Solid-State Block Polyelectrolytes

A DISSERTATION

SUBMITTED TO THE FACULTY OF THE GRADUATE SCHOOL

OF THE UNIVERSITY OF MINNESOTA

BY

David Justin Goldfeld

IN PARTIAL FULFILLMENT OF THE REQUIREMENTS

FOR THE DEGREE OF

DOCTOR OF PHILOSOPHY

Marc A. Hillmyer, Adviser

July 2020

Acknowledgements

It has been more than ten years since I was first mistaken as having a Ph.D. (not because of anything I did, but because I have always looked older than I am and was standing in a research laboratory). Most of my life, I knew I was going to be in STEM; originally working towards being an engineer, and later discovering that I work much better as a scientist who occasionally does engineering on the side.

Over my time in academia, I have become a good scientist. While most people will not be surprised I wrote that sentence, they may be surprised to know that I understand more than anyone that it has nothing to do with my genetic abilities (which I've been told are lacking) or work ethic (really, I have never been that efficient). I am a good scientist because I have had the privilege of learning from many of the best at all stages of my career. I have received guidance, assistance, advice, and more resources than I could have ever imagined from many of the best scientists and engineers in the world. The group of people that have contributed to making me who I am today is too large to properly enumerate in a thesis acknowledgement (this is not, unfortunately, an autobiography), but nonetheless, I will try to mention a number of those that stick out as playing a major role specifically in my pursuits of a scientific career, or in the past five years of my life in Minnesota. There are many who will not fit in the following acknowledgments; thank you to everyone that has had a positive impact in my life. I can never repay you all.

Thank you first to the brilliant Dr. Jeffrey Gaw, the high school teacher that inspired me to pursue chemistry. He gave me the first test I received below a 30% (which was curved significantly higher) and taught me how calculus can be done intuitively to inform

physics which guides chemistry. I think he would be proud to know I was sufficiently convinced by his love of chemical physics to acquire a B.A. in physics, and a B.S., M.S., and now Ph.D. in chemistry.

I owe a great deal of thanks to Prof. Shelley Minteer at Saint Louis University. My work in her lab was my introduction to real scientific research as a part of the Students and Teachers as Research Scientists (STARS) program through the University of Missouri-St. Louis. Although we had relatively little face time, she let me play with the expensive toys at a major research university and provided me with a number of learning experiences in biochemistry, electrochemistry, and materials science.

There is no way for me to ever give proper thanks the inimitable Prof. Dong Qin, who hired me, a high school student passing a baby CV to random professors, to work in her lab at Washington University in St. Louis. Dong is a fantastic scientist, always full of energy and excitement for interesting experiments. I was lucky to have her work in lab alongside me, teaching me to work with noble metal nanostructures. She is the most inspiring scientist I have ever met. I would also like to thank Brent Riggs, a master of photolithography for teaching me to use cleanroom equipment during my time there, which has been a recurring theme in every stage of my career since then.

I would like to thank Prof. Younan Xia, who hired me after my time working for Prof. Qin. He didn't usually hire high school students, but I'm glad he was willing to give it a try. My time in his lab was the first time I truly experienced the joys, and frustrations, of doing chemistry (and exceedingly expensive noble metal chemistry at that). Thank you for teaching me all of the best expensive Chinese restaurants in St. Louis, and that no matter

how famous and busy a professor is, they can always find a bit of time to take a young scientist out to lunch. We have shared many meals since that time, and I am always thankful he is willing to block out time on his seminar circuit to grab a meal with me whenever we are in the same town, whether it be St. Louis, Atlanta, Chicago, or Minneapolis, to help me decide on a college, research jobs, or graduate schools, and discuss many other aspects of my scientific and personal life. Dong and Younan, you have both been incredible mentors and friends for nearly a decade now, and I cannot thank you enough; I know I wouldn't be here without both of you.

For my time in college, I first want to thank Prof. Paul Kohl at the Georgia Institute of Technology. Prof. Kohl was the third professor of engineering I worked with that had never studied engineering and was an entertaining professor who was always filled with ideas (and he also taught me how to overcome any fear of hydrofluoric acid).

Most of my scientific work as an undergrad was with the incomparable Prof. Matthew Tirrell. Matt gave me continuous support for four years in his lab, and he saved me from a number of "problematic" situations. I learned over time that his work is motivated simply by the drive to do good, and I have the deepest respect for his attitude toward making academia, and the world, a better place for everyone. I would not be in graduate school, and probably would not have graduated college, without Matt. Thank you, Matt, for always keeping me on track.

I have many people from the Tirrell Group to thank, but none more so than Dr. Matthew Kade, the man, the legend, who taught me the basics of all of polymer science and most of organic chemistry. He is a genius and also a scientist that taught me about life

as much as polymers. I look back fondly on our endeavors with a huge smile, and I can't wait for the next one. In addition, thank you to Prof. Sarah Perry, Prof. Lorraine Leon, Prof. Handan Acar, and Prof. Samanvaya Srivastava for helping to shape my four years at UChicago (and Argonne National Laboratory); your friendship and mentorship was invaluable. I also have to thank my comrades Khatcher Margossian, Dr. Charles Pierce, and Adam Levi, who I would not have made it through without, and the administrative staff, in particular Maria Rubio. I also owe a very special thanks to Diana Morgan, who kept me alive and well even when we were traversing questionable waters. Nowhere I do science can compare to a lab where I can simply shout your name down the hall and make plans for lunch.

For my time at Lawrence Berkeley National Laboratory, I would like to thank Prof. Nathaniel Lynd, who welcomed me into the Joint Center for Artificial Photosynthesis. I had the opportunity to learn anionic polymerization from the master himself, and also got to know him well. Thank you, Nate, for showing me some invaluable polymerization techniques, making polymers to send *to space (!)*, as well as showing me around the Bay Area.

Since coming to Minnesota, I've had the opportunity to learn from the best there is in polymer science. Thank you to Prof. Timothy Lodge, Prof. Frank Bates, and Prof. Mahesh Mahanthappa for teaching me more about polymers than I thought mankind had figured out. Thank you also to Prof. Phillippe Buhlmann and Prof. Christopher Ellison, who rounded out my committee and always kept me on my toes. I would also like to thank the entire polymer group, including all of the students and postdocs, that have made an

entire community of polymer-minded people here. I can guarantee there is nowhere on Earth that does polymers better than Minnesota.

Thank you to the Center for Sustainable Polymers, who I was a part of for several years of my time here, and to the administrator that made it work, Laura Seifert. I'm sorry I had to bother you with so many questions. My time in the CSP was funded by some of my dearest friends. Thank you to my friend John Parnell; you have been a joy to get to know better over the past decade and you are one of the strongest and kindest people I have ever met. I would also like to thank Dundee and Ian Butcher for believing we could do something unique and change the world. Your support has never wavered, and I am confident we are going to do it.

I am extremely thankful to have had the pleasure over the past five years of working in the Hillmyer Group. You are all without a doubt the most fun collective in polymers. A special thank you to South Office, including Dr. Stacey Saba, Dr. Ozcan Altintas, Dr. Ingrid Haugan-Smidt, Emily Wilborn (my movie watching, TV binging office/labmate), Dr. Jay Werber, and Dr. Babu Gaddam, for listening to me for many years. I'm sure you figured out quickly I will never run out of hot takes. Thank you to my friends Dr. Sebla Onbulak, the best driving student I ever instructed, Dr. Debbie Schneiderman, who helped me do my first high pressure experiments, Dr. Angelika Neitzel, who never believed in doing what everyone expects, Dr. Leonel Barreda, who will one day build a car out of magnesium, Dr. Esra Altay, the calm in the storm, Dr. Lucie Fournier, a fantastic photographer, and Dr. Christopher DeRosa, who always had a kind and gentle solution to any problem, even when I was about to smash something with a hammer. I also must thank

Dr. Nicholas Hampu, my foil through five years, who has told me nine of the ten wildest stories I have ever heard.

Thank you to the two undergraduate researchers that worked with me during my time here, Devin Dykes and José Valdez. They were both sharp as tacks and also genuine people that I'm confident will continue on to impactful endeavors. I hope I managed to teach you a little bit about science, life, and how to make mistakes along the way.

I worked closely with two postdoctoral researchers during my time at Minnesota, and they are most likely responsible for any content herein that actually worked. Thank you to Prof. Madalyn Radlauer, who was a great friend and mentor. We started a difficult project and I can't imagine how I would have gotten it off the ground without you. You are one of the best teachers (and DMs) I have ever met, and SJSU is lucky to have you. I would also like to thank Dr. Eric Silver (a.k.a. New Maddy), who spent the final few years of my Ph.D. struggling with me to control the fickle beasts that are polyelectrolytes. Your innate knowledge of obscure black and white European movies from the 1950s and appreciation of strange music has opened my eyes to an entire world of content, and certainly kept me entertained.

I also owe thanks to my advisor, Prof. Marc Hillmyer. You let me pursue a number of unorthodox projects (and projects created/run in unorthodox ways) and whenever there was a holdup, a problem, or even if the experiments are working, you could always find a different lens through which to view the problem, a different experiment to compliment the data, or a new expansive idea about what comes next.

Thank you to the University of Minnesota Rocket Team, who invited me to be a mentor for the past four years. Special thanks to Michael Siirila, Jacqueline Sotraidis, and Christopher Gosch, who started the Propulsion program, and to the many undergraduates who have run it since they graduated. I've had a wonderful time learning from each of you, and I hope I taught you some chemical safety along the way. I would like to thank Prof. Jeffrey Schott who helped me establish the program, Gary Stroick who taught me all about rockets and saved my life at least once in the New Mexico desert, Kate Greenberg and Adam Krajicek for helping us build the safest propulsion program in the world, and Officer Michael Coan of the Minneapolis Bomb Squad for finding us a place to do it. Thank you also to Connor Reilly, who is taking over the mentor role into the future. *Per aspera, ad astra.*

Special thanks to my dearest friends through grad school. I know I would not have survived without each of you. Thank you to Claire Dingwell for always reminding the world that all dogs are good dogs, and Katherine Jones for helping run Trash TV night. I might still have faith in the world if not for the seasons of *Are You the One?, The Bachelor,* and *The Bacholorette* that I've watched. Thank you to Meghan McGreal and Connie Anderson, who know how to embrace the emo and enjoy it. You both understand the struggle is real, and are always down for the most efficient ways to crush it nonetheless.

Thank you to the leader of my climbing/workout crew, Dr. Tyler Mann; you did a remarkable job holding us together and keeping us in shape. Thank you to all of my broomball players who withstood me coaching (*read screaming*) from the sidelines for many years. You were all spectacular players, and I'm proud to have had, by far, the best

female broomballers at the U. I am confident we thoroughly crushed the undergrad fraternity teams in another universe (because really, in this universe, how are we ever supposed to compete with a team of 19 year old lifelong hockey players...).

Thank you to my dearest roommate of all five (!) years of grad school, Kiall Suazo, for letting me fill our apartment with junk and share lots of food when one of us was going hungry. Thank you to the absolute strongest 4, weakest 5 that I've ever known, *the* Dr. Guilhem De Hoe. We've probably had too many adventures for one lifetime, and I'm sure one day we'll suffer for it. But until then, here's to many more. Thank you to Nicholas Bible, my co-teacher of welding and design, who embraced the real definition of bourgeoisie while being helpful, innovative, and an always available editor. I wish I would have found you down the street earlier in life. The biggest thanks goes to my partner in crime for the last many years, Beth Dewing. I'm scared to count the number of movies we've seen together, the number of restaurants we've eaten at, or the number of rock walls we've climbed, but I know that I enjoyed every single adventure nonetheless. The support of all of my friends is what keeps me from truly losing every bit of sanity grad school tried to claw away from me.

I was also kept sane by my dearest friends from outside of Minnesota. Thank you to Ricky Stewart, William Craft, and Mark Maskeri for sticking by me as my best friends. From adventures in the Twin Cities to regular D&D sessions at a distance, your friendship has been a staple. And thank you to Ricky and Amber for letting us appoint ourselves the Best Men and schedule your wedding. Thank you to my two other favorite couples that also let me serve as Best Man during my time in grad school: my dearest friend Andy Cook,

who has been listening to me spout garbage about everything for well over 20 years, and his wife Natalie, and my brother Danny and his wife Alexis, who have always been a joy to see whenever I return home. If you've attended any of my Best Man speeches, you would be unfazed by the 3,000 word length of this acknowledgements section, and are perhaps underwhelmed.

Thank you to my dearest cousin Adrienne, who traveled across Europe with me and has been my bestie as long as either of us can remember. There is no one I would rather be stuck with in a public stairwell in the town square of Aix-en-Provence. Thank you to the rest of my dearest family–Ma, Kim, Tammy, and Gary and many others. Your support has meant the world and your visits (including seeing the Dixie Chicks, touring breweries, riding steamboats, and attending graduations), phone calls, and video chats are the highlights of my time wherever I live. Even at a distance, I always feel your love.

Despite the literal hundreds of people I've thanked above, in some ways everyone has really meant nothing compared to my biggest champions. All the thanks and all my love must really be given to my parents, Pam and Joe. They have answered every phone call, traveled across the country too many times to count, and never believed I could do anything wrong (even when I might have). They fought for me when I was attacked, demolished barriers when something blocked my path, and lit flares when I couldn't find my way. They have kept me joyful, talked me through the hard parts, and tried really, really hard to understand the science I've been working on. Mom and Dad, you are the true heroes of this story.

I will conclude this never-ending monologue with a small footnote: the world today looks a lot different than what I expected when I started here in 2015, with Barack Obama as my President and the world in an upswing. I'm writing this dissertation from quarantine, stuck inside so as to avoid potentially spreading COVID-19. I had a few remaining experiments that were underway during partial reopening when campus was shut down again due to the Minneapolis riots over the death of George Floyd. In academia, we are often shielded from the negative events going on in the outside world, but I'm hopeful that recent events will lead to a wake-up call. Maybe we'll see the importance of scientific research. Maybe we'll try to increase the presence of underrepresented groups in STEM. Maybe we'll do something to prevent the murder of Black people by the very police that should be protecting them. Maybe we'll finally understand that Black Lives Matter.

I hope we will.

For Austin Hudson-LaPore and Leonard Kirchdoerfer; two scientists and dearest friends.

Manibus date lilia plenis.

Abstract

While polyelectrolytes are, in general, hydrophilic and soluble in water, there are many applications that benefit from immobilized solid-state charged materials, including membrane separations and batteries. One convenient method to immobilize polyelectrolytes in a solid-state configuration is using block polymer materials self-assembled to contain charged polyelectrolyte domains immobilized by neutral supporting domains. We used this strategy to work towards charge mosaic materials, a proposed design for a piezodialysis-based water desalination system. In a charge mosaic membrane, there are both positively and negatively charged polymer domains that are spatially separated and independently cross the thickness of the material.

In **Chapter 2**, we first developed a new technique to integrate this design into thin films. Through the synthesis of neutral ABC triblock polymers, we casted thin films with three microphase separated domains. We then demonstrated the functionalization of these materials in a mild, 2-in-1 postpolymerization modification that converted the A domain (poly(*n*-propyl styrene sulfonic ester)) to a negatively charged polyanion and the C domain (poly(vinylbenzyl chloride)) to a positively charged polycation in a mild, single step vapor exposure. While these materials demonstrated successful microphase separation with a simple functionalization that maintained morphology, they had poor long-range order and suffered from brittle mechanical properties that prevented their effective use as active layers in membrane separations.

During the synthesis of an ABC triblock polymer for charge mosaic applications, we found a previously unreported miscibility between polystyrene and poly(vinylbenzyl

chloride). Although both polymers had been used together in a number of previous applications, their solid-state structure had never been adequately explored. In **Chapter 4**, we attempted to characterize the Flory-Huggins interaction parameter between these two polymers using small-angle X-ray scattering of homogeneous polymer blends. We then synthesized a vinylbenzyl chloride derivative, vinylbenzyl nitrate, that demonstrated both microphase separation from polystyrene as well as facile postpolymerization modification and explosive properties.

Chapter 3 attempted to solve the mechanical problems associated with the triblock polymers by integrating poly(styrene sulfonic ester) and poly(vinylbenzyl chloride) into a system that undergoes polymerization-induced microphase separation (PIMS). PIMS monoliths were made through a simple radical polymerization initiated in a homogeneous mixture of a macroinitiator dissolved in mono- and di-functional monomers. The PIMS technique results in strong materials that contain a bicontinuous structure comprising a percolating macroinitiator domain crossing the thickness of the crosslinked matrix. We used PIMS to produce solid monoliths using the neutral polyelectrolyte precursors previously used in the ABC triblock polymers. The macroinitiator domain was then functionalized to yield either a positively charged polycation material or a negatively charged polyanion material, confirmed using oppositely charged dyes and infrared characterization.

The integration of both positive *and* negative charges into a PIMS system is approached in **Appendix A**. Simply mixing macroinitiators, a procedure based on previous literature, showed unexpected macrophase separation in the monolith. The use of block

polymer macroinitiators to overcome solubility differences between the segments is presented as a potential solution and the synthesis of the first block polymer PIMS is demonstrated. Finally, we introduced the potential of using a polyelectrolyte as the matrix domain.

Appendix B presents a proposed model for controlling swelling in the PIMS polyelectrolyte domain. By adding a poly(lactide) block to the poly(styrene sulfonic ester) macroinitiator, a degradable domain is introduced that can be selectively removed to free swelling space for the polyelectrolyte. We hypothesize that control over the swelling will provide a model system for the systematic variation of ion conductivity and provide insights into the fundamental effects of ion density, water content, and morphology.

A slightly different project is explored in **Chapter 5**, where we develop a poly(lactide) based foam for use in floral foam applications. We formulate a mix of surfactants that make the hydrophobic, low melt-strength poly(lactide) into a rigid, low density ($<0.02\ g \cdot cm^{-3}$), hydrophilic foam that readily absorbs water and supplies it to inserted flowers. The foam is compostable and made from renewable materials, making it a significant improvement over the petroleum based, non-degradable materials that are currently commercially available.

Table of Contents

Table of Tables

Table of Figures

Table of Schemes

Chapter 1. Introduction

1.1 Limited resources

One focus of the current sustainability movement is understanding that Earth has limited resources for consumption by humans. Despite centuries of expansion upon the assumption that there would always be more natural material to work with, we have begun to run out of critical resources. One of the first resources that has seen critical stress has been considered the most important resource since the founding of civilization–freshwater.

For millennia, humans have built their cities at sources of freshwater. It is important to note the need specifically for freshwater, which is specified as water containing less than 500 parts per million (ppm) of salt. Though the oceans contain 97% of the Earth's water, the saltwater they contain is unsuitable for most uses. Instead, rivers, streams, lakes, and underground aquifers have supplied society with the entirety of its freshwater needs.

There are three main draws on water resources. The first is drinking water and sanitation. Although it is the smallest portion of necessary water, estimated at only 7.5 liters of water per person per day,[1] it is the one we are most intimate with as it passes through our homes and must meet the highest purity standards. We use water for drinking, cooking, and basic hygiene, as well as cleaning and waste disposal. Even though this is the water we directly interact with, it makes up only about 10% of overall water use.[2]

The largest consumer of water is agriculture. On average worldwide, nearly 70% of the water withdrawn from freshwater sources is used for irrigation, livestock, and aquaculture.[2] While this water consumption is less tangible to us than what we consume in

our homes, it is just as vital of a resource. When there is not enough water to grow sufficient food, famine can lead to the collapse of entire civilizations. Water scarcity due to droughts contributed to the collapse of numerous civilizations, including the Maya civilization in Mexico and the Tang Dynasty in China.[3] Even in modern times, Syria was driven into civil war in 2011 partly by a mass exodus of rural individuals to the major cities after years of crop failure and massive losses of livestock.[4]

The remainder of overall water consumption is even further removed from our lives in the form of industrial and energy uses. Water has played an important role in industrial practices since before the industrial revolution. Leather tanneries,[5] paper mills, and textile factories[6] consume tremendous amounts of water in their respective production processes. Even without directly consuming the water, a number of industries after the industrial revolution began using water as a main source of power. Minneapolis rapidly became the largest flour producer in the world when more than twenty mills were built along St. Anthony Falls on the Mississippi river to power their machines.[7] Today, large quantities of water are used to generate electricity. The state of Texas alone withdraws more than 9 billion gallons of freshwater per day just to generate electricity.[8] The presence of industry also causes regional variance in the end-use of water. Africa uses less than 10% of their freshwater withdrawals for industrial purposes, and a vast majority for agriculture. At the same time, Europe has more advanced industrialization and a climate with higher rainfall, so almost 60% of their withdrawn freshwater is used in industry.[2]

After such long periods of rapid growth, human civilization has begun to experience widespread water scarcity. While droughts have always caused temporary periods of water

scarcity, some areas now consume more water than rainfall and runoff will replenish. Throughout the 20th century, water use grew by more than twice the rate of population growth. In drier climates like the southwest United States, municipalities and farms consistently consume more than the entirety of the rainwater that falls in the region. Even so, the population and agricultural industries in the area continue to expand. Periods of permanent or intermittent water scarcity are currently affecting the southwest United States, most of North Africa and the Middle East, and large parts of South and East Asia, costing upwards of $500 billion annually (**Figure 1.1**).[9]

Climate change has created further challenges to maintaining healthy water supplies. Changes in weather patterns have led to droughts in widespread areas. Certain dry climates are predicted to steadily receive less rainfall, while other areas are expected to see dramatic increases in extreme weather events, leading to severe flooding and water management problems. The United Nations predicts that the adaptations needed to improve industrial and municipal water management systems and successfully combat the effects of climate change will cost $10-20 billion annually, with up to $7 billion more needed for flood protection.[10]

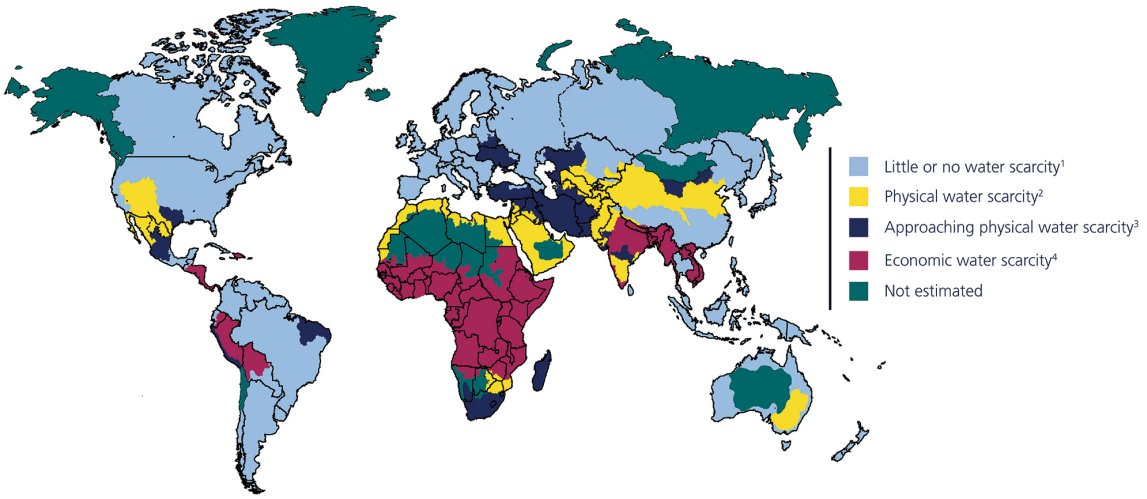

Figure 1.1. Notes: [1] Little or no water scarcity. Abundant water resources relative to use, with less than 25% of water from rivers withdrawn for human purposes. [2] Physical water scarcity (water resources development is approaching or has exceeded sustainable limits). More than 75% of river flows are withdrawn for agriculture, industry, and domestic purposes (accounting for recycling of return flows). This definition – relating water availability to water demand – implies that dry areas are not necessarily water scarce. [3] Approaching physical water scarcity. More than 60% of river flows are withdrawn. These basins will experience physical water scarcity in the near future. [4] Economic water scarcity (human, institutional, and financial capital limit access to water even though water in nature is available locally to meet human demands). Water resources are abundant relative to water use, with less than 25% of water from rivers withdrawn for human purposes, but malnutrition exists.[11]

1.2 Water purification

There is no single solution to the current and future lack of clean water. A combination of water management, conservation of existing resources, and catchment and distribution infrastructure will be required to sustain growing populations in the near future. Efforts like gray water reuse, improved transport pipelines, increased water efficiency, and collection and use of storm drain runoff will play a vital role in the future of clean water. While these systems are easy to implement in new sustainable developments, it is both difficult and exceedingly expensive to retrofit existing communities. At the same time, these efforts only improve use of existing resources, while much of the current and

developing water scarcity is in areas that do not have enough renewable water resources to sustain the population (**Figure 1.2**).

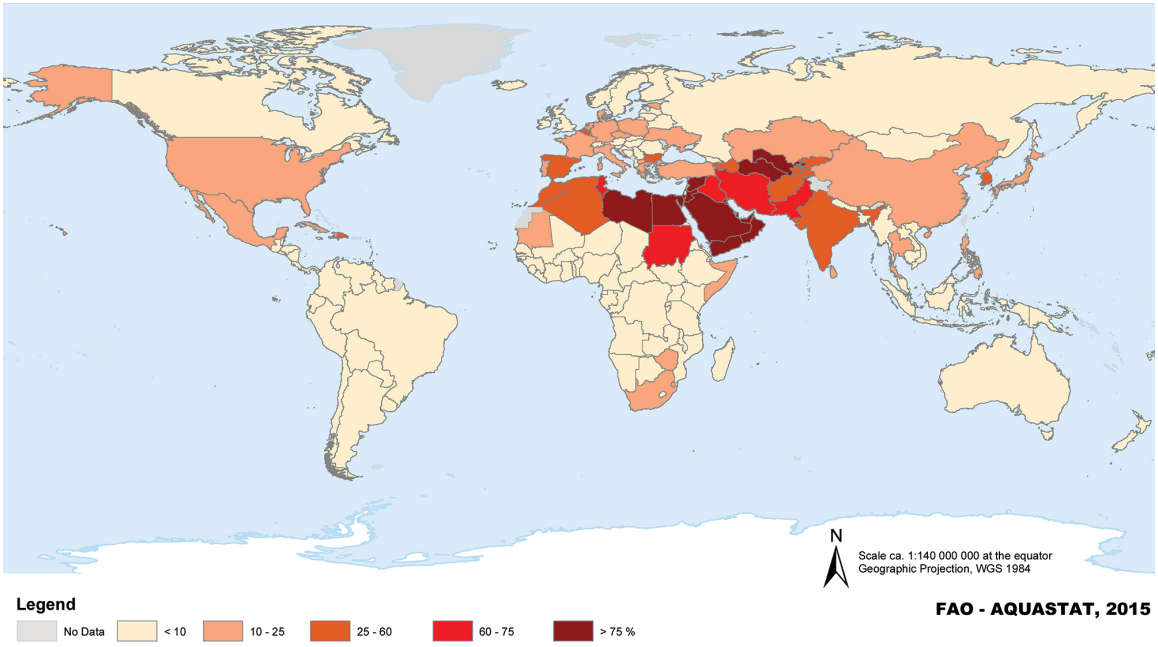

Figure 1.2. Proportion of renewable water resources withdrawn: the Millenium Development Goal Water Indicator from the United Nations Food and Agriculture Organization.

One of the most promising ways to combat this water scarcity is the development of new technologies for water purification. The implementation of water purification is based on the simple observation that we have a scarcity of *freshwater*, but anywhere along a coast has a near infinite supply of *saltwater*. Water desalination should therefore allow for an endless supply of freshwater; the problem is that removing the salt from oceanwater is an extremely expensive process.[12]

The simplest process for water desalination is thermal desalination (distillation), during which the water is evaporated and condensed, leaving behind the salt in the distillation pot and producing purified water. Vaporizing water, however, requires a

tremendous amount of heat input, and even the best heat recovery systems cannot make up for the lost energy. For that reason, the majority of new water desalination operations use reverse osmosis (RO).[13]

Reverse osmosis is a separation technique that uses a semipermeable membrane to remove a solute from a solution. The contaminant (salt) is filtered out of the solution by size. The contaminated feed is placed on one side of a semipermeable membrane that allows extremely small molecules to move through but excludes larger solutes. The separation process follows the solution-diffusion model, [14] which assumes a nonporous but diffusive active layer of polymer that serves as the separation site. Water and solutes both partition into the active layer and then diffuse across the thickness of the polymer driven by a chemical potential gradient. The solute then desorbs from the membrane on the downstream side. For RO desalination processes, the membrane structure is more permeable to water than salt. When several atmospheres of pressure are applied to the feed, the difference in pressure drives the water to cross the membrane while the salt is held back. The water that passes through the membrane (filtrate) comes out desalinated and salt concentration on the high-pressure side (concentrate) increases.

Despite its significantly lower energy consumption relative to distillation, RO still requires a large amount of energy–so much that it is often more economical to pay for freshwater transport over large distances. A large part of the cost of RO desalination stems from its efficiency; energy use in RO remains higher than the theoretical minimum energy. When salt dissolves in water, it is entropically driven to do so. The charged molecules are driven to solvate into water, *releasing* energy as they do so (the solvated ions are at a lower

Gibbs free energy, ΔG). To remove the salt, the process of dissolution has to be reversed, which necessitates an *input* of energy.[12] The theoretical minimum energy of an RO system running at 50% water recovery is 1.06 $kWhm^{-3}$, but current systems generally run between 3-6 $kWhm^{-3}$.[15]

Increasing efficiency of RO systems over time has led to limited use in some countries, most notably Israel. After building the world's largest RO desalination plant with an output of 40 billion gallons of potable water per year, the country now gets more than 50% of its freshwater from RO desalination and has successfully avoided severe water shortages.[16] However, new technologies are needed because many countries lack the economic resources required to undertake such a large scale and energy intensive project. At the same time, the drive to reduce greenhouse gas emissions has brought energy efficiency to the forefront of water desalination research worldwide.

While some excess energy is lost in the pressurization of the water, a large part of the inefficiencies in RO systems are from the semipermeable membrane. Currently, the standard for RO membranes is aromatic thin-film composite polyamide membranes, which are fabricated through the interfacial polymerization of *m*-phenylenediamine and trimesoyl chloride. These polymer membranes, however, do not have perfect selectivity for water over solutes, meaning there is not a high enough rejection of salt and small neutral molecules (in particular boron) for applications including drinking water and agriculture. The water often has to go through significant pre- and post-treatment and may require more than one pass through a RO system, driving up the energy and economic cost. Calculations show that efficiency in RO processes will be most improved by focusing research efforts

on the development of more selective membranes.[17] To improve selectivity in RO membranes, new materials and membrane processing techniques will need to be developed.

1.3 Polymers

Even after more than a hundred years of refinement of the understanding of elements and the development of the periodic table, polymers were outside of the understanding of chemistry. The idea of a molecule containing thousands of atoms seemed so absurd that more than a decade after Einstein helped define quantum mechanics,[18] the first chemists to propose the idea of polymers were ridiculed. Broadly, the chemistry community refused to believe that a single molecule could be so large.

Hermann Staudinger proposed the existence of polymers in his paper *Über Polymerisation* in 1920 after studying natural rubber.[19] He proposed that giant molecules existed, made up of a vast number of repeating units. Other chemists believed he was confusing his theory with many individual molecules that were stuck together, forming colloidal structures, rather than properly measuring the molar mass of individual molecules. Staudinger would, of course, prove to be right, and in doing so change the way we use chemistry in our daily lives.

The idea of polymers was slowly accepted in the chemical community, and it turned out there had been polymers around us, and inside of us, the entire time. Cellulose is a polymer, starches are polymers, even the proteins and DNA inside of each of our cells are polymers. While polymers were not described in chemical form until the 1920s, they had been in commercial use for millennia. Cellulose had been harvested from trees and

processed into paper, cotton and silk had been spun into yarn and woven into textiles, and gelatin had become a common ingredient in kitchens of wealthy landowners.

Chemical modification had also started on polymers, including the synthesis of sulfur crosslinked rubbers to make thermoset materials,[20] nitrocellulose to produce Celluloid,[21] and the mass production of Bakelite resins from phenol and formaldehyde.[22] Despite their introduction into the marketplace in a number of applications, there was little understanding of why these materials behaved the way they did and how they could be manipulated to make better materials.

Over a remarkably short period of time, chemists made tremendous advancements in polymer materials science. By the end of World War II, low-density polyethylene could be produced at scale, neoprene had been invented and produced by DuPont to be used as a chemical resistant material,[23] butadiene and nitriles were copolymerized into Buna rubber in Germany, and styrene/butadiene copolymers were produced as a synthetic rubber in the U.S.[24] For the first time, soft materials were designed with critical evaluation of material properties, and they were put to use in important, widespread applications.

The incredible range of properties we can access with polymers made them a staple of modern consumer products. It is nearly impossible to purchase a product without a polymer included as a component–either a thermoplastic as the constituent material, a plastic bag as packaging, an adhesive that binds components together, or even a coating that protects underlying metal from corrosion. Polymer pipes and insulation have become standard construction materials and polymer hoses and foams have become essential components in motor vehicles. In polymer chemist speak, plastic is ubiquitous.

1.4 Polymer blends

Polymers made from different monomers can have remarkably different properties. One way to make materials containing properties from two different polymers is to simply mix two polymers together into a polymer blend. Materials properties, however, are rarely additive. In fact, many polymers are incompatible and will not mix together at all. Two polyethylene sheets can be melted and pressed together to form a single piece, like the seal on the edge of a trash bag. Pressing a melted polyethylene sheet against a melted polypropylene sheet, however, will result in two pieces of plastic that will still freely delaminate from each other.

Paul Flory derived what is now called Flory-Huggins solution theory in the early 1940s.[25,26] The theory builds a mathematical model describing the dissolution of a polymer chain in a solvent by constructing a square lattice where each monomer occupies a lattice point and is surrounded on all sides by solvent molecules and/or other monomers (**Figure 1.3**). He then quantified the enthalpic force that drives different substances to segregate into separate domains; monomers like to be surrounded by other monomers and solvent likes to be surrounded by solvent. The enthalpic interaction, therefore, usually opposes dissolving the polymer and is quantified using solubility parameters of the polymer in different solvents. At the same time, entropic forces drive the polymer to dissolve in the same way sodium chloride is driven to dissolve in water. These drives to mix and/or segregate can be quantitatively calculated, which allows determination of when a polymer will dissolve based on degree of polymerization (i.e., length), solubility parameters, and temperature.

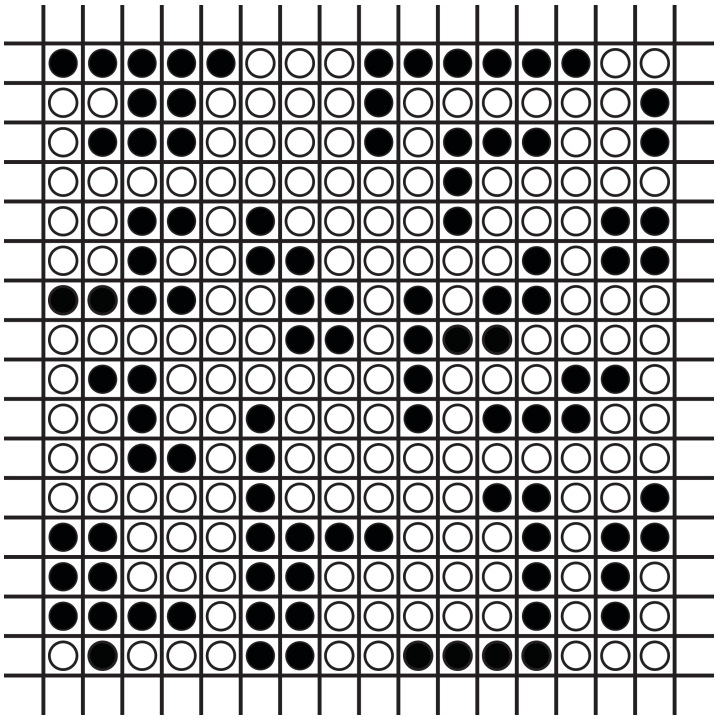

Figure 1.3. Square lattice of polymer (in black) in solution (white).

Flory-Huggins solution theory can be expanded into blends by simply replacing the solvent component with a second polymer.[27] This polymer-polymer interaction is described by the Flory-Huggins interaction parameter χ, which, like the solubility parameters of a polymer in a solvent, describes the miscibility of one polymer in another. Depending on this χ value and the length of each polymer, it is possible to estimate the volume fractions of two polymers that will mix together at any given temperature. While some blends will be fully compatible, others will instead undergo macrophase separation. Even after mechanically mixing in the melt, incompatible polymers will form two separate phases, one rich in polymer A and one rich in polymer B, like oil on water. A system of two miscible polymers is investigated in **Chapter 4**, and an alternative polymer proposed to increase the effective χ. Polymer blends often have limited applicability because

macrophase separation precludes the formation of a homogeneous and coherent material and leads to poor material properties.

1.5 Polymer architecture

One method to prevent the macrophase separation of two polymers is to incorporate the two different monomers into a single polymer chain called a copolymer. Many monomers, especially those with similar chemical structures, will freely polymerize one after the other, so a copolymer can be made by simply mixing two monomers in the polymerization.[27,28] The material properties will change in turn, sometimes averaging the properties between that of the two separate homopolymers and sometimes manifesting entirely new behaviors. Mixing certain monomers can also increase functionalities in the material, adding the ability to crosslink or blend in additives. The ability to mix two or more monomers opens up a vast library of possibilities to reach desired material properties starting with materials that already exist and polymerization techniques that are well understood.

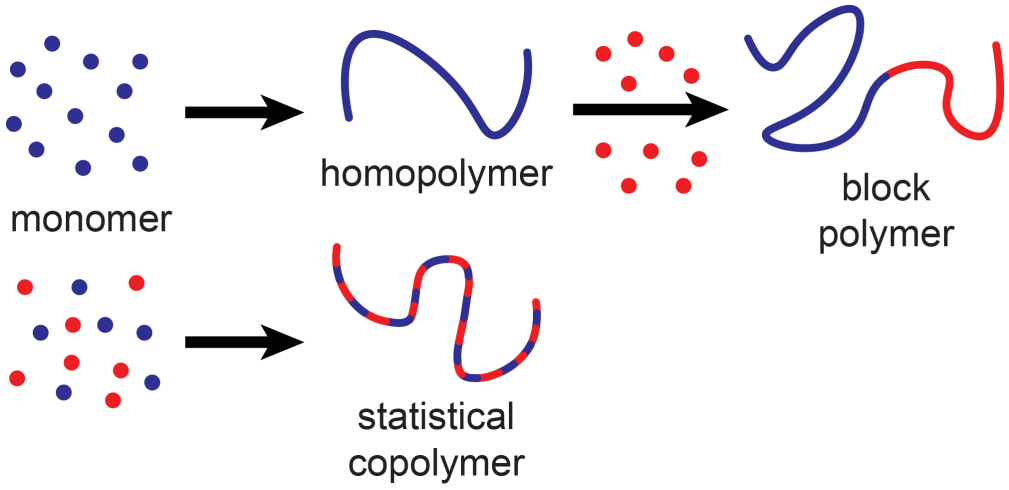

Figure 1.4. Schematic of the synthesis of a homopolymer, statistical copolymer, and block polymer; here the latter is made via chain extension.

Polymer architectures can dramatically change the material properties of a polymer–Error! Reference source not found. investigates the application of branched p olymers to compostable foams. Other work in this dissertation revolves primarily around block polymers, a further subset of polymer architectures (**Figure 1.4**). A block polymer can be made by chemically coupling different blocks together on their ends[29] or by growing a chain of a different monomer off the end(s) of a polymer macroinitiator in a process known as chain extension.[30] The resulting polymer contains two or more segments of two or more differing monomers in a controlled order.

1.6 Block polymer morphology

Block polymers have properties that are distinct from both homopolymers (which contain a single monomer) and copolymers. The application of Flory-Huggins solution theory to different components in a single chain reveals a new set of variable parameters with a notable impact on material performance and functionality. As discussed in **Section 1.4**, two polymers with different chemical structures may separate into two distinct macrophases. In a diblock polymer, however, polymer A is covalently bonded to polymer B. They cannot physically separate from each other. This drive to segregate coupled with the inability to separate leads to the formation of morphologies consisting of small domains of A and B that minimize the free energy of the system as much as possible through a process known as self-assembly. These two separate domains, one rich in polymer A and one rich in polymer B, can form complex arrangements, from parallel stacked sheets called lamellae to asymmetric quasicrystals (**Figure 1.5**).[31,32]

The morphology that self-assembles in a block polymer system is dependent on many factors including the Flory-Huggins interaction parameter, the length of each block, the relative conformational asymmetry (the stiffness of the chains), and processing conditions (temperature, confinement, shear forces, etc.). One strategy to increase long-range order in these systems is to anneal the block polymer after initial processing. Thermal annealing consists of heating the sample to an elevated temperature for an extended period of time, whereas solvent annealing involves exposure of a polymer sample to solvent or solvent vapor. These techniques increase chain motion through thermal means or plasticization, respectively, and allow the sample to relax into the lowest free-energy state, or equilibrium morphology.

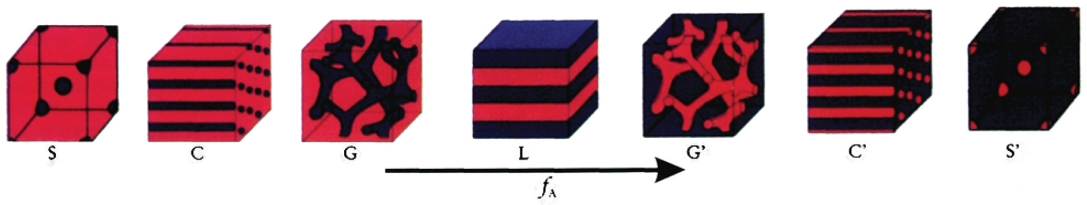

Figure 1.5. Possible morphologies found in diblock polymers including spherical (S), cylindrical (C), gyroid (G), and lamellar (L) depending on the composition and χN. Reproduced from Bates and Fredrickson[31] with the permission of the American Institute of Physics.

The self-assembly of these domains into different morphologies has a dramatic effect on the applicability of block polymer materials to certain technologies. Spherical morphologies with minority "hard" domains interspersed between soft domains can make thermoplastic elastomers for elastic, high impact applications.[33] Lamellar morphologies can be used to create nanometer scale lines on semiconductor chips.[34] Hexagonally packed cylinders can be used as transport channels across a membrane.[35] **Chapter 2** and **Chapter**

3 use block polymer self-assembly to develop new polyelectrolyte materials for water purification applications.

1.7 Polyelectrolytes and coacervation

Polyelectrolytes are a subset of polymers that contain fixed charges along the polymer chain. Adding charges to a polymer drastically changes its behavior, in some ways merging the behavior of neutral polymers with that of a salt. Many biopolymers are actually polyelectrolytes including proteins, DNA, and RNA. For decades, polyelectrolytes have been closely studied, and have been used in applications ranging from food additives[36] to tissue scaffolds[37] to superabsorbent materials.[38] One of the features that makes them so applicable to our lives is that polyelectrolytes are, in general, hydrophilic. Similar to most small molecule salts, they dissolve readily in water and in solution behave in ways we still do not fully comprehend.

There are a variety of polymer structures that are encompassed by the term polyelectrolyte. In the simplest form, polyelectrolytes can be either negatively or positively charged. In general, we refer to the charge of the polymer as the fixed charge bound to the polymer chain, but it is important to note that every charge along a polymer chain will contain an oppositely charged counterion. When we refer to a polyanion (negatively charged polyelectrolyte) or a polycation (positively charged polyelectrolyte), we generally imply pairing each charge along the polymer chain with a small inorganic counterion (such as Na^+, Cl^-, etc.).

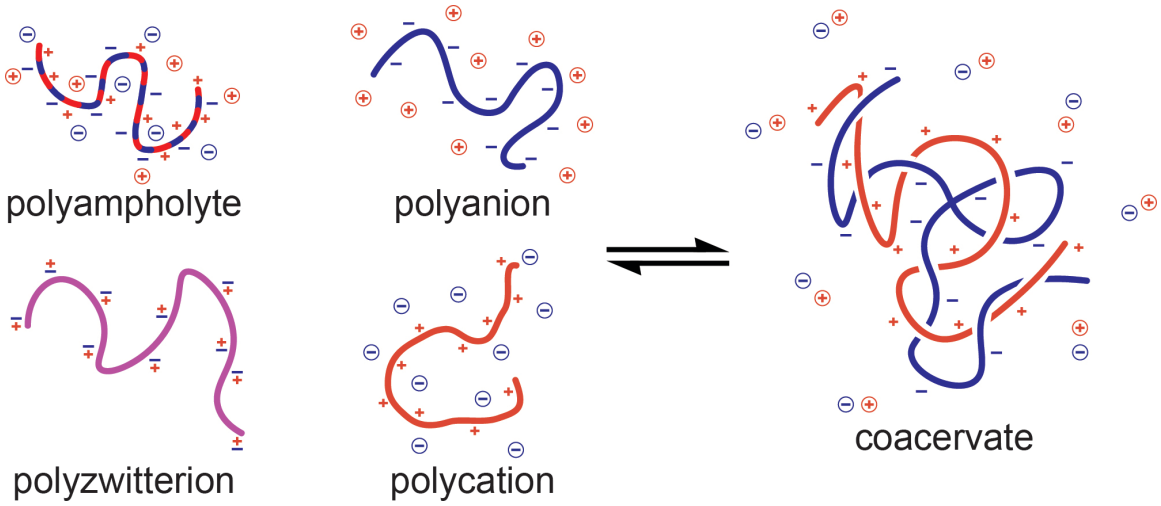

Figure 1.6. Schematic of polyampholyte, polyzwitterion, polyanion, polycation, and coacervate architecture.

More complex geometries can also be made using polyelectrolytes (**Figure 1.6**).[39] Polyampholytes are made from a combination of anionic and cationic monomers, resulting in a polymer containing both charges on different repeat units. Polyzwitterions contain monomers where each repeat unit contains both a negative and positive charge. Many polyelectrolytes are synthesized with neutral comonomers, or block polymer structures containing polyelectrolytes covalently linked to neutral blocks. Many of these are also used in crosslinked materials to make hydrogels[40] and absorbent materials.[38]

The variable properties from the myriad possibilities in architecture are further complicated by the long-range attraction of charges. Two neutral molecules have little effect on each other unless they are in contact, and similarly two neutral polymer chains will not interact at a distance. A charge, however, creates an electric field that spans the area outside of immediately adjacent molecules. Every part of a polyelectrolyte system is interacting with every other part.[41] The complexity of polyelectrolyte systems therefore scales quickly, and their behavior is difficult to accurately predict in even simple systems.

One phenomenon commonly observed in polyelectrolyte systems is known as coacervation. If a polycation is added to an aqueous solution of a polyanion, the system will contain both positive and negative charges that attract each other. Even though both polyelectrolytes contain small molecule counterions, the counterions are entropically driven to free themselves from even a loose solvated binding to the larger polymer chain and move into solution. To do that, the polyanion comes together with the polycation to balance charges and release the small counterions. Since the polymers contain multiple charges per chain, they will tend to physically crosslink between each other and a crosslinked, polymer-rich phase will macrophase separate from the rest of the solution. This liquid-liquid phase separation is known as coacervation,[42] and its behavior has been studied extensively.[43]

Adding small molecule salts can disrupt the coacervation of two polyelectrolytes,[44] as can the presence of different small molecule counterions in solution.[45] Some coacervates are temperature sensitive and they can be affected by characteristics like the stereochemistry of the polymer backbone.[46] Even after extensive study, these systems are not completely understood.

1.8 Applications

Despite their complexity, polyelectrolytes have a wide variety of applications in modern technology. When a single polyelectrolyte is immobilized as a solid to prevent dissolution, the material will only swell when submerged in water. The swollen material can contain an extremely high charge density due to the proximity of charges along the polymer chain. With a sufficient amount of water to facilitate transport and a sufficiently

high charge density, the material becomes an ion-exchange material capable of passing large amounts of a single charge of ion. In an immobilized anionic material, cations will pass freely through the material, but neutral molecules and anions will be rejected. Similarly, a cationic material will only facilitate passage of anions.[47] These materials are useful for applications like electrochemical reference electrodes,[48] batteries, and purification technologies. **Appendix A** investigates the behavior of disordered polyelectrolyte materials under different amounts of swelling.

Charge mosaic membranes were hypothesized by Karl Sollner in the early 1950s.[49] These separation membranes consist of a mosaic of spatially separated positive and negative polyelectrolyte domains crossing the thickness of a membrane. The material allows cations to cross through the anionic domains and anions through the cationic domains (**Figure 1.7**). When a pressure is applied to saltwater on one side of the membrane, water will begin to flow through the swollen membrane. Because the ion density is so high, counterions within the polyelectrolyte will be carried through the membrane at a high concentration. The water that is pushed through the membrane comes out on the low-pressure side at a higher salt concentration than the original water feed, a process known as salt enrichment.

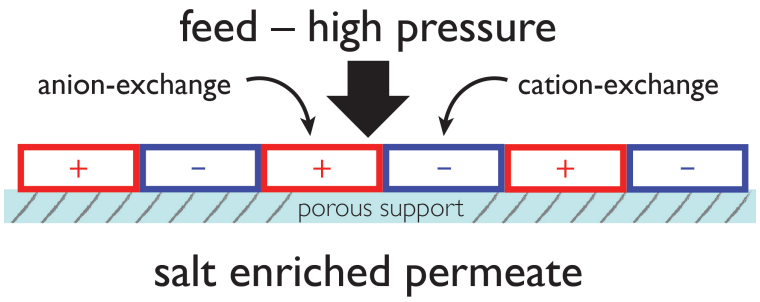

Figure 1.7. Schematic of a charge mosaic membrane containing spatially separated anion- and cation-exchange domains.

Because the anion flow and cation flow are spatially separated, an electric current is created between the separate domains.[50] The electrical current slows down the flow of ions, significantly decreasing the salt flux. The current connects the anionic and cationic domains and is therefore proportional to the distance between them. By decreasing the distance between the positive and negative domains, the flux of salt and therefore efficiency of the membrane will significantly increase. The salt flux (J_s) can be modeled by the equation:[51-53]

$$J_s = \frac{L_{12}(\Delta\mu_1 + V_1\Delta P) + L_{22}(\Delta\mu_2 + V_2\Delta P)}{1 + 2L_{22}\rho l}$$

where $\Delta\mu_1$ and $\Delta\mu_2$ are the chemical potentials of the water and salt, respectively; V_1 and V_2 are the partial volumes of the water and salt, respectively; ΔP is the pressure difference across the membrane; ρ is the electrical resistivity of the solution; l is the effective electrical current path length; and L_{ij} describes the phenomenological flux coefficients for the effect of the flow of the *j*th component on the flux of the *i*th component (such that $J_i = \sum F_j L_{ij}$ for all forces F_j).

The effective electrical current path length plays an important role in the total flux. For any filtration system, the flux coefficients are a constant value based on material properties. Similarly, the chemical potential, partial volumes, resistivity, and pressure difference will be dependent upon operational parameters including the chemical makeup of the incoming feed and the applied pressure for maximum efficiency. The path length, however, can be independently controlled by the geometry of the positive and negative

domains and a large path length can drive the salt flux to negligible levels, regardless of the other variables. For that reason, charge mosaic researchers have continually worked towards smaller feature sizes. The first examples of charge mosaic membranes were formed from separate anionic and cationic membranes submerged in the same saltwater.[50] Later efforts included macroscale arrangement of polyanions and polycations through processes like arranging millimeter scale beads in a square lattice pattern in a silicone supporting matrix.[54] To reach efficiency levels that are approaching a commercially viable system, however, the distance needs to reach a significantly smaller scale.[55]

Using block polymers to shrink the domains to small scales was investigated early in the charge mosaic literature. The first report was from Shell Development Company, where they attempted to use symmetric ABA triblock polymers that were cast onto porous supports and then functionalized.[56] Due to degradation of the microstructure (i.e., the morphology) on functionalization, no salt enrichment was observed. Distributing particulates of anion exchange material in a cation exchange film was equally unsuccessful. Only after lining up perforated films of polyanions and polycations was any salt enrichment observed. The only successful work in charge mosaic membranes occurred in the late 1980s, when a pentablock polymer was used to make a crosslinked lamellar film before functionalization to yield polyelectrolyte domains.[57] The technology was successfully commercialized but was only ever used for niche separation applications. The large domain sizes of the pentablock and significant loss of morphology during functionalization decreased the efficiency to well below the requirements for water desalination.[58]

Chapter 2 focuses on the next steps in block polymer charge mosaic membranes. Thin films of an ABC triblock polymer were assembled and subsequently functionalized in a single step to produce a dually charged material. The functionalization was performed with a mild reagent that preserved the block polymer morphology. **Chapter 3** expands on that work by applying the mild postpolymerization functionalization to a bicontinuous disordered system made through polymerization-induced microphase separation (PIMS). The PIMS strategy uses a controlled radical polymerization to form a block polymer off the end of a macroinitiator in a bulk monomer solution that contains a small amount of crosslinker. As the block polymer grows, the interaction between the blocks increases until the two polymers are driven to microphase separate. Before an equilibrium morphology is reached, as in the case with annealed block polymers, a bicontinuous morphology is kinetically trapped, forming a monolith with a percolating macroinitiator domain through the material. The work in **Chapter 3** successfully creates both positively and negatively charged PIMS monoliths, which are built upon in **Appendix A** by working towards a tricontinuous material incorporating both anionic and cationic domains. PIMS materials are further modified to control the swelling of individual polyelectrolyte domains in **Appendix B**.

1.9 References

[1] Sphere. The Sphere Handbook: Humanitarian Charter and Minimum Standards in Humanitarian Response (Fourth Edition). **2018**, 1–458.

[2] Food and agriculture organization of the United Nations. Coping with Water Scarcity : an Action Framework for Agriculture and Food Security. **2012**, 1–100.

[3] Yancheva, G.; Nowaczyk, N. R.; Mingram, J.; Dulski, P.; Schettler, G.; Negendank, J. F. W.; Liu, J.; Sigman, D. M.; Peterson, L. C.; Haug, G. H. Influence of the Intertropical Convergence Zone on the East Asian Monsoon. *Nature* **2007**, *445*, 74–77.

[4] Gleick, P. H. Water, Drought, Climate Change, and Conflict in Syria. *Weather, Climate, and Society* **2014**, *6*, 331–340.

[5] Sundar, V. J.; Ramesh, R.; Rao, P. S.; Saravanan, P.; Sridharnath, B.; Muralidharan, C. Water Management in Leather Industry. *Journal of Scientific Industrial Research* **2001**, *60*, 443–450.

[6] *Security of Industrial Water Supply and Management*; Atimtay, A. T., Sikdar, S. K., Eds.; 2011; pp 1–261.

[7] Minneapolis Flour Milling Boom. *Minnesota Historical Society*. https://www.mnhs.org/millcity/learn/history/flour-milling (accessed June 9, 2020).

[8] Dieter, C. A.; Maupin, M. A.; Caldwell, R. R.; Harris, M. A.; Ivahnenko, T. I.; Lovelace, J. K.; Barber, N. L.; Linsey, K. S. *Estimated Use of Water in the United States in 2015*; U.S. Department of the Interior and U.S. Geological Survey: Reston, Virginia, 2018; pp 1–76.

[9] Sadoff, C. W.; Hall, J. W.; Grey, D.; Aerts, J. C. J. H.; Ait-Kadi, M.; Brown, C.; Cox, A.; Dadson, S.; Garrick, D.; Kelman, J.; McCornick, P.; Ringler, C.; Rosegrant, M.; Whittington, D.; Wiberg, D. Securing Water, Sustaining Growth: Report of the GWP/OECD Task Force on Water Security and Sustainable Growth. **2015**, 1–171.

[10] The United Nations World Water Development Report 4. **2012**, *1-3*, 1–909.

[11] The United Nations World Water Development Report 2016: Water and Jobs; 2016. **2016**, 1–164.

[12] Elimelech, M.; Phillip, W. A. The Future of Seawater Desalination: Energy, Technology, and the Environment. *Science* **2011**, *333*, 712–717.

[13] Greenlee, L. F.; Lawler, D. F.; Freeman, B. D.; Marrot, B.; Moulin, P. Reverse Osmosis Desalination: Water Sources, Technology, and Today•S Challenges. *Water Research* **2009**, *43*, 2317–2348.

[14] Geise, G. M.; Paul, D. R.; Freeman, B. D. Fundamental Water and Salt Transport Properties of Polymeric Materials. *Progress in Polymer Science* **2014**, *39*, 1–42.

[15] Subramani, A.; Jacangelo, J. G. Emerging Desalination Technologies for Water Treatment: a Critical Review. *Water Research* **2015**, *75*, 164–187.

[16] Kershner, I. Aided by the Sea, Israel Overcomes an Old Foe: Drought. *New York Times*. May 30, 2015, p A1.

[17] Werber, J. R.; Deshmukh, A.; Elimelech, M. The Critical Need for Increased Selectivity, Not Increased Water Permeability, for Desalination Membranes. *Environ. Sci. Technol. Lett.* **2016**, *3*, 112–120.

[18] Einstein, A. Über Einen Die Erzeugung Und Verwandlung Des Lichtes Betreffenden Heuristischen Gesichttspunkt. *Annalen der Physik* **1905**, *322*, 132–148.

[19] Staudinger, H. Über Polymerisation. *Berichte der deutschen chemischen Gesellschaft A and B Series* **1920**, *53*, 1073–1085.

[20] Goodyear, C. Improvement in the Mode of Preparing Caoutchouc with Sulphur for the Manufacture of Various Articles. February 24, 1839.

[21] Parkes, A. Improvements in the Manufacture of Parkesine or Compound of Pyroxyline, and Also Solutions of Pyroxyline Known as Collodion. In *Patents for inventions*; 1857; pp 255–256.

[22] American Chemical Society National Historic Chemical Landmarks. Bakelite: the World's First Synthetic Plastic. *American Chemical Society*. http://www.acs.org/content/acs/en/education/whatischemistry/landmarks/bakelite.html (accessed June 9, 2020).

[23] Carothers, W. H.; Williams, I.; Collins, A. M.; Kirby, J. E. Acetylene Polymers and Their Derivatives. Ii. a New Synthetic Rubber: Chloroprene and Its Polymers. *Journal of the American Chemical Society* **1931**, *53*, 4203–4225.

[24] Wendt, P. The Control of Rubber in World War II. *Southern Economic Journal* **1947**, *13*, 203–227.

[25] Flory, P. J. Thermodynamics of High Polymer Solutions. *J. Chem. Phys.* **1941**, *9*, 660–660.

[26] Flory, P. J. Thermodynamics of High Polymer Solutions. *J. Chem. Phys.* **1942**, *10*, 51–61.

[27] Hiemenz, P. C.; Lodge, T. P. *Polymer Chemistry*, Second. CRC Press: New York, 2007; pp 1–598.

[28] Odian, G. *Principles of Polymerization*; John Wiley & Sons, Inc.: Hoboken, New Jersey, 2004; pp 1–839.

[29] He, Y.; He, W.; Wei, R.; Chen, Z.; Wang, X. Synthesizing Amphiphilic Block Copolymers Through Macromolecular Azo-Coupling Reaction. *Chem. Commun.* **2012**, *48*, 1036–1038.

[30] Mühlebach, A.; Gaynor, S. G.; Matyjaszewski, K. Synthesis of Amphiphilic Block Copolymers by Atom Transfer Radical Polymerization (ATRP). *Macromolecules* **1998**, *31*, 6046–6052.

[31] Bates, F. S.; Fredrickson, G. H. Block Copolymers—Designer Soft Materials. *Physics Today* **1999**, *52*, 32–38.

[32] Lee, S.; Bluemle, M. J.; Bates, F. S. Discovery of a Frank-Kasper Σ Phase in Sphere-Forming Block Copolymer Melts. *Science* **2010**, *330*, 349–353.

[33] Brunwin, D. M.; Fischer, E.; Henderson, J. F. Developments in Self-Reinforced Elastomers. *Journal of Polymer Science Part C* **1969**, *26*, 135–147.

[34] Kim, H.-C.; Park, S.-M.; Hinsberg, W. D. Block Copolymer Based Nanostructures: Materials, Processes, and Applications to Electronics. *Chem. Rev.* **2010**, *110*, 146–177.

[35] Yang, S. Y.; Ryu, I.; Kim, H. Y.; Kim, J. K.; Jang, S. K.; Russell, T. P. Nanoporous Membranes with Ultrahigh Selectivity and Flux for the Filtration of Viruses. *Adv. Mater.* **2006**, *18*, 709–712.

[36] Furia, T. E. *CRC Handbook of Food Additives*, Second Edition. CRC Press: Boca Raton, Florida, 1973; Vol. 1.

[37] Wan, A. C. A.; Yim, E. K. F.; Liao, I.-C.; Le Visage, C.; Leong, K. W. Encapsulation of Biologics in Self-Assembled Fibers as Biostructural Units for Tissue Engineering. *J. Biomed. Mater. Res.* **2004**, *71A*, 586–595.

[38] Graham, A. T.; Buchholz, F. L. *Modern Superabsorbent Polymer Technology*; Wiley-VCH: New York, 1998.

[39] Lowe, A. B.; McCormick, C. L. Synthesis and Solution Properties of Zwitterionic Polymers. *Chem. Rev.* **2002**, *102*, 4177–4190.

[40] Mondal, S.; Das, S.; Nandi, A. K. A Review on Recent Advances in Polymer and Peptide Hydrogels. *Soft Matter* **2020**, *16*, 1404–1454.

[41] Muthukumar, M. 50th Anniversary Perspective: a Perspective on Polyelectrolyte Solutions. *Macromolecules* **2017**, *50*, 9528–9560.

[42] Overbeek, J. T. G.; Voorn, M. J. Phase Separation in Polyelectrolyte Solutions. Theory of Complex Coacervation. *J. Cell. Comp. Physiol.* **1957**, *49*, 7–26.

[43] Sing, C. E.; Perry, S. L. Recent Progress in the Science of Complex Coacervation. *Soft Matter* **2020**, *16*, 2885–2914.

[44] Spruijt, E.; Sprakel, J.; Lemmers, M.; Stuart, M. A. C.; van der Gucht, J. Relaxation Dynamics at Different Time Scales in Electrostatic Complexes: Time-Salt Superposition. *Phys. Rev. Lett.* **2010**, *105*, 1426–4.

[45] Perry, S. L.; Li, Y.; Priftis, D.; Leon, L.; Tirrell, M. The Effect of Salt on the Complex Coacervation of Vinyl Polyelectrolytes. *Polymers* **2014**, *6*, 1756–1772.

[46] Perry, S. L.; Leon, L.; Hoffmann, K. Q.; Kade, M. J.; Priftis, D.; Black, K. A.; Wong, D.; Klein, R. A.; Pierce, C. F.; Margossian, K. O.; Whitmer, J. K.; Qin, J.; de Pablo, J. J.; Tirrell, M. Chirality-Selected Phase Behaviour in Ionic Polypeptide Complexes. *Nature Communications* **2019**, *6*, 6052-6059.

[47] Sollner, K.; Gregor, H. P. Membrane Equilibria Which Involve Only the Ions of Strong in Organic Electrolytes. *Journal of the American Chemical Society* **1945**, *67*, 346–346.

[48] Chopade, S. A.; Anderson, E. L.; Schmidt, P. W.; Lodge, T. P.; Hillmyer, M. A.; Bühlmann, P. Self-Supporting, Hydrophobic, Ionic Liquid-Based Reference Electrodes Prepared by Polymerization-Induced Microphase Separation. *ACS Sens.* **2017**, *2*, 1498–1504.

[49] Neihof, R.; Sollner, K. A Quantitative Electrochemical Theory of the Electrolyte Permeability of Mosaic Membranes Composed of Selectively Anion-Permeable and Selectively Cation-Permeable Parts and Its Experimental Verification. I. an Outline of the Theory and Its Quantitative Test in Model Systems with Auxiliary Electrodes. *J. Phys. Chem.* **1950**, *54*, 157–176.

[50] Neihof, R.; Sollner, K. A Quantitative Electrochemical Theory of the Electrolyte Permeability of Mosaic Membranes Composed of Selectively Anion-Permeable Parts, and Its Experimental Verification: II. a Quantitative Test of the Theory in Model Systems Which Do Not Involve the Use of Auxiliary Electrodes. *The Journal of General Physiology* **1955**, *38*, 613–622.

[51] Leitz, F. B.; Alexander, S. S.; Douglas, A. S. Research on Piezodialysis. *United States Department of the Interior* **1969**, 1–156.

[52] Leitz, F. B.; Alexander, S. S.; de Winter, D. M.; Plummer, C. W. Research on Piezodialysis : Second Report. *United States Department of the Interior* **1970**, 1–76.

[53] Leitz, F. B.; Sharr, J.; OMeara, J. W.; Gillam, W. S.; Johnson, S. Research on Piezodialysis: Third Report. *United States Department of the Interior* **1972**, 1–89.

[54] Weinstein, J. N.; Caplan, S. R. Charge-Mosaic Membranes: Enhanced Permeability and Negative Osmosis with a Symmetrical Salt. *Science* **1968**, *161*, 70–72.

[55] Bolto, B.; Hoang, M.; Tran, T. Review of Piezodialysis — Salt Removal with Charge Mosaic Membranes. *Desalination* **2010**, *254* (1-3), 1–5.

[56] Lopatin, G.; Newey, H. A. Ionic Block Copolymers as Piezodialysis Membranes. In *Reverse Osmosis Membrane Research*; Lonsdale, H. K., Podall, H. E., Eds.; Springer US: Boston, MA, 1972; pp 317–327.

[57] Hirahara, K.; Takahashi, S.-I.; Iwata, M.; Fujimoto, T.; Miyaki, Y. Artificial Membranes From Multiblock Copolymers. 5. Transport Behaviors of Organic and Inorganic Solutes Through a Charge-Mosaic Membrane. *Industrial Engineering Chemistry Research* **1986**, No. 25, 305–313.

[58] Isono, Y.; Ito, H.; Hirahara, K.; Fujimoto, T.; Miyaki, Y. Weak Acid-Strong Base Type Charge-Mosaic Membrane. I. Carboxylic Acid-Quaternary Amine System. *Journal of Membrane Science* **1989**, *43*, 205–216.

Chapter 2. Synthesis and Self-Assembly of Block Polyelectrolyte Membranes through a Mild, 2-in-1 Postpolymerization Treatment*

* The work in this chapter was completed in close collaboration with Dr. Eric Silver and Dr. Madalyn Radlauer in the Department of Chemistry at the University of Minnesota. Reprinted (adapted) with permission from Goldfeld, D. J.; Silver, E. S.; Radlauer, M. R.; Hillmyer, M. A. Synthesis and Self-Assembly of Block Polyelectrolyte Membranes through a Mild, 2-in-1 Postpolymerization Treatment. *ACS Applied Polym. Mater.* **2020**, *2*, 817–825.

2.1 Abstract

Block polymer systems containing spatially separated positive and negative charges are desirable for a number of applications, including biomedical devices, membrane separations, and coatings. Unfortunately, the tendency of positive and negative block polymers to charge cancel and form an insoluble coacervate precipitate leads to processing difficulties in the fabrication of charged thin films. We use postpolymerization modifications to simultaneously add both negative and positive charges to self-assembled neutral ABC triblock polymer thin films. Using reversible addition−fragmentation chain transfer polymerization, we synthesized triblock terpolymers consisting of poly(n-propyl styrene sulfonic ester), poly(4-chlorostyrene), and poly(vinylbenzyl chloride). The chemical functionalization of both charged blocks was accomplished simultaneously through exposure to gaseous trimethylamine in a single step at room temperature, simplifying the synthetic procedure and preserving the microstructure of the thin film. The quantitative functionalization was tracked through attenuated total reflectance infrared spectroscopy, and the thin film morphology was evaluated using intermodulation atomic force microscopy, transmission electron microscopy, and grazing-incidence small-angle X-ray scattering.

2.2 Introduction

Polyelectrolytes are polymers containing fixed charges along the length of the polymer chain.[1,2] Both polyanions and polycations are used for a variety of applications, including battery materials,[3] membrane separations,[4] and biomedical devices.[5] Due to their broad applicability, polyelectrolytes have been studied extensively in terms of their solution self-

assembly,[6] network formation and swelling behavior,[7,8] and interfacial phenomena.[9] More recent work includes studies on block polyelectrolytes, which are polymer chains with covalently linked, chemically distinct blocks of a polyelectrolyte segment connected to a neutral block in a variety of architectures, including A−B diblock polymers, A−B−A triblock polymers, and other multiblocks.[10−13]

A polyampholyte is a polyelectrolyte that contains both negative and positive charges on separate monomers within the polymer chain.[14,15] A subset of this polymer class is block polyampholytes, where blocks of polyanions are covalently attached to blocks of polycations. These have been investigated for their phase behavior in solution, including the formation of complex coacervates with additives like pharmaceuticals and genetic material leading to nanoparticle self-assembly.[10−13] Despite studies into the solution-state behavior of these systems, the solid-state assembly of block polyampholytes has been relatively unexplored.[16−18] Applications that would benefit from spatially separated positively and negatively charged polymer domains include antibiofouling coatings, separation membranes, and selective physical adsorption of anionic and cationic targets to surfaces.[3,19] For example, in wastewater treatment, a common issue when using reverse osmosis (RO) membranes is that as more water is filtered, the water remaining on the high-pressure side increases in concentration, leading to both higher incidences of scaling (buildup of salt precipitates on the membranes) and higher osmotic pressure resulting in increased pressure and energy requirements. A membrane capable of piezodialysis being incorporated periodically into the purification route would help to decrease the salt concentration in the water feed, thereby decreasing the energy needs of the water plant and

also decreasing scaling and thus extending the lifetimes of RO membranes. According to theory, smaller domain spacings lead to higher fluxes of salts through the membranes, improving energy efficiency. While previous systems have been fabricated with domain spacings on the micron scale, further reduction of the charged domains to the nanometer scale should lead to increased ion fluxes.[20–22] To achieve spatially separated nanoscale domains of opposite charge, we take advantage of block polymer self-assembly.[23,24] Self-assembled morphologies in thin films are an area of current interest,[24–27] and the behavior of block polyampholytes in thin films is largely unknown.

In the system described here, we separate the two charged blocks with a neutral spacer, so the films will maintain domains of a fixed positive charge separated from domains of a fixed negative charge, which we expect will display a number of distinctive behaviors compared to both zwitterionic systems (where a fixed positive and fixed negative charge are contained in a single monomer unit)[28] and polyelectrolyte complexes (which allow the fixed charges on different parts of the polymer chain to come together into a separate phase, releasing mobile ions into solution).[29,30]

Complex coacervation prevents the straightforward fabrication of self-assembled films containing spatially separated opposite charges. When a polyanion and polycation are in a solution together, the entropically driven release of counterions leads to a liquid−liquid macrophase separation into a phase rich in polymer and a supernatant rich in small molecule counterions.[21–34] These charge-canceled aggregates cannot segregate into separate domains as they form solid-state complexes, leading to a single domain of fixed positive and negative charges together, often as gels or solid precipitates.[7,35]

One possible way to self-assemble a microphase-separated structure of positive and negative charges in the solid state is to synthesize a neutral polymer that can later be functionalized to contain charges (**Figure 2.1a**). The neutral precursor polymer can be processed in common organic solvents, and self-assembly can be assisted using standard thin film practices, such as solvent vapor or thermal annealing (**Figure 2.1b**).[25] These systems can be characterized in the solid state using a variety of characterization techniques, including atomic force microscopy (AFM), transmission electron microscopy (TEM), grazing-incidence small-angle X-ray scattering (GISAXS), and attenuated total reflectance infrared (ATR-IR) spectroscopy.

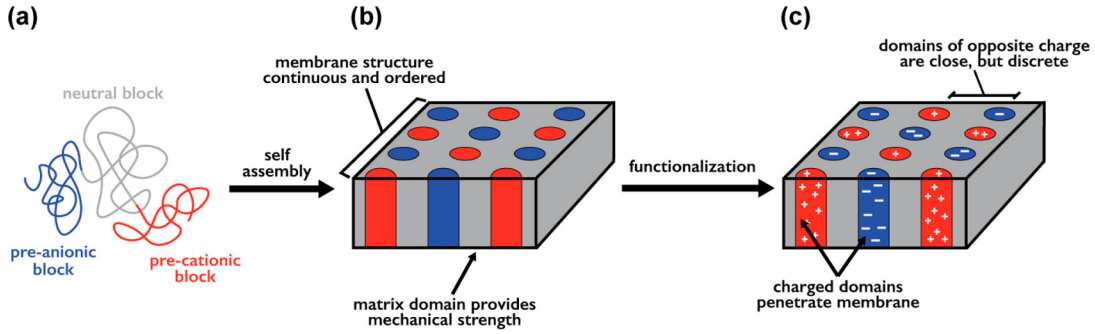

Figure 2.1. Schematic of (a) a neutral triblock polymer and subsequent self-assembly into (b) a thin film with cylinder-on-square lattice morphology. The thin film is then functionalized to yield (c) an ordered array of spatially separated positively and negatively charged domains.

After the neutral block polymer has assembled into a desired morphology, postpolymerization modification can be used to convert the domains to their respective charged species (**Figure 2.1c**). Such strategies have been demonstrated in the past for polymers in the solid state, but the modification strategies have typically used harsh reagents and conditions, for example exposure to pure sulfuric or chlorosulfonic acid at temperatures near or exceeding 100 °C.[16,17] These conditions are inefficient and can lead

to large defects in the solid-state structures of the polymers, characterized by substantial changes in the morphology from the softening of the polymers and undesired chemical degradation.[16–18] In addition, it is often difficult or impossible to show the extent of conversion to charged groups, and these reactions generally fall short of quantitative conversion. Our goal is to use a system that is easily functionalized under mild conditions and can be readily monitored to quantify conversion.

Once the polymer is functionalized in the solid state, the polyelectrolytes still suffer from a strong tendency to swell in the presence of water or high humidity.[16] The swelling allows the polyanion and polycation chains to move within the structure, which can lead to the loss of separation between the domains and the rearrangement of the morphology. To prevent this, we use a neutral, unreactive matrix B block in the center of an ABC triblock polymer system to contain the charged domains and keep them separated after functionalization to polyelectrolytes. Since the eventual applications often involve submersion of the membranes into water (where the charged polyelectrolytes are completely soluble), it is vital to have a glassy and hydrophobic support material with a glass transition temperature (T_g) much higher than room temperature to hold the membrane together and separate the positive and negative domains while they swell under osmotic pressure. One possible idealized morphology would be a cylinder-on-square lattice morphology,[36–38] which has a neutral B block separating alternating cylinders of the A and C charged blocks, consisting of first a polyanion domain, then a spacer, and then a polycation domain. The neutral B block needs to be chemically stable under the conditions

of functionalization (mildly acidic/basic conditions). It is also advantageous for the support block to be processable in common solvents.

There are several commercially available derivatives of styrene that are negatively and positively charged like styrenesulfonate, 4-vinylbenzoic acid, and N,N,N-trimethyl-4-vinylanilium chloride. There are similarly a wide variety of substituted styrenes that are inert to many chemical transformations, including 4-methylstyrene, 4-tert-butylstyrene, and 4-chlorostyrene. Most of these styrene derivatives can be used to make polymers that are glassy at room temperature, and many of them are well studied and readily available.[39–41] The ideal system will have three blocks that are processable in similar solvents and have similar surface energies to simplify thin film self-assembly into the desired perpendicularly oriented morphologies. We achieved this by using a styrene backbone through all three blocks of the ABC triblock polymer with covalently attached masked functional groups that are converted to anions and cations after polymerization. Herein, we detail the synthesis, solid-state conversion to polyanions and polycations, and self-assembly properties of a series of diblock and triblock polymers (**Scheme 2.1**).

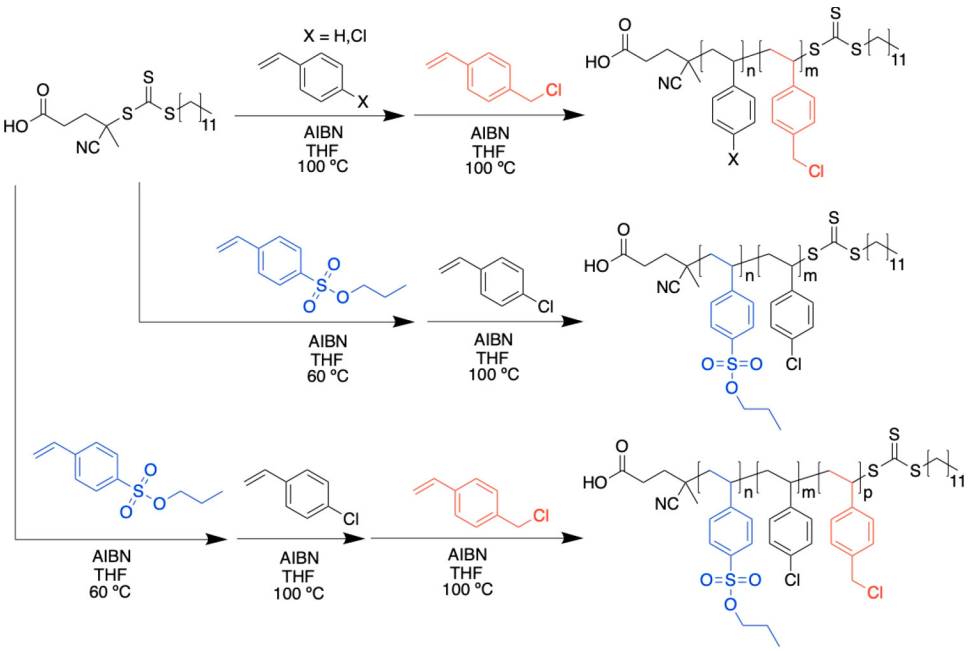

Scheme 2.1. Synthesis of Diblock and Triblock Polymers Using RAFT Polymerization to Yield AB, BC, and ABC Block Polymers Containing PSSE, PS, P4ClS, and PVBC

2.3 Experimental

2.3.1 Materials

Unless otherwise noted, all chemicals were purchased from Sigma Aldrich and used as received. Styrene (99%) was distilled after drying over calcium hydride. Azobisisobutyronitrile (AIBN) (98%) was recrystallized from methanol and dried under reduced pressure. Vinylbenzyl chloride (90%) and 4-chlorostyrene (98%) were run through a plug of basic alumina to remove inhibitors. N-Propyl styrene sulfonate was synthesized according to literature procedures starting from sodium styrene sulfate.[42–43] The chain transfer agent (4-Cyano-4-[(dodecylsulfanylthiocarbonyl)sulfanyl]pentanoic acid; CTA) was synthesized according to previous literature procedures.[44]

2.3.2 Instrumentation

NMR spectra were recorded on a Bruker Advance III HD 500 spectrometer. Chemical shifts are reported in δ units, expressed in ppm downfield from tetramethylsilane using residual protiosolvent as an internal standard ($CDCl_3$, ^1H: 7.26 ppm). Size exclusion chromatography (SEC) was performed in THF (25 °C, 1 mL/min) on an Agilent Infinity 1260 HPLC system equipped with three Waters Styragel HR columns, a Wyatt DAWN HELEOS-II 18-angle laser light scattering detector, and a Wyatt Optilab T-rEX differential refractive index detector. Absolute weight-average molar mass was determined using light scattering detector with a dn/dc = 0.171 mL g^{-1} for PVBC, 0.1249 mL g^{-1} for PSSE, and 0.185 mL g^{-1} for PS and P4ClS. Thermal gravimetric analysis (TGA) was performed on a TA Instruments Q500 under house nitrogen at a heating rate of 10 °C min^{-1}. Differential scanning calorimetry (DSC) analyses were performed on a TA Instruments Discovery DSC using standard aluminum T-zero pans with hermetic lids. Scans were conducted under house nitrogen at a heating or cooling rate of 10 °C min^{-1}. Infrared spectroscopy measurements were performed on a Bruker Alpha Platinum ATR spectrometer and a Thermo Scientific Nicolet iS50 FT-IR spectrometer with a built-in diamond attenuated total reflection set up and a DLaTGS detector. Transmission electron microscopy (TEM) measurements were performed on a FEI Tecnai G2 Spirit BioTWIN instrument with a LaB6 gun and an accelerating voltage of 120 kV in bright-field mode. TEM sample preparation is detailed below in polymer thin film preparation. Transmission small angle X-ray scattering (SAXS) measurements were performed on a SAXSLab GANESHA300XL instrument of the Characterization Facility at the University of

Minnesota. Cu Kα X-rays (λ = 1.54 Å) generated by a Xenocs Geni3DX source were collimated through 2 sets of 4-bladed slits (JJ X-ray, A/S). 2D-SAXS patterns were acquired using a Dectris EIGER R 1M detector (7.72 cm x 7.99 cm rectangular area) with 1030 x 1065 pixels (75 μm x 75 μm pixel size) at a sample-to-detector distance of 46.8 cm. Samples were sealed in an ambient temperature holder with Kapton tape windows. All 2D-SAXS pattern were azimuthally-integrated to obtain one-dimensional scattered intensity I(q) versus q plots. Grazing-incidence small-angle X-ray scattering (GISAXS) Data was collected at the 8-ID-E beamline of the Advanced Photon Source at Argonne National Laboratory. An X-ray wavelength of 10.915 keV = 1.14 Å was used to irradiate the sample and the scattering intensity distribution was capture by a Pilatus 1M detector at an incident angle of 0.14°. The intensities (I) are plotted with respect to q, where $q = (4\pi/\lambda) \sin(\theta/2)$, λ is the wavelength of the incident X-ray beam and θ is the scattering angle. Reactive ion etching was performed on a Vision 320 AV Etcher using O_2 plasma at a 50 sccm flow rate and a pressure of 50 mTorr for 15 s at the MN Nano Center. Ellipsometry of thin films was performed on a J. A. Wollam Co., Inc. V-VASE using measurements at 3 angles and a Cauchy model for the polymer films. Atomic force microscopy measurements were performed on a Bruker Nanoscope V Multimode 8 with a Multifrequency Lockin Amplifier (MLA)™ attachment from Intermodulation Products.

2.3.3 Synthesis of poly(*n*-propyl styrene sulfonic ester) (PSSE)

An oven-dried Schlenk flask was fitted with a Teflon stopcock and flame dried three times, backfilling with argon (g) after each cycle. The flask was then placed under an atmosphere of argon (g) and charged with *n*-propyl styrene sulfonate (SSE) monomer

(3.4997 g, 15.5 mmol, 187 equiv.), 4-cyano-4-[(dodecylsulfanylthiocarbonyl)sulfanyl]-pentanoic acid (CTA) (0.0337 g, 0.083 mmol, 1 equiv.), and AIBN (0.0046 g, 0.028 mmol, 0.3 equiv.), and dissolved in dry THF (10 mL). The reaction was then put through three cycles of freeze-pump-thaw, after which the reaction flask was backfilled with 5 psig of argon (*g*) and sealed. The flask was placed in a preheated oil bath (60 °C) and stirred for five days. The reaction was stopped by submerging the reaction flask in a N_2 (*l*) bath for 1 min, and then warming to room temperature. Subsequently, the solution mixture was precipitated in methanol and filtered through a 0.2 μm pore PVDF membrane, and the isolated solid was dried under vacuum to yield PSSE as a white solid (2.947 g, 84% isolated yield, $M_{n,NMR}$ = 59 kg mol^{-1}, $M_{n,SEC}$ = 47 kg mol^{-1}, $M_{w,SEC}$ = 53 kg mol^{-1}, $Đ$ = 1.11) ^{1}H NMR (500 MHz, $CDCl_3$): δ 0.91 (899H, s, -CH_3), 1.62 (1550H, m, -CH_2-), 2.46 (81H, br s,), 2.71 (88H, br s,), 3.25 (2H, br s, -S-CH_2-), 4.07 (569H, br s, O-CH_2-), 6.74 (558H, br s, Ar-H), 7.70 (604H, br s, Ar-H).

2.3.4 Synthesis of polystyrene macroinitiator (PS)

An oven-dried Schlenk flask was fitted with a Teflon stopcock and flame dried three times, backfilling with 5 psi of argon (*g*) after each cycle. The flask was then placed under an atmosphere of argon (*g*) and charged with styrene monomer (5 mL, 4.53 g, 43.5 mmol, 3360 equiv.), CTA (0.0052 g, 0.013 mmol, 1 equiv.) and a 5 mL solution of AIBN (0.00065 g, 0.0038 mmol, 0.3 equiv.) in THF. The reaction was then degassed through three cycles of freeze-pump-thaw. After the last thawing, the flask was backfilled with 5 psig of argon (*g*) and sealed. The flask was placed in a preheated oil bath (100 °C) and stirred for 19 h. The reaction was stopped by submerging the flask in a N_2 (*l*) bath for

1 min and then warming to room temperature. The polymer was precipitated in methanol and then filtered through 0.2 μm pore PVDF membrane and the solid was dried under vacuum to yield PS as a white solid (1.138 g, 25% isolated yield, $M_{n,NMR}$ = 74 kg mol^{-1}, $M_{n,SEC}$ = 80 kg mol^{-1}, $M_{w,SEC}$ = 93 kg mol^{-1}, $Đ$ = 1.17) ^{1}H NMR (500 MHz, $CDCl_3$): δ 0.90 (4.46H, t, -CH_3), 1.45 (464H, multiplet, -CH_2- and -CH- backbone), 3.25 (2H, m, S-CH_2-), 6.59 (707H, m, Ar-H).

2.3.5 Synthesis of poly(vinylbenzyl chloride) (PVBC)

An oven-dried Schlenk flask was fitted with a Teflon stopcock and flame dried three times, backfilling with 5 psig of argon (*g*) after each cycle. The flask was then placed under an atmosphere of argon (*g*) and charged with vinylbenzyl chloride monomer (1 mL, 1.08 g, 7.10 mmol, 100 equiv.), CTA (0.0286 g, 0.0710 mmol, 1 equiv.), and AIBN (0.0023 g, 0.014 mmol, 0.2 equiv.). The reaction was then degassed through three cycles of freeze-pump-thaw. After the last thawing, the flask was backfilled with 5 psig of argon (*g*) and sealed. The flask was placed in a preheated oil bath (70 °C) and stirred for 8 h. The reaction was stopped by submerging the flask in a N_2 (*l*) bath for 1 min and then warming to room temperature. The polymer was precipitated in methanol and then filtered through 0.2 μm pore PVDF membrane and the solid was dried under vacuum to yield PVBC as a pale yellow solid (0.473 g, 44% isolated yield, $M_{n,NMR}$ = 9 kg mol^{-1}, $M_{n,SEC}$ = 14 kg mol^{-1}, $M_{w,SEC}$ = 15 kg mol^{-1}, $Đ$ = 1.06) ^{1}H NMR (500 MHz, $CDCl_3$): δ 0.89 (4.6H, t, -CH_3), 1.40 (197H, m, -CH_2-, -CH-), 3.25 (2H, m, -S-CH_2-), 4.52 (113H, br s, -CH_2-Cl), 6.49 (227H, m, Ar-H).

2.3.6 Synthesis of poly(4-chlorostyrene) macroinitiator (P4ClS)

An oven-dried Schlenk flask was fitted with a Teflon stopcock and flame dried three times, backfilling with 5 psig of argon (*g*) after each cycle. The flask was then placed under an atmosphere of argon (*g*) and charged with 4-chlorostyrene (2 mL, 2.31 g, 16.67 mmol, 3600 equiv.), CTA (0.0018 g, 0.0046 mmol, 1 equiv.) and AIBN (0.0002 g, 0.0013 mmol, 0.3 equiv.). The reaction was then degassed through three cycles of freeze-pump-thaw. After the last thawing, the flask was backfilled with 5 psig of argon (*g*) and sealed. The flask was placed in a preheated oil bath (120 °C) and stirred for 3 h. The reaction was stopped by submerging the flask in a N_2 (*l*) bath for 1 min and then warming to room temperature. The polymer was precipitated in methanol and then filtered through a 0.2 µm pore PVDF membrane and the solid was dried under vacuum to yield P4ClS as a white solid (0.919 g, 40% isolated yield, $M_{n,NMR}$ = 92 kg mol^{-1}, $M_{n,SEC}$ = 97 kg mol^{-1}, $M_{w,SEC}$ = 137 kg mol^{-1}, $Đ$ = 1.41) ^{1}H NMR (500 MHz, $CDCl_3$): δ 0.88 (2H, t, -CH_3), 1.32 (2121H, m, -CH_2- and -CH-backbone), 3.74 (2H, m, -S-CH_2-), 6.40 (2654H, m, Ar-H).

2.3.7 Synthesis of poly(*n*-propyl styrene sulfonate ester)-*block*-poly(4-chlorostyrene) (PSSE–P4ClS)

An oven-dried Schlenk flask was fitted with a Teflon stopcock and flame dried three times, backfilling with 5 psig of argon (*g*) after each cycle. The flask was then placed under an atmosphere of argon (*g*) and charged with PSSE macroinitiator (0.0997 g, 0.0016 mmol, 1 equiv.), 4-chlorostyrene (1 mL, 1.155 g, 8.33 mmol, 5208 equiv.), and a 1 mL solution of AIBN (0.00009 g, 0.00048 mmol, 0.3 equiv.) in THF. The reaction was then degassed through three cycles of freeze-pump-thaw. After the last thawing, the flask

was backfilled with 5 psig of argon (*g*) and sealed. The flask was placed in a preheated oil bath (100 °C) and stirred for 4 h. The reaction was stopped by submerging the flask in a N_2 (*l*) bath for 1 min and then warming to room temperature. The polymer was precipitated in methanol and then filtered through 0.2 μm pore PVDF membrane and the solid was dried under vacuum to yield PSSE-*b*-P4ClS as a white solid (0.324 g, 26% isolated yield, $M_{n,NMR}$ = 225 kg mol^{-1}, $M_{n,SEC}$ = 113 kg mol^{-1}, $M_{w,SEC}$ = 130 kg mol^{-1}, $Đ$ = 1.15) ^{1}H NMR (500 MHz, $CDCl_3$): δ 0.91 (3H, br s, -CH_3), 1.32 (25H, m, -CH_2- and -CH-backbone), 4.08 (2H, br s, -O-CH_2-), 6.40 (26H, m, Ar-H), 7.67 (2H, m, Ar-H).

2.3.8 Synthesis of poly(styrene)-block-poly(vinylbenzyl chloride) (PS-PVBC)

An oven-dried Schlenk flask was fitted with a Teflon stopcock and flame dried three times, backfilling with 5 psig of argon (*g*) after each cycle. The flask was then placed under an atmosphere of argon (*g*) and charged with PS macroinitiator (0.100 g, 0.0065 mmol, 1 equiv.), vinylbenzyl chloride (0.92 mL, 1 g, 6.55 mmol, 1016 equiv.), and a 1 mL solution of AIBN (0.00053 g, 0.0033 mmol, 0.5 equiv.) in THF. The reaction was then degassed through three cycles of freeze-pump-thaw. After the last thawing, the flask was backfilled with 5 psig of argon (*g*) and sealed. The flask was placed in a preheated oil bath (100 °C) and stirred for 3 h. The reaction was stopped by submerging the flask in a N_2 (*l*) bath for 1 min and then warming to room temperature. The polymer was precipitated in hexanes and then filtered through 0.2 μm pore PVDF membrane and the solid was dried under vacuum to yield PS-*b*-PVBC as a white solid (0.220 g, 20% isolated yield, $M_{n,NMR}$

= 36 kg mol^{-1}, $M_{n,SEC}$ = 17 kg mol^{-1}, $M_{w,SEC}$ = 22 kg mol^{-1}, $Đ$ = 1.32) ^{1}H NMR (500 MHz, $CDCl_3$): δ 0.86 (0.1H, t, -CH_3), 1.43 (7H, m, -CH_2- and -CH-backbone), 4.51 (2H, br s, -CH_2-Cl), 6.49 (9H, m, Ar-H).

2.3.9 Synthesis of poly(4-chlorostyrene)-*block*-poly(vinylbenzyl chloride) (P4ClS-PVBC)

An oven-dried Schlenk flask was fitted with a Teflon stopcock and flame dried three times, backfilling with 5 psig of argon (*g*) after each cycle. The flask was then placed under an atmosphere of argon (*g*) and charged with P4ClS macroinitiator (0.0993 g, 0.0010 mmol, 1 equiv.), vinylbenzyl chloride (0.06 mL, 0.065 g, 0.40 mmol, 393 equiv.), and a 1 mL solution of AIBN (0.00007 g, 0.00043 mmol, 0.4 equiv.) in THF. The reaction was then degassed through three cycles of freeze-pump-thaw. After the last thawing, the flask was backfilled with 5 psig of argon (*g*) and sealed. The flask was placed in a preheated oil bath (100 °C) and stirred for 4 h. The reaction was stopped by submerging the flask in a N_2 (*l*) bath for 1 min and then warming to room temperature. The polymer was precipitated in methanol and then filtered through 0.2 μm pore PVDF membrane and the solid was dried under vacuum to yield P4ClS-*b*-PVBC as a white solid (0.086 g, 52% isolated yield, $M_{n,NMR}$ = 114 kg mol^{-1}, $M_{n,SEC}$ = 76 kg mol^{-1}, $M_{w,SEC}$ = 141 kg mol^{-1}, $Đ$ = 1.87) ^{1}H NMR (500 MHz, $CDCl_3$): δ 0.88 (0.2H, t, -CH_3), 1.32 (26H, m, -CH_2- and -CH-backbone), 4.50 (2H, br s, -CH_2-Cl), 6.40 (30H, m, Ar-H).

2.3.10 Synthesis of poly(*n*-propyl styrene sulfonate ester)-*block*-poly(4-chlorostyrene)-*block*-poly(vinylbenzyl chloride) (PSSE-P4ClS-PVBC)

An oven-dried Schlenk flask was fitted with a Teflon stopcock and flame dried three times, backfilling with 5 psig of argon (*g*) after each cycle. The flask was then placed under an atmosphere of argon (*g*) and charged with PSSE-*b*-P4ClS macroinitiator (0.1004 g, 0.0014 mmol, 1 equiv.), vinylbenzyl chloride (0.25 mL, 0.27 g, 1.8 mmol, 1267 equiv.), and a 1 mL solution of AIBN (0.00008 g, 0.0004 mmol, 0.3 equiv.) in THF. The reaction was then degassed through three cycles of freeze-pump-thaw. After the last thawing, the flask was backfilled with 5 psig of argon (*g*) and sealed. The flask was placed in a preheated oil bath (100 °C) and stirred for 1 h. The reaction was stopped by submerging the flask in a N_2 (*l*) bath for 1 min and then warming to room temperature. The polymer was precipitated in methanol and then filtered through 0.2 μm pore PVDF membrane and the solid was dried under vacuum to yield PSSE-*b*-P4ClS-*b*-PVBC as a white solid (0.088 g, 24% isolated yield, $M_{n,NMR}$ = 78 kg mol^{-1}, $M_{n,SEC}$ = 27 kg mol^{-1}, $M_{w,SEC}$ = 31 kg mol^{-1}, $Đ$ = 1.10) ^{1}H NMR (500 MHz, $CDCl_3$): δ 0.91 (3H, br s, -CH_3), 1.32 (18H, m, -CH_2- and -CH- backbone). 4.07 (2H, br s, -O-CH_2- from SSE monomer), 4.54 (0.7H, br s, -CH_2-Cl from VBC monomer), 6.40 (15H, m, Ar-H), 7.70 (2H, m, Ar-H).

2.3.11 Thin Film Preparation

Thin films of block polymers were spin coated on bare silicon wafers cut to 2 cm x 2 cm squares which were then cut into 1 cm x 1 cm squares after spin coating for the various measurements. In the case of AFM and GISAXS samples, the polymer of interest was dissolved to a concentration of 2 wt% in chlorobenzene. The wafers were first cleaned by

adding chlorobenzene to the wafer and spinning at 2000 rpm for 60 s with a ramp rate of 2000 rpm/s. The polymer solution was then spin coated onto the wafer spinning at 2000 rpm for 60 s with a ramp rate of 2000 rpm/s. The film thickness was then determined by ellipsometry measurements, as detailed in the Instrumentation section above. In the case of ATR-IR samples, the polymer of interest was dissolved to a concentration of 10 wt% in chlorobenzene. The wafers were first cleaned by adding chlorobenzene to the wafer and spinning at 1500 rpm for 60 s with a ramp rate of 1500 rpm/s. The polymer solution was then spin coated onto the wafer spinning at 1500 rpm for 60 s with a ramp rate of 2000 rpm/s. The film thickness was then determined by ellipsometry measurements at 3 angles and then fitting to a two-layer model, Layer 1 being a native silicon oxide substrate and Layer 2 being a Cauchy fit. The thin films were annealed in a homemade solvent vapor annealing chamber composed of all metal parts with two flow-controlled inlet valves, one for flowing dry N_2 (*g*) to purge the sample chamber and one to flow dry N_2 (*g*) through a solvent well of chlorobenzene to bubble solvent vapor into the sample chamber. The thin films were annealed for 4 min to a 50% swelling in thickness (monitored by an interferometer), followed by rapid flushing of the chamber with N_2 (*g*), approximately 1 s. Details on the construction of this solvent vapor annealing chamber and a schematic for the vapor and gas inlets can be found in our previous work by Baruth, et al.[45] For TEM samples, the same recipe was followed for the AFM and GISAXS samples, but instead of spin coating onto bare silicon, the polymer solutions were spin coated onto silicon wafers coated in LOR3A lift-off resist (400 nm thick). The polymer coated wafers were then solvent vapor annealed, as detailed above, and subsequently developed in 2.5 wt% aqueous

tetramethylammonium hydroxide solutions and the free films were floated onto TEM grids. The polymer films on TEM grids were then exposed to trimethylamine vapor in a sealed glass chamber for 1 hr and then allowed to air out for 24 h. The functionalized films were then exposed to 0.1 wt% aqueous solution of phosphotungstic acid for 10 min, and then washed with deionized water to remove excess salts and dried under ambient conditions overnight.

2.3.12 Intermodulation Atomic Force Microscopy

Intermodulation atomic force microscopy is a technique developed at the Section of Nanostructure Physics at the Royal Institute of Technology (KTH) in Stockholm, Sweden.[46–47] The technique is an enhanced form of normal AFM tapping mode that uses multiple frequencies to record small variations in the mechanical and surface properties of the substrate.

The technique relies on exact determination of the resonant frequency, determined by ambient vibrations caused by air flow around the undriven tip. The tip is then driven at both the resonant frequency and the first harmonic mode at the same time. These two drive frequencies cause constructive and destructive interference that form integer linear combinations of the drive frequencies, in our case forming a beat. The AFM scan is then calibrated so that each pixel in the image is recorded on a single beat.

The phase scan of the image is recorded at both drive frequencies as well as the linear combinations at higher harmonics. This allows for analysis at upwards of 20 distinct frequencies, each one with a slightly different amount of contrast highlighting small and large differences in the collected data. By comparing the data at a variety of frequencies, it

is straightforward to identify artifacts as well as distinguish minute differences in the surface that may only be visible at higher or lower frequency modes.

Each beat also produces a force and dissipation curve, similar to a force curve that can be viewed in a normal AFM in tapping mode. In contrast to standard AFM, intermodulation AFM records the force and dissipation curves at every pixel. The force curves can later be analyzed either pixel by pixel, or by averaging over a region, for instance a region with a high phase to contrast with a region with a low phase.

When we compare two sets of curves, we can clearly distinguish a soft, dissipative region from a hard, glassy region in a polymer substrate. Even with small differences beneath the surface, intermodulation has the ability to carefully assess each pixel and region and determine its aggregate mechanical and surface interaction properties. This allows us to confirm that differences we see in phase are, in fact, different polymer domains and are not artifacts of the instrumentation.

2.4 Results and Discussion

2.4.1 Pre-Cationic Block

Our target for the positively charged C block of the ABC polymer is an initially neutral polymer that can be functionalized postpolymerization to carry a permanent positive charge. One of the most commonly used polymers for this purpose is poly(vinylbenzyl chloride) (PVBC). Vinylbenzyl chloride (VBC) is a commercially available styrene derivative that contains a benzyl chloride functional group that is stable under radical polymerization conditions and can be functionalized with a variety of nucleophiles after polymerization. The most common functionalization is exposure of the

PVBC to an amine.[48] Using a protected primary amine yields a pH-sensitive polycationic block,[49] and using a trialkylamine yields a poly(vinylbenzyl trialkylammonium chloride) (PVBAC) with positive fixed charges installed at every repeat unit.[50] PVBAC has been studied in a variety of applications,[51] including anion exchange membranes and gene delivery.[50,52] In addition, PVBC is ideal for our system since it is a stable, neutral polymer that is glassy at room temperature ($T_g \sim 108$ °C)[53,54] and soluble in a wide range of organic solvents. It can be polymerized in a controlled manner through radical addition−fragmentation chain transfer (RAFT) polymerization[55] techniques and adds easily onto styrenic macroinitiators to form block polymers with well-defined molar masses and low dispersities.[56]

PVBC is commonly copolymerized with styrene to form both statistical copolymers, i.e., the well-known Merrifield resins,[57] and to form block polymers of poly(styrene)-*b*-poly(vinylbenzyl chloride) or poly(vinylbenzyl chloride)-*b*-poly(styrene).[58−60] However, these polymers are typically converted to the charged ammonium state immediately after synthesis for the solution-state self-assembly of amphiphiles or solid-state ion-conductive membranes. As a result, the only evidence of the solid-state morphology of poly(styrene)-*b*-poly(vinylbenzyl chloride) in literature is a differential scanning calorimetry (DSC) study showing a merged T_g for a single sample without further investigating the effects of the molar mass or volume fraction on the diblock behavior.[53] We first investigated the solid-state self-assembly behavior of this diblock before incorporation into our target triblock polymers.

We initially synthesized a homopolymer of polystyrene through RAFT polymerization using a commercially available chain transfer agent (4-cyano-4-[(dodecylsulfanylthiocarbonyl)-sulfanyl]pentanoic acid; CTA) and azobis-(isobutyronitrile) (AIBN) as a radical thermal initiator. The initial block was then chain extended by growing a block of PVBC from the PS macroinitiator to yield PS_{140}-*b*-$PVBC_{140}$ (subscripts indicate the average degree of polymerization) with a molar mass (M_n) = 36 kg mol^{-1} and dispersity ($Đ$) = 1.32 (**Figure 2.2** and **Figure 2.3**; polymer sample data are summarized in **Table 2.1**). The isolated diblock was then evaluated for efficiency in converting the benzyl chloride functional group to a trimethylammonium group through exposure to trimethylamine (TMA) (**Scheme 2.2**). PVBC homopolymer could be functionalized by suspending it in a 45% by weight solution of TMA in water, where after functionalization to the charged state, the polymer dissolved. After isolating the PVBAC, Fourier-transform infrared spectroscopy (FTIR) showed the disappearance of the C−Cl wag and the emergence of the C−N stretch (**Figure 2.4**). Thin films (30−60 nm) of the diblock PS_{140}-*b*-$PVBC_{140}$ were then spin coated from chlorobenzene onto silicon wafers and then converted to PS_{140}-*b*-$PVBAC_{140}$ by exposure to TMA vapor in a sealed glass chamber. Similarly, the IR band for the C−Cl wag at 1266 cm^{-1} disappeared, and the new C−N stretch at 1220 cm^{-1} appeared after 1 h of exposure (**Figure 2.5**).

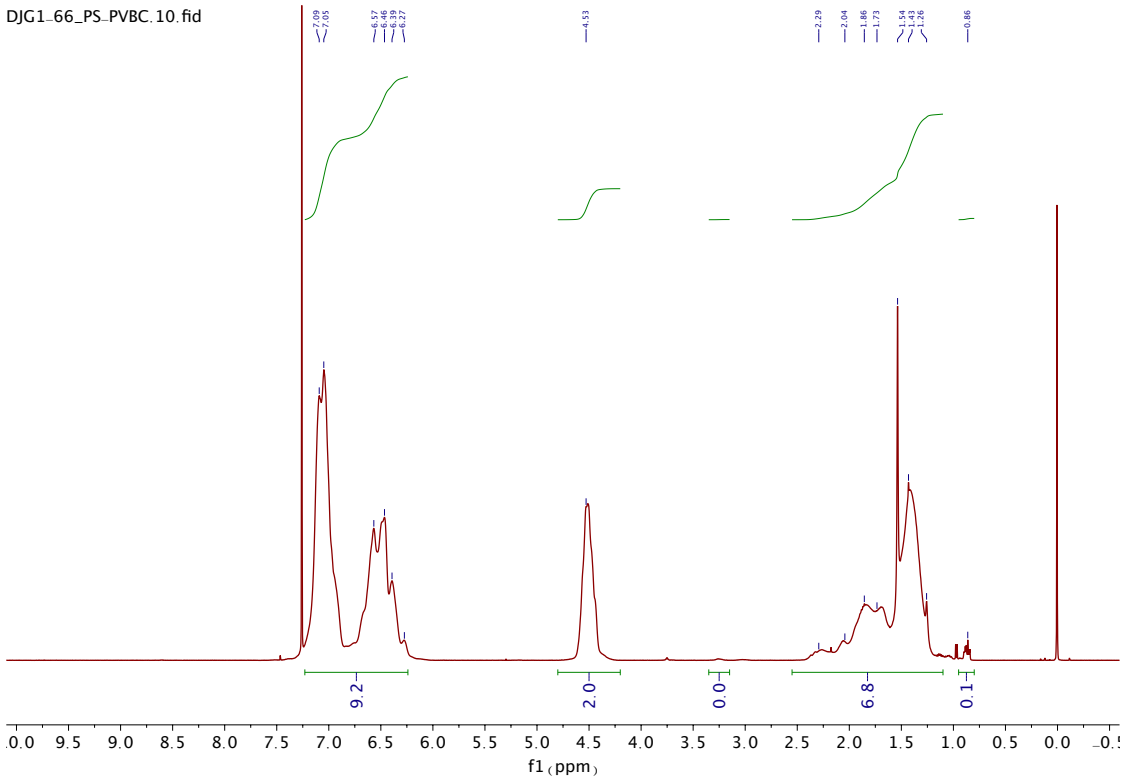

Figure 2.2. ^{1}H NMR spectrum of PS_{140}-*b*-$PVBC_{140}$

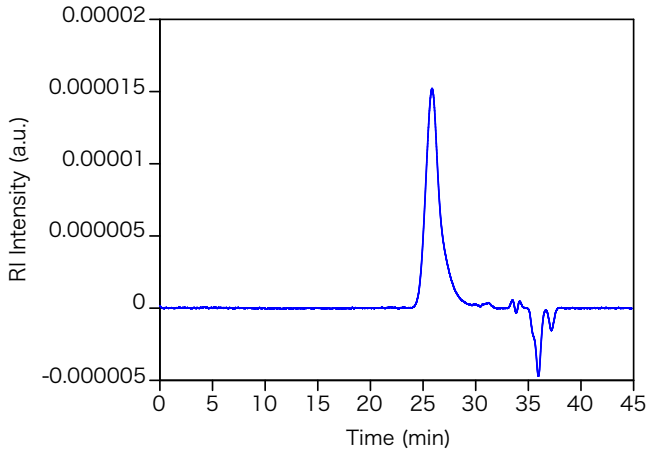

Figure 2.3. THF SEC chromatogram of PS_{140}-*b*-$PVBC_{140}$

Polymer	$M_{n,NMR}$ (kg mol^{-1})	$M_{n,SEC}$ (kg mol^{-1})	$M_{w,SEC}$ (kg mol^{-1})	$Đ$
$PSSE_{110}$	25	25	26	1.06
$PSSE_{260}$	59	47	53	1.11
PS_{140}	15	15	16	1.03
PS_{710}	74	80	93	1.17
PS_{1290}	134	70	89	1.27
$PVBC_{56}$	9	14	15	1.06
$PVBC_{301}$	163	46	66	1.44
$P4ClS_{700}$	92	97	137	1.41
$PSSE_{260}$-$P4ClS_{1585}$	278	113	130	1.15
$PSSE_{110}$-$P4ClS_{305}$	67	31	34	1.12
$PSSE_{260}$-$P4ClS_{565}$	137	30	55	1.81
PS_{140}-$PVBC_{140}$	36	17	22	1.32
PS_{710}-$PVBC_{400}$	135	81	134	1.66
PS_{1290}-$PVBC_{650}$	232	72	121	1.69
$P4ClS_{700}$-$PVBC_{110}$	114	76	141	1.87
$PSSE_{110}$-$P4ClS_{305}$-$PVBC_{70}$	78	27	31	1.10
$PSSE_{260}$-$P4ClS_{565}$-$PVBC_{140}$	158	44	53	1.19

Table 2.1. Polymer samples and their molar masses by ^{1}H NMR spectroscopy and THF SEC with light scattering

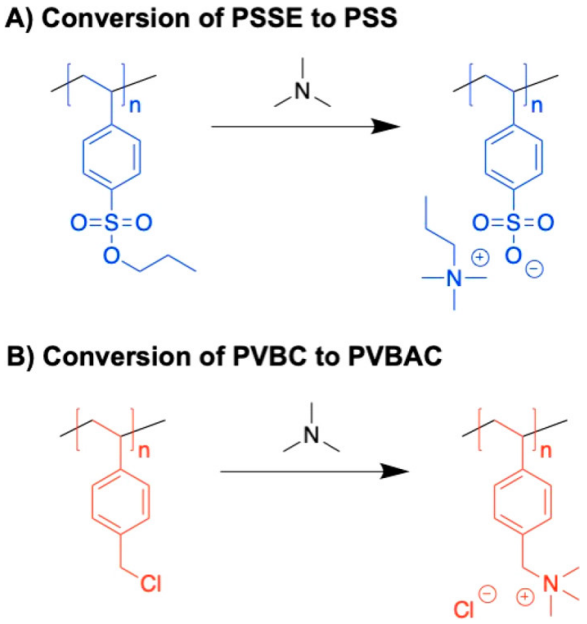

Scheme 2.2. Conversion of the Neutral Homopolymers to Their Ionic Counterparts: (A) Poly(n-propyl styrene sulfonic ester) (PSSE) is exposed to trimethylamine, and the propyl group undergoes an SN2 reaction to form poly(styrene sulfonate) (PSS). (B) Poly(vinylbenzyl chloride) (PVBC) is exposed to trimethylamine, and the benzyl chloride

functional group undergoes an SN2 reaction to form poly(vinylbenzyl trimethylammonium chloride) (PVBAC).

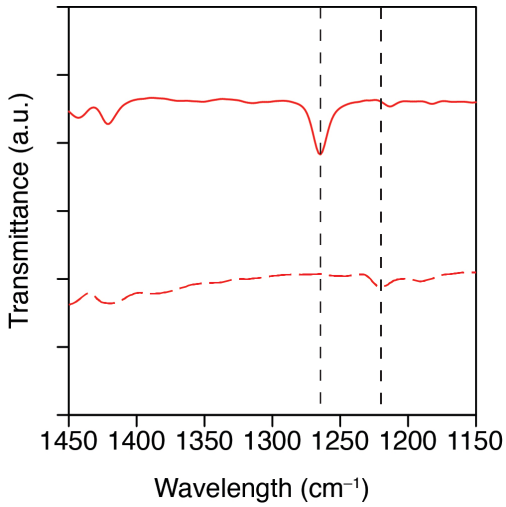

Figure 2.4. FT-IR spectrum of PVBC homopolymer before (solid line) and after (dashed line) exposure to 45% wt/wt trimethylamine solution for 17 h at 60 °C. Dashed lines are added as guides for the eye to note the C–Cl wag at 1266 cm^{-1}, the C–N stretch at 1220 cm^{-1}.

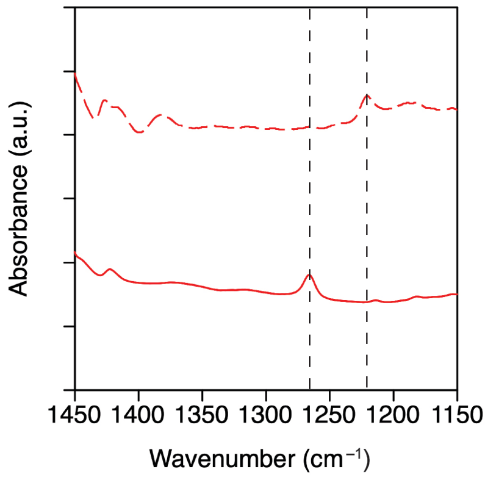

Figure 2.5. ATR-IR spectrum of PS_{140}-$PVBC_{140}$ before (solid line) and after (dashed line) exposure to 45% wt/wt trimethylamine vapor for 1 h. Dashed lines are added as guides for the eye to note the C–Cl wag at 1266 cm^{-1}, the C–N stretch at 1220 cm^{-1}.

While the thin films of PS_{140}–$PVBC_{140}$ readily converted to PS-*b*-PVBAC, the PS-*b*-PVBC thin films exhibited no observable microphase separation at any molar mass

by AFM measurements or GISAXS analysis (**Figure 2.6**, **Figure 2.7**, and **Figure 2.8**). By AFM, the films were smooth, without any features observable in the height or phase measurements even when employing the intermodulation AFM technique (**Figure 2.9**). Intermodulation AFM is useful for our experiments, as the cantilever tip is driven simultaneously at two different frequencies, which allows for the resolution of small differences in surface interactions between distinct domains. In addition, due to this method of driving the cantilever at two simultaneous frequencies, force and dissipation curves for each pixel within the AFM scan are generated simultaneously, which will be applied further below to aid in distinguishing unique domains within the material (for a more in-depth discussion of this technique and how it differs from typical AFM tapping mode techniques, please see **Section 2.3.12**).[46] By GISAXS, no scattering peaks were observed outside of the Yoneda band (**Figure 2.6**). Small-angle X-ray scattering (SAXS) of the solvent cast bulk samples similarly showed no scattering peaks for any PS−PVBC sample (**Figure 2.10a**). Furthermore, by DSC, we observed a single T_g for the diblock at 103 °C (**Figure 2.10b**), similar to the behavior previously reported by Knauss and co-workers.[53] This behavior is most likely due to an exceedingly small Flory−Huggins interaction parameter, χ_{ij}, between PS and PVBC.

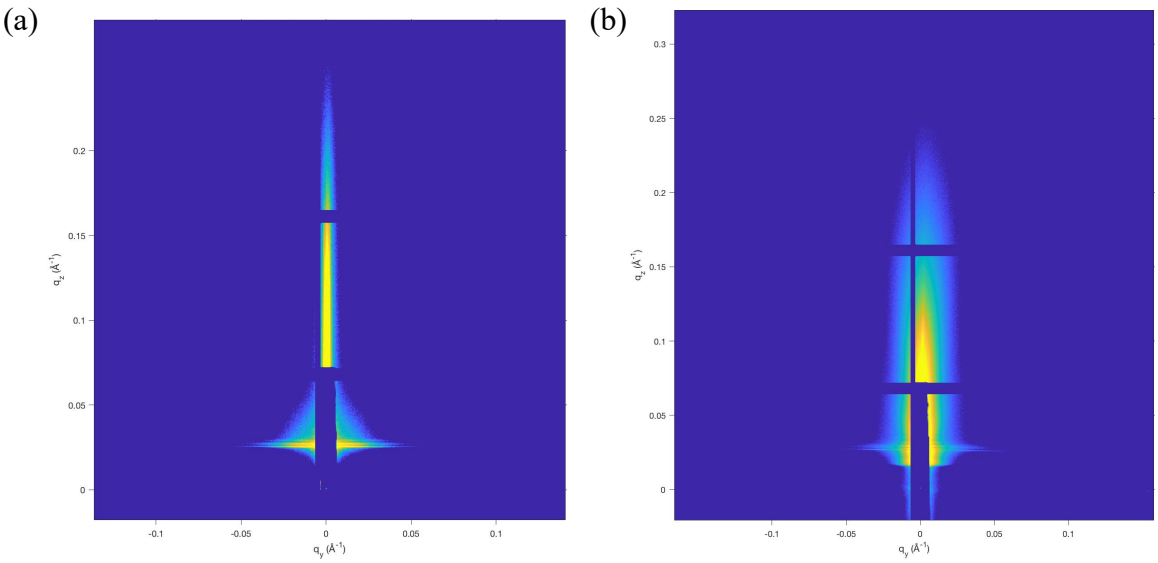

Figure 2.6. GISAXS scattering pattern of PS_{140}-$PVBC_{140}$ film after solvent vapor annealing in chlorobenzene (a) before and (b) after exposing to TMA vapor for 1 hour. Incident angle of 0.14° and an exposure time of 20 s.

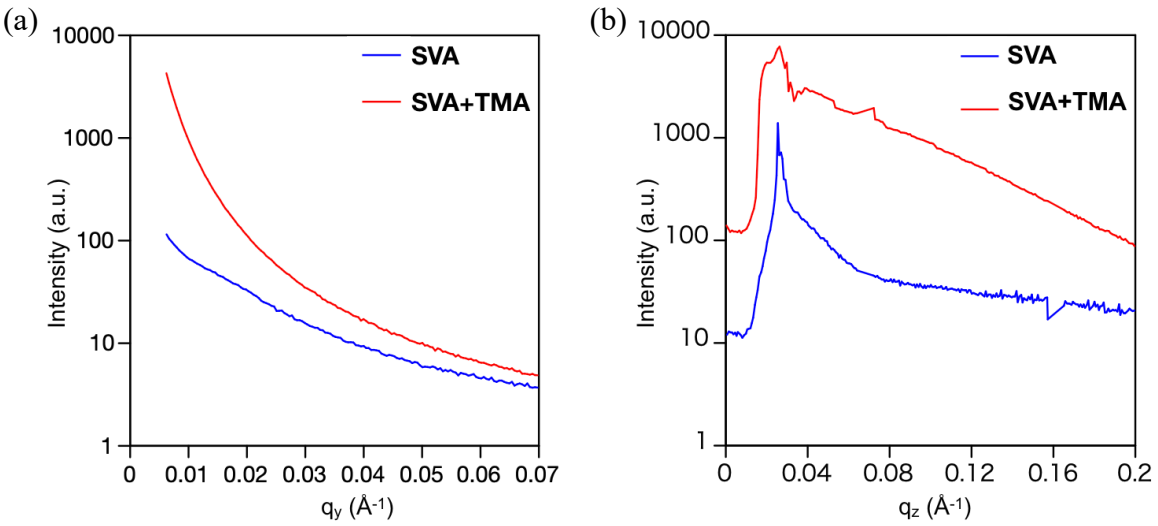

Figure 2.7. Line cut along the (a) q_y and (b) q_z axis of the GISAXS scattering pattern of PS_{140}-$PVBC_{140}$ film before and after exposure to TMA vapor.

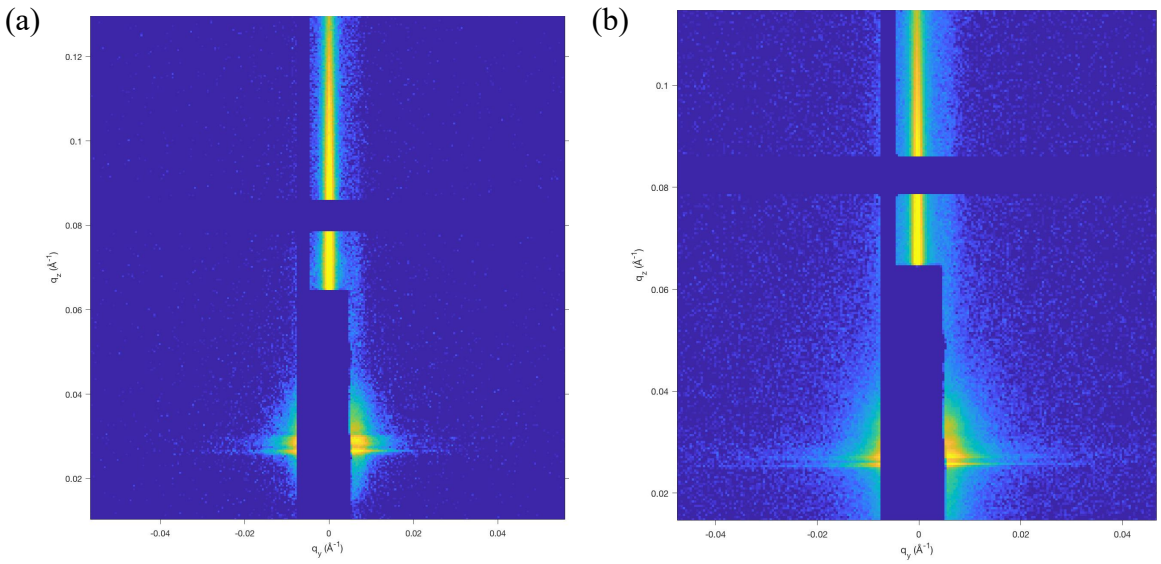

Figure 2.8. GISAXS scattering pattern of (a) PS_{710}-$PVBC_{400}$ and (b) PS_{1290}-$PVBC_{650}$ films after solvent vapor annealing in chlorobenzene. Incident angle of 0.14° and an exposure time of 20 s.

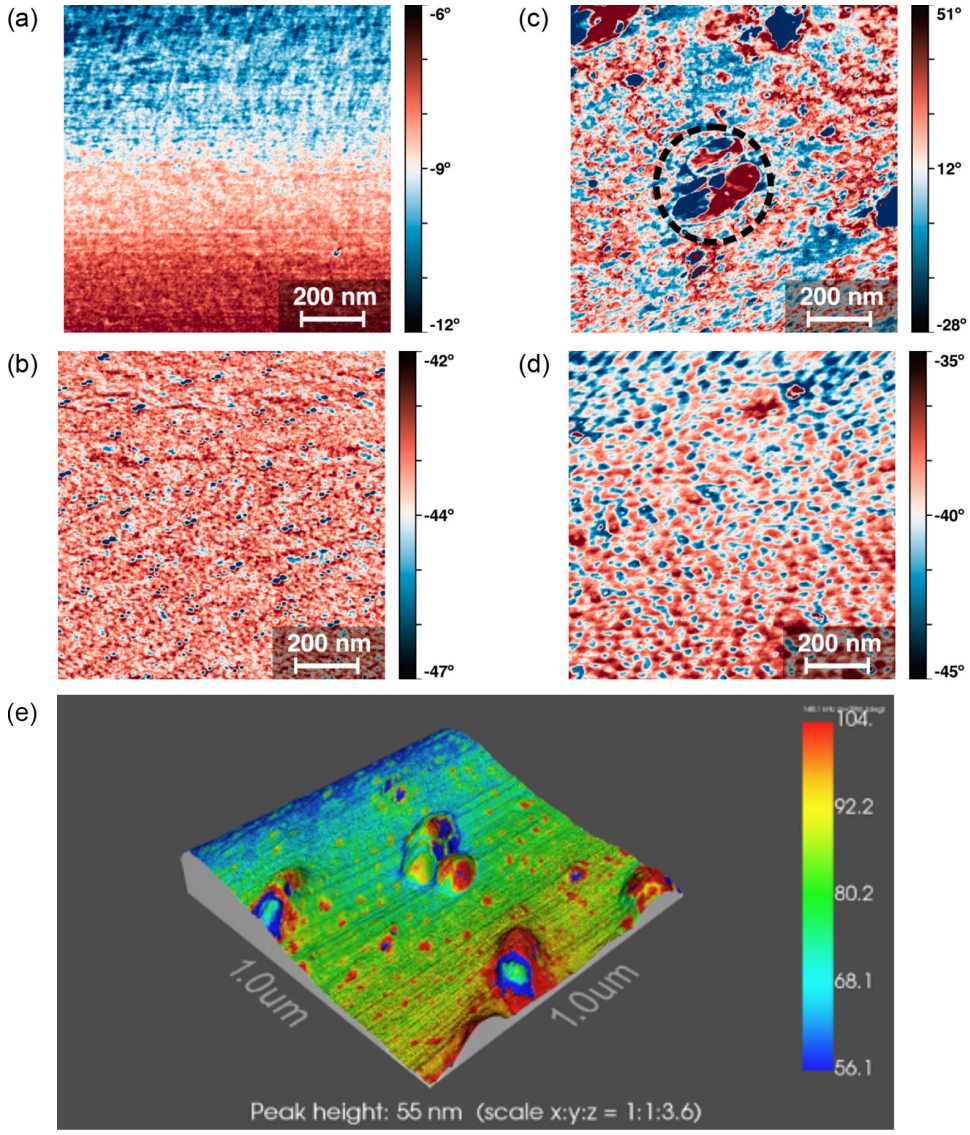

Figure 2.9. Intermodulation AFM phase images of (a) PS_{140}−$PVBC_{140}$, (b) $P4ClS_{700}$−$PVBC_{110}$, and (c) $PSSE_{260}$−$P4ClS_{1585}$ diblock polymers, as well as (d) $PSSE_{110}$−$P4ClS_{305}$−$PVBC_{70}$ triblock spin coated to make 50−70 nm films on bare silicon and solvent vapor annealed in chlorobenzene. In image (a), the apparent shift from blue to red is due to the inherent drift of the AFM tip over time during measurements. Image (c) has a few disordered features in the phase image such as the one highlighted with a black dashed circle, this is due to a large height defect on the surface, which can be seen in (e) the overlay of height and phase images.

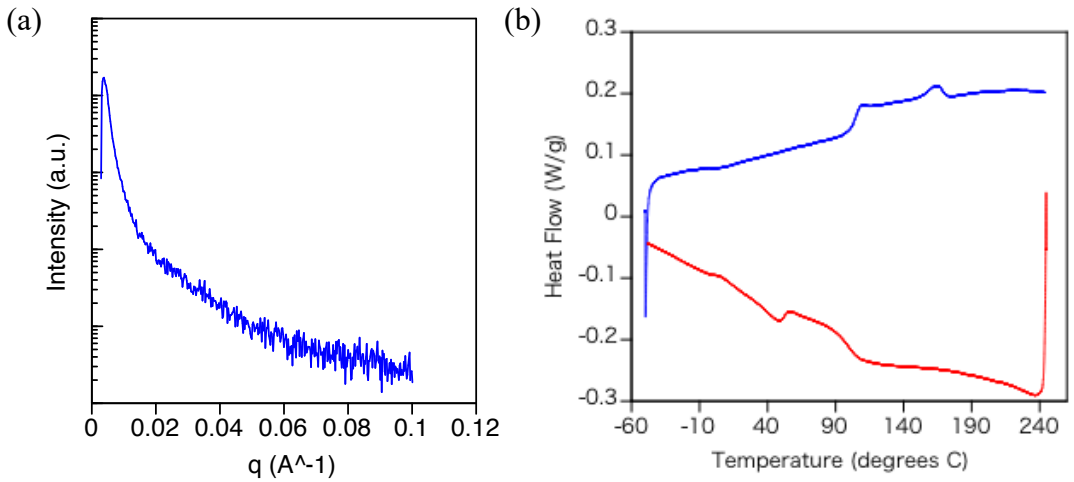

Figure 2.10. (a) Transmission SAXS 1D plot and (b) DSC plot of PS_{140}-$PVBC_{140}$.

Because microphase separation was not observed for the PS−PVBC polymers, we attempted to increase the interaction parameter between our B and C blocks by replacing the proton at the 4 position of styrene with a chloride through the use of poly(4-chlorostyrene) (P4ClS) as an alternative neutral block. Unfortunately, there have been no previous studies of the solid-state behavior of block polymers containing P4ClS and PVBC. P4ClS−PVBC diblock polymers were synthesized by RAFT polymerization, first growing P4ClS from the CTA and then adding VBC onto the isolated and characterized P4ClS macroinitiator, yielding a diblock polymer $P4ClS_{700}$−$PVBC_{110}$ with M_n = 114 kg mol^{-1} and $Đ$ = 1.87 (**Figure 2.11** and **Figure 2.12**). By intermodulation AFM, we observed that the thin films of $P4ClS_{700}$−$PVBC_{110}$ exhibited circular domains ~50 nm in diameter, both before and after solvent vapor annealing with chlorobenzene (**Figure 2.9b**). Upon exposure to TMA vapor for 1 h, the circular domains became more distorted and grew in size to 100 nm with "sticky", dissipative force curves, indicative of swollen alkyl ammonium domains (**Figure 2.13**). Because charged polymers can absorb humidity from the air, their water

content is variable, which leads to changes in their T_g values. As a result, DSC data on the functionalized polyelectrolytes are inconsistent and cannot be used to help confirm microphase separation.[61] To further confirm the self-assembled morphology, we stained the TMA exposed films with an aqueous phosphotungstic acid ($H_3PW_{12}O_{40}$) solution and collected TEM images. The phosphotungstate is negatively charged, and therefore it should interact with the positively charged PVBAC domains and increase the contrast in the TEM image. We observed regularly spaced dark, circular domains around 80−100 nm in diameter (PVBAC) within a lighter matrix (P4ClS) (**Figure 2.14a**). GISAXS experiments indicate that the domains likely permeate through the film; a diffuse Bragg sheet scattering pattern is indicative of microphase separation of the two blocks within the film (**Figure 2.14b**).

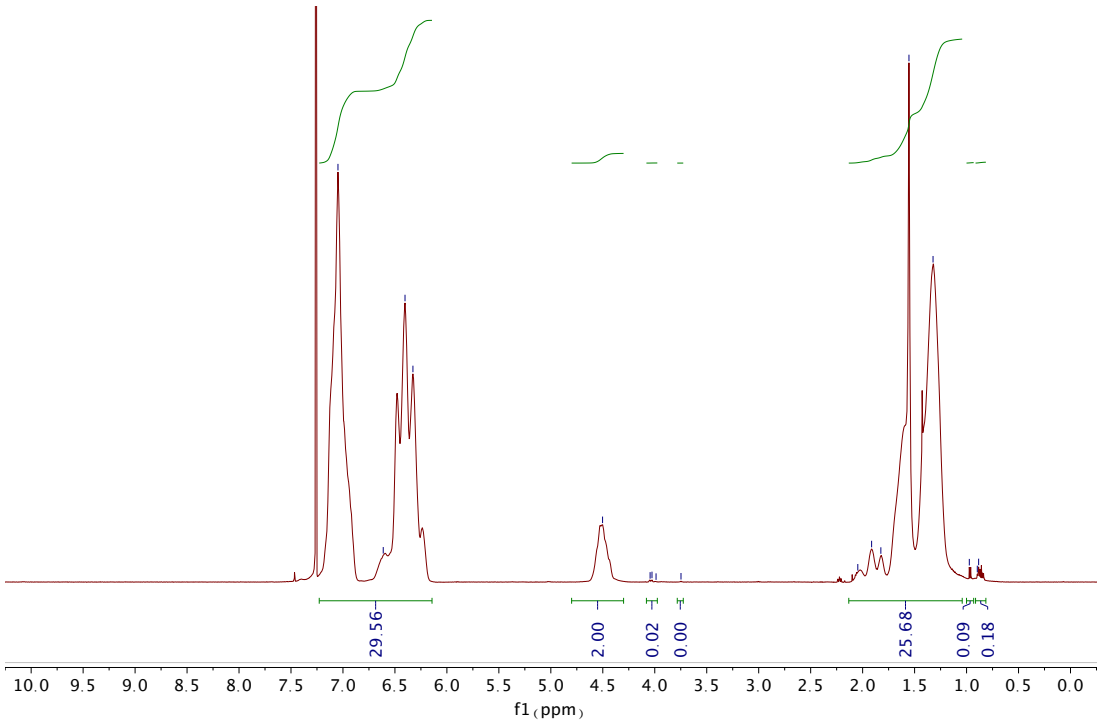

Figure 2.11. ^{1}H NMR spectrum of P4ClS$_{700}$-PVBC$_{110}$

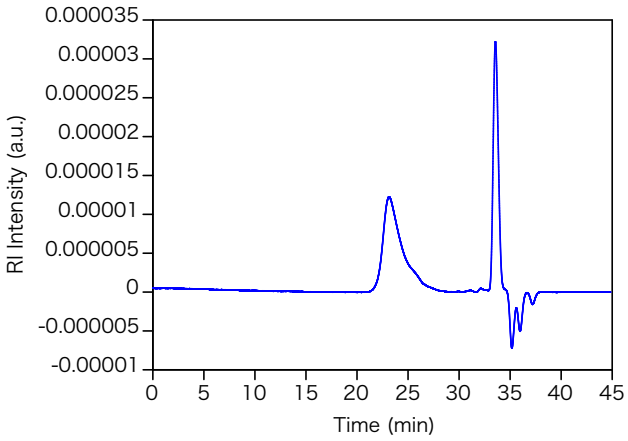

Figure 2.12. P4ClS$_{700}$-PVBC$_{110}$ SEC Chromatogram

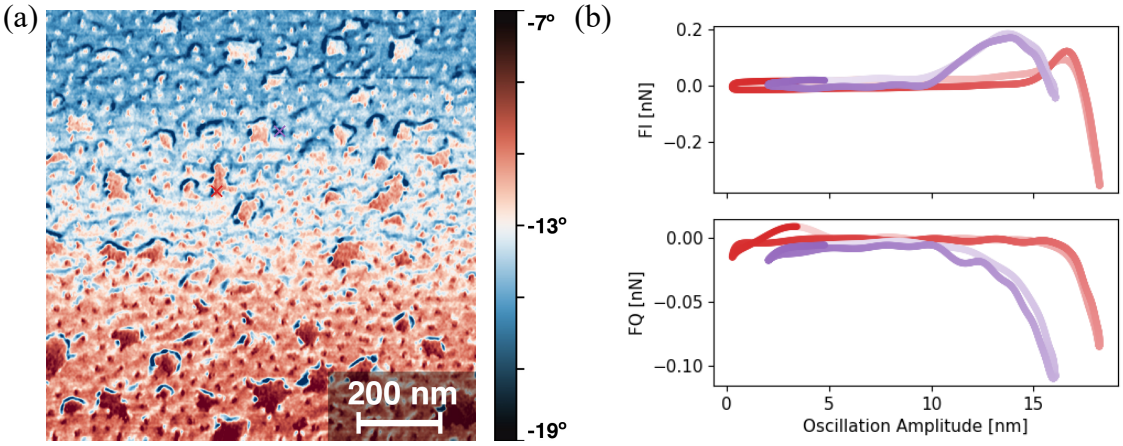

Figure 2.13. (a) An intermodulation AFM scan of P4ClS$_{700}$-PVBC$_{110}$ after TMA exposure and (b) the force (top) and dissipation (bottom) curves where the red "X" and lines correspond to a PVBAC domain and the purple "X" and lines correspond to a P4ClS domain.

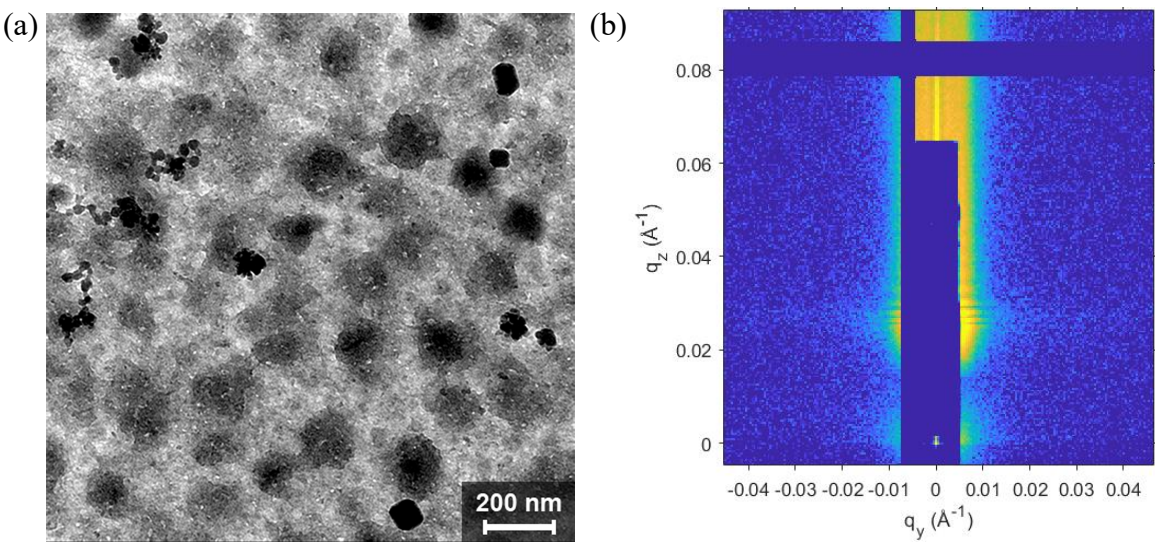

Figure 2.14. (a) Transmission electron microscopy image of P4ClS$_{700}$−PVBC$_{110}$ 50 nm thick film after solvent vapor annealing with chlorobenzene and staining by submersion in a 0.1 wt% aqueous solution of phosphotungstic acid. (b) GISAXS scattering pattern of P4ClS$_{700}$-PVBC$_{110}$ film after solvent vapor annealing in chlorobenzene. Incident angle of 0.14° and an exposure time of 20 s.

To determine the rate of the functionalization of PVBC in a P4ClS matrix, ATR-IR data were collected for a P4ClS$_{700}$−PVBC$_{110}$ diblock polymer film of 1 μm thickness (to increase the signal intensity) as a function of TMA exposure time. **Figure 2.15** shows the IR band due to the C−Cl wag disappearance and the peak due to the C−N stretch appearance within an hour of TMA exposure, consistent with the S_N2 displacement of chloride by trimethylamine. GISAXS data of the "thick" films (>200 nm) indicate parallel features, suggesting that the morphology of the diblock polymer P4ClS$_{700}$−PVBC$_{110}$ films buries parallel PVBC layers at these thicknesses (**Figure 2.14b**). As a result, we observe a slower functionalization than that seen in a PVBC homopolymer because the domains are less accessible in the thicker films of the diblock polymers. In the thinner films that we used for morphological characterization (<100 nm), we identified perpendicularly oriented morphologies on the surface of our films in AFM, which likely increases the rate of the

functionalization. From these results, we conclude that the P4ClS$_{700}$–PVBC$_{110}$ is microphase separated, and that the PVBC can be readily functionalized to the corresponding polycation under mild conditions.

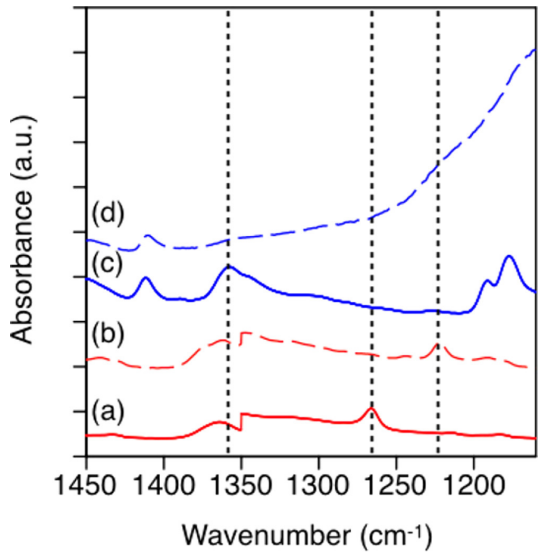

Figure 2.15. ATR-IR spectra of 1 μm thick films of diblock polymers P4ClS$_{700}$–PVBC$_{110}$ (a) before and (b) after 1 h of TMA exposure and PSSE$_{260}$-P4ClS$_{1585}$ (c) before and (d) after 12 h of TMA exposure. Black dashed lines are added to highlight the C–Cl wag at 1266 cm^{-1}, the C–N stretch at 1220 cm^{-1}, and the S=O stretch at 1357 cm^{-1}.

2.4.2 Pre-Anionic Block

Our target polymer for the preanionic A block is poly(*n*-propyl styrene sulfonic ester) (PSSE), which can be converted to the polyanion poly(styrene sulfonate) (PSS) (**Scheme 2.2**).[62] PSS is a common polyelectrolyte, with uses in ion-exchange resins,[52] ion-exchange membranes for batteries,[63] and potassium binders for chronic kidney disease.[64] The initial *n*-propyl styrene sulfonic ester (SSE) monomer was synthesized according to literature methods by converting sodium styrene sulfate to the acid chloride and then condensing with *n*-propanol.[42–43,65] The SSE was then polymerized through RAFT polymerization using CTA and AIBN as a radical thermal initiator to form PSSE.

Thermogravimetric analysis (**Figure 2.16a**) showed a partial mass loss at ~200 °C, which is consistent with literature reports of thermal alkyl deprotection of the sulfonic ester. Previously reported methods for deprotecting PSSE to PSS use a strong base to hydrolyze the ester group, such as sodium hydroxide.[62,65] Suspending the PSSE homopolymer in an aqueous solution of 30 wt% NaOH and heating to 70 °C led to deprotection of the sulfonic ester to the sulfonate, which could be monitored by FT-IR spectroscopy (**Figure 2.16b**).

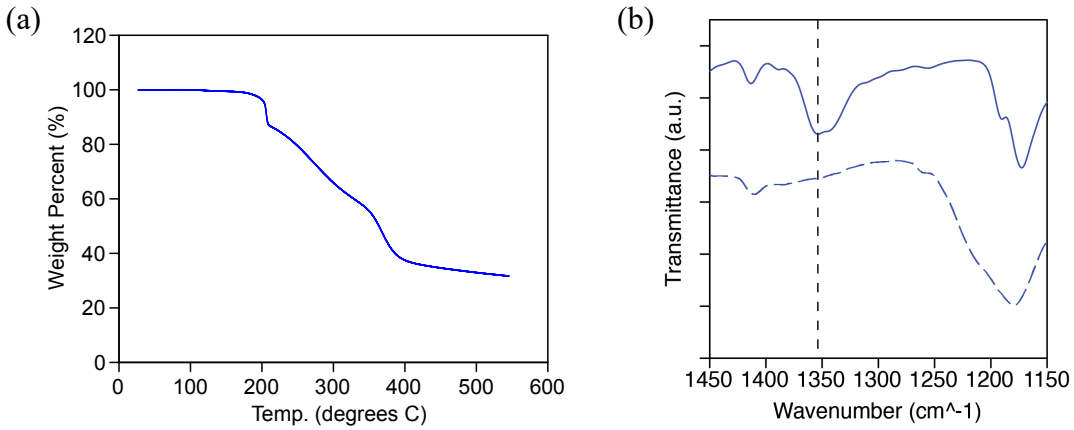

Figure 2.16. (a) TGA plot of PSSE. (b) FT-IR spectrum of PSSE homopolymer before (solid plot) and after (dashed plot) exposure to 30 wt. % NaOH in 5:6 vol./vol. of H_2O/MeOH for 48 h at 70 °C. Dashed vertical line is added as a guide for the eye to note the S=O stretch at 1350 cm^{-1}.

To confirm whether PSSE would microphase separate from P4ClS and to further confirm the sulfonic ester deprotection in a block copolymer, a PSSE macroinitiator was chain extended with 4ClS in the presence of AIBN to yield a diblock polymer, $PSSE_{260}$–$P4ClS_{1585}$, with M_n = 225 kg mol^{-1} and $Đ$ = 1.15 (**Figure 2.17** and **Figure 2.18**). Polymer solutions were spin coated onto silicon wafers to produce 50 nm thick films (see **2.3.11** for spin coating and annealing recipes), and intermodulation AFM was used to determine the microphase separated morphology of the thin film (**Figure 2.9c**). Again, disordered circular domains were observed, consistent with segregation of the two blocks.

To verify that these nanoscale features permeated through the thin films, we measured the GISAXS of the $PSSE_{260}$−$P4ClS_{1585}$ thin films, which revealed perpendicular features with D spacing around 45 nm, in agreement with our observations by AFM (**Figure 2.19**).

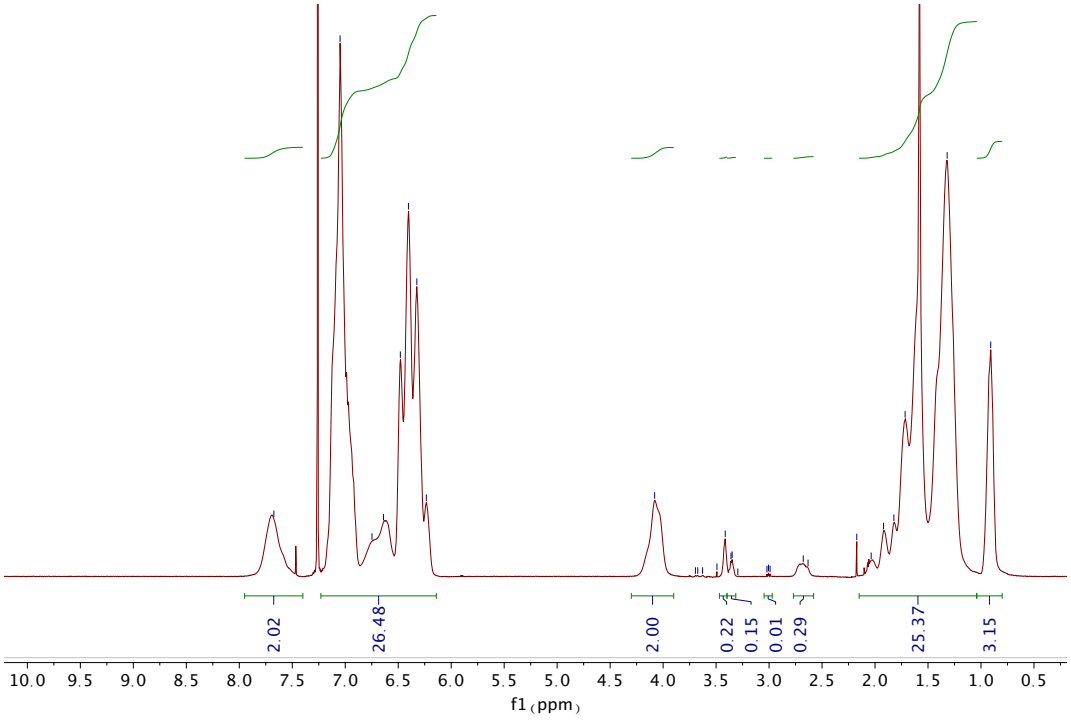

Figure 2.17. ^{1}H NMR spectrum of $PSSE_{260}$-$P4ClS_{1585}$

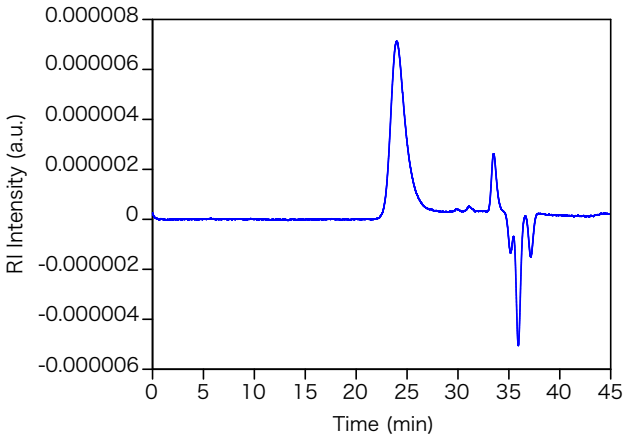

Figure 2.18. $PSSE_{260}$-$P4ClS_{1585}$ SEC Chromatogram

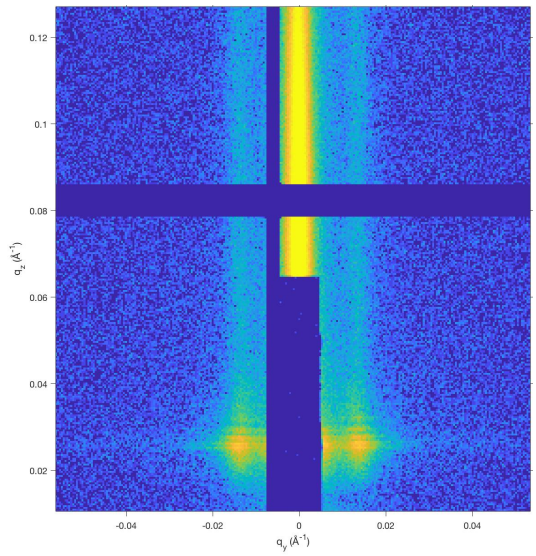

Figure 2.19. GISAXS scattering pattern of $PSSE_{260}$-$P4ClS_{1585}$ film after solvent vapor annealing in chlorobenzene. Incident angle of 0.14° and an exposure time of 20 s.

During the course of these studies, various bases were evaluated for deprotecting the n-propyl sulfonic ester. We developed a strategy using an aqueous 45% solution of trimethylamine (TMA) (the same amine used to convert PVBC to the cationic block PVBAC). The conversion of PSSE to PSS in a 45% TMA aqueous solution was monitored by FTIR spectroscopy of the isolated solid polymer after lyophilization, which showed full conversion after 8 h (**Figure 2.20**). Functionalization to the sulfonate in the solid state could also be achieved by simple exposure to TMA vapor in a sealed chamber. After 12 h of exposure to TMA vapor, we observed a quantitative conversion of $PSSE_{260}$−$P4ClS_{1585}$ to PSS_{260}−$P4ClS_{1585}$, as determined by ATR-IR spectroscopy, where the peak at 1357 cm^{-1} attributed to asymmetric S=O stretching of the sulfonic ester disappeared (**Figure 2.15**). GISAXS showed retention of the microphase separated morphologies with no observable change in the scattering pattern (**Figure 2.21**).

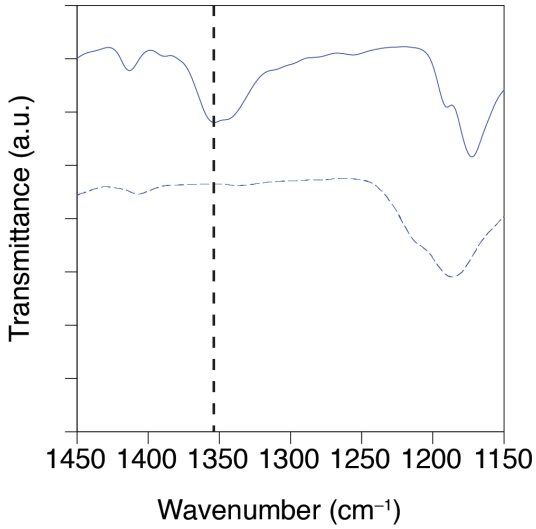

Figure 2.20. FT-IR spectrum of PSSE homopolymer before (solid line) and after (dashed line) exposure to 45% wt/wt trimethylamine solution for 8 h at 80 °C. Dashed lines are added as guides for the eye to note the S=O stretch at 1350 cm^{-1}.

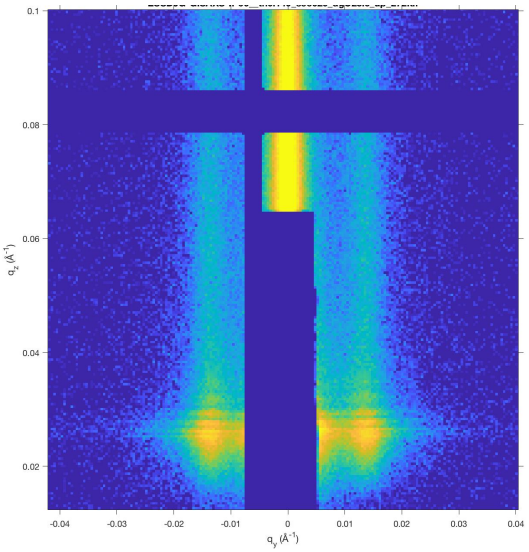

Figure 2.21. GISAXS scattering pattern of $PSSE_{260}$-$P4ClS_{1585}$ film after solvent vapor annealing in chlorobenzene and exposure to 45% wt/wt trimethylamine solution vapors. Incident angle of 0.14° and an exposure time of 20 s.

2.4.3 Triblock Polyampholytes

To obtain our desired microphase-separated anionic and cationic thin films, we targeted the synthesis of the neutral ABC triblock precursor poly(*n*-propyl styrene sulfonic

ester)-*block*-poly(4-chlorostyrene)-*block*-poly-(4-vinylbenzyl chloride) (PSSE-*b*-P4ClS-*b*-PVBC). As detailed above, the individual PSSE-*b*-P4ClS and P4ClS-*b*-PVBC diblock polymers displayed clear microphase separation behavior. The last step was to combine all three homopolymers into one ABC triblock terpolymer to ultimately obtain negative and positive domains within a neutral matrix. Starting with the $PSSE_{110}$–$P4ClS_{305}$ diblock polymer as the macroinitiator, PVBC was grown via RAFT polymerization to yield $PSSE_{110}$–$P4ClS_{305}$–$PVBC_{70}$ with M_n = 78 kg mol^{-1} and $Đ$ = 1.10 (**Figure 2.22** and **Figure 2.23**). Thermal analysis by DSC showed a single, merged T_g due to the small difference between the T_g values of the component polymers. A solution of the triblock polymer in chlorobenzene was spin coated onto native oxide silicon wafers to yield 68 nm thick films, which were solvent vapor annealed in chlorobenzene and then analyzed by intermodulation AFM. The phase image in **Figure 2.9d** shows circular domains on the order of 50 nm, illustrative of microphase separation of the polymer blocks. The domains were confirmed to permeate through the thickness of the film through GISAXS measurements (**Figure 2.24**).

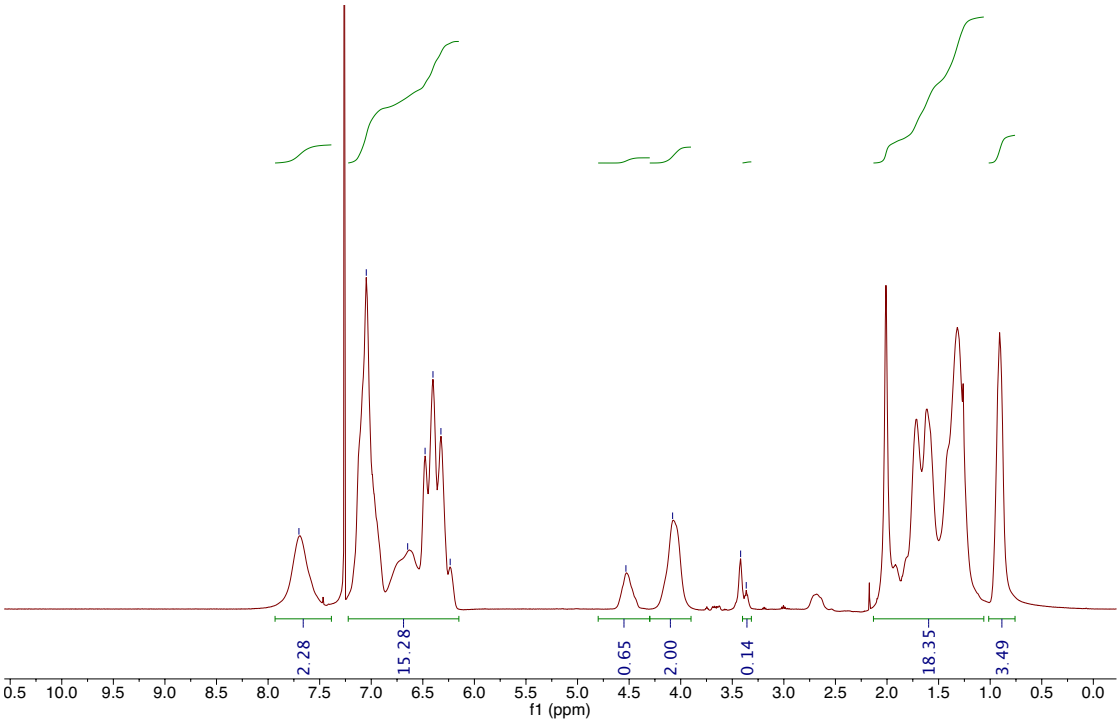

Figure 2.22. ^{1}H NMR spectrum of $PSSE_{110}$-$P4ClS_{305}$-$PVBC_{70}$

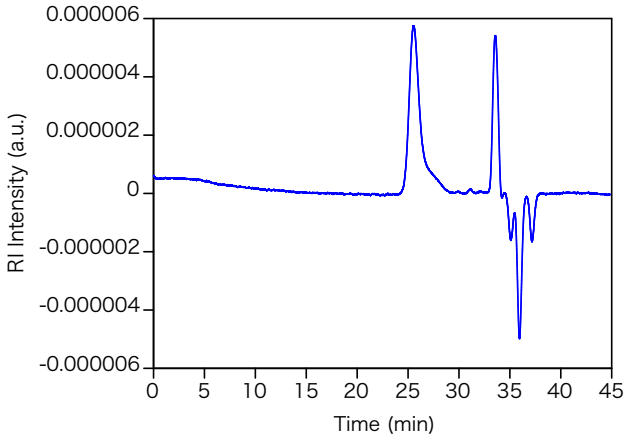

Figure 2.23. $PSSE_{110}$-$P4ClS_{305}$-$PVBC_{70}$ SEC Chromatogram

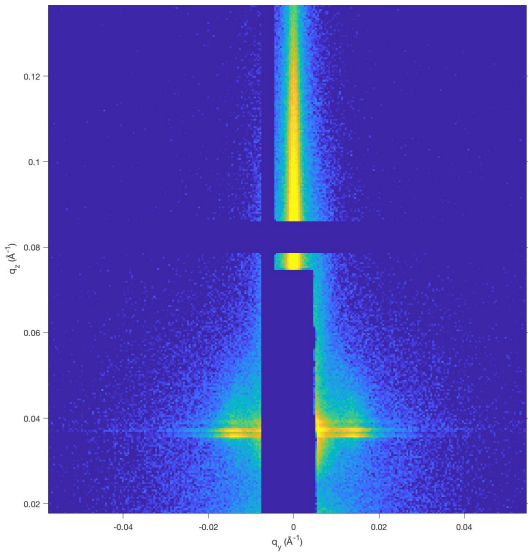

Figure 2.24. GISAXS scattering pattern of $PSSE_{110}$-$P4ClS_{305}$-$PVBC_{70}$ film after solvent vapor annealing in chlorobenzene. Incident angle of 0.14° and an exposure time of 20 s.

Functionalization of the pre-anionic-*b*-neutral-*b*-pre-cationic triblock simultaneously to the anionic-*b*-neutral-*b*-cationic triblock polymer in the solid state was attempted by exposing the film to TMA vapor in a sealed chamber. The reaction progress was followed by ATR-IR spectroscopy, as previously detailed in the diblock polymer sections. However, the vibrational bands at 1270 cm^{-1}, indicative of the C−Cl wag, and at 1350 cm^{-1}, indicative of the S=O stretch of the sulfonate ester, did not decrease as a function of TMA exposure time (**Figure 2.25**).

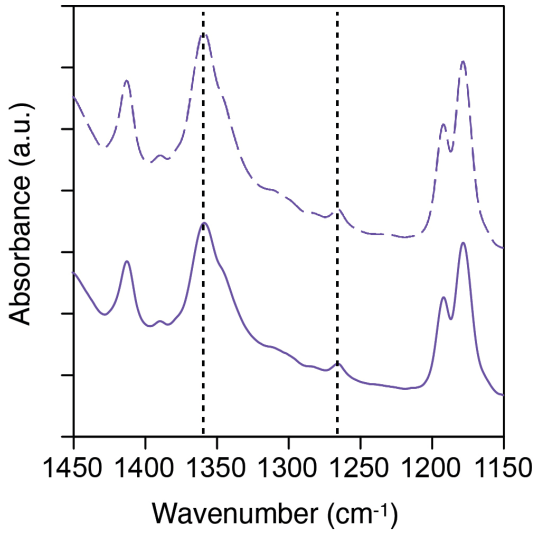

Figure 2.25. ATR-IR spectrum of $PSSE_{260}$-$P4ClS_{565}$-$PVBC_{140}$ triblock polymer before (solid plot) and after (dashed plot) exposure to 45% wt/wt trimethylamine vapor for 12 h. Vertical dashed lines are added as guides for the eye to note the C–Cl wag at 1266 cm^{-1} and the S=O stretch at 1357 cm^{-1}.

Because the respective diblock polymers become fully functionalized in a short period of time, it seemed likely that there was some surface phenomenon preventing TMA from accessing the preanionic and precationic domains. To try to clean the surface, an unexposed sample of the polymer thin film was plasma etched with oxygen for 15 s, reducing the thickness from 68 to 57 nm. ATR-IR showed that the plasma etching did not result in the deprotection of the thin film. The etched film was then exposed to TMA vapor. ATR-IR showed complete functionalization of both the anionic A block and the cationic C block after 24 h of vapor exposure (**Figure 2.26**). We suspect that the surface energies lead to a thin layer of P4ClS that obscures the other blocks from functionalizing in the TMA vapor, but is thin enough that characterization shows the domains underneath the layer; a quick plasma etch treatment exposes the underlying layers that are then functionalized. AFM of the film after etching showed large height features, making the determination of

the phase difference difficult (**Figure 2.27**), but after functionalization with TMA (**Figure 2.28**), the intermodulation AFM image was consistent with the microphase separation, confirming that the thin film maintains separate domains throughout the functionalization process. To further support this, we measured the force and dissipation curves of the microphase separated domains, revealing a softer red domain (the oscillation amplitude is higher, indicating that the tip pushes further into the material) consistent with the force curves of the PVBAC domains in the P4ClS−PVBAC diblock thin film (see **Figure 2.13**). Conversely, the blue domain is noticeably harder, consistent with these domains being comprised of different polymer blocks. We propose that the increase in the number of observable domains by AFM is a result of the increased contrast due to the A and C blocks becoming charged and, therefore, having a greater interaction with the tip when compared to the previous glassy preionic blocks.

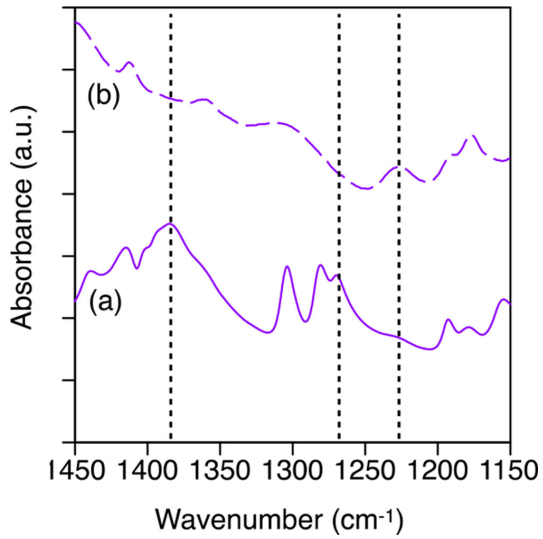

Figure 2.26. ATR-IR spectra of 57 nm thick films of plasma-etched triblock polymers $PSSE_{110}$−$P4ClS_{305}$−$PVBC_{70}$ (a) before (solid) and (b) after (dashed) exposure to TMA. Black dashed lines are added as guides for the eye to note the C−Cl wag at 1266 cm^{-1}, the C−N stretch at 1220 cm^{-1}, and the S=O stretch at 1357 cm^{-1}.

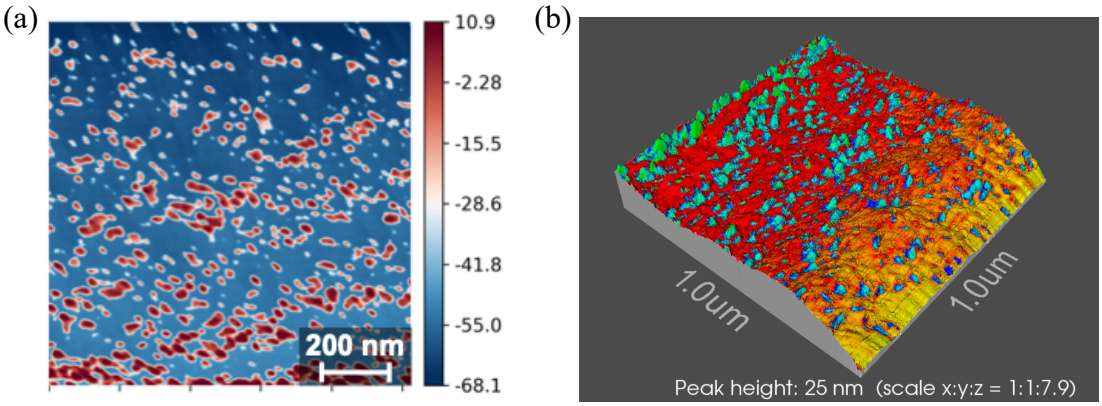

Figure 2.27. Intermodulation AFM scan of $PSSE_{110}$-$P4ClS_{305}$-$PVBC_{70}$ after plasma etching (a) the phase image scan and (b) the scanned image with the height data overlaid on the phase data.

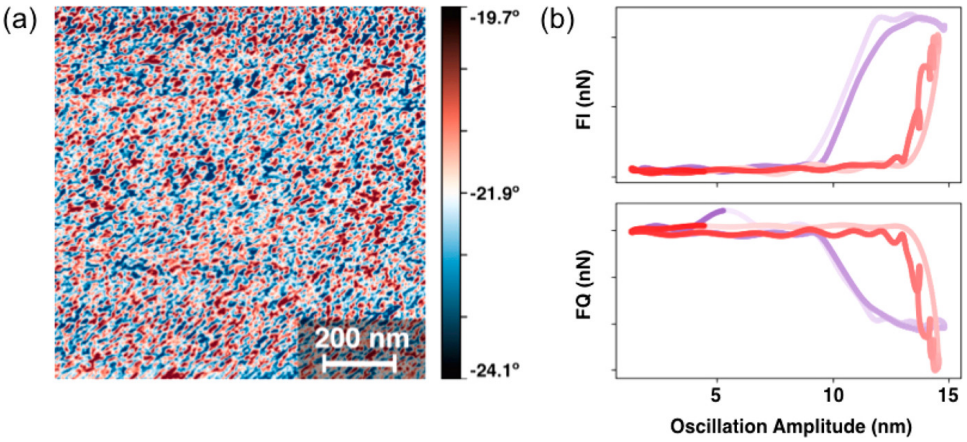

Figure 2.28. (a) Intermodulation AFM phase image of 57 nm thick film of $PSSE_{110}$–$P4ClS_{305}$–$PVBC_{70}$ triblock polymer after plasma etch and subsequent exposure to TMA vapor for 24 h. (b) Force (top) and dissipation (bottom) curves taken from a representative point within the blue domain (PSS, purple line) and red domain (PVBAC, red line).

This novel single-step functionalization of PSSE–P4ClS–PVBC to simultaneously convert both preionic A and C blocks to anionic and cationic blocks, respectively, improves the ease of synthesis and fabrication compared to previous methods reported for multiblock functionalization.[16–18] Using TMA in the vapor phase, a convenient and mild base, allows a wider range of functional groups and side chains to be incorporated into the system

without adverse side reactions that commonly occur when using harsh acids to convert polystyrene to poly(styrene sulfonate). The use of TMA also precludes the need for harsh, basic conditions previously employed to deprotect sulfonic esters to sulfonates in these polymer systems, e.g., 30 wt % NaOH at 70 °C for 2 days, which can lead to the decomposition of functional groups like esters to carboxylic acids, the degradation and corrosion of prefabricated membranes and silicon supports, or the chain scission of diblock polymers linked through ester linkages. Furthermore, the postfunctionalization purification now simply requires placing the films under vacuum to remove excess physisorbed TMA vapor, as opposed to washing or neutralization procedures. In previous work, these harsh conditions led to the loss of ordering in thin films of diblock and triblock polymers, the creation of holes in the membranes, and the need for BABCB pentablock polymers, where the neutral B block (polyisoprene) was cross-linked to immobilize the ionic domains.[16–18] Through this 2-in-1 functionalization, two synthetic steps and multiple purification steps are removed, resulting in an efficient and convenient way to achieve charged polymer domains using mild reagents. These factors mean the morphology of the thin films as well as any support structures are well maintained through the transformation.

2.5 Conclusion

Polyelectrolytes are used for a wide variety of applications, but their solid-state behavior has been relatively unexplored. We describe a combined method of fabrication for solid-state polyelectrolyte-containing thin films that uses a neutral triblock polymer to form microphase-separated morphologies. The polymers are then functionalized in a single step using mild reagents to yield a thin film containing spatially segregated positively and

negatively charged domains. The domains are held together by a glassy poly(4-chlorostyrene) matrix that maintains the morphology of the film through the functionalization step. Conversion to poly(styrene sulfonate) as an anionic block and poly(4-vinylbenzyl trimethylammonium chloride) as a cationic block is easily monitored using ATR-IR spectroscopy and shown to reach quantitative conversion in thin films after exposure to TMA vapor. Finally, AFM and GISAXS show retention of the morphology before and after TMA vapor exposure. Future work on the solid-state morphology and its use in various applications will allow us to apply this simplified functionalization procedure. More efforts are needed in fabricating thin films with clear microphase separated morphologies that maintain long-range order before and after functionalization. Further work can make use of this single step postpolymerization strategy with different B blocks that will allow for higher χ_{ij} parameters and different processing conditions, leading to thin films and bulk morphologies with long-range order and varying mechanical properties that can be tuned for a range of applications, including piezodialysis of wastewater and solid-state electrolytes for emerging battery technologies.

2.6 References

[1] Pinto, M. R.; Schanze, K. S. Conjugated Polyelectrolytes: Synthesis and Applications. *Synthesis* **2002**, *9*, 1293−1309.

[2] Freyer, J. L.; Brucks, S. D.; Campos, L. M. Fully charged: Maximizing the potential of cationic polyelectrolytes in applications ranging from membranes to gene delivery through rational design. *J. Polym. Sci., Part A: Polym. Chem.* **2017**, *55*, 3167−3174.

[3] Zhang, W.; Zhao, Q.; Yuan, J. Porous Polyelectrolytes: The Interplay of Charge and Pores for New Functionalities. *Angew. Chem., Int. Ed*. **2018**, *57*, 6754−6773.

[4] Zhao, Q.; An, Q. F.; Ji, Y.; Qian, J.; Gao, C. Polyelectrolyte complex membranes for pervaporation, nanofiltration and fuel cell applications. *J. Membr. Sci*. **2011**, *379*, 19−45.

[5] Scranton, A. B.; Rangarajan, B.; Klier, J. *Biomedical Applications of Polyelectrolytes;* Springer-Verlag: Berlin, Germany, 1995; Vol. *122*.

[6] Bronich, T. K.; Kabanov, A. V.; Kabanov, V. A.; Yu, K.; Eisenberg, A. Soluble Complexes from Poly(ethylene oxide)-*block*-polymethacrylate Anions and *N*-Alkylpyridinium Cations. *Macromolecules* **1997**, *30*, 3519−3525.

[7] Hunt, J. N.; Feldman, K. E.; Lynd, N. A.; Deek, J.; Campos, L. M.; Spruell, J. M.; Hernandez, B. M.; Kramer, E. J.; Hawker, C. J. Tunable, high modulus hydrogels driven by ionic coacervation. *Adv. Mater.* **2011**, *23*, 2327−2331.

[8] Nowak, A. P.; Breedveld, V.; Pakstis, L.; Ozbas, B.; Pine, D. J.; Pochan, D.; Deming, T. J. Rapidly recovering hydrogel scaffolds from self-assembling diblock copolypeptide amphiphiles. *Nature* **2002**, *417*, 424−428.

[9] Raviv, U.; Glasson, S.; Kampf, N.; Gohy, J.-F.; Jérôme, R.; Klein, J. Lubrication by charged polymers. *Nature* **2003**, *425*, 163−165.

[10] Gucht, J. v. d.; Spruijt, E.; Lemmers, M.; Cohen Stuart, M. A. Polyelectrolyte complexes: bulk phases and colloidal systems. *J. Colloid Interface Sci*. **2011**, *361*, 407−422.

[11] Kimerling, A. S.; Rochefort, W. E.; Bhatia, S. R. Rheology of Block Polyelectrolyte Solutions and Gels: A Review. *Ind. Eng. Chem. Res*. **2006**, *45*, 6885−6889.

[12] Delaney, K. T.; Fredrickson, G. H. Theory of polyelectrolyte complexation−Complex coacervates are self-coacervates. *J. Chem. Phys.* **2017**, *146*, 224902.

[13] Yang, S.; Vishnyakov, A.; Neimark, A. V. Self-assembly in block polyelectrolytes. *J. Chem. Phys.* **2011**, *134*, 054104.

[14] Lowe, A. B.; McCormick, C. L. Synthesis and Solution Properties of Zwitterionic Polymers. *Chem. Rev.* **2002**, *102*, 4177−4190.

[15] Dobrynin, A. V.; Colby, R. H.; Rubinstein, M. Polyampholytes. *J. Polym. Sci., Part B: Polym. Phys.* **2004**, *42*, 3513−3538.

[16] Isono, Y.; Tanisugi, H.; Endo, K.; Fujimoto, T.; Hasegawa, H.; Hashimoto, T.; Kawai, H. Morphological and Mechanical Properties of Multiblock Copolymers. *Macromolecules* **1983**, *16*, 5−10.

[17] Fujimoto, T.; Ohkoshi, K.; Miyaki, Y.; Nagasawa, M. A New Charge-Mosaic Membrane from a Multiblock Copolymer. *Science* **1984**, *224*, 74−76.

[18] Miyaki, Y.; Iwata, M.; Fujita, Y.; Tanisugi, H.; Isono, Y.; Fujimoto, T. Artificial Membranes from Multiblock Copolymers. 2. Molecular Characterization and

Morphological Behavior of Pentablock Copolymers of the ISIAI Type. *Macromolecules* **1984**, *17*, 1907−1912.

[19] Mendes, P. M.; Yeung, C. L.; Preece, J. A. Bio-nanopatterning of Surfaces. *Nanoscale Res. Lett.* **2007**, *2*, 373−384.

[20] Gao, P.; Hunter, A.; Summe, M. J.; Phillip, W. A. A Method for the Efficient Fabrication of Multifunctional Mosaic Membranes by Inkjet Printing. *ACS Appl. Mater. Interfaces* **2016**, *8*, 19772−19779.

[21] Rajesh, S.; Yan, Y.; Chang, H.-C.; Gao, H.; Phillip, W. A. Mixed Mosaic Membranes Prepared by Layer-by-Layer Assembly for Ionic Separations. *ACS Nano* **2014**, *8*, 12338−12345.

[22] Higa, M.; Masuda, D.; Kobayashi, E.; Nishimura, M.; Sugio, Y.; Kusudou, T.; Fujiwara, N. Charge mosaic membranes prepared from laminated structures of PVA-based charged layers: 1. Preparation and transport properties of charged mosaic membranes. *J. Membr. Sci.* **2008**, *310*, 466−473.

[23] Bates, F. S.; Fredrickson, G. H. Block Copolymers–Designer Soft Materials. *Phys. Today* **1999**, *52*, 32−38.

[24] Albert, J. N. L.; Epps, T. H. Self-assembly of block copolymer thin films. *Mater. Today* **2010**, *13*, 24−33.

[25] Luo, M.; Epps, T. H. Directed Block Copolymer Thin Film Self-Assembly: Emerging Trends in Nanopattern Fabrication. *Macromolecules* **2013**, *46*, 7567−7579.

[26] Segalman, R. A. Patterning with block copolymer thin films. *Mater. Sci. Eng., R* **2005**, *48*, 191−226.

[27] Choi, J.; Huh, J.; Carter, K. R.; Russell, T. P. Directed Self-Assembly of Block Copolymer Thin Films Using Minimal Topographic Patterns. *ACS Nano* **2016**, *10*, 7915−7925.

[28] Laschewsky, A. Structures and Synthesis of Zwitterionic Polymers. *Polymers* **2014**, *6*, 1544−1601.

[29] Philipp, B.; Dautzenberg, H.; Linow, K.-J.; Kötz, J.; Dawydoff, W. Polyelectrolyte Complexes - Recent Developments and Open Problems. *Prog. Polym. Sci.* **1989**, *14*, 91−172.

[30] Wang, Q.; Schlenoff, J. B. The Polyelectrolyte Complex/Coacervate Continuum. *Macromolecules* **2014**, *47*, 3108−3116.

[31] Ahmed, L. S.; Xia, J.; Dubin, P. L.; Kokufuta, E. Stoichiometry and the Mechanism of Complex Formation in Protein-Polyelectrolyte Coacervation. *J. Macromol. Sci., Part A: Pure Appl.Chem.* **1994**, *31*, 17−29.

[32] Chollakup, R.; Smitthipong, W.; Eisenbach, C. D.; Tirrell, M. Phase Behavior and Coacervation of Aqueous Poly(acrylic acid)-Poly(allylamine) Solutions. *Macromolecules* **2010**, *43*, 2518−2528.

[33] Antonov, M.; Mazzawi, M.; Dubin, P. L. Entering and Exiting the Protein−Polyelectrolyte Coacervate Phase via Nonmonotonic Salt Dependence of Critical Conditions. *Biomacromolecules* **2010**, *11*, 51−59.

[34] Qin, J.; Priftis, D.; Farina, R.; Perry, S. L.; Leon, L.; Whitmer, J.; Hoffmann, K.; Tirrell, M.; de Pablo, J. J. Interfacial Tension of Polyelectrolyte Complex Coacervate Phases. *ACS Macro Lett.* **2014**, *3*, 565−568.

[35] Kelly, K. D.; Schlenoff, J. B. Spin-Coated Polyelectrolyte Coacervate Films. *ACS Appl. Mater. Interfaces* **2015**, *7*, 13980−13986.

[36] Tang, C.; Sivanandan, K.; Stahl, B. C.; Fredrickson, G. H.; Kramer, E. J.; Hawker, C. J. Multiple Nanoscale Templates by Orthogonal Degradation of a Supramolecular Block Copolymer Lithographic System. *ACS Nano* **2010**, *4*, 285−291.

[37] Guliyeva, A.; Vayer, M.; Warmont, F.; Faugère, A. M.; Andreazza, P.; Takano, A.; Matsushita, Y.; Sinturel, C. Thin Films with Perpendicular Tetragonally Packed Rectangular Rods Obtained from Blends of Linear ABC Block Terpolymers. *ACS Macro Lett.* **2018**, *7*, 789−794.

[38] Tang, C.; Lennon, E. M.; Fredrickson, G. H.; Kramer, E. J.; Hawker, C. J. Evolution of Block Copolymer Lithography to Highly Ordered Square Arrays. *Science* **2008**, *322*, 429−432.

[39] Malhotra, S. L.; Lessard, P.; Minh, L.; Blanchard, L. P. Thermal Decomposition and Glass-Transition Temperature Study of Poly-*p*-methylstyrene. *J. Macromol. Sci., Chem.* **1980**, *14*, 517−540.

[40] Malhotra, S. L.; Lessard, P.; Blanchard, L. P. The Thermal Decomposition and Glass Transition Temperature of Poly(*p*-tert-butylstyrene). *J. Macromol. Sci., Chem.* **1981**, *A15*, 121−141.

[41] Thermal Transitions of Homopolymers: Glass Transition & Melting Point. https://www.sigmaaldrich.com/technical-documents/articles/materials-science/polymer-science/thermal-transitions-ofhomopolymers.html (accessed June 7, 2019).

[42] Schuh, K.; Prucker, O.; Rühe, J. Surface Attached Polymer Networks through Thermally Induced Cross-Linking of Sulfonyl Azide Group Containing Polymers. *Macromolecules* **2008**, *41*, 9284−9289.

[43] Kolomanska, J.; Johnston, P.; Gregori, A.; Fraga Domínguez, I.; Egelhaaf, H.-J.; Perrier, S.; Rivaton, A.; Dagron-Lartigau, C.; Topham, P. D. Design, synthesis and thermal behaviour of a series of well-defined clickable and triggerable sulfonate polymers. *RSC Adv.* **2015**, *5*, 66554−66562.

[44] Moad, G.; Chong, Y. K.; Postma, A.; Rizzardo, E.; Thang, S. H. Advances in RAFT polymerization: the synthesis of polymers with defined end-groups. *Polymer* **2005**, *46*, 8458–8468.

[45] Baruth, A.; Rodwogin, M. D.; Shankar, A.; Erickson, M. J.; Hillmyer, M. A.; Leighton, C., Non-lift-off Block Copolymer Lithography of 25 nm Magnetic Nanodot Arrays. *ACS Appl. Mater. Interfaces* **2011**, *3*, 3472-3481.

[46] Haviland, D. B. Quantitative force microscopy from a dynamic point of view. *Curr. Opin. Colloid Interface Sci.* **2017**, *27*, 74−81.

[47] ImAFM Overview. Intermodulation Products AB, Sweden. https://intermodulation-products.com/support/tutorials (accessed June 7, 2019).

[48] Thunhorst, K. L.; Noble, R. D.; Bowman, C. N., Preparation of Functionalized Polymers by Reactions of Poly(Vinylbenzyl Chloride). In *Polymer Modification*; Swift, G., Carraher, C. E., Jr., Bowman, C. N., Eds.; Plenum Publishing: New York, NY, 1997; pp 97−107.

[49] Ting, W.-H.; Dai, S. A.; Shih, Y.-F.; Yang, I. K.; Su, W.-C.; Jeng, R.-J. Facile synthetic route toward poly(vinyl benzyl amine) and its versatile intermediates. *Polymer* **2008**, *49*, 1497−1505.

[50] Haladjova, E.; Mountrichas, G.; Pispas, S.; Rangelov, S. Poly(vinylbenzyl trimethylammonium chloride) Homo and Block Copolymers Complexation with DNA. *J. Phys. Chem. B* **2016**, *120*, 2586−2595.

[51] Lloyd, W. G.; Durocher, T. E. Nucleophilic Displacements upon Poly(vinylbenzyl chloride). *J. Appl. Polym. Sci.* **1963**, *7*, 2025−2033.

[52] Alexandratos, S. D. Ion-Exchange Resins: A Retrospective from Industrial and Engineering Chemistry Research. *Ind. Eng. Chem. Res.* **2009**, *48*, 388−398.

[53] Li, Y.; Jackson, A. C.; Beyer, F. L.; Knauss, D. M. Poly(2,6-dimethyl-1,4-phenylene oxide) Blended with Poly(vinylbenzyl chloride)-*b*-polystyrene for the Formation of Anion Exchange Membranes. *Macromolecules* **2014**, *47*, 6757−6767.

[54] Cao, Y.-C.; Wang, X.; Mamlouk, M.; Scott, K. Preparation of alkaline anion exchange polymer membrane from methylated melamine grafted poly(vinylbenzyl chloride) and its fuel cell performance. *J. Mater. Chem.* **2011**, *21*, 12910−12916.

[55] Moad, G.; Rizzardo, E.; Thang, S. H. Radical addition−fragmentation chemistry in polymer synthesis. *Polymer* **2008**, *49*, 1079−1131.

[56] Couture, G.; Améduri, B. Kinetics of RAFT homopolymerisation of vinylbenzyl chloride in the presence of xanthate or trithiocarbonate. *Eur. Polym. J.* **2012**, *48*, 1348−1356.

[57] Merrifield, R. B. The Synthesis of a Tetrapeptide. *J. Am. Chem. Soc.* **1963**, *85*, 2149−2154.

[58] Wang, X.; Goswami, M.; Kumar, R.; Sumpter, B. G.; Mays, J. Morphologies of block copolymers composed of charged and neutral blocks. *Soft Matter* **2012**, *8*, 3036−3052.

[59] Hickner, M. A.; Herring, A. M.; Coughlin, E. B. Anion exchange membranes: Current status and moving forward. *J. Polym. Sci., Part B: Polym. Phys.* **2013**, *51*, 1727−1735.

[60] Lacroix-Desmazes, P.; Delair, T.; Pichot, C.; Boutevin, B. Synthesis of Poly(chloromethylstyrene-b-styrene) Block Copolymers by Controlled Free-Radical Polymerization. *J. Polym. Sci., Part A: Polym. Chem.* **2000**, *38*, 3845−3854.

[61] Zhang, Y.; Batys, P.; O'Neal, J. T.; Li, F.; Sammalkorpi, M.; Lutkenhaus, J. L. *ACS Cent. Sci*. **2018**, *4*, 638−644.

[62] Chen, L.; Hallinan, D. T., Jr.; Elabd, Y. A.; Hillmyer, M. A. Highly Selective Polymer Electrolyte Membranes from Reactive Block Polymers. *Macromolecules* **2009**, *42*, 6075−6085.

[63] Higgins, T. M.; Park, S. H.; King, P. J.; Zhang, C. J.; McEvoy, N.; Berner, N. C.; Daly, D.; Shmeliov, A.; Khan, U.; Duesberg, G.; Nicolosi, V.; Coleman, J. N. A Commercial Conducting Polymer as Both Binder and Conductive Additive for Silicon Nanoparticle-Based Lithium-Ion Battery Negative Electrodes. *ACS Nano* **2016**, *10*, 3702−3713.

[64] Hunt, T. V.; DeMott, J. M.; Ackerbauer, K. A.; Whittier, W. L.; Peksa, G. D. Single-dose sodium polystyrene sulfonate for hyperkalemia in chronic kidney disease or end-stage renal disease. *Clin. Kidney J.* **2019**, *12*, 408−413.

[65] Lienkamp, K.; Schnell, I.; Groehn, F.; Wegner, G. Polymerization of Styrene Sulfonate Ethyl Ester by ATRP: Synthesis and Characterization of Macromonomers for Suzuki Polycondensation. *Macromol. Chem. Phys.* **2006**, *207*, 2066−2073.

Chapter 3. Bicontinuous ion-exchange materials through polymerization-induced microphase separation*

* This work was completed in close collaboration with Dr. Eric Silver of the Department of Chemistry at the University of Minnesota.

3.1 Abstract

Polymerization-induced microphase separation has been used to prepare solid cross-linked monoliths containing bicontinuous and nanostructured polymer domains. We use this process to fabricate a monolith containing either a negatively or positively charged polyelectrolyte domain inside of the neutral styrene/divinylbenzene derived matrix. First, the materials are made with a neutral *pre*-ionic polymer containing masked charged groups. The monoliths are then functionalized to a charged state by treatment with trimethylamine; small-angle X-ray scattering shows no significant morphological change in the microphase-separated structure upon post-polymerization modification. By exchanging dyes with the counterions in the material, we corroborated the continuity of the charged domains. Using ion-exchange capacity measurements, we estimate the accessible charge within the material based on macroinitiator molar mass and loading.

3.2 Introduction

Polyelectrolytes are polymers containing charges along their chain.[1] They are an important part of many applications involving ion transfer and sequestration, including ion exchange resins and separators in batteries and fuel cells.[2,3] Their usefulness in these applications stems from the generally desirable mechanical properties of polymers[3] and their large number of fixed charges at a high charge density.

Often, practical considerations call for crosslinking polyelectrolytes or functionalizing domains in a microphase-separated system. The ideal material often has high ion conductivity across macroscopic distances, limited transfer of oppositely charged or neutral solutes, and robust mechanical properties.[4,5] Several studies have attempted to

correlate ion conductivity with tunable properties of such polymer systems.[3,6-9] Conductivity is expected to improve as the charge density in the material increases.[10] However, solvent swelling plays an important role, and ion conductivity in water-containing systems has been shown to initially increase as water content decreases, followed by a significant decrease at water contents that are insufficient to solvate the ions.[7] Interfacial curvature and dimensions of the charged domains have also proven to be important factors.[11] These parameters have been controlled by adjusting the level of functionalization along the polymer chain.[12] But, a series of studies showed that in systems at lower levels of functionalization, the charged monomers gathered into smaller hydrated portions of the domain while the uncharged monomers formed undesirable dry, hydrophobic domains.[7]

Similar roadblocks have been shown in systems that use crosslinking instead of functionalization to limit swelling. The first limitation is the crosslinking density–even at high crosslink densities, the polymer still swells because of the osmotic driving force.[13] Zeldovich and Khokhlov highlighted potential drawbacks in highly crosslinked systems where inhomogeneities were found in the areas surrounding each crosslink.[14]

Polymerization-induced microphase separation (PIMS) is a useful approach to nanostructured monoliths.[15] The synthesis starts with a macroinitiator consisting of a polymer chain end-capped with a reversible addition-fragmentation chain transfer agent (RAFT CTA). The macroinitiator is then dissolved in a mixture of monofunctional and difunctional monomers. An exogenous radical initiator leads to polymer chain extension through controlled radical polymerization. The forming block polymer reaches a molar

mass where microphase separation of the macroinitiator from the actively polymerizing matrix occurs. Simultaneously, crosslinking in the matrix kinetically traps the system, forming a bicontinuous network of percolating nanoscale domains. Variation in the macroinitiator loading and molar mass allows tuning of domain size. When using a degradable polymer CTA, etching of the macroinitiator domain can lead to high porosities and surface areas.[16]

PIMS monoliths are desired for applications where synthetic ease and interconnectivity of domains is advantageous. In this communication we use postpolymerization modification with the PIMS synthetic methodology to prepare charged monoliths that contain either positive or negative charges via polyelectrolyte domains percolating through a styrene/divinylbenzene (S/DVB) matrix (**Figure 3.3**). These systems demonstrate high charge density, low swelling, and. sequestration of oppositely charged molecules.

3.3 Experimental

3.3.1 Materials

Unless otherwise noted, all chemicals were purchased from Sigma-Aldrich and used as received. Styrene (99%) was distilled after drying over calcium hydride. Azobisisobutyronitrile (AIBN) (98%) was recrystallized from methanol and dried under reduced pressure. Vinylbenzyl chloride (90%) and divinylbenzene (80% technical grade) were run through a plug of basic alumina to remove inhibitors. Dichloromethane, tetrahydrofuran, and toluene were purified via a GC-SPS-4-CM glass contour 800-L solvent purification system obtained from Pure Process Technologies (Nashua, NH). The

chain transfer agent (4-Cyano-4-[(dodecylsulfanylthiocarbonyl)sulfanyl]pentanoic acid; CTA) was synthesized according to previous literature procedures.[17]

3.3.2 Instrumentation

NMR spectra were recorded on a Bruker Advance III HD 500 spectrometer. Chemical shifts are reported in δ units, expressed in ppm downfield from tetramethylsilane using residual protio- solvent as an internal standard ($CDCl_3$, ^1H: 7.26 ppm).

Size exclusion chromatography (SEC) was performed in THF (25 °C, 1 mL min^{-1}) on an Agilent Infinity 1260 HPLC system equipped with three Waters Styragel HR columns, a Wyatt DAWN HELEOS-II 18-angle laser light scattering detector, and a Wyatt Optilab T-rEX differential refractive index detector. Absolute weight-average molar mass was determined using light scattering detector with a dn/dc = 0.1710 mL g^{-1} for PVBC and 0.1156 mL g^{-1} for PoSSE, as determined using a batch dn/dc calculation (**Section 3.3.6**).

Thermal gravimetric analysis (TGA) was performed on a TA Instruments Q500 under house nitrogen at a heating rate of 10 °C·min^{-1}. Differential scanning calorimetry (DSC) analyses were performed on a TA Instruments Discovery DSC using standard aluminum T-zero pans with hermetic lids. Scans were conducted under house nitrogen at a heating and cooling rate of 10 °C·min^{-1}.

Infrared spectroscopy measurements were performed on a Bruker Alpha Platinum ATR spectrometer with a built-in diamond attenuated total reflection set up.

Transmission small-angle X-ray scattering (SAXS) measurements were performed on a SAXSLab GANESHA300XL instrument of the Characterization Facility at the University of Minnesota. Cu Kα X-rays (λ = 1.54 Å) generated by a Xenocs Geni3DX

source were collimated through 2 sets of 4-bladed slits (JJ X-ray, A/S). 2D-SAXS patterns were acquired using a Dectris EIGER R 1M detector (7.72 cm x 7.99 cm rectangular area) with 1030 x 1065 pixels (75 μm x 75 μm pixel size) at a sample-to-detector distance of 46.8 cm. All 2D-SAXS pattern were azimuthally-integrated to obtain one-dimensional scattered intensity I(q) versus q plots.

UV-vis spectroscopy was measured with a Shimadzu spectrometer. Spectra were obtained between 200 and 800 nm at 1 nm intervals. Dye concentration calibration curves were calculated using dilution of stock solutions.

Images of samples were taken using an Epson Perfection V600 Photo Flatbed Scanner. The images were cropped and white balanced in Photoshop using the black text and white paper of the background to increase contrast (white balance applied evenly across each image).

3.3.3 Synthesis of *n*-octyl styrene sulfonic ester (oSSE)

n-Octyl styrene sulfonic ester was synthesized using a modified procedure described previously[18] by adding *p*-styrene sulfonyl chloride (6.1 g) dropwise to a stirring solution of 1-octanol (6.3 g, 1.5 eq) and DABCO (4.3 g, 1.2 eq) in 80 mL dry dichloromethane at 0 °C. The mixture was warmed to room temperature and stirred overnight. The reaction mixture was then washed with DI water (3x100 mL) and brine (100 mL). The organic phase was dried over $MgSO_4$ and 20 mg of butylated hydroxytoluene (BHT) was added before removing the solvent with a rotary evaporator followed by drying overnight under high vacuum, leaving a clear, colorless oil. The monomer was then purified using a silica plug with a 95:5 hexanes:ethyl acetate mix. The

monomer was recovered in 48% overall isolated yield (4.3 g) as a spot at R_f = ~0.5 by TLC with 9:1 hexanes:ethyl acetate. Solvent was removed by rotary evaporator after adding 20 mg of BHT and the monomer was dried under high vacuum overnight. The monomer, a clear and colorless oil, was stored at -20 °C under argon. ^{1}H NMR (500 MHz, $CDCl_3$): δ (ppm) 0.86 (3H, t, -CH_3, J = 7.0 Hz), 1.19-1.35 (10H, bm, (-CH_2-)$_5$), 1.64 (2H, m, O-CH$_2$-CH_2-), 4.04 (2H, t, O-CH_2, J = 6.6 Hz), 5.47 (1H, d, -C=CH, J = 10.9 Hz), 5.91 (1H, d, -C=CH, J = 17.6 Hz), 6.76 (1H, dd, -CH=C, J = 10.9, 17.6 Hz), 7.55 (2H, d, Ar-H_2, J = 8.1 Hz), 7.86 (2H, d, Ar-H_2, J = 8.0 Hz)

3.3.4 Synthesis of poly(*n*-octyl styrene sulfonic ester) (PoSSE)

An oven-dried Schlenk flask was fitted with a Teflon stopcock and flame dried three times, backfilling with argon after each cycle. The flask was then placed under an atmosphere of argon and charged with *n*-octyl styrene sulfonate (oSSE) monomer (7.8 g, 26.3 mmol, 67 equiv.), 4-cyano-4-[(dodecylsulfanylthiocarbonyl)sulfanyl]pentanoic acid (CTA) (0.159 g, 0.393 mmol, 1 equiv.), and AIBN (0.0189 g, 0.115 mmol, 0.3 equiv.), and dissolved in dry THF (2.7 mL g^{-1} monomer). The reaction was freeze-pump-thawed three times and the reaction flask was backfilled with 5 psig of argon. The flask was placed in a preheated oil bath (60 °C) and stirred for five days. The reaction was stopped by submerging the reaction flask in a liquid N_2 bath for 1 min, and then warming to room temperature. Subsequently, the solution mixture was precipitated in methanol and filtered through a 0.2 μm pore PVDF membrane, and the isolated solid was dried under vacuum to yield PSSE as a white solid (4.19 g, 54% isolated yield, $M_{n,NMR}$ = 21 kg mol^{-1}, $M_{n,SEC}$ = 21 kg mol^{-1}, $M_{w,SEC}$ = 21 kg mol^{-1}, $Đ$ = 1.02) ^{1}H NMR (500 MHz, $CDCl_3$): δ (ppm) 0.91

(218H, s, -CH_3), 1.62 (1090H, m, -CH_2-), 3.25 (2H, br s, -S-CH_2-), 4.07 (142H, br s, O-CH_2-), 6.74 (126H, br s, Ar-*H*), 7.70 (140H, br s, Ar-*H*).

3.3.5 Synthesis of poly(vinylbenzyl chloride) (PVBC)

An oven-dried Schlenk flask was fitted with a Teflon stopcock and flame dried three times, backfilling with 5 psig of argon after each cycle. The flask was then placed under an atmosphere of argon and charged with vinylbenzyl chloride monomer (16.2 g, 106 mmol, 325 equiv.), CTA (0.132 g, 0.33 mmol, 1 equiv.), and AIBN (0.0161 g, 0.098 mmol, 0.3 equiv.). The reaction was then freeze-pump-thawed three times and backfilled with 5 psig of argon. The flask was placed in a preheated oil bath (100 °C) and stirred for 1 h. The reaction was stopped by submerging the flask in a liquid N_2 bath for 1 min. The polymer was precipitated in methanol and filtered through 0.2 μm pore PVDF membrane. The solid was dried under vacuum to yield PVBC as a pale yellow solid (0.473 g, 44% isolated yield, $M_{n,NMR}$ = 24 kg mol^{-1}, $M_{n,SEC}$ = 12 kg mol^{-1}, $M_{w,SEC}$ = 13 kg mol^{-1}, $Đ$ = 1.122) ^{1}H NMR (500 MHz, $CDCl_3$): δ (ppm) 0.89 (5.8H, t, -CH_3), 1.40 (274H, m, -CH_2-, -C*H*-), 3.25 (2H, m, -S-CH_2-), 4.52 (154H, br s, -CH_2-Cl), 6.49 (305H, m, Ar-*H*).

3.3.6 Batch d*n*/dc measurements

d*n*/d*c* was determined for both polymers by dissolving 6 concentrations (0.5, 1, 2, 3, 4, and 5 mg/mL) of polymer into HPLC grade THF. The solution refractive index was measured at a flow rate of 0.2 mL/min using a Wyatt Optilab T-rEX differential refractive index detector at a wavelength of 658 nm.

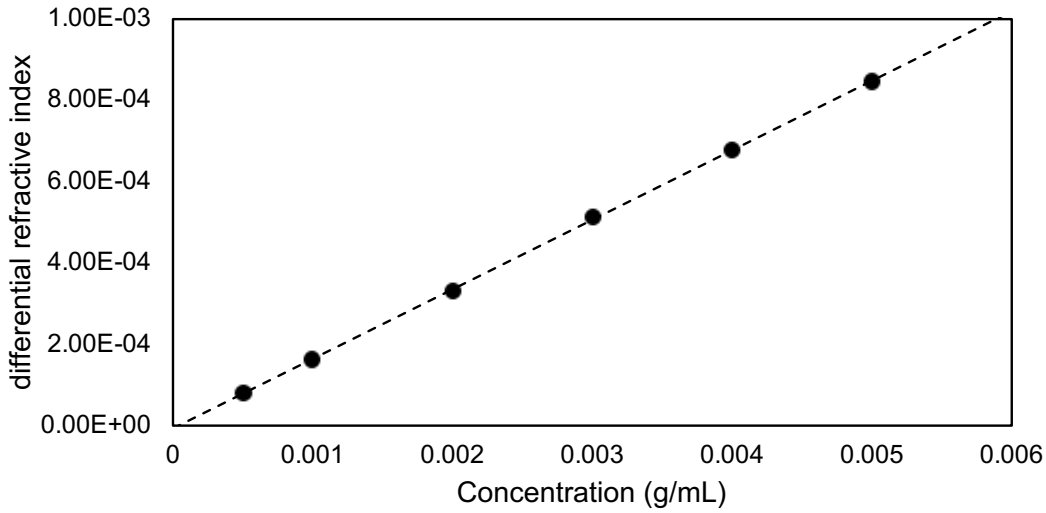

Figure 3.1. Batch d*n*/dc measurement for poly(vinylbenzyl chloride). Final d*n*/dc = 0.1710 ± 0.0007 mL g^{-1}.

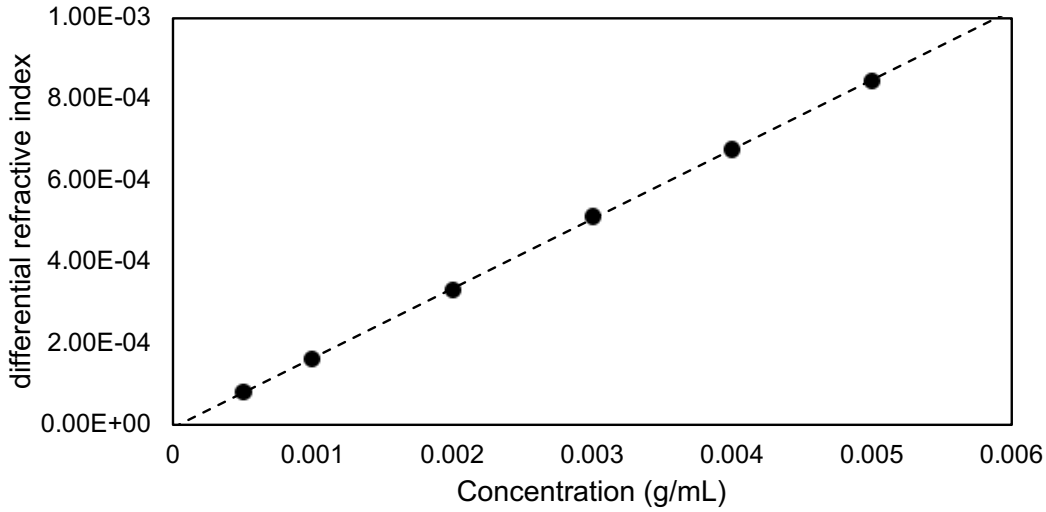

Figure 3.2. Batch d*n*/dc measurement for poly(vinylbenzyl chloride). Final d*n*/dc = 0.1156 ± 0.0009 mL g^{-1}.

3.3.7 Silanation of vials

Vials for making PIMS were silanated to prevent the monolith from sticking to the glass. 1 dram glass vials were washed thoroughly with DI water and acetone and then placed in an oven at 111 °C to dry. The dry vials were cooled to room temperature on the bench in a large jar and then filled with dry toluene. 2 drops of trichloro(3,3,3-

trifluoropropyl)silane were added to each vial and the jar was sealed overnight. The next day, each vial was rinsed out with dry toluene followed by a 1:1 DI water:methanol mixture and then dried in an oven before use.

3.3.8 Synthesis of PIMS monoliths

Macroinitiator (either PVBC or PoSSE, 0.260 g or 0.390 g, for 20 wt% or 30 wt%) was combined in a scintillation vial with styrene (0.792 g or 0.693 g) and divinylbenzene (0.248 g or 0.237 g) mixed at a 4:1 S:DVB molar ratio. The solution was sonicated at room temperature for 20 min to dissolve the macroinitiator. After sonication, a scoop of AIBN (~1 mg) was added and stirred into the mixture. The PIMS solution was then divided into three silane treated vials. The headspace was purged with dry argon and the vials capped and then sealed with parafilm. The vials were then suspended in an oil bath at 70 °C for 24 hours. The solidified PIMS were removed from the oil bath and air-cooled to room temperature. The vials were then shattered with a hammer to remove the solidified PIMS. The recovered PIMS were then placed under high vacuum overnight to remove residual monomer. PIMS monoliths were imaged and then sanded flat and polished using 600-5000 grit sandpaper to remove the skin layer and make a standard geometry.

3.3.9 Functionalization of PIMS

PIMS monoliths were functionalized by soaking in 3 mL of 45 wt% trimethylamine in water for 24 hours. After functionalization, the PIMS were rinsed in DI water and placed under high vacuum overnight to remove excess TMA. The dried monoliths were massed, imaged, and measured with ATR-IR to check functionalization.

3.3.10 Exposure of PIMS monoliths to dye solutions

PIMS monoliths were exposed to positively charged toluidine blue and negatively charged methyl red solutions to assess the polymer charges. 1 mg of toluidine blue or methyl red was dissolved into 100 mL of 0.1 M phosphate buffer in water mixed at a pH of 7.0. The solution was sonicated for 30 min to ensure dissolution of the dye. PIMS monoliths were placed into 15 mL polypropylene centrifuge tubes with 3 mL of dye stock solution and soaked for 24 h. After exposure, the PIMS were removed, rinsed in DI water, and dried with a delicate task wiper. The monoliths were weighed and imaged at each exposure step. UV-vis spectroscopy was used to assess the residual dye remaining in solution after exposure to the PIMS. The spectrometer was baselined with a cuvette of phosphate buffer and then used to measure the absorbance of each dye solution left after PIMS exposure and a control solution from a centrifuge tube without a sample.

The UV-vis absorption was calibrated using dilution of stock solutions that showed the following relationship between dye concentration and absorption for each dye:

Methyl Red: Absorbance = 35293 · (Concentration in M)

Toluidine Blue: Absorbance = 28622 · (Concentration in M) + 0.0337

Using the above calibration curve, the amount of dye remaining in solution was measured for each sample. Subtracting from the original amount of dye, the amount of absorbed dye was calculated for each PIMS sample.

3.3.11 Ion exchange capacity (IEC) measurements

IEC of the PIMS monoliths was determined through pH measurements of ionic exchange solutions. First, a neutral PIMS was exposed to TMA following the above

procedure. After drying and characterization, the PIMS was broken into chucks and ground into small pieces using a glass pestle and mortar. For PoSSE PIMS, the powdered material was soaked in a 0.1 M hydrochloric acid solution for two exposures of 24 h each. The material was then rinsed multiple times with DI water in a fritted funnel to remove excess acid.

The ground up PVBC PIMS was put in the bottom of a tared scintillation vial, which was packed with a known amount of Pyrex glass wool to contain the powder at the bottom of the vial. The material was first soaked in 0.1 M sodium hydroxide solution for two exposures for 24 h each. The material was then soaked in DI water for multiple washes until the water reached a plateau pH below 8.

After rinsing with water, the vial was heated in a 40 °C vacuum oven overnight to remove any residual water. The vial was then weighed to determine the amount of dry PIMS remaining (as some was lost during the exposures). Finally, 10 mL of 1 M sodium chloride solution was added to each vial and allowed to equilibrate for three days.

2 mL of salt solution were removed from each vial and 1 drop of 0.01 M phenolphthalein was added. The solution was then titrated to light pink using either 0.001 M hydrochloric acid (for PVBC PIMS) or 0.001 M sodium hydroxide solution (for PoSSE PIMS). The amount titrated was then used to back calculate the concentration of ions present in each PIMS, which was normalized by the mass of the dry PIMS.

3.4 Results and Discussion

We previously reported a thin film system containing a neutral ABC triblock polymer consisting of pre-anionic (poly(*n*-propyl styrene sulfonic ester)), a neutral styrenic

block, and pre-cationic (poly(*p*-vinylbenzyl chloride)) [PVBC] blocks to produce three distinct domains that could be converted through exposure to a trialkylamine solution to both positive and negative charges.[19] Here, we use that general strategy in a PIMS scheme to create bicontinuous, nanostructured, and charged materials (**Figure 3.3**).

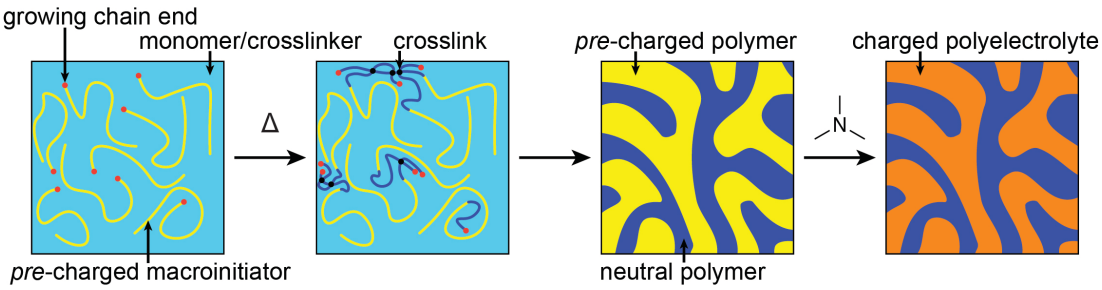

Figure 3.3. Schematic of polymerization-induced microphase separation to create percolating charged domains.

n-Octyl styrene sulfonic ester (oSSE) monomer was synthesized following a similar method to the synthesis of *n*-propyl styrene sulfonic ester previously reported,[18] substituting 1-octanol for 1-propanol. The oSSE monomer has not been previously reported; full characterization is included in **Section 3.3.3**. oSSE was polymerized using a trithiocarbonate RAFT CTA as an initiator,[17] which produced poly(*n*-octyl styrene sulfonate ester) (PoSSE) samples of controlled molar masses and relatively low dispersities ($Đ < 1.5$). Two molar masses were used in this study, M_n = 21 and 55 kg·mol^{-1}. PVBC homopolymer was prepared in an analogous manner to produce two macroinitiators of comparable molar masses M_n = 24 and 46 kg·mol^{-1}.

The selected macro-chain transfer agent (MacroCTA) was dissolved in a trichloro(3,3,3-trifluoropropyl)silane-treated vial in a 4:1 molar ratio of S:DVB at either 20 or 30 wt% loadings (samples referred to as MacroCTA-M_n-loading). MacroCTA loadings below 20 wt% did not consistently result in monoliths with interconnected

domains. In addition, the high molar mass PoSSE macroinitiator was only sparingly soluble in the S/DVB mixture, even at 20 wt%. Thus, in the case of PoSSE, we emphasized the use of the low molar mass material. A small amount of AIBN was added to the vials and the mixtures were purged with argon, sealed, and heated in an oil bath at 70 °C for 24 h. After cooling, the vials were broken apart and the monoliths were subjected to reduced pressure overnight to remove any unreacted S/DVB. The as-synthesized samples are optically transparent with a yellow tint due to the trithiocarbonate end groups (**Figure 3.4**); they were then sanded flat and polished to remove any macroscopic surface imperfections.

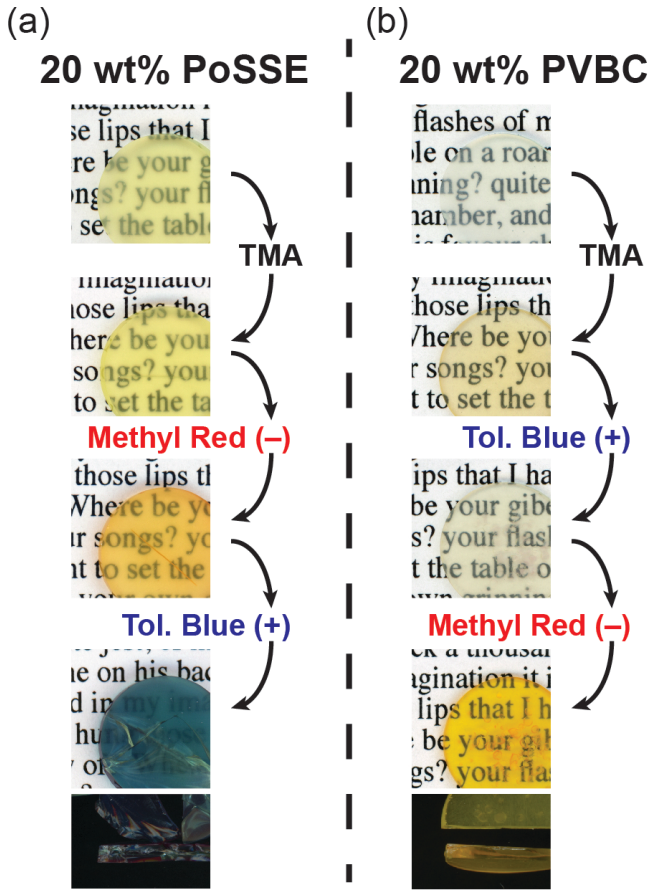

Figure 3.4. Images of (a) PoSSE-21k-20 and (b) PVBC-24k-20 monoliths as made, after functionalization with TMA, and after exposure to positively and negatively charged dyes.

Small-angle X-ray scattering (SAXS) of the monoliths showed a broad disordered peak in all of the samples, consistent with previous PIMS systems (**Figure 3.5**).[16] The principle scattering peak, q*, corresponded to domain spacings of 19 and 54 nm for the PoSSE-21k-20 and PoSSE-55k-20 materials, respectively. Similarly, the q* for the PVBC containing PIMS indicated domain spacings of 15 and 43 nm for the PVBC-24k-20 and PVBC-46k-20 samples, respectively. A peak was expected for the PoSSE PIMS since we have previously shown that other poly(styrene sulfonic esters) will microphase separate from polystyrene in related block polymer systems. In the case of PVBC, however, there have been no examples of a PS-PVBC block polymer showing microphase separation. The fact that PVBC PIMS scatter in our system indicates that PVBC and PS are characterized by a small positive Flory-Huggins interaction parameter. At some molar mass and/or degree of crosslinking in the PIMS system, the PS block on the end of the growing PVBC chains reaches a molar mass or level of crosslinking that is high enough to drive microphase separation.

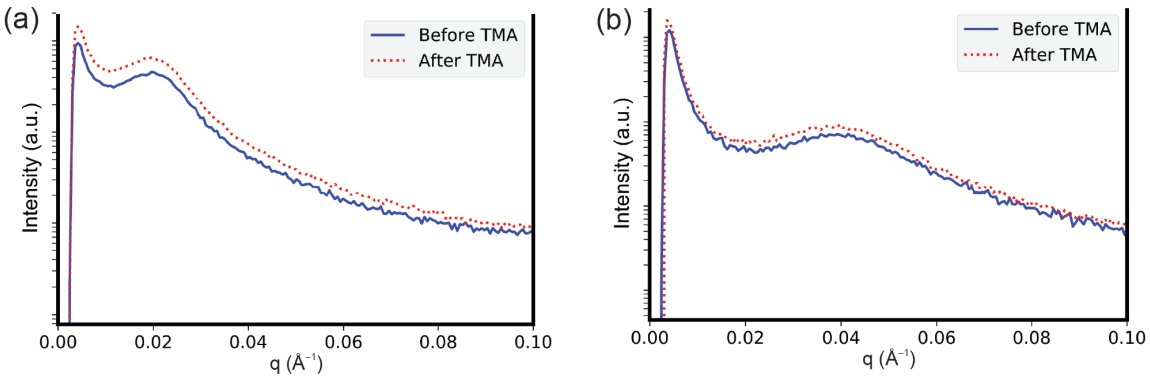

Figure 3.5. Transmission SAXS data of (a) a representative PoSSE-55k-20 PIMS (solid blue line) before and (dotted red line) after TMA exposure and (b) PVBC-24k-20 (solid line) before and (dashed line) after TMA exposure.

Attenuated total reflectance infrared spectroscopy (ATR-IR) suggests the macroinitiators remained largely intact during the PIMS process as the C–Cl stretch of the PVBC and the asymmetric S–O–C stretch of the sulfonic ester were retained. To convert the neutral macroinitiator domains into charged polyelectrolytes, the monoliths were soaked in an aqueous solution containing 45 wt% trimethylamine (TMA). ATR-IR showed complete disappearance of the C–Cl and S–O–C peaks in the PVBC and PoSSE monoliths, respectively (**Figure 3.6)**. ATR-IR data was acquired on various points of both the exterior and interior of the monolith to corroborate complete functionalization throughout the sample. Transmission SAXS was measured of the functionalized disks, showing a negligible change in the observed scattering pattern, indicating morphological integrity (**Figure 3.5**).

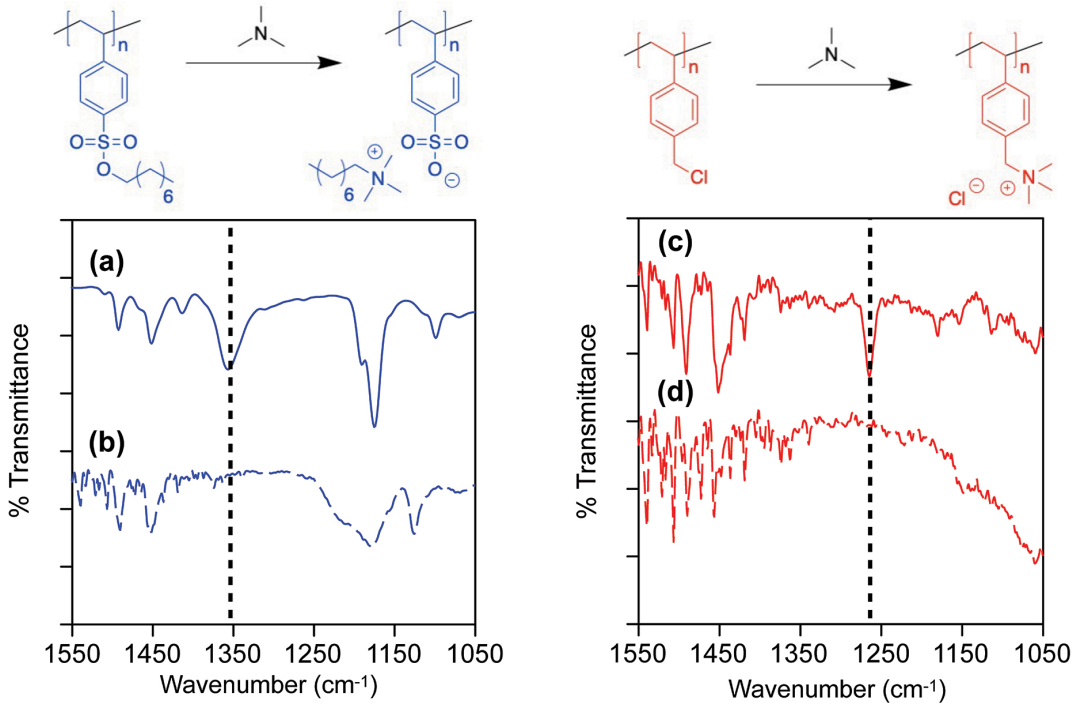

Figure 3.6. ATR-IR of (a) unfunctionalized and (b) TMA exposed PoSSE-62k-30 PIMS and (c) unfunctionalized and (d) TMA exposed PVBC-24k-20 PIMS.

The monoliths were functionalized in 24 hours upon exposure to TMA, even over significant thicknesses (millimeters). We attribute this rather rapid conversion to the functionalized polymer drawing amine into the polyelectrolyte domain, directly exposing the deeper parts of the sample to base solution. The monoliths may react faster than 24 h, but the exposure time was kept at 24 h to help ensure quantitative conversion.

After functionalization, the monoliths became more hydrophilic and slightly swelled in the presence of water. Although the outer dimensions of the sample remained essentially constant, the mass increased by around 4-6% after soaking in water. This low level of swelling resulted in some loss in mechanical integrity, and some monoliths, in particular those with 30 wt% macroinitiator loading, often cracked or broke into pieces after functionalization, especially as the swollen monoliths were subsequently dried. Similarly, exposure to trimethylamine revealed macrophase separation and inhomogeneities in both the PoSSE-55k-20 and PoSSE-55k-30 samples.

We further confirmed the successful functionalization using ion exchange with charged dyes. Each PIMS sample was soaked for 24 h in two different phosphate-buffered solutions, one containing negatively charged methyl red dye and the other positively charged toluidine blue dye. The unfunctionalized PIMS samples remained transparent and only a small amount of dye appeared to physisorb onto the surface. Further, the monoliths were the same mass before and after soaking. In contrast, the charged monoliths again increased in mass by around 4% from their dry weight, indicative of swelling and dye

uptake. The monoliths clearly absorbed the complementary-charged dye, emerging either dark orange or dark blue through the thickness of the material (**Figure 3.4**).

Ultraviolet-visible absorption spectroscopy (UV-vis) was used to determine the amount of dye absorbed into the monolith. Before functionalization, the PIMS monoliths absorbed a statistically negligible amount of dye after 24 h (**Figure 3.7**). After functionalization, the PoSSE monoliths absorbed a vast majority of the positively charged toluidine blue dye in solution and little of the negatively charged methyl red. The PVBC monoliths displayed the opposite behavior, absorbing almost all of the methyl red in solution, but not the toluidine blue. Fracturing the monoliths showed blue (for the PoSSE PIMS) or orange (for the PVBC PIMS) through the thickness of the sample (**Figure 3.4**). These data are consistent with the PIMS samples consisting of percolating, connected domains that allow the charged dyes to permeate through the material. This also indicates that despite the low swelling in the monoliths, the passive ion exchange kinetics allow some diffusion across several millimeters in a 24 h timespan.

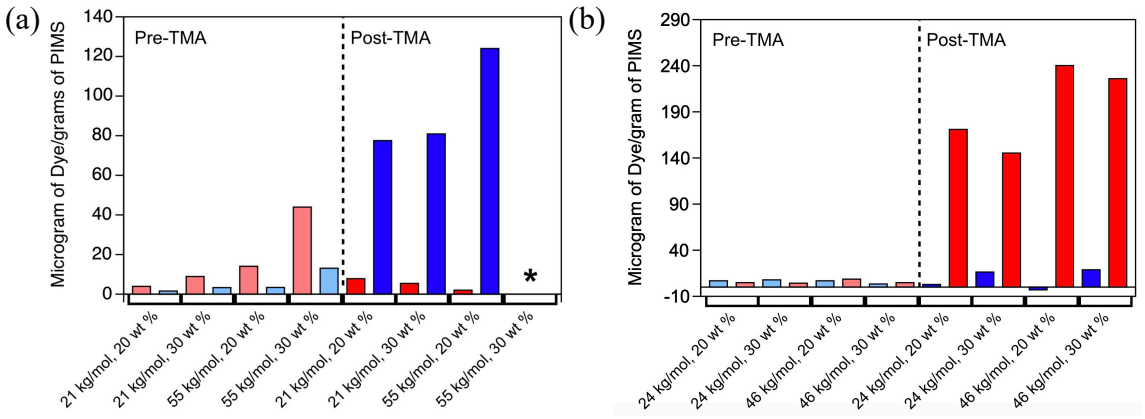

Figure 3.7. Dye absorption of methyl red (red) and toluidine blue (blue) dyes before and after TMA exposure for (a) PoSSE and (b) PVBC PIMS. *PoSSE-55k-30 disintegrated during testing which increased solution turbidity enough to obscure UV absorption.

The theoretical charge density of the materials is high. The sulfonic ester and the vinylbenzyl chloride guarantee a single charge per monomer with 100% functionality according to IR analysis. As an example, the PoSSE-21k-30 monolith contains 300 mg of PoSSE polymer in a 1 g sample. The sample therefore contains 1 mmol of charged monomers in each gram of dry monolith.

Because the crosslinked matrix has a fixed geometry, the volume of the PoSSE domain should not significantly change after functionalization to poly(styrene sulfonic acid). The only volume that can be consumed in swelling is the space freed up by removal of the *n*-octyl chains. If we then assume that the density of the PoSSE is the same as the density of the matrix (at roughly 1 g/cm^3), we calculate there to be approximately 2 charges·nm^{-3} within the polyelectrolyte domain.

Such a high charge density is difficult to achieve in soft materials; common ion exchange polymers have a dry charge density around 0.6 charge·nm^{-3}.[20] Deformation and expansion under swelling further decreases the charge density. In the materials we have prepared, however, the glassy matrix retains the shape and the covalent anchoring of the polyelectrolyte prevents leaching of the charged domain into the surrounding space. These restrictions force the volume to remain constant, even in the presence of excess water. Based on the ~4% swelling we measure in PoSSE-21k-30, we estimate that the monoliths absorb only 2.2 water molecules per charge. Water content at such a low level may be incapable of fully solvating the ions in the polyelectrolyte domain; common ion exchange polymers swell at least 10%.[20] In addition, because every monomer contains a charge, we expect the water to be evenly distributed throughout the polyelectrolyte domain.

We sought to verify the number of charges in the monoliths by measuring their ion exchange capacity (IEC). To do this, we functionalized PoSSE monoliths with TMA and crushed them into a powder to increase the accessible surface area. We then soaked the powder in 0.1 M H_2SO_4 to exchange the tetraalkylammoniums for protons. After the acid soak, the crushed material was rinsed with water multiple times and was then soaked in 1 M NaCl solution to exchange the protons for sodium ions. The salt solution was then titrated with sodium hydroxide to neutral using phenolphthalein as an indicator. The IEC indicated there was about half the expected number of charges in the monolith ($4 \cdot 10^{-4}$ mol charge/g monolith for PoSSE-62k-30 compared to a theoretical ion capacity of $1 \cdot 10^{-3}$ mol charge/g monolith).

We suspect this discrepancy could be caused by several factors. The first is the kinetics of passive exchange. With the swelling as low as the mass indicates, diffusion is likely quite slow to the center of the monoliths without any driving force. Secondly, the functionalization of the sulfonic ester with amines may be preventing efficient ion exchange with harder ions (protons).[21] If the softer ammoniums are staying bound to the sulfonic acid groups, even a high local concentration of protons will have trouble exchanging. Finally, the samples used were relatively small (less than 150 mg) which decreases the precision of the pH titration.

A similar trend was seen in the IEC of the PVBC PIMS. Instead of soaking in acid, the functionalized PIMS was soaked in 0.1 M NaOH solution to displace the chloride ions with hydroxide ions. After soaking in water to remove excess ions, the monolith was soaked in 1 M NaCl solution to release the hydroxide ions. The pH was then titrated to

neutral using HCl and phenolphthalein as the indicator. Again, this showed a lower ion exchange capacity than theoretically predicted ($8 \cdot 10^{-4}$ mol charges/g monolith for PVBC-24k-30 compared to the theoretical $2 \cdot 10^{-3}$ mol charge/g monolith). We again attribute this to the kinetics of the passive exchange, which are likely restricting the accuracy of the measurement.

3.5 Conclusions

Through the use of polymerization induced microphase separation, we have shown the ability to create polyelectrolyte-containing monoliths with high charge densities. Using two different macroinitiators, we formed monoliths with either positive or negative charges. By then exposing them to oppositely charged dyes, we showed through passive ion exchange that the domains percolate throughout the thickness of the monolith and contain only positive or negative fixed charges. We measured the ion concentration in an effort to show the extremely high ion densities and low levels of solvation. The ease of fabrication makes these materials good candidates for use in battery separators and separations membranes, among other applications.[2-5]

3.6 References

[1] Jenkins, A. D.; Kratochvíl, P.; Stepto, R. F. T.; Suter, U. W. Glossary of Basic Terms in Polymer Science (IUPAC Recommendations 1996). *Pure Applied Chemistry* **1996**, *68*, 2287–2311.

[2] Mauritz, K. A.; Moore, R. B. State of Understanding of Nafion. *Chem. Rev.* **2004**, *104*, 4535–4586.

[3] Kraytsberg, A.; Ein-Eli, Y. Review of Advanced Materials for Proton Exchange Membrane Fuel Cells. *Energy Fuels* **2014**, *28*, 7303–7330.

[4] Lee, H.; Yanilmaz, M.; Toprakci, O.; Fu, K.; Zhang, X. A review of recent developments in membrane separators for rechargeable lithium-ion batteries. *Energy Environ. Sci.* **2014**, *7*, 3857–3886.

[5] Harry, K. J. Lithium dendrite growth through solid polymer electrolyte membranes. PhD Thesis, University of California, Berkeley: Berkeley, CA, 2016.

[6] Chen, X. C.; Kortright, J. B.; Balsara, N. P. Water Uptake and Proton Conductivity in Porous Block Copolymer Electrolyte Membranes. *Macromolecules* **2015**, *48*, 5648–5655.

[7] Kim, S. Y.; Park, M. J.; Balsara, N. P.; Jackson, A. Confinement Effects on Watery Domains in Hydrated Block Copolymer Electrolyte Membranes. *Macromolecules* **2010**, *43*, 8128–8135.

[8] Jeon, C.; Han, J. J.; Seo, M. Control of Ion Transport in Sulfonated Mesoporous Polymer Membranes. *ACS Appl. Mater. Interfaces* **2018**, *10*, 40854–40862.

[9] Chen, L.; Hallinan, D. T., Jr.; Elabd, Y. A.; Hillmyer, M. A. Highly Selective Polymer Electrolyte Membranes from Reactive Block Polymers. *Macromolecules* **2009**, *42*, 6075–6085.

[10] Wang, P.; Anderko, A.; Young, R. D. Modeling Electrical Conductivity in Concentrated and Mixed-Solvent Electrolyte Solutions. *Ind. Eng. Chem. Res.* **2004**, *43*, 8083–8092.

[11] Jackson, G. L. Nanoconfined Water and Water-mediated Ion Transport in Model Lyotropic Liquid Crystals. PhD Thesis, University of Wisconsin-Madison: Madison, WI, 2018.

[12] Serpico, J. M.; Ehrenberg, S. G.; Fontanella, J. J.; Jiao, X.; Perahia, D.; McGrady, K. A.; Sanders, E. H.; Kellogg, G. E.; Wnek, G. E. Transport and Structural Studies of Sulfonated Styrene−Ethylene Copolymer Membranes. *Macromolecules* **2002**, *35*, 5916–5921.

[13] Rumyantsev, A. M.; Pan, A.; Ghosh Roy, S.; De, P.; Kramarenko, E. Y. Polyelectrolyte Gel Swelling and Conductivity vs Counterion Type, Cross-Linking Density, and Solvent Polarity. *Macromolecules* **2016**, *49*, 6630–6643.

[14] Zeldovich, K. B.; Khokhlov, A. R. Osmotically Active and Passive Counterions in Inhomogeneous Polymer Gels. *Macromolecules* **1999**, *32*, 3488–3494.

[15] Seo, M.; Hillmyer, M. A. Reticulated Nanoporous Polymers by Controlled Polymerization-Induced Microphase Separation. *Science* **2012**, *336*, 1422–1425.

[16] Schulze, M. W.; Hillmyer, M. A. Tuning Mesoporosity in Cross-Linked Nanostructured Thermosets via Polymerization-Induced Microphase Separation. *Macromolecules* **2017**, *50*, 997–1007.

[17] Moad, G.; Chong, Y. K.; Postma, A.; Rizzardo, E.; Thang, S. H. Advances in RAFT polymerization: the synthesis of polymers with defined end-groups. *Polymer* **2005**, *46*, 8458–8468.

[18] Kolomanska, J.; Johnston, P.; Gregori, A.; Domínguez, I. F.; Egelhaaf, H.-J.; Perrier, S.; Rivaton, A.; Dagron-Lartigau, C.; Topham, P. D. Design, synthesis and thermal behaviour of a series of well-defined clickable and triggerable sulfonate polymers. *RSC Advances* **2015**, *5*, 66554–66562.

[19] Goldfeld, D. J.; Silver, E. S.; Radlauer, M. R.; Hillmyer, M. A. Synthesis and Self-Assembly of Block Polyelectrolyte Membranes through a Mild, 2-in-1 Postpolymerization Treatment. *ACS Appl. Poly. Mater.* **2020**, *2*, 817–825.

[20] *AmberLite™ HPR9200 Cl Product Data Sheet*, 1st ed.; Dupont, 2019; pp 1–4.

[21] Boyd, G. E.; Larson, Q. V. The Binding of Quaternary Ammonium Ions by Polystyrenesulfonic Acid Type Cation Exchangers. *J. Am. Chem. Soc.* **1967**, *89*, 6038–6042.

Chapter 4. Determining the interaction parameter between polystyrene and poly(vinylbenzyl chloride) and a substitute polymer for microphase separated morphologies*

* This work was completed in collaboration with Dr. Eric Silver and Dr. Madalyn Radlauer of the Department of Chemistry at the University of Minnesota.

4.1 Introduction

Polystyrene (PS) is a widely used polymer in applications ranging from packing foam to disposable serviceware.[1] Derivatives of polystyrene that can be prepared by straightforward syntheses have been used as functionalizable polymers with tunable mechanical properties. Some of these polymers are made through post-polymerization modification of the parent polystyrene (e.g., sulfonation to poly(styrene sulfonate))[2] while other monomer derivatives of styrene are directly polymerizable, including methylstyrenes,[3] *tert*-butylstyrene,[4] sodium styrene sulfonate,[5] and vinylbenzoic acid.[6]

One of the most common styrenic derivatives is 4-vinylbenzyl chloride (VBC), which contains a chlorine substituted methylene in the para position of the aromatic ring. It is a bench stable monomer that is easily polymerized to poly(vinylbenzyl chloride) (PVBC) through normal free-radical and controlled-radical polymerizations.[7] PVBC is commonly used as a precursor to poly(vinylbenzyl ammonium chloride) (PVBAC), which is synthesized by exposing PVBC to aqueous ammonia solutions.[8] The resulting water-soluble polymer is cationic at certain pHs, and derivatives that form quaternary ammoniums using a trialkylamine (such as trimethylamine or tributylamine) result in permanent positive charges along the polymer chain and are used in a variety of anion exchange membranes.[9,10]

While ion-exchange resins often use VBC as a comonomer, multiple systems have also been described synthesizing both PS-*block*-PVBC (PS-*b*-PVBC) and PVBC-*b*-PS for uses including anion exchange membranes[11] and DNA complexation.[12] Despite the extensive use of VBC as a separate block or comonomer in PS systems, there has been

little study of their solid-state behavior, often because the PVBC is regularly functionalized in the step directly following polymer synthesis. Several studies have concluded, however, that PS and PVBC do not microphase separate in block polymer systems. In one study, a block polymer of PS-*b*-PVBC was shown to have a single glass transition temperature (T_g).[11] However, the T_g of PS and PVBC homopolymer are similar (~100 °C) and may be observed as one T_g even if the sample exhibits microphase separation. More recently, in work included in **Chapter 2**, we showed solid state PS-*b*-PVBC did not microphase separate, even at overall molar masses approaching 100 kg/mol, according to atomic force microscopy as well as transmission and grazing-incidence small-angle X-ray scattering (SAXS) measurements. Combined, these works suggest that PS is miscible with PVBC even at high molar masses and this is characterized by an extremely small (≈ 0) positive Flory-Huggins interaction parameter (χ). No study has quantitatively evaluated χ between PS and PVBC, which would quantify the enthalpic drive of the two polymers to separate.[13]

Chapter 3 includes the only evidence to suggest that χ is greater than zero, putting a lower bound on its value ($\chi > 0$). The work on charged systems in polymerization-induced microphase separation successfully used PVBC as a macroinitiator for a system where a polymerizing, actively crosslinking styrene/divinylbenzene (S/DVB) block led to polymerization-induced microphase separation (PIMS) forming a bicontinuous crosslinked monolith. The separate domains were confirmed using transmission SAXS, the first report of X-ray scattering observed in a PS/PVBC system under the assumption that a lightly crosslinked S/DVB behaves enthalpically similarly to PS. The system demonstrates that at

some molar mass, a PS-*b*-PVBC polymer will have a χN high enough to drive microphase separation, meaning the $\chi_{PS\text{-}PVBC}$ is necessarily greater than zero.

In an effort to more precisely quantify $\chi_{PS–PVBC}$, we use SAXS measurements of a homopolymer blend to place an approximate upper limit on the value of $\chi_{PS\text{-}PVBC}$. We also report vinylbenzyl nitrate ($VBNO_3$), a derivative monomer of vinylbenzyl chloride that can be polymerized to poly(vinylbenzyl nitrate) ($PVBNO_3$) in a similar fashion to PVBC and functionalized to a cationic ammonium polyelectrolyte. (143k PS)-*b*-(185k $PVBNO_3$) shows clear microphase separation with PS by differential scanning calorimetry, atomic force microscopy, and grazing-incidence SAXS, making it a suitable substitution for PS-*b*-PVBC in applications requiring solid-state microphase separation. We conclude that it has a significantly higher χ with PS than PVBC but are unable to quantify a precise $\chi_{PS\text{-}PVBNO3}$ due to thermal constraints associated with $PVBNO_3$.

4.2 Experimental

4.2.1 Materials

Unless otherwise noted, all chemicals were purchased from Sigma Aldrich and used as received. Styrene (99%) was distilled after drying over calcium hydride. Azobisisobutyronitrile (AIBN) (98%) was recrystallized from methanol and dried under reduced pressure. 4-Vinylbenzyl chloride (90%) was run through a plug of basic alumina to remove inhibitors. The chain transfer agent (4-Cyano-4-[(dodecylsulfanylthiocarbonyl)sulfanyl]pentanoic acid; CTA) was synthesized according to previous literature procedures.[14]

4.2.2 Instrumentation

NMR spectra were recorded on a Bruker Advance III HD 500 spectrometer. Chemical shifts are reported in δ units, expressed in ppm downfield from tetramethylsilane using residual protiosolvent as an internal standard ($CDCl_3$, ^1H: 7.26 ppm). Size exclusion chromatography (SEC) was performed in THF (25 °C, 1 mL/min) on an Agilent Infinity 1260 HPLC system equipped with three Waters Styragel HR columns, a Wyatt DAWN HELEOS-II 18-angle laser light scattering detector, and a Wyatt Optilab T-rEX differential refractive index detector. Absolute weight-average molar mass was determined using light scattering detector with a d*n*/dc = 0.171 mL g^{-1} for PVBC, 0.185 mL g^{-1} for PS, and 0.1494 mL g^{-1} for $PVBNO_3$ (**Section 4.2.6**). Thermal gravimetric analysis (TGA) was performed on a TA Instruments Q500 under house nitrogen with a heating rate of 10 °C min^{-1}. Differential scanning calorimetry (DSC) analyses were performed on a TA Instruments Discovery DSC using standard aluminum T-zero pans with hermetic lids. Scans were conducted under house nitrogen at a heating or cooling rate of 10 °C min^{-1}. Infrared spectroscopy measurements were performed on a Bruker Alpha Platinum ATR spectrometer with a built-in diamond attenuated total reflection set up and a DLaTGS detector. Ellipsometry of thin films was performed on a J. A. Wollam Co., Inc. V-VASE using measurements at 3 angles and a Cauchy model for the polymer films. Atomic force microscopy measurements were performed on a Bruker Nanoscope V Multimode 8 with a Multifrequency Lockin Amplifier (MLA)™ attachment from Intermodulation Products. Grazing-incidence small-angle X-ray scattering (GISAXS) Data was collected at the 8-ID-E beamline of the Advanced Photon Source at Argonne National Laboratory. An X-ray

wavelength of 10.915 keV = 1.14 Å was used to irradiate the sample and the scattering intensity distribution was capture by a Pilatus 1M detector at an incident angle of 0.14°. The intensities (I) are plotted with respect to q, where $q = (4\pi/\lambda)\sin(\theta/2)$, λ is the wavelength of the incident X-ray beam and θ is the scattering angle.

4.2.3 Transmission SAXS measurements of PS/PVBC blends

Transmission small angle X-ray scattering (SAXS) measurements were performed on a SAXSLab GANESHA300XL instrument of the Characterization Facility at the University of Minnesota. Cu Kα X-rays (λ = 1.54 Å) generated by a Xenocs Geni3DX source were collimated through 2 sets of 4-bladed slits (JJ X-ray, A/S). 2D-SAXS patterns were acquired using a Dectris EIGER R 1M detector (7.72 cm x 7.99 cm rectangular area) with 1030 x 1065 pixels (75 µm x 75 µm pixel size) at a sample-to-detector distance of 46.8 cm.

Polymer blend samples were prepared by first removing the trithiocarbonate end-group from the RAFT-grown homopolymers of PS and PVBC. Following previous literature,[15] the homopolymers were dispersed in THF with AIBN radical initiator and tributyltin hydride, which acted as a radical trap. The mixture was heated to 70 °C for three hours and the polymer was then precipitated into methanol, filtered with a 0.2 µm PVDF filter, and dried overnight under high vacuum. NMR confirmed quantitative removal of the CTA end-groups. The homopolymers were then weighed out to their critical composition,[16] following the equation:

$$\phi_2 = \frac{N_2^{1/2}}{N_1^{1/2} + N_2^{1/2}}$$

where ϕ_i is the volume fraction of the i^{th} component and N_i is the degree of polymerization normalized to a chosen reference volume. The PS has an M_w = 85 mol^{-1} and the PVBC has a molar mass of M_w = 13 kg mol^{-1}, which means the critical composition is ϕ_2 = 0.718 and ϕ_1 = 0.282.

0.078 g of PVBC and 0.0307 g of PS were mixed together in 1 mL of benzene and frozen in N_2 (l). The solid sample was lyopholized under high vacuum overnight. The remaining powder was melt-pressed to 1 mm thickness at 140 °C using steel spacers to control the thickness and secured to a Linkam hot-stage with metal clips. The samples were placed under vacuum and equilibrated at each temperature for 10 min before measurement. Measurements were taken from 40 °C to 160 °C in 20 °C increments. All 2D-SAXS patterns were azimuthally-integrated to obtain the absolute one-dimensional scattered intensity I(q) versus q plots. The included SAXSLab software applied an absolute calibration to the data based on the thickness of the material, the incident X-ray intensity based on a blank collection between each measurement, the number of photons scattered, and the number of photons transmitted through the sample.[17]

4.2.4 Synthesis of vinylbenzyl nitrate

Vinylbenzyl chloride (1 g, 6.6 mmol, 1 equiv.) was stirred with silver nitrate (2.23 g, 13.1 mmol 2 equiv.) in acetonitrile (5 mL) for 3 days at room temperature. The precipitated silver chloride was filtered off and the resulting solution diluted with ice water (200 mL) and extracted with DCM (2x5 mL). The solvent was removed by rotary evaporation and the resulting yellow oil purified through a silica plug using 30:70 DCM:hexanes, where the monomer moves at an $R_f \approx 0.5$. The solvent was removed by

rotary evaporation and the resulting $VBNO_3$ monomer dried under vacuum to yield a clear, colorless oil (85% yield). T_m = 11 °C. ^{1}H NMR in $CDCl_3$ (δ,ppm): 5.31 (d, 1H, J = 10.9 Hz), 5.41 (s, 2H), 5.79 (d, 1H, J = 17.6 Hz), 6.72 (dd, 1H, J = 17.6, 10.9 Hz), 7.36 (d, 2H, J = 7.7 Hz), 7.44 (d, 2H, J = 7.7 Hz) (**Figure 4.1**); ^{13}C NMR in $CDCl_3$ (δ,ppm): 74.7, 115.3, 126.8, 129.5, 131.6, 136.2, 138.9 (**Figure 4.2**); **HRMS (EI+):** Calculated for $C_9H_9NO_3^+$ (M^+): 179.0577, Found 179.0576 (**Figure 4.3**)

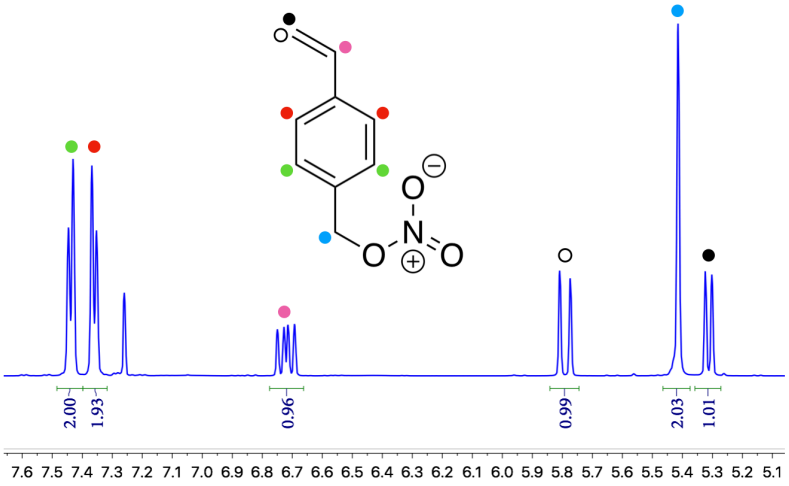

Figure 4.1. ^{1}H NMR spectrum of $VBNO_3$

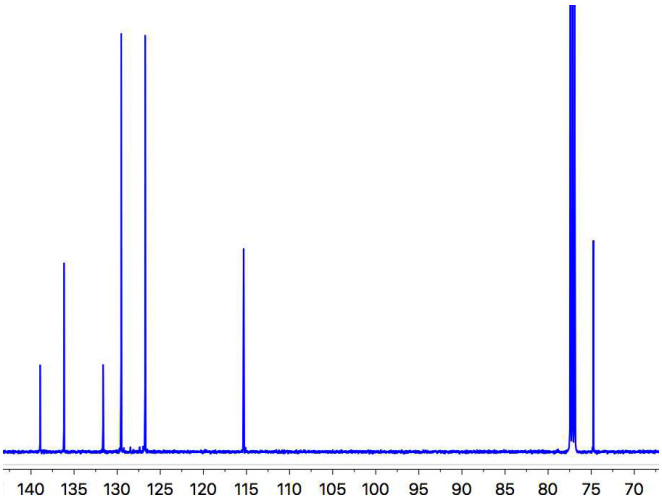

Figure 4.2. ^{13}C NMR spectrum of $VBNO_3$

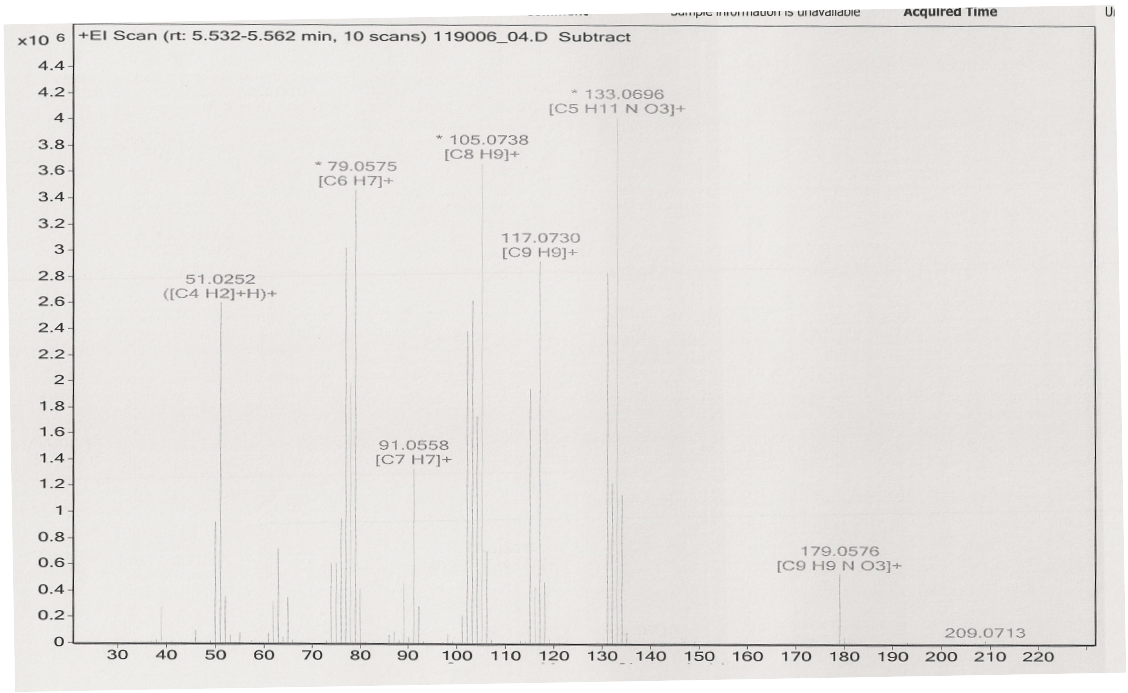

Figure 4.3. High resolution GC-MS spectrum of $VBNO_3$

4.2.5 Synthesis of poly(vinylbenzyl nitrate) through RAFT polymerization

A typical reversible addition-fragmentation chain transfer (RAFT) polymerization combined CTA (11.3 mg, 28 µmol, 1 equiv.), azobisisobutyronitrile (1.4 mg, 8.5 µmol, 0.3 equiv.), and $VBNO_3$ (1 g, 5.6 mmol, 200 equiv.) in dry THF (2.7 mL, 2.7 mL/g monomer) in a flame-dried Schlenk flask. The mixture was freeze-pump-thawed three times and then backfilled with 5 psig of argon. The polymerization mixture was heated to 80 °C for 6-48 hours and the polymerization stopped by immersion in N_2 (*l*). The reaction mixture was diluted in 2-3 mL THF and precipitated into 100 mL methanol. The polymer was removed by filtration through a 0.2 µm PVDF filter and dried under high vacuum overnight.

4.2.6 Batch d*n*/dc measurements

For d*n*/dc of pol(vinylbenzyl chloride), see **Section 3.3.6**. d*n*/d*c* was determined for $PVBNO_3$ polymer by dissolving 6 concentrations (0.5, 1, 2, 3, 4, and 5 mg/mL) of polymer into HPLC grade THF. The solution refractive index was measured at a flow rate of 0.2 mL/min using a Wyatt Optilab T-rEX differential refractive index detector at a wavelength of 658 nm.

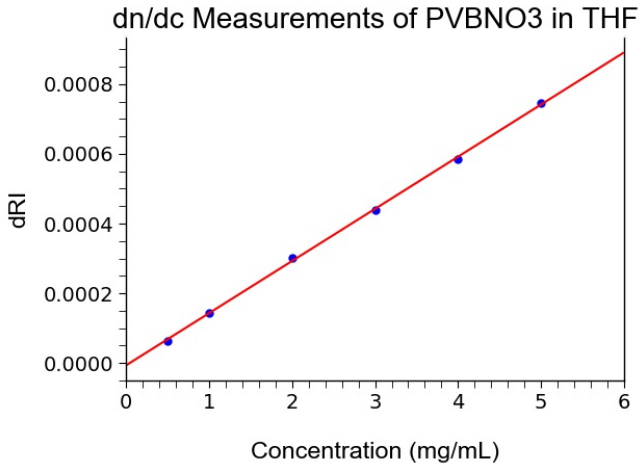

Figure 4.4. d*n*/dc measurement of $PVBNO_3$ in THF, giving a slope of 0.1494 ± 0.0018 mL g^{-1}.

4.3 Discussion and Results

4.3.1 Determining an upper bound for $\chi_{PS-PVBC}$

Making an estimate of the Flory-Huggins interaction parameter, χ_{ij}, between two polymers is often done by measuring the order-to-disorder transition of a diblock polymer as the sample is heated above its order-to-disorder transition temperature (T_{ODT}). The transition is usually found either through rheological experiments (where a change in modulus at T_{ODT} indicates a transition from an ordered to disordered state) or scattering

experiments (where either X-ray or neutron scattering shows the loss of a clear ordered morphology upon traversing T_{ODT}).

The mean field theoretical models predict that T_{ODT} for a dymmetric diblock polymer occurs when $\chi_{ij}N = 10.5$. That means that for systems with small interaction parameters, the polymer needs a high molar mass (and hence high N) to show microphase separation at accessible temperatures (T_{ODT} must be above the highest T_g in the system to observe the transition). $\chi_{PS–PVBC}$ is so small that there have been no reported diblock polymers of a high enough molar mass to observe a T_{ODT}.

The block polymer limit can be circumvented using homopolymer blends. In a mix of two differing homopolymers of the same relative number of repeat units, a polymer melt will macrophase separate at a $\chi_{ij}N > 2$. A simple test can be done to determine if $\chi_{ij}N$ is greater than 2 by drop casting a solution of two homopolymers mixed in a volatile solvent. When the solvent has evaporated, a macrophase separated system will turn opaque if there is a sufficient difference in refractive index, and a miscible homopolymer blend will remain optically transparent. Trials with PS and PVBC homopolymers up to 100 kg mol^{-1} remained clear, demonstrating that even homopolymers at high molar masses will not macrophase separate at room temperature.

These data show that $\chi_{PS–PVBC}$ is exceedingly small. Similarly small interaction parameters have been observed in previous studies, originating with the determination that deuterated analogues of a hydrogen-containing polymer will have an exceedingly small, but greater than zero, interaction parameter.[18] In these polymer systems where higher molar masses are difficult to reach, or the interaction parameter is too low to achieve phase

separation, a technique was developed based on a binary homogeneous blend scattering equation derived by De Gennes.[16] The correlation function is based on mean-field random-phase approximation for a mixture of amorphous polymers mixed at a volume fraction of component 1, Φ:

$$S^{-1}(q) = [N_1 \Phi g_D(R_{g1}, q)]^{-1} + [N_2(1-\Phi) g_D(R_{g2}, q)]^{-1} - 2\chi \tag{4.1}$$

where

$$g_D(R_g, q) = 2\left[R_g^2 q^2 + e^{-R_g^2 q^2} - 1\right] / R_g^4 q^4 \tag{4.2}$$

and in which $q = 4\pi\lambda^{-1}\sin(\theta/2)$ is the scattering wave vector, N is the number of volume normalized segments per polymer molecule, and $R_g = b(N/6)^{1/2}$ is the radius of gyration for a Gaussian coil where b is the statistical segment length of the polymer and is a fit parameter in the model. The equation models fluctuations in a blend of two homopolymers, which even without any macrophase separation will show some scattering because of density fluctuations in the material. These fluctuations can be measured using standard scattering characterization with techniques that allow for absolute intensity calibration.

Bates *et al.* demonstrated this concept using neutron scattering on a blend of low molar mass deuterated and non-deuterated polybutadiene.[18] The polymers were mixed at a critical composition and their calibrated scattering at various temperatures was fit to the De Gennes model. The final calculated equation for χ using the segmental volume of polybutadiene was:

$$\chi = \frac{0.326}{T} - 2.3 \cdot 10^{-4} \tag{4.3}$$

The χ measured around room temperature was therefore on the order of 10^{-3}. Similar work has been done with neutron scattering on other systems including poly(vinyl ethylene) and poly(ethylethylene),[19] polypropylene,[20] and polylactide.[21]

In this work, we use absolute intensity SAXS measurements to find the effective χ from a PS/PVBC homogeneous binary blend. Using a SAXSLab Ganesha system, we are able to calibrate intensity using sample thickness, the number of incident photons (measured during a blank collection between each sample), the number of scattered photons, and the number of transmitted photons. We can analyze the data using SasView5,[22] which allows the calculation of the X-ray scattering length densities (SLD) at 1.54 Å wavelength X-rays of $9.57 \cdot 10^{-6}$ Å^{-2} for polystyrene and $10.0 \cdot 10^{-6}$ Å^{-2} for poly(vinylbenzyl chloride). Plotting the data for temperatures from 40 °C to 140 °C in 20 °C increments, we can see from the overlap that all of the data sets are nearly identical (**Figure 4.5**). At temperatures of 160 °C and above, we see inconsistent data, likely due to change in sample shape from flow at higher temperatures.

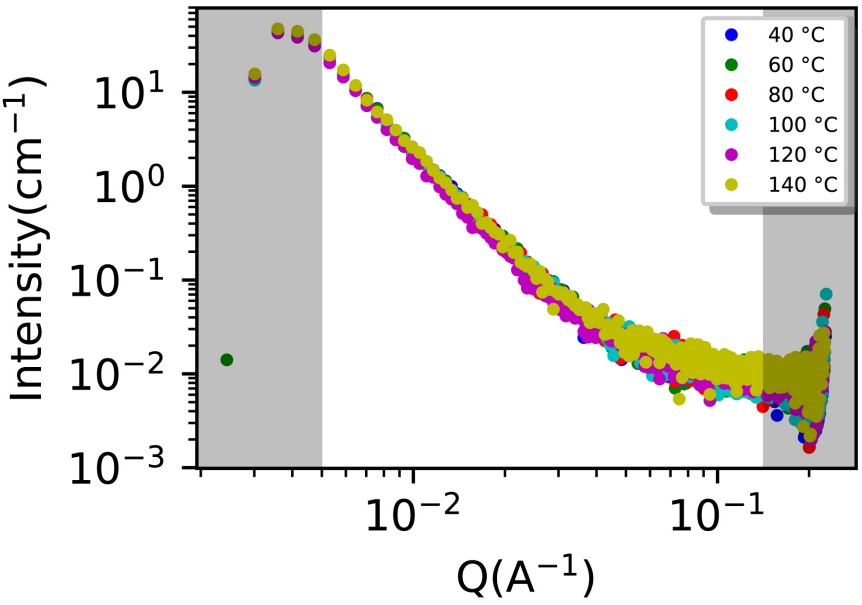

Figure 4.5. $I(q)$ v. q for all data sets 40-140 °C. The shaded region at low and high q shows data points excluded from the fitting.

We can take these data and fit them in three formats to attempt to estimate the effective interaction parameter. First is to fit the random phase approximation (RPA) equation to a graph of $I(q)$ v. q by using a Levenberg-Marquardt algorithm to fit the equation:

$$I(q) = (\mathrm{SLD}_1 - \mathrm{SLD}_2)^2 \cdot S(q) \tag{4.4}$$

where $S(q)$ is defined using **Eq. (4.1)**. Following precedent, the data was restricted to the q range between 0.005 Å^{-1} and 0.15 Å^{-1} due to scattering from imperfections in the material at low q and low signal at high q. The equation requires the fitting of χ as well as the statistical segment lengths for both PS and PVBC. The following parameters have been derived or measured for both polymers used in this experiment:

	N	ρ (g/cm^3)	ϕ	V (cm^3/mol)	SLD (10^{-6} Å^{-2})
PS	816	1.046	0.269	99.57	9.57
PVBC	86	1.120	0.731	136.3	10.0

Table 4.1. Parameters used for fitting the shape independent RPA model of two-component homogeneous polymer blends.

After multiple attempts, we were unable to fit the equations to the data (the errors for each variable were on the order of magnitude or above of the fit value). To try to calculate a more suitable fit, we attempted to add in fitting parameters for both intensity (to compensate for errors in SLD calculations) and background (to compensate for nonsample scattering), but were unable to reach a better result.

The second method for determining χ is to use an intermediate q approximation to narrow the RPA model (**Eq. (4.1)**)[20] which results in the following equation:

$$S(q)^{-1} = \frac{1}{N_{\mathrm{PS}}\phi_{\mathrm{PS}}} + \frac{1}{N_{\mathrm{PVBC}}\phi_{\mathrm{PVBC}}} - 2\chi + \frac{q^2 b^2}{12}\frac{1}{\phi_{\mathrm{PS}}\phi_{\mathrm{PVBC}}} \tag{4.5}$$

where:

$$b^2 = \frac{b_{\mathrm{PS}}^2}{V_{\mathrm{PS}}\phi_{\mathrm{PS}}} + \frac{b_{\mathrm{PVBC}}^2}{V_{\mathrm{PVBC}}\phi_{\mathrm{PVBC}}} \tag{4.6}$$

We can therefore plot I^{-1} v. q^2 and fit to a line to calculate χ from the y-intercept c. By converting $S(q)$ to $I(q)$ using **Eq. (4.4)** and rearranging to isolate the interaction parameter, we find that the relation between c and χ is:

$$\chi = -\frac{1}{2}\left[c(\mathrm{SLD}_{\mathrm{PS}} - \mathrm{SLD}_{\mathrm{PVBC}})^2 - \frac{1}{N_{\mathrm{PS}}\phi_{\mathrm{PS}}} - \frac{1}{N_{\mathrm{PVBC}}\phi_{\mathrm{PVBC}}}\right] \tag{4.7}$$

After converting the PS/PVBC data to $I(q)^{-1}$ v. q^2, however, we find that the data is not linear over a significant q range and there is a large amount of noise. Restricting the

q values (this time between 0.01 $Å^{-1}$ and 0.15 $Å^{-1}$), we fit a line to the data to try to approximate what an upper bound to the χ value might reasonably fall. Below is a representative plot and linear fit for the data at 40 °C:

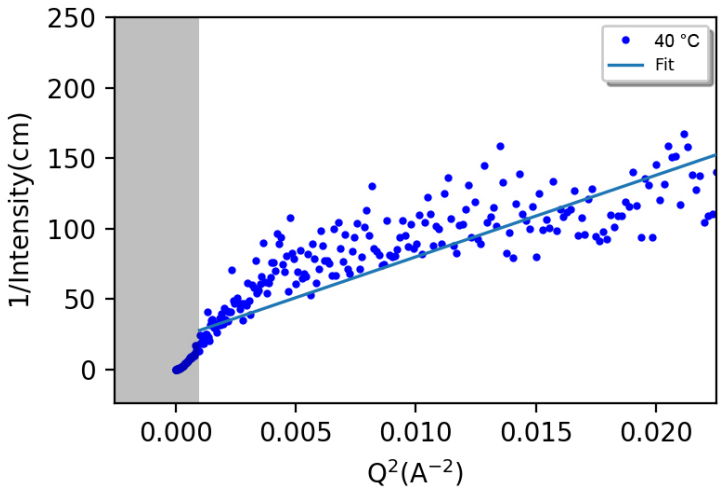

Figure 4.6. Representative $I^{-1}(q)$ v. q^2 plot for 40 °C. The shaded region at low q represents data that is excluded from the linear fit.

Despite the poor fits of these lines, the data show y-intercepts ranging from 21.9 cm at 40 °C to 2.9 cm at 120 °C, corresponding to $\chi_{PS–PVBC}$ between $1 \cdot 10^{-2}$ and $1.02 \cdot 10^{-2}$. Further adjusting the fit by changing the range of included data does not appreciably change the estimated effective interaction parameter as they all have a small absolute value for c, rendering the first term of **Eq. (4.7)** significantly smaller than the latter two (which are experimental parameters independent of the fit). These numbers are likely unreliable due to the high noise and poor fit to a linear model. The poor quality of data is further visible by plotting each set as a Kratky plot, or $q^2I(q)$ v. q. In a system that followed expected behavior, there would be a steady increase in this plot at low q leading to a plateau from which the statistical segment length of the polymer can be calculated. In our data,

there is instead a sharp decrease at low q followed by a steady rise. The same pattern is noted in all data sets.

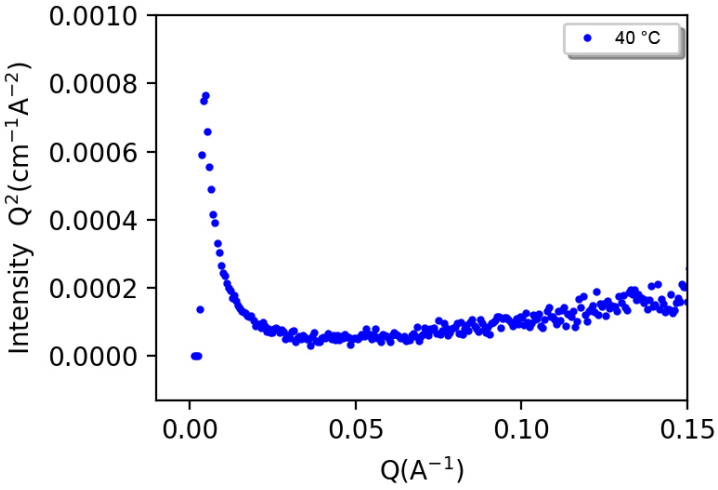

Figure 4.7. Representative Kratky plot for 40 °C.

The data collection through a lab source SAXS has not previously been used for χ measurements in homogeneous polymer blends. The higher noise and presence of significant incoherent scattering in X-rays likely means that it is not a suitable method for these procedures, despite the capability for absolute intensity calibration. Future neutron scattering studies may be able to further specify the χ value between PS and PVBC.

4.3.2 Vinylbenzyl nitrate as a substitute

Because of the exceedingly low interaction parameter between PS and PVBC, we started investigating other styrenic monomers that are room-temperature stable and easily polymerizable, have a significantly higher drive to microphase separate from PS, and can be modified postpolymerization to a polyelectrolyte through similar mechanisms as PVBC. We targeted a replacement that was similarly easy to polymerize through controlled-radical

polymerization and would allow for synthesis of a wide range of block polymer architectures.

Nitrate containing molecules are often stable analogues of chlorine containing compounds. Although nitrate is a poorer leaving group than chloride, it is still readily displaced by amines, carboxylates, hydroxides, and amides through S_N2 substitution.[23] We replace the chlorine in VBC with a nitrate group, forming a stable analogue of VBC.

Vinylbenzyl nitrate (VBNO3) is made through the room temperature reaction of silver nitrate with VBC (**Scheme 4.1**). Following previous syntheses of similar compounds,[24] vinylbenzyl chloride was stirred with silver nitrate in acetonitrile for 3 days at room temperature. After filtering off the silver chloride byproduct, the final monomer was obtained after flash chromatography through a short silica plug. The colorless oil product was stable at room temperature in air and could be stored for extended periods (>6 months) in a freezer with small amounts of butylated hydroxytoluene inhibitor.

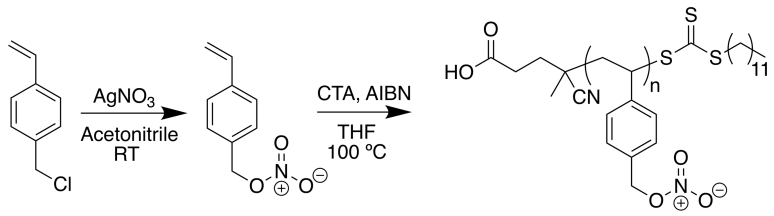

Scheme 4.1. Synthetic scheme for the synthesis of $VBNO_3$ and $PVBNO_3$.

4.3.3 Polymerization of vinylbenzyl nitrate

Because of the susceptibility of $VBNO_3$ to reactivity with a wide range of nucleophiles, it cannot be polymerized using anionic polymerization like many other styrenic monomers. Instead, $VBNO_3$ was polymerized using controlled radical polymerization similar to the polymerization of VBC. Well-controlled RAFT

polymerization of $VBNO_3$ yielded polymers with well-controlled molar masses and narrow dispersities ($Đ < 1.2$ for short polymerization times) (**Table 4.2**).

Reaction time (h)	[M]:[I]	$M_{n,NMR}$ (kg · mol^{-1})	$M_{n,SEC}$ (kg · mol^{-1})	$Đ$
6	200	36.7	4.2	1.07
12	200	37.4	19.4	1.05
6	550	*	24	1.10
42	550	*	95	1.45

Table 4.2. Samples of $PVBNO_3$. *samples did not have identifiable end group

Kinetic tracking of the polymerization showed a consistent increase in molar mass, with a quick initiation to 12.7 kg/mol after one hour and then consistent addition of 1.4 kg/mol per hour, showing first order kinetics with respect to monomer consumption. After six hours, a final molar mass of 22.4 kg/mol was reached according to THF SEC-MALS (**Figure 4.8**). The dispersity monotonically increased over the reaction time from 1.02 to 1.12.

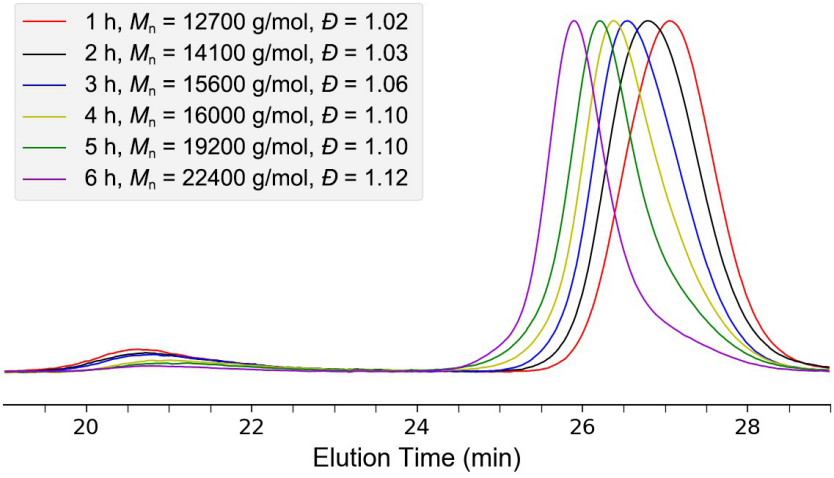

Figure 4.8. Normalized differential refractive index data of $PVBNO_3$ over a 6 hr polymerization. M_n and $Đ$ were calculated using SEC. Corresponding M_n by NMR: 1 h = 20.3 kg · mol^{-1}, 2 h = 25.3 kg · mol^{-1}, 3 h = 31.4 kg · mol^{-1}, 4 h* = 50.8 kg · mol^{-1}, 5 h* = 70.1 kg · mol^{-1}, 6 h* = 56.3 kg · mol^{-1}. *indicates poor end group resolution by NMR.

4.3.4 Thermal properties of $PVBNO_3$

Organic nitrate esters are known to thermally degrade under elevated temperatures through a variety of mechanisms.[25] Poly(vinylbenzyl nitrate) is stable at room temperature. It is shock stable and has no reaction when hammered against a steel plate. Thermogravimetric analysis (TGA) under both nitrogen and air showed the polymer is thermally stable to 170 °C. It slowly begins to lose 5% of its mass until a rapid mass loss of 55% at 193-200 °C, for all heating rates above 1 °C min^{-1} (**Figure 4.9a-c**). The remaining 45% mass is stable to above 320 °C. The extremely fast decomposition likely follows an explosive decomposition path, which results in the degradation of the polymer to formaldehyde (and potentially other low-carbon aldehydes) along with nitrogen dioxide, nitric oxide, and water. At the slowest heating rate, we see a much slower decomposition rate as well (**Figure 4.9d**). The sample first has a partial decomposition of 25% mass loss

likely corresponding to the release of nitrogen dioxide; it then slowly loses mass until it reaches the same 55% plateau as the faster heating rates. The slower decomposition pathway is also observed in other alkyl nitrates, generating a remaining alkyl radical after the release of NO_2 that can undergo a variety of reactions with the remaining material.[26] The result is a mix of more complex products including alkyl nitrites and nitromethane along with nitrogen dioxide and nitric oxide.[25,26] Since the polymer is more heavily weighted with carbon, a carbonaceous char remains for all samples that is thermally stable to high temperatures. Differential scanning calorimetry (DSC) at 10 °C/min heating rate showed a clear glass transition temperature, T_g, at 72 °C (**Figure 4.10**).

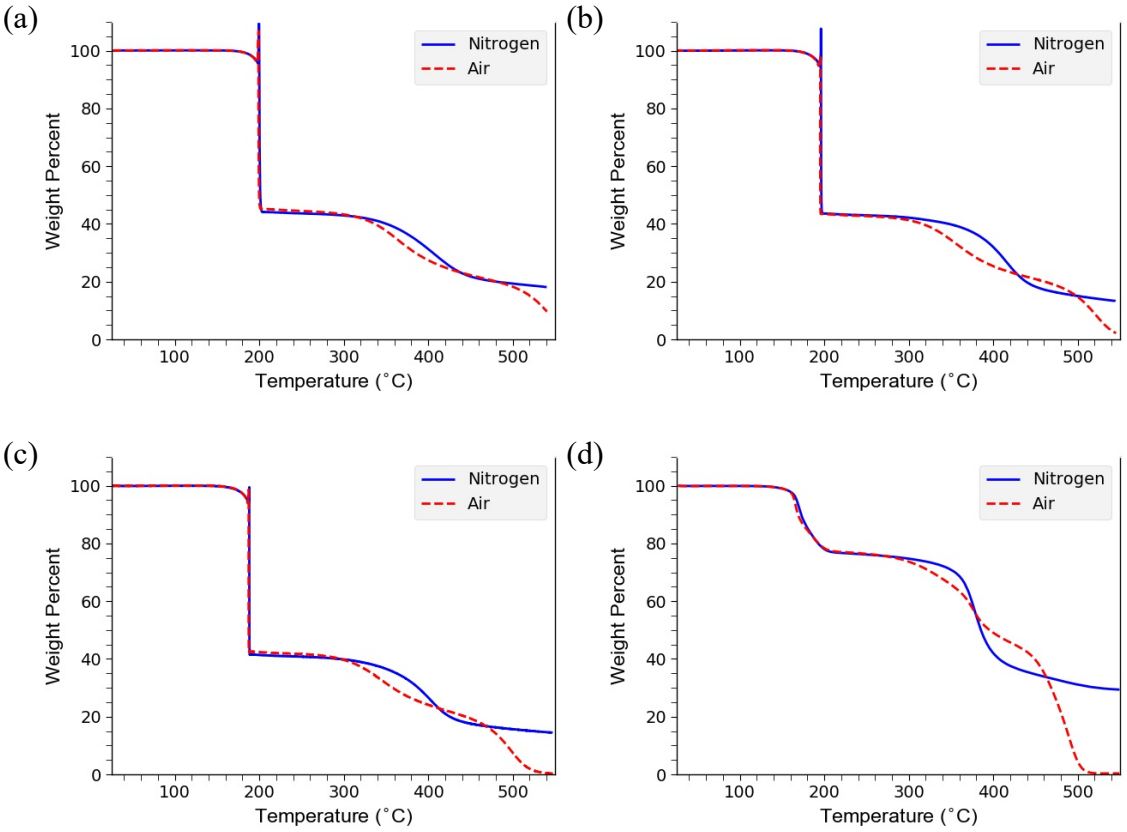

Figure 4.9. TGA analysis of $PVBNO_3$ under nitrogen (solid blue line) and air (dashed red line) with heating rates of (a) 20 °C min^{-1}, (b) 10 °C min^{-1}, (c) 5 °C min^{-1}, and (d) 1 °C min^{-1}

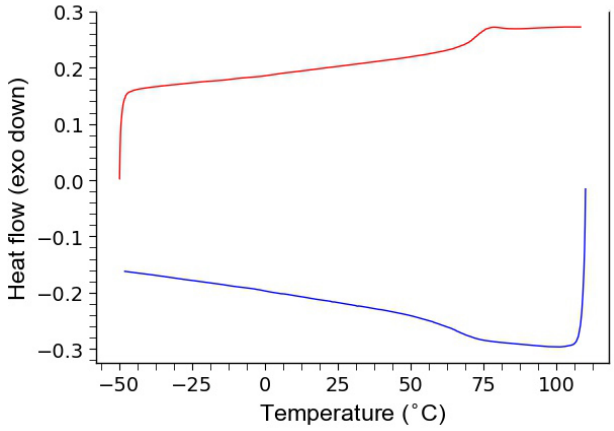

Figure 4.10. DSC analysis of $PVBNO_3$ (10 °C min^{-1} heating rate, 2nd heating curve shown)

4.3.5 Functionalization of $PVBNO_3$ with trimethylamine

The ease of functionalization was demonstrated by submerging $PVBNO_3$ in a 22.5 wt% solution of trimethylamine (TMA) in water. The polymer, which is not water soluble, immediately disperses in TMA solution into a cloudy mixture. After 30 min, the reaction mixture turned clear, similar to the functionalization of PVBC. The mixture was stirred overnight, diluted 10x with water, and freeze-dried to remove solvent and excess TMA. ATR-IR spectroscopy showed complete disappearance of the two (1275 cm^{-1} and 1622 cm^{-1}) nitrate peaks and the appearance of a strong N-C stretch at 1326 cm^{-1} and an N-C wag at 1480 cm^{-1} (**Figure 4.11**), indicative of complete conversion to the poly(vinylbenzyl trimethylammonium nitrate) derivative (PVBAN).

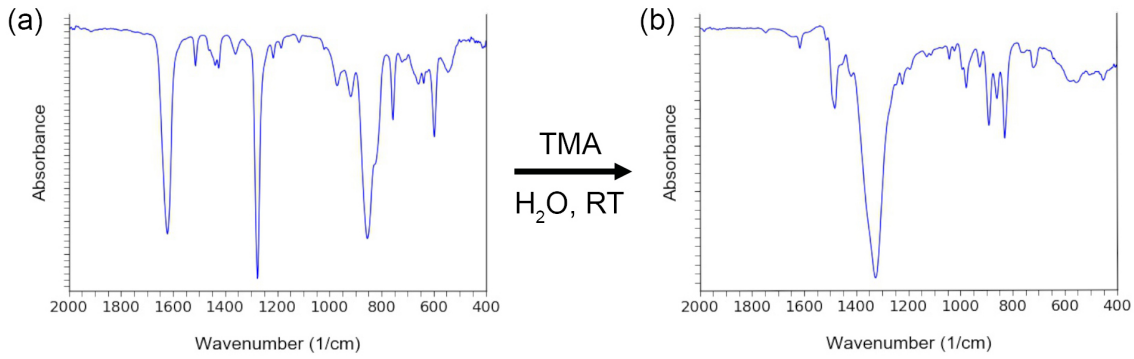

Figure 4.11. ATR-IR of (a) $PVBNO_3$ and (b) PVBAN showing the disappearance of nitrate ester peaks at 1275 cm^{-1} and 1622 cm^{-1} and appearance of ammonium peaks at 1326 cm^{-1} and 1480 cm^{-1}.

To test the kinetics of $PVBNO_3$ functionalization, a diblock polymer (PS–$PVBNO_3$) was synthesized by addition of $PVBNO_3$ to a PS (M_n = 134 kg mol^{-1}) macroinitiator to prevent dissolution of the functionalized polymer into aqueous solution (M_n = (134 kg mol^{-1} PS)-*b*-(185 kg mol^{-1} $PVBNO_3$)). The diblock polymer was spin coated from a 10 wt% solution in chlorobenzene onto native oxide silicon wafers to produce a thin film around 1 μm thick. Using ATR-IR, we monitored the disappearance of nitrate peaks and the appearance of ammonium peaks over time after exposure to TMA vapor inside of a sealed chamber (**Figure 4.12**). The thin film was completely functionalized to the trimethylammonium nitrate in less than 1 hour according to this IR spectroscopic analysis.

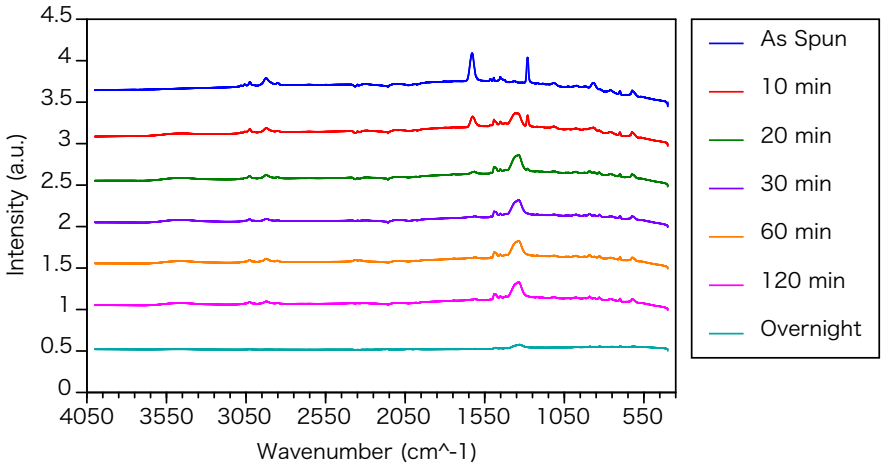

Figure 4.12. ATR-IR spectra of PS–PVBNO$_3$ films on silicon wafer substrates exposed to trimethylamine vapor for varying periods of time: as spun (blue), 10 min (red), 20 min (green), 30 min (purple), 60 min (orange), 120 min (magenta), and overnight (teal).

4.3.6 Confirmation of microphase separation in PS-*b*-PVBNO$_3$

VBNO$_3$ was shown to efficiently add to PS using RAFT chain extension to form a PS–PVBNO$_3$ block polymer. We then sought to confirm that $\chi_{PS–PVBNO3}$ is a larger interaction parameter than $\chi_{PS–PVBC}$, making PVBNO$_3$ a more suitable monomer choice in applications requiring solid-state microphase separation. Unfortunately, TGA of the diblock PS–PVBNO$_3$ showed thermal instability similar to the PVBNO$_3$ homopolymer with significant degradation at temperatures above 150 °C (**Figure 4.13a**). Visible polymer degradation at higher pressures was visually noted after DSC measurements in hermetically sealed pans, leading to a measurement ceiling temperature around 120 °C. The instability precludes determining an order-to-disorder transition in any PS–PVBNO$_3$ block polymers through SAXS or rheology as the working range to see the transition would be restricted between the T_g of PS (~105 °C) and 120 °C (~15 °C range).

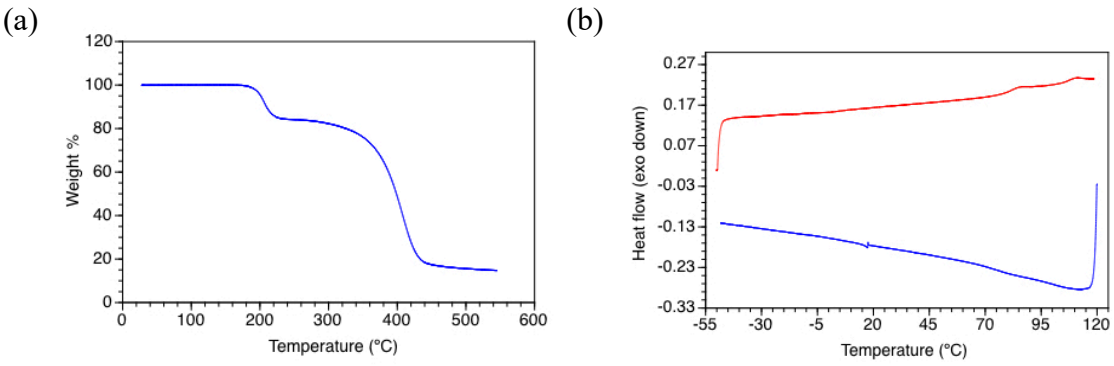

Figure 4.13. (a) TGA analysis of PS–PVBNO$_3$ under nitrogen with a heating rate of 10 °C min^{-1} and (b) DSC analysis of PS–PVBNO$_3$ (10 °C min^{-1} heating rate, 2nd heating curve shown)

Because of the restriction preventing direct measure of $\chi_{PS–PVBNO3}$, we sought to demonstrate microphase separation by identifying separated polymer domains using thin film characterization. After spinning a 67 nm thick thin film from a 1 wt% solution in chlorobenzene, the sample was solvent vapor annealed in chlorobenzene. AFM showed clear separation into two separate domains using intermodulation AFM (**Figure 4.14**). Although disordered, the AFM results strongly suggest a positive $\chi_{PS–PVBNO3}$ that will drive a reasonably sized block polymer to microphase separate.

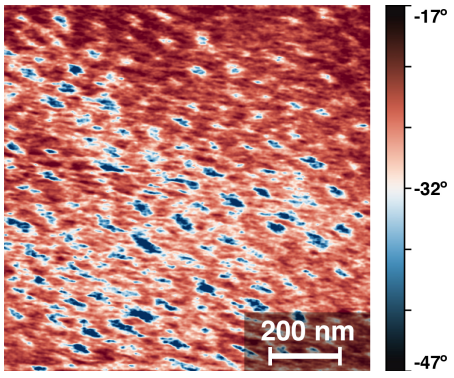

Figure 4.14. Intermodulation AFM image (see **2.3.12**) of PS-*b*-PVBNO$_3$ diblock polymer spin coated on native silicon oxide wafer and solvent vapor annealed with chlorobenzene.

The microphase separation was further demonstrated using grazing-incidence small-angle X-ray scattering. Unlike the previous reported GISAXS of PS–PVBC, which showed no indication of parallel or perpendicular features (and in fact showed no scattering at all), the PS–$PVBNO_3$ thin film showed apparent scattering, indicating a disordered, perpendicular-oriented microphase separated morphology (**Figure 4.15**). This clear microphase separation is further indication that there is a significant positive interaction parameter between PS and $PVBNO_3$.

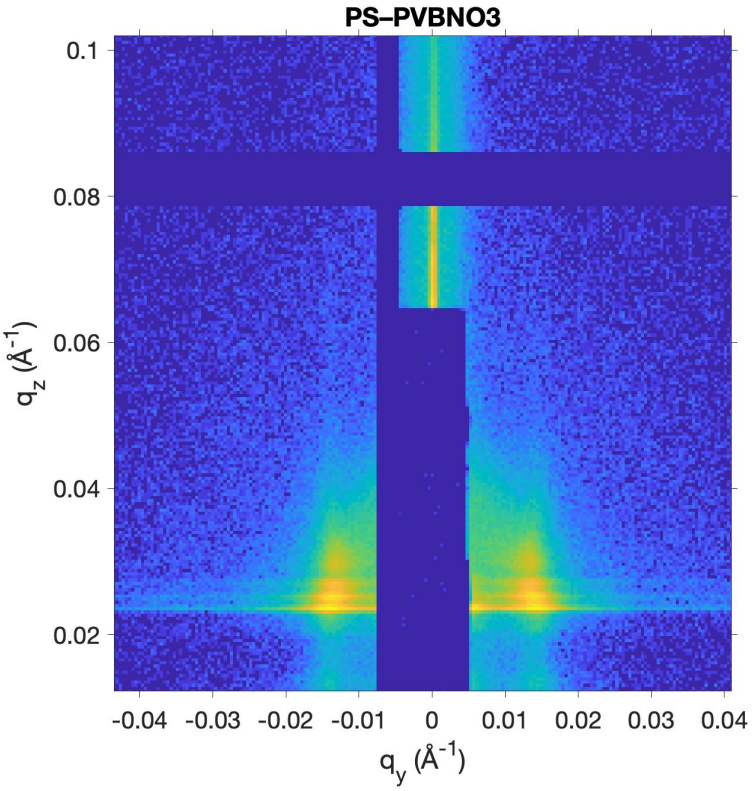

Figure 4.15. GISAXS of 87 nm thick film of (134k PS)-*b*-(37k $PVBNO_3$) on native silicon oxide showing vertical features scattering at q_y = 0.015 Å^{-1}.

4.4 Conclusions

Polystyrene and poly(vinylbenzyl chloride) have become standard monomers in block polymer and polyelectrolyte synthesis. Unfortunately, previous studies have shown that the Flory-Huggins interaction parameter between PS and PVBC is positive, but exceedingly small. We used transmission SAXS through a homogeneous polymer blend to attempt to place an upper bound on the value of $\chi_{PS-PVBC}$. We then propose an alternative monomer, $VBNO_3$ as a drop-in substitute for VBC. $PVBNO_3$ is a stable analogue of the commonly used PVBC polycationic precursor. The straightforward synthesis uses VBC as a precursor under mild conditions with common commercially available reagents. $PVBNO_3$ has similar selectivity for nucleophiles and offers a variety of interesting properties, including oxidative capabilities and differing solubility. $PVBNO_3$ should be considered as an alternative pre-cationic polymer in applications incompatible with PVBC.

4.5 References

[1] Maul, J.; Frushour, B. G.; Kontoff, J. R.; Eichenauer, H.; Ott, K. -H.; Schade, C. "Polystyrene and Styrene Copolymers" *Ullmann's Encyclopedia of Industrial Chemistry* **2007**, Wiley-VCH, Weinheim.

[2] Brown, D. W. and Lowry R. E. Molecular weight standards from sulfonation of polystyrene. *J. Polymer Sci.* **1979**, *17*, 1039–1046.

[3] Mays, J. W. and Hadjichristidis, N. Synthesis of high molecular weight near-monodisperse poly(4-methylstyrene) by anionic polymerization. *Polymer Bulletin* **1989**, *22*, 471–474.

[4] Kennemur, J. G.; Hillmyer, M. A.; Bates, F. S. Synthesis, Thermodynamics, and Dynamics of Poly(4-tert-butylstyrene-b-methyl methacrylate). *Macromolecules* **2012**, *45*, 7228–7236.

[5] Kolomanska, J.; Johnston, P.; Gregori, A.; Dominguez, I. F.; Egelhaaf, H. -J.; Perrier, S.; Rivaton, A.; Dagron-Lartigau, C.; Topham, P. D. Design, synthesis and thermal

behaviour of a series of well-defined clickable and triggerable sulfonate polymers. *RSC Adv.* **2015**, *5*, 66554–66562.

[6] Abreu, A. S.; Oliveira, M.; Rodrigues, P. V.; Moura, I.; Botelho, G.; Machado, A. V. Synthesis and characterization of polystyrene-block-poly(vinylbenzoic acid): a promising compound for manipulating photoresponsive properties at the nanoscale. *J. Mater. Sci.* **2015**, *50*, 2788–2796.

[7] Strube, O. I. and Schmidt-Naake, G. Synthesis of Reactive Triblock Copolymers via Reversible Addition-Fragmentation Chain Transfer (RAFT) Polymerization. *Macromol. Symp*. **2009**, *275–276*, 13–23.

[8] Thunhorst, K. L.; Noble, R. D.; Bowman, C. N. Preparation of Functionalized Polymers by Reactions of Poly(Vinylbenzyl Chloride). In *Polymer Modification*; Swift, G.; Carraher, C. E.; Bowman, C. N., Eds.; Springer Science+Business Media, LLC: New York; 1997; pp 97–107.

[9] Couture, G.; Alaaeddine, A.; Boschet, F.; Ameduri, B. Polymeric materials as anion-exchange membranes for alkaline fuel cells. *Prog. Polym. Sci.* **2011**, *36*, 1521–1557.

[10] Merrifield, R. B. The Synthesis of a Tetrapeptide. *J. Am. Chem. Soc*. **1963**, *85*, 2149−2154.

[11] Li, Y.; Jackson, A. C.; Beyer, F. L.; Knauss, D. M. Poly(2,6-dimethyl-1,4-phenylene oxide) Blended with Poly(vinylbenzyl chloride)-b-polystyrene for the Formation of Anion Exchange Membranes. *Macromolecules* **2014**, *47*, 6757−6767.

[12] Haladjova, E.; Mountrichas, G.; Pispas, S.; Rangelov, S. Poly(vinylbenzyl trimethylammonium chloride) Homo and Block Copolymers Complexation with DNA. *J. Phys. Chem. B* **2016**, *120*, 2586−2595.

[13] Hiemenz, P. C.; Lodge, T. P. *Polymer Chemistry, 2nd ed.*; CRC Press: Boca Raton, FL, 2007.

[14] Moad, G.; Chong, Y. K.; Postma, A.; Rizzardo, E.; Thang, S. H. Advances in RAFT Polymerization: the Synthesis of Polymers with Defined End-Groups. *Polymer* **2005**, *46*, 8458–8468.

[15] Postma, A.; Davis, T. P.; Evans, R. A.; Li, G.; Moad, G.; O'Shea, M. S. Synthesis of Well-Defined Polystyrene with Primary Amine End Groups Through the Use of Phthalimido-Functional RAFT Agents. *Macromolecules* **2006**, *39*, 5293–5306.

[16] de Gennes, P. G. *Scaling Concepts in Polymer Physics*; Cornell Univ. Press: Ithaca, New York, 1979.

[17] *Standardless absolute intensity calibration on SAXSLAB's SAXS instruments*. Technical documentation for Xenocs, Inc.: Grenoble, France, Sept. 22, 2015. http://saxslab.com/wp-content/uploads/2015/08/standardless-AI-calibration_v1.3.pdf (accessed June 6, 2020).

[18] Bates, F. S.; Wignall, G. D.; Koehler, W. C. Critical Behavior of Binary Liquid Mixtures of Deuterated and Protonated Polymers. *Phys. Rev. Lett.* **1985**, *55*, 2425–2428.

[19] Bates, F. S.; Fetters, L. J.; Wignall, G. D. Thermodynamics of Isotopic Polymer Mixtures: Poly(vinyl ethylene) and Poly(ethylethylene). *Macromolecules* **1988**, *21*, 1086–1094.

[20] Jones, T. D.; Chaffin, K. A.; Bates, F. S.; Annis, B. K.; Hagaman, E. W.; Kim, M.-H.; Wignall, G. D.; Fan, W.; Waymouth, R. Effect of Tacticity on Coil Dimensions and Thermodynamic Properties of Polypropylene. *Macromolecules* **2002**, *35*, 5061–5068.

[21] Anderson, K. S.; Hillmyer, M. A. Melt Chain Dimensions of Polylactide. *Macromolecules* **2004**, *37*, 1857–1862.

[22] M. Doucet, et al. *SasView*, Version 5.0.2. http://doi.org/10.5281/zenodo.3011184.

[23] Smith, M. B. and March, J. *Advanced Organic Chemistry 6th ed.*; Wiley Interscience: Hoboken, NJ; 2007; pp 501–502.

[24] Ferris, A. F.; McLean, K. W.; Marks, I. G.; Emmons, W. D. Metathetical Reactions of Silver Salts in Solution. III. The Synthesis of Nitrate Esters. *J. Am. Chem. Soc.* **1953**, *75*, 4078.

[25] Boschan, R.; Merrow, R. T.; Van Dolah, R. W. The Chemistry of Nitrate Esters. *Chem. Rev.* **1955**, *55*, 485–510.

[26] Francisco, M. A.; Krylowski, J. Chemistry of Organic Nitrates: Thermal Chemistry of Linear and Branched Organic Nitrates. *Ind. Eng. Chem. Res.* **2005**, *44*, 5439–5446.

Chapter 5. Polylactide Foams with Tunable Mechanical Properties and Wettability using a Star Polymer Architecture and a mixture of surfactants*

* The work in this chapter was completed in close collaboration with Dr. Philip Dirlam in the Department of Chemistry at the University of Minnesota. Reprinted (adapted) with permission from Dirlam, P. T.; Goldfeld, D. J.; Dykes, D. C.; Hillmyer, M. A. Polylactide Foams with Tunable Mechanical Properties and Wettability using a Star Polymer Architecture and a Mixture of Surfactants. *ACS Sustain. Chem. Eng.* **2019**, *7*, 1698–1706.

5.1 Abstract

Commercially available low-density, hydrophilic foams are principally produced from nonrenewable petrochemical feedstocks and suffer from challenging disposal avenues and effective recycling. We aim to develop a biodegradable alternative using materials from sustainable chemical feedstocks. Here we report the preparation of expanded poly(lactide) via carbon dioxide-mediated batch foaming under relatively mild conditions (6 MPa CO_2, $T \leq 50$ °C). By changing architecture, temperature, and surfactant loading, we obtain tunable densities from 0.05 to 0.3 g/cm^3 and compressive strengths from 1.2 to 0.05 MPa. The use of poly(lactide) with a multiarm star architecture is preferable over the linear analogue in preparing low-density foams. Polysorbate and poloxamer type surfactants were incorporated with 4-arm star poly(lactide) enabling further reduction in foam densities and imparting persistent wettability to inherently hydrophobic poly(lactide). The practical utility of these biodegradable poly(lactide) foams was demonstrated as a potential replacement for current phenolic resin-based foams.

5.2 Introduction

Foams from renewable resources that biodegrade in the environment are desirable for numerous applications. Rigid, open-cell foams are used as acoustic insulation,[1] tissue scaffolds,[2–4] and in a variety of packaging applications. Currently, the majority of these foams are made from fossil fuels and are typically polyurethane- or phenolic resin-based materials that are difficult to dispose of and nearly impossible to recycle.

In particular, we are interested in applications of foam in decorative floral arrangements, where a hydrophilic foam provides structural support to cut flower stems

pierced into the foam and held at specific orientations while supplying water to keep the stems rigid and flowers from wilting. The current standard commercial floral foam is a phenolic foam, manufactured using an alkane blowing agent.[5] All components are nonrenewable, derived from petroleum, and can be considered toxic. The foaming process produces a cross-linked hydrophobic foam with trace formaldehyde that is then treated with a surfactant to allow for uptake of water into the entirety of the foam pore space.[5] After use in a floral arrangement, the foam is mechanically damaged and has limited capacity to reabsorb water leading it to be discarded, with no available method for recycling or reuse. Our goal is to develop a compostable, biorenewable alternative that has similar mechanical properties, water compatibility, and floral longevity.

The most promising method of mass-produced foams meeting these specifications is the use of a common biorenewable polymer and a benign physical blowing agent. Previous work has revolved around the foaming of poly(lactide) (PLA), which is currently the most widely produced synthetic compostable polymer.[6] One previously explored foaming method involves the dissolution of carbon dioxide, an environmentally friendly, nontoxic, and nonflammable gas, into the polymer which is then depressurized in either a batch setting or as it exits an extruder to produce a low-density foam.[7] The initial CO_2 treatment step causes notable glass transition temperature (T_g) depression (plasticization) of the PLA leading to a saturated mixture of up to 20 wt% CO_2 in PLA (at 35 °C and 5 MPa).[8−10] Upon decompression, the mixture becomes unstable toward bubble nucleation and growth, and gaseous CO_2 evolves out of the blend. When the decompression rate is rapid, the resulting thermodynamic instability provokes the nucleation of CO_2 bubbles

dispersed throughout the PLA matrix. Continued decompression perpetuates CO_2 evolution and results in a foam growth regime as CO_2 diffuses out of the PLA and into nucleated bubbles, facilitating expansion. During CO_2 evolution, the system cools and the degree of PLA plasticization continually decreases. Foam growth stops when the decreasing temperature of the foam and the increasing T_g of PLA intersect.[11]

However, PLA foams produced using CO_2 as a physical blowing agent are usually closed cell and are often brittle or relatively dense (>0.2 g/mL). Most previous research attributes these problems with PLA foaming to low melt strength, which prevents a PLA melt from maintaining structural integrity under extensional stress as the foam cells rapidly grow. The most common method of overcoming this obstacle is the introduction of long-chain branching by copolymerization of a multifunctional monomer[12] or using one of a variety of chain extenders,[13–17] usually a multiepoxide (or similar functional group) containing small molecule additive. While these attempts have achieved moderate success in the extrusion foaming of PLA,[18] the chemical structure of the chain-extended PLA is often poorly defined. To study the effect of polymer branching on the behavior of PLA in CO_2 mediated batch foaming, it is desirable to use PLA with well-defined architectures. Here we specifically focus on multiarm star polymers.

In this report, we investigate the effect of polymer architecture, foaming temperature, and the incorporation of surfactants on PLA foams physically blown with CO_2 under relatively mild conditions. The physical and mechanical properties of foams prepared with linear PLA were compared with well-defined 3-arm and 4-arm PLA. This has enabled us to definitively establish the utility of polymer branching relative to a linear

architecture for preparing low-density PLA foams with CO_2, which is only previously reported in a generalized patent on the topic.[19] We also report the first use of polysorbate surfactants as additives capable of moderating the CO_2 driven expansion of PLA to produce coherent, lower-density materials. Furthermore, the incorporation of poly(ethylene oxide)-poly(propylene oxide)-poly(ethylene oxide) (PEO-PPO-PEO) triblock polymers into a PLA-based formulation were investigated to impart wettability to the resulting foams. The combination of these insights enabled development of a PLA based formulation that allowed the preparation of low-density, hydrophilic foams with a degree of open-cell character. These foams are composed of biodegradable materials and prepared with green chemical processing techniques were tested as an alternative to phenolic resin-based floral foams.

5.3 Experimental

5.3.1 Materials

(±)-Lactide was donated by Altasorb and recrystallized two times from toluene prior to use. Tin(II) 2-ethylhexanoate ($Sn(Oct)_2$) (Sigma Aldrich) was distilled under reduced pressure prior to use. Dry toluene and dry dichloromethane were obtained from a solvent purification system (Pure Process Technology). Pentaerythritol (99%, Sigma-Aldrich), 1,1,1-tris(hydroxymethyl)propane (≥98%, Sigma-Alrdich), benzyl alcohol (99%, Sigma Aldrich), 1,8-diazabicyclo[5.4.0]undec-7-ene (DBU, 98%, Sigma-Aldrich), polysorbate 20, 40, 60, 80 (Alfa-Aesar) and Poloxamer 188 (Pluronic F68, Anatrace) were commercially available and used as received. Colorants (Keyplast Blue B, and Keyplast Yellow 2GH) were donated by Milliken and used as received. All solvents including

methanol, hexanes, dichloromethane and ethyl acetate were commercially available and used as received.

5.3.2 Instrumentation and Methods

Size exclusion chromatography (SEC) was performed in a chloroform mobile phase with an Agilent 1100 series liquid chromatograph with an HP 1047A differential refractometer running three Agilent PLgel 5 μm Mixed-C columns at 35 °C and a flow rate of 1 mL/min. Molar masses were calculated using ChemStation software (Agilent), calibrated against low dispersity linear polystyrene standards. ^{1}H NMR spectroscopy was conducted with a Bruker Avance III HD 400 in $CDCl_3$, chemical shifts are reported relative to residual chloroform signal (7.26 ppm). Molar mass was estimated as the product of the repeat unit molar mass and degree of polymerization determined via end group analysis utilizing the terminal methine signal (4.35 ppm) as an internal standard to calculate the degree of polymerization relative to the polymer signal (5.2 ppm). Differential scanning calorimetry was conducted on a TA Instruments Q-1000 DSC under nitrogen. Samples were analyzed in hermetically sealed aluminum pans. Samples were subjected to two cycles of heating from 0 °C to 160 °C and then cooling to 0 °C at 10 °C/min. Glass transitions are reported as determined from the second heating cycle as the inflection point. Foam density was calculated by determining the volume of cylindrical foam samples by measuring the dimensions with a caliper or via water displacement for samples with poorly defined shape and dividing by the mass. Foam void volume (V_{void}) was determined as the difference between the measured foam volume (V_{foam}) and the volume of poly(lactide) (or poly(lactide)/surfactant blend) (V_{PLA}) comprising the structure of the foam sample as

determined from the foam mass and assuming a density of 1.25 g/cm^3 (i.e. $V_{void} = V_{foam} - V_{PLA}$) . Compression testing was conducted according to a procedure adapted from ASTM D1621 on a Shimadzu Autograph AGS-X equipped with two parallel stainless steel plates at a uniaxial compression rate of 1 mm/min on cylindrical foam samples with D = 1.021 cm and H ≈ 1 cm compressed parallel to the direction of foam rise. Compressive strength was calculated with Trapezium software by taking the stress at 10% strain. Scanning electron microscopy (SEM) was conducted with a Hitachi S3500N. SEM samples were sputter coated with Au/Pt (ca. 3 nm) prior to imaging. Imaging was conducted with an accelerating voltage of 10 kV. Images were analyzed using ImageJ software. Foam cell diameter was approximated by assuming spherical cells where the cross-sectional area was determined using morphological segmentation with the MorphoLibJ plug-in for ImageJ.[20] Rheology master curves were measured using 25 mm parallel plates on a TA Instruments Rheometric Series ARES Classic. Frequency sweeps were performed at 1% strain at 90, 120, and 150 ºC with autoadjusting strain for low signal. In-phase (G') and out-of-phase (G'') stress response was recorded from 0.01 rad/s to 100 rad/s. Time-temperature superposition (TTS) was performed using TA Orchestrator software with a reference temperature of 150 ºC, where curves were horizontally shifted according to calculated a_T values to build a master curve.

5.3.3 Experimental Procedures

All glassware utilized in the synthesis of poly((±)-lactide) (PLA) was dried at 110 °C in an oven overnight or flame dried prior to use. All materials utilized in the synthesis of PLA were stored and handled in a N_2 filled glovebox.

5.3.3.1 General Procedure for the Preparation of 3-Arm and 4-Arm Star PLA

The bulk polymerization of (±)-lactide to afford 3-arm and 4-arm star PLA was conducted according a procedure adapted from Hillmyer et al.[21] The following is a specific example of the general procedure used for the preparation of 4-arm star PLA using pentaerythritol as the initiator; for 3-arm star PLA 1,1,1-tris(hydroxymethyl)propane was used as the initiator. To a 300 mL pressure vessel equipped with a magnetic stir bar was successively added pentaerythritol (310 mg, 2.28 mmol), (±)-lactide (80.0 g, 0.555 mol) and a 25 mM solution of $Sn(Oct)_2$ in dry toluene (0.8 mL, 20 μmol $Sn(Oct)_2$). The pressure vessel was sealed and the bottom portion of the reaction vessel was submerged in an oil bath at 160°C and stirred for ca. 15 min to allow for melting and mixing of the initiator and a portion of the lactide. When a clear solution of initiator and (±)-lactide was afforded the reaction vessel was submerged further and the reaction mixture was heating at 160 °C with stirring for 3 hours. The crude polymer was allowed to cool to RT, dissolved in dichloromethane and then precipitated into an excess of methanol. The supernatant was decanted off and the precipitate was dissolved in dichloromethane. The polymer was then precipitated a second time into an excess of hexanes. The supernatant was decanted off and the precipitate was dissolved in a minimal amount of dichloromethane and transferred to a polypropylene container. The solution was concentrated under a stream of nitrogen and then placed in a vacuum oven at 60 °C for a minimum of 16 hours to remove residual solvent affording the polymer as a clear, colorless glass in 88% isolated yield. ^{1}H NMR (400 MHz, $CDCl_3$; 25 °C): δ (ppm) = 5.2 [bm, -COC**H**(CH_3)O-], 4.35 [m, -COC**H**(CH_3)OH end group], 4.15 [bs, C(C**H**$_2$)$_4$-pentaerythritol], 1.56

[bm, -COCH(C**H**$_3$)O-], M_n = 44.0 kg/mol, SEC ($CHCl_3$): M_n = 50.5 kg/mol, $Đ$ = 1.26. DSC: T_g = 46 °C.

5.3.3.2 General Procedure for the Preparation of Linear PLA

The following is a specific example of the general procedure used to synthesize linear PLA. To a 200 mL round bottom flask equipped with a magnetic stirbar was added (±)-lactide (20 g, 0.14 mol) and dry CH_2Cl_2 (100 mL). The mixture was stirred until a homogenous solution resulted and then benzyl alcohol (42 µL, 0.40 mmol) was added. The solution was stirred briefly and then the polymerization was initiated with the addition of DBU (0.10 mL, 0.69 mmol) as a catalyst. The reaction vessel was sealed with a rubber septum, removed from the glove box and stirred at room temperature for 1 h. Acetic acid (ca. 0.1 mL) was then added to deactivate the catalyst and stop the polymerization. The reaction mixture was concentrated *in vacuo* to a volume of 50 mL and then added dropwise to an excess of methanol. The supernatant was decanted off and the precipitate was dissolved in dichloromethane. The polymer was then precipitated a second time into an excess of hexanes. The supernatant was decanted off and the precipitate was dissolved in a minimal amount of dichloromethane and transferred to a polypropylene container. The solution was concentrated under a stream of nitrogen and then placed in a vacuum oven at 60 °C for a minimum of 16 hours to remove residual solvent affording the polymer as a clear, colorless glass in 81% isolated yield. ^{1}H NMR (400 MHz, $CDCl_3$; 25 °C): δ (ppm) = 7.34 [bm, **Ph**-CH_2O- benzyl alcohol] 5.36 [m, Ph-C**H**$_2$O-, benzyl alcohol], 5.2 [bm, -COC**H**(CH_3)O-], 4.36 [m, -COC**H**(CH_3)OH end group], 1.56

[bm, -COCH(C**H**$_3$)O-], M_n = 26.7 kg/mol, SEC ($CHCl_3$): M_n = 46.4 kg/mol, $Đ$ = 1.09. DSC: T_g = 54 °C.

5.3.3.3 General Procedure for Preparing Poly(Lactide) and Poly(Lactide)/Additive Blend Foams

The following is a specific example of the general procedure used to prepare PLA and PLA/additive (e.g. surfactants and colorants) blend foams. For samples prepared without additives the PLA was utilized without the initial solvent casting steps described in the following. To a polypropylene jar equipped with a magnetic stirbar was added polysorbate 80 (100 mg), poloxamer 188 (100 mg), (poly((±)-lactide) (1.8 g) and dichloromethane (10 mL). The mixture was stirred until a homogeneous solution was afforded and the stir bar was then removed. The solution was concentrated under a stream of nitrogen and then placed in a vacuum oven at 60 °C for a minimum of 8 hours to remove residual solvent. The polypropylene container with PLA or solvent cast PLA/surfactant blend was then loaded into a 1 L stainless steel pressure vessel. The vessel was sealed, charged with CO_2 (0.7 MPa, gauge pressure), and vented to atmospheric pressure. This was repeated a total of three times to purge to pressure vessel with CO_2. The pressure vessel was then heated to the desired temperature with a water bath and subsequently pressurized with CO_2 (6 MPa, gauge pressure). The sample was incubated under CO_2 at the desired temperature for 5 hours. The vessel was then rapidly depressurized to atmospheric pressure (2.3 MPa/s) through a ball-valve outlet with inner diameter of 4.7 mm and the expanded polymer sample was removed from the pressure vessel. To obtain samples with well-

defined dimensions for density and compressive strength testing, cylindrical samples were extracted from larger foams using a cork borer tool.

5.4 Results and Discussion

5.4.1 Impact of PLA Architecture and Foaming Temperature

Molecularly defined PLA can provide insights into the complex process of carbon dioxide foaming of this biorenewable material. While previous reports have used chain extender techniques to try to increase the melt strength of linear PLA,[13−17] well-defined chemical branching shows properties much more beneficial to melt processing techniques. Commercially produced poly((−)-lactide) (PLLA) is a semicrystalline polymer with a practical melting point around 155 °C. CO_2 is insoluble in the crystalline domains of PLLA, which have to melt to allow CO_2 dissolution.[22] To avoid foaming at high temperature, we synthesized all PLA in this study from a racemic mixture of (+)-lactide and (−)-lactide, yielding poly((±)-lactide), an amorphous polymer with a glass transition around 45 °C. Using mono-, tri-, and tetrafunctional initiators for our polymerizations, we synthesized linear, 3-arm, and 4-arm PLA stars with a number-average molar mass (M_n) between 10 and 50 kg/mol (see **Table 5.1**) via ring-opening transesterification polymerization (ROTEP) of (±)-lactide (**Scheme 5.1**). We note that the tin catalyst used for bulk ROTEP of lactide is not directly biosourceable. However, the use of tin(II) 2-ethylhexanoate at a catalytic loading of 100 ppm and its status as an FDA-approved indirect additive for food contact packaging[23] mitigate the deleterious impact stemming from its use.

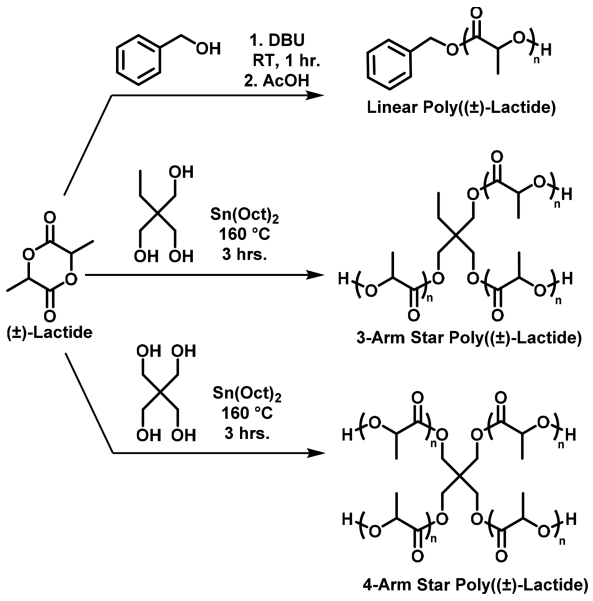

Scheme 5.1. Synthesis of Linear and Star-Shaped PLA via ROTEP.

Foams were prepared with linear and star PLA to ascertain the effects of polymer architecture on the CO_2-mediated expansion of PLA. Previous studies have shown dramatic differences in the rheological properties of linear vs star PLA.[24–27] Consistent with other polymers, star PLA has been shown to have both a higher zero shear viscosity and higher shear thinning than the linear analogue. The activation energies are independent of architecture, and while the relaxation times are similar for fast relaxations, they diverge at low relaxation times. The phenomenon is attributed to hindered reptation,[28] which proposes that polymer chain self-diffusion is constrained by branch points. The constraint necessitates disentanglement that relies on chain end diffusion toward the branch point; as the arms get longer, a deep arm retraction becomes unlikely, and the star material exhibits a longer relaxation time than the linear polymer.

Architecture	M_n (SEC, kg/mol)	Arm M_n (kg/mol)	Result of CO_2 Treatment	Density of Expanded Sample (g/cm^3)
Linear	8.57	4.3	No Significant Expansion	-
Linear	16.5	8.3	No Significant Expansion	-
Linear	46.4	23.2	Expansion	0.21
3-Arm	8.23	2.7	Incoherent	-
3-Arm	16.2	5.4	Incoherent	-
3-Arm	35	11.7	Expansion	0.10
3-Arm	44.3	14.8	Expansion	0.11
3-Arm	51	17.0	Expansion	0.09
4-Arm	9.47	2.4	Incoherent	-
4-Arm	17.2	4.3	Incoherent	-
4-Arm	35.7	8.9	Expansion	0.10
4-Arm	50.5	12.6	Expansion	0.10

**All samples were treated with 6 MPa (gauge pressure) CO_2 at ambient temperature for 5 hours with subsequent rapid decompression*

Table 5.1. Result of CO_2 Foaming Procedure on PLA with Various Molar Masses.

We believe these characteristics are attractive for a foaming process. While both linear and star PLA samples are believed to rapidly expand upon CO_2 depressurization, the viscosity of the star polymer is lower at higher shear rates experienced at the fastest expansion times. This phenomenon is further exaggerated by the solution created upon CO_2 dissolution in the polymer. A solution of star polymer has a much lower viscosity than a solution of linear polymer due to the restricted size of the branched structure.[29] The lower viscosity will likely facilitate cell growth as the material rapidly expands. More importantly, the viscosity of the star polymer should rapidly surpass that of the linear polymer when both the shear rate slows and the CO_2 vaporizes as the foam growth rate comes to a rapid halt. The star polymer will reach a viscosity up to two orders of magnitude higher than the linear analogue, which should prevent cells from collapsing as it vitrifies

under depressurization. The linear analogue will maintain a lower viscosity, likely leading to significant cell coalescence and collapse, and hence a higher-density foam.

While many previous studies focused on PLLA, Dorgan et al. showed that varying the (+)-lactide content in the final polymer had little to no effect on the rheological properties.[30] Full rheological characterization of the amorphous PLA used in our studies in both linear, 3-arm star, and 4-arm star architectures showed the expected trends in viscosity and modulus (**Figure 5.1**).

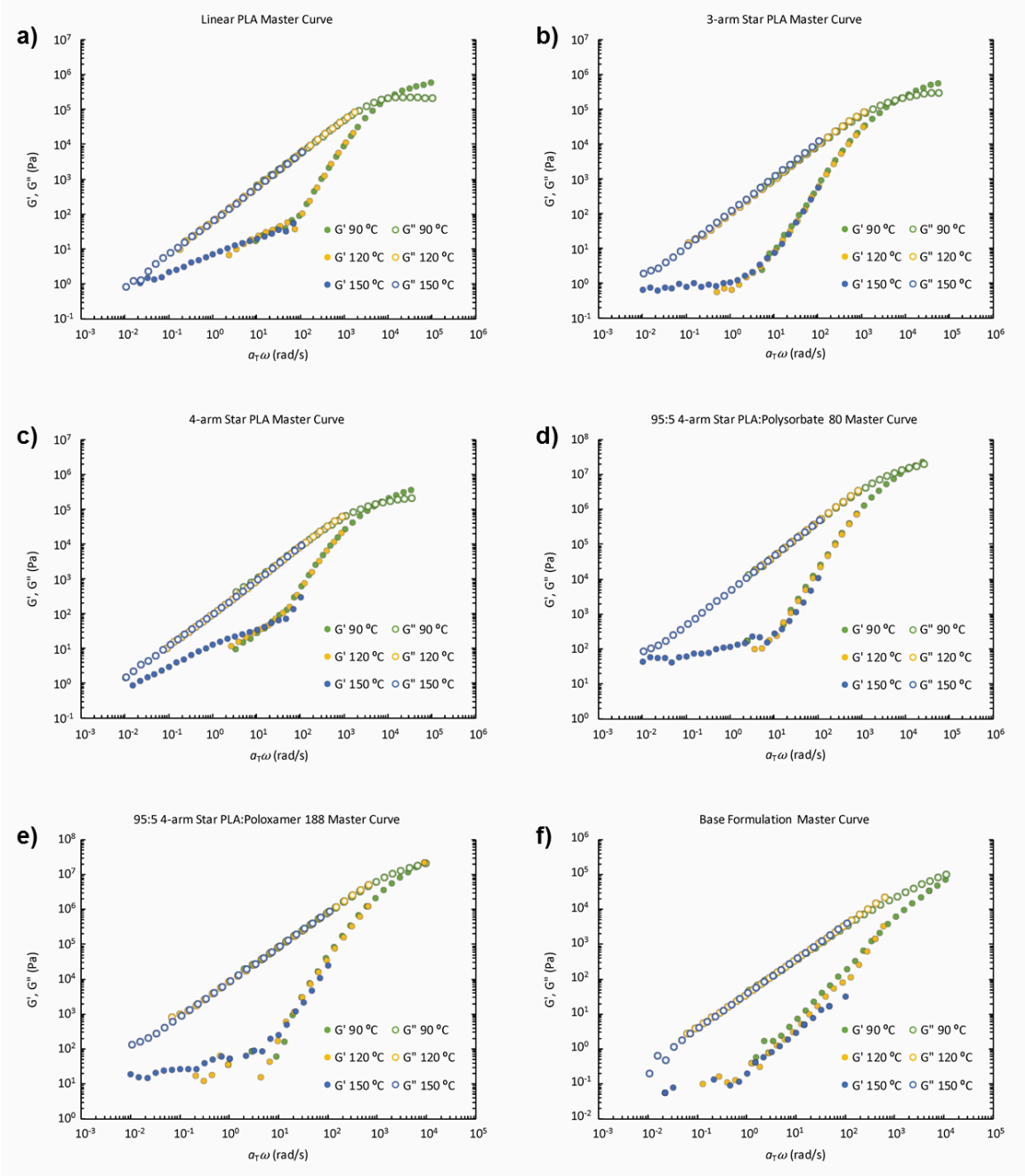

Figure 5.1. Rheology master curves for a) linear PLA, b) 3-arm PLA, c) 4-arm PLA, d) 4-arm PLA with 5 wt% polysorbate 80, e) 4-arm PLA with 5 wt% poloxamer 188, f) 4-arm PLA base formulation with 5 wt% polysorbate 80 and 5 wt% poloxamer 188. Master curves were constructed by applying shift factors (a_T) to dynamic frequency sweep data obtained at 90, 120, and 150 °C at 1% strain (with autoadjust strain increases at low signal). The low frequency data where G' is below 1 Pa (particularly in (b), (e), and (f)) is unreliable due to diminishing signal from low torque, even at increased strain.

Polymer samples were treated in a 1 L high-pressure batch reactor with CO_2 (6 MPa gauge pressure) for 5 h at various temperatures followed by rapid depressurization (~2.3 MPa/s) (**Figure 5.2**). As predicted, introducing branches into the polymer architecture dramatically influenced the density of the expanded foams. Foams prepared using linear PLA with a molar mass of 46 kg/mol showed considerably lower expansion at room temperature relative to the 3-arm and 4-arm star polymers with comparable molar masses of 51 kg/mol. Likely, the low viscosity of the linear polymer as the foam growth nears its end causes significant cell coalescence as the cell walls fall apart. Once the cells have merged, there is likely total collapse of the foam, leading to little expansion of the material. There were also stark differences observed between the flow properties of the linear and star PLA under carbon dioxide pressure. Linear PLA did not flow to a significant extent after 5 h, at any temperature up to 50 °C under carbon dioxide pressures up to 6 MPa; the expanded pieces recovered from the reactor retained the general shape of the original melt-pressed samples. In contrast, every molar mass 3-arm and 4-arm star PLA that we prepared was found to flow sufficiently to take the shape of its container regardless of temperature (21−50 °C). We attribute this difference to the flow properties of star and linear polymer solutions. Under CO_2 pressure, up to 20 wt % carbon dioxide will dissolve into the polymer. A star polymer in this case will have a lower viscosity than the linear polymer as the branch points restrict the size of the individual chains. The combination of a lower viscosity with a lower glass transition temperature means that the star polymers flow much more readily under CO_2 pressure than the linear analogues at the same temperature.

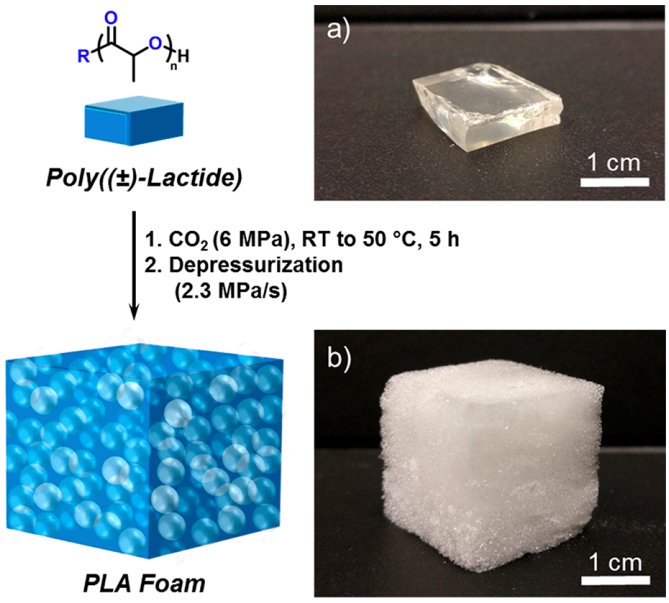

Figure 5.2. Schematic of PLA foaming using CO2 as a physical blowing agent with representative images of PLA (a) before and (b) after CO2 treatment and subsequent rapid depressurization.

The effect of molar mass on the CO_2 foaming of PLA was determined over a limited range (**Table 5.1**). Both 3- and 4-arm star PLA with a molar mass (<35 kg/mol) led to incoherent, flaky particulate samples after CO_2 foaming. The polymers began to form coherent foams after surpassing the previously measured branch molar mass (M_B), which is related to the entanglement molar mass (M_e) normalized by the number of arms in the architecture.[27] It is likely that below M_B, the poor rheological properties give little stability to the quickly growing carbon dioxide bubbles, and the cell walls tear apart into separate pieces. Low molar mass linear PLA was also unsuitable for preparing foamed materials. It showed virtually no expansion, likely because the lower molar mass material will have an extremely low viscosity during foaming as well as during the final vitrification, giving an even lower degree of CO_2 bubble stabilization and precluding the formation of any cellular structure.

Temperature played a vital role in the foaming process, similar to the effect seen in previous works.[31–34] Increasing the temperature in increments of 10 °C between room temperature and 50 °C showed linearly decreasing densities for all polymer architectures with M_n of ca. 50 kg/mol (**Figure 5.3**). The linear PLA foams had average densities ranging from 0.24 g/cm^3 to 0.15 g/cm^3 when prepared between 21 and 50 °C, respectively. These densities for linear PLA foams were approximately 2.5 times higher than both the 3- and 4-arm polymer foams, which were nearly identical at all tested foaming temperatures and ranged from 0.097 g/cm^3 to 0.060 g/cm^3. Because of this, the star polymers were emphasized in our studies aimed at generating biodegradable foams because their densities approached the target density of commercial floral foam (0.03−0.05 g/cm^3).

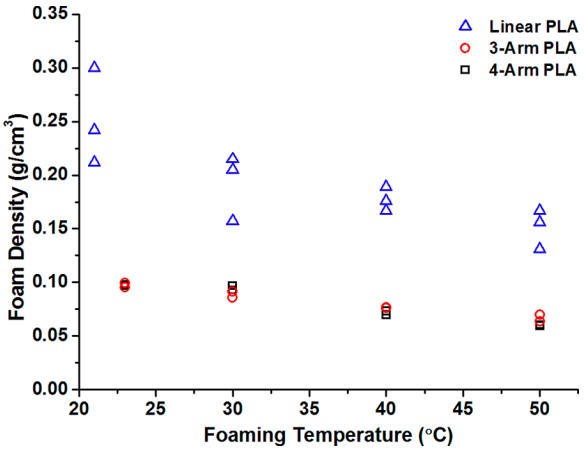

Figure 5.3. PLA foam density versus CO2 foaming temperature for linear, 3-arm star, and 4-arm star PLA with comparable molar masses of 46, 51, and 51 kg/mol, respectively.

We then measured the compressive mechanical properties to compare the 3- and 4-arm PLA foamed at various temperatures (**Figure 5.4**). Cylindrical samples were compressed between two plates at a send speed of 1 mm/min, and the compressive strength was determined as the stress at 10% compressive strain. There was no significant difference

in compressive strength between foams prepared with the 3- or 4-arm PLA. Foams prepared with either star shaped PLA at the same temperature exhibited compressive strengths ranging from 1.2 to 0.4 MPa for foaming temperatures of 23 and 50 °C, respectively. We expected the 3-arm and 4-arm star polymers to behave similarly throughout the foaming process as their rheological properties are relatively similar. While increasing branch number causes an increase in viscosity, the predicted and observed difference is only notable at high molar masses with a large increase in the number of branches.[27] The moderate change from three to four arms at molar masses that only slightly surpass the branch entanglement molar mass has a negligible effect compared to the difference with the linear analog.

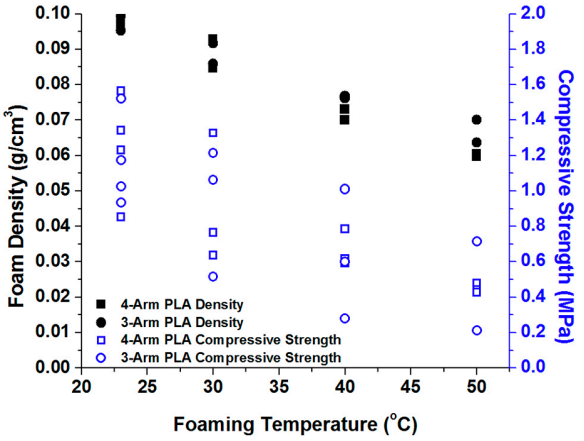

Figure 5.4. Plot of compressive strength versus foaming temperature for PLA foams prepared with 3-arm and 4-arm PLA of comparable molar mass (ca. 50 kg/mol).

Multiarm star polymer architecture and mild heating enables access to PLA foams with a range of compressive strengths principally dictated by the foam density, which is controlled by foaming temperature. However, further reduction of PLA foam density was

needed to approach the target compressive strength of commercial phenolic floral foam (0.05 MPa).

5.4.2 Surfactant Additives

With the improved foaming capability of multiarm star architecture, we sought to further decrease the density of the expanded PLA to better match the target density for floral foam applications, approximately 10^{-2} g/cm^3. It is common practice to introduce surfactants to polymer foam formulations to facilitate stabilization of growing bubbles during polymer foam growth.[35,36] Interestingly, to our knowledge, there has not been a report of using this strategy as a route to modifying PLA foams physically blown with CO_2. We found that addition of as little as 0.5 wt % of surfactant to our 4-arm star PLA led to lower-density foams while maintaining coherent, homogeneous samples with consistent mechanical properties.

We focused on the use of polysorbate surfactants as additives. Polysorbate surfactants are commercially available surfactants made from the addition of hydrophilic (PEO) chains onto a sorbitan backbone that is then coupled to a variety of hydrophobic fatty acids designated by a numerical identifier. These emulsifiers are safe for use in consumer products and are commonly found in pharmaceuticals, cosmetics, and food products. Based on a sugar, fatty acid, and PEO chain, polysorbates are biodegradable and can also be partially biosourced.[37,38]

In PLA/polysorbate blends, the negative Flory−Huggins interaction parameter between PLA and PEO should lead to the PEO component of the surfactant embedding in the PLA matrix.[39] Nonpolar hydrocarbons are not miscible with PLA, and therefore, the

fatty acid component of the polysorbate is assumed to be incompatible with the PLA matrix and phase separate.[40] The contrasting molecular interactions between the PEO and fatty acid segments of polysorbate with the PLA matrix may lead to micelle formation. During depressurization, heterogeneous nucleation of carbon dioxide bubbles will occur at the interface generated by micelles to a greater extent than homogeneous nucleation occurring in the polymer matrix. The polysorbate likely coats the nucleated bubble and then maintains the structural integrity along the interface as the bubble expands dramatically over a short period of time. Such stability allows for the growth of coherent foams even at lower melt strengths. The addition of even a small amount of polysorbate changed the outcome of PLA foaming. Lower molar mass PLA stars that foamed to incoherent flakes were shown to form coherent foams with as little as 0.5 wt % added polysorbate.

Polysorbates with four different fatty acid constituents were used to optimize conditions for a PLA foam. Polysorbate 80 (oleic acid), polysorbate 60 (stearic acid), polysorbate 40 (palmitic acid), or polysorbate 20 (lauric acid) was added to 50 kg/mol 4-arm star PLA before foaming. **Figure 5.5** shows the density of the foams with 5 wt% of the different surfactant additives.

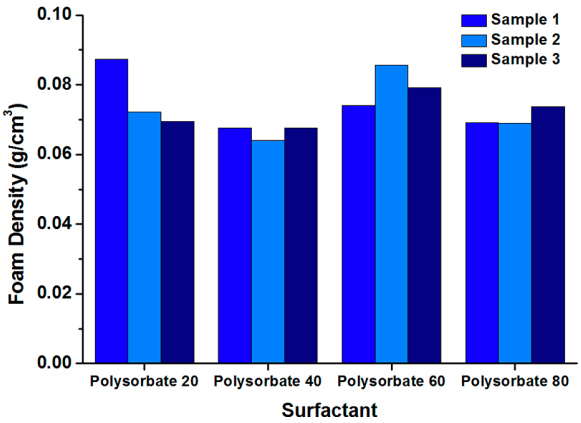

Figure 5.5. Density of foams prepared with a variety of polysorbate surfactants at 22 °C with 95:5 wt:wt loading of 50 kg/mol 4-arm PLA:polysorbate. Results of density determination for three samples of each polysorbate composition are presented.

Both polysorbate 40 and polysorbate 80 led to foams with similar densities between 0.065 and 0.07 g/cm^3, a 10% average decrease in density compared to polysorbate 20 and polysorbate 60. For the remaining experiments in this study, polysorbate 80 was used as an additive to control foam density. We optimized the surfactant loading by examining the effect that various loadings of polysorbate had on the density of foams prepared at ambient temperature. The density of PLA foams decreased from 0.097 g/cm^3 without any polysorbate additives to densities as low as 0.065 g/cm^3 at 2.5 wt% loading, the minimum density at any loading (**Figure 5.6**). Previous studies have shown that the addition of a small amount of block polymer surfactants will lead to the creation of micelles that serve as nucleation sites during foaming.[41,42] Increasing surfactant concentration increases the concentration of micelles, helping to nucleate a higher number of well-controlled cells. After passing a certain surfactant content, however, the concentration of the surfactant in the bulk material starts to increase. The mixing decreases the difference in surface energy between the surfactant micelles and the bulk and reduces the nucleation efficiency of the micelles, causing a loss of nucleation sites and a well-recorded decrease in cell count and increase in foam density. A minimum in the foam density results around 2.5 wt % polysorbate 80.

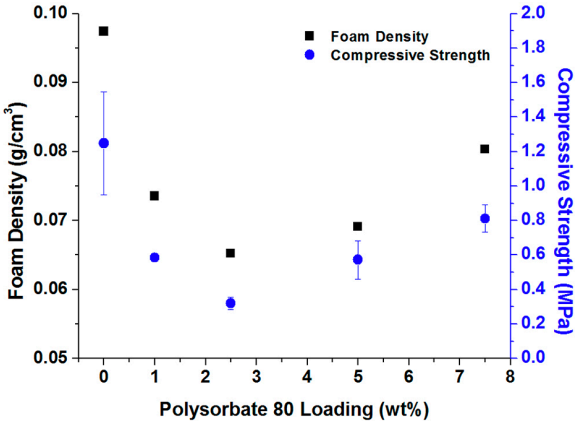

Figure 5.6. Density and compressive strength of 50 kg/mol 4-arm star PLA foamed at 23 °C with varying loadings of polysorbate 80.

The compressive strength of foams containing polysorbate 80 was again strongly associated with foam density ranging from 0.3 to 1.2 MPa for the lowest- and highest-density foams, respectively (**Figure 5.6**). Notably, there was no observable change in compression properties due to polysorbate content beyond the effect on foam density. This is apparent upon comparison of the foams containing 1 and 5 wt% polysorbate, which had similar densities and compressive strengths. Indeed, an association is apparent when comparing the compressive strength versus density for all 3- and 4-arm star PLA foams regardless of foaming temperature or polysorbate content (**Figure 5.7**). The compressive strength appears to be principally dependent upon the resulting foam density.

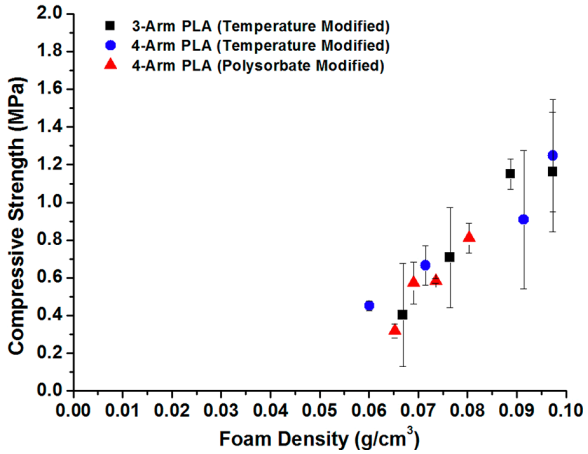

Figure 5.7. Plot of compressive strength versus density for PLA based foams with density modified by foaming at temperatures from 22 to 50 °C (3-arm PLA and 4-arm PLA) and polysorbate 80 incorporation at loadings of 1, 2.5, 5, and 7.5 wt%.

5.4.3 Hydrophilicity and Water Uptake

In the past, water uptake into PLA foams has been a common research target to make foams suitable for use as a tissue scaffold among other applications.[2] In floral foam, water uptake is vital to maintaining the aesthetic quality of inserted flowers, which need constant access to water to prevent wilting. An ideal foam holds a maximum amount of water allowed by the pore structure (100% water uptake) without drawing water from the stems as the foam dries. There are two requirements to reach high water uptake levels. The first is hydrophilicity of the material walls. PLA is, in general, a hydrophobic material−insoluble in water with a water contact angle of 80°.[43] Even after foaming with 5 wt% polysorbate surfactant, PLA foams do not absorb water. One method to overcome this limitation is the application of a surfactant to the foam surface after production but before exposure to water. This process is used for wettability in commercial phenolic floral foams[5] but is undesirable for two reasons. First, the application of a surfactant post foam formation introduces an additional processing step. Second, the foam is not inherently

hydrophilic. After wetting the foam and washing away the applied surfactant, it does not readily rewet.

We sought to improve upon these shortcomings by introducing a hydrophilic material directly into the polymer blend before foaming. Poloxamer is a nonionic surfactant triblock polymer containing a central poly(propylene oxide) (PPO) chain and PEO end blocks. In this study, we use poloxamer 188, which has an 1800 g/mol PPO midblock with a 3600 g/mol PEO block on each end. Poloxamers have been previously demonstrated to be miscible with PLA with a propensity to concentrate at the surface of PLA blends and impart wettability.[43–46] Some limited studies on semi-crystalline PLA have shown that poloxamer will concentrate at the surface of a blend with poly(L-lactide) and that the hydrophobicity of the PPO chain drives the PPO segments away from the polymer-air interface.[47,48] This leads to the PPO block embedding in the PLA matrix and coating the surface with hydrophilic PEO. A similar arrangement may occur under carbon dioxide processing conditions, where the polymer/carbon dioxide solution will favor the more hydrophobic PPO block over the hydrophilic PEO. Additionally, poloxamer is ideal for our application, as it has been shown to be biodegradable.[49]

Addition of poloxamer to 4-arm PLA at higher loadings of 5 and 7.5 wt% caused notable change in the resulting foams with increased densities of 0.12 g/cm^3 and 0.14 g/cm^3. To mediate this undesirable increase in density, we incorporated polysorbate and increased the foaming temperature to reach our target compressive strength. This strategy was successful when a formulation of 90:5:5 wt% PLA:polysorbate 80:poloxamer 188 foamed at 40 °C produced a low-density (0.06 g/cm^3) foam with a hydrophilic surface.

Water absorption of this base formulation was evaluated by placing cylindrical samples in a water bath at ambient temperature for ~3 min and recording the mass of water absorbed. The base formulation including poloxamer had a water uptake of 27% relative to the void volume (i.e., total foam volume less the volume occupied by PLA/polysorbate/poloxamer) whereas foams prepared solely with polysorbate additives did not absorb water. Further, by integrating the hydrophilic elements into the structural material of the foam, the foams were capable of absorbing water, drying out, and then reabsorbing the same mass of water.

The second characteristic needed to absorb water is an open-cell structure with connections between the void spaces in the foam. Most reported PLA foams have consisted of closed-cell foams and several approaches have been attempted to perforate cell walls, including dissolving out salts or polymers that leave behind pathways between cells.[50−52] In general, these foams suffer from inhomogeneous structures and poor mechanical properties while requiring a high loading of additives. Another approach to the open-cell structure incorporates low T_g polymer domains that rupture more readily during the foaming process.[53] It requires the addition of an immiscible polymer into the blend that is either distributed through the matrix or covalently bound as a block polymer. The blend can complicate melt processing of the polymer and may require additional additives as compatibilizers.

The most convenient strategy for increasing the open-cell content is addition of a plasticizer or secondary blowing agent that extends the foam growth regime and softens the foam cell walls.[54,55] The longer growth period allows for greater cell wall extensional strain and the softening increases the ease of wall perforation. An ideal solvent for foaming

has moderate volatility and good solubility in PLA so it could easily be loaded directly into the reactor with the sample before foaming. Furthermore, after the foaming process is complete, any residual solvent is easily removed via vaporization. Ethyl acetate was chosen as it has the desired volatility and miscibility with PLA in addition to being nontoxic and biorenewable.[56] It was added at several loadings directly to PLA/polysorbate/poloxamer blends (2 g scale) before foaming with CO_2. A low loading of ethyl acetate proved to have the most pronounced effect in increasing open-cell nature, increasing the water absorbed into the foams to nearly 50% of the void volume (**Figure 5.8**). However, when this strategy was implemented for the preparation of large foam prototypes (20 g scale) the results were inconsistent with foams prepared on a smaller scale.

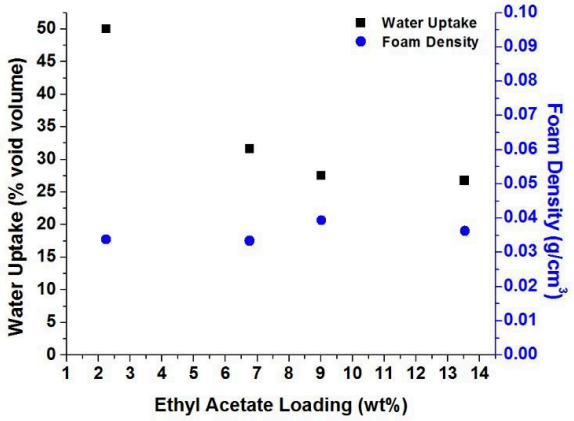

Figure 5.8. Plot of water uptake and density versus ethyl acetate used as a secondary blowing agent/plasticizer for foams composed of 90:5:5 wt% PLA:polysorbate 80:poloxamer 188 foamed at 40 °C. The ethyl acetate loading is given as an additive wt% relative to the total mass of the PLA and surfactant blend. Water uptake was determined in terms of void volume calculated assuming a density of 1.25 g/cm^3 for PLA/polysorbate/poloxamer blend. All samples were prepared with 2 g of PLA/surfactant blend.

We also investigated the use of higher CO_2 treatment pressures to extend the foam growth regime and increase water uptake (**Figure 5.9**). This was determined to be an

ineffective strategy as higher CO_2 treatment pressures were found to be inversely associated with water uptake in the resulting foams. This could be attributed to the more rapid initial depressurization event associated with the higher initial CO_2 pressures being released under the same conditions (i.e. through a valve with a fixed diameter). The higher initial depressurization rate leads to an increase in bubble nucleation and subsequently a shorter bubble growth regime.

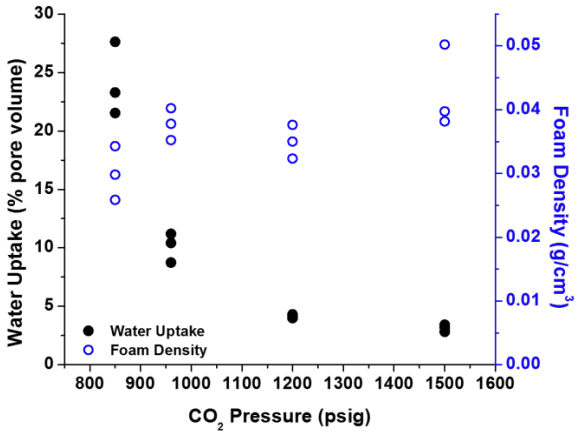

Figure 5.9. Plot of water uptake and density versus CO_2 treatment pressure for 90:5:5 wt% PLA:polysorbate 80:poloxamer 188 foamed at 55 °C.

5.4.4 PLA Foams in Floral Foam Applications

A formulation was optimized for the use of expanded PLA foams as a structural support for cut flower arrangements (i.e., floral foam). The targeted mechanical properties were a rigid foam that can hold a large number of floral stems inserted close together in a single foam piece, while remaining soft enough to be punctured with angle-cut flower stems of varying sizes. Second, the foam must absorb enough water to provide hydration to a cut flower stem for several days. All components are nontoxic, biodegradable, compostable, and can be biosourced as an alternative to the current petroleum-based

phenolic floral foam standards. We combined 4-arm star PLA with polysorbate to control foam density and poloxomer to impart wettability while maintaining at least 90 wt% PLA in the formulation.

The general conditions used to prepare low-density foams with a wettable surface (90:5:5 wt % PLA:polysorbate 80:poloxamer 188 foamed at 40 °C) yielded foam with a density of 0.060 g/cm^3 and a compressive strength of 80 kPa. To better match the expected structural integrity of commercial floral foam, which was determined to have a density of 0.03−0.05 g/cm^3 and a compressive strength of 45 kPa, the foaming temperature of the PLA formulation was increased to 45 °C. This effectively lowered the foam density to 0.049 g/cm^3 and corresponding compressive strength to 48 kPa to give a foam with an excellent match to the compression properties of the commercial material (**Figure 5.10**).

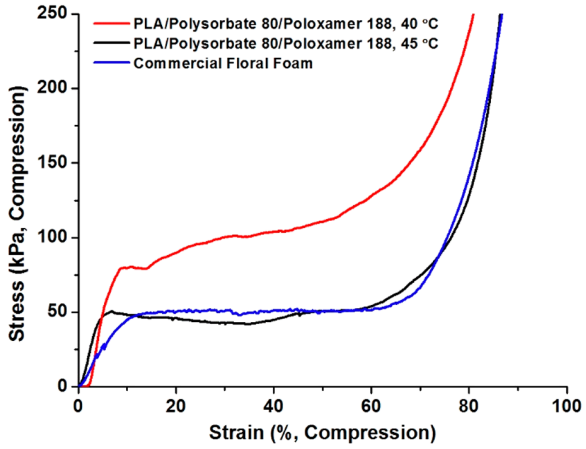

Figure 5.10. Compression stress versus strain curves for a commercial phenolic-based floral foam and PLA foams prepared with a 90:5:5 wt% 4-arm PLA:polysorbate 80:poloxamer 188 formulation foamed at 40 and 45 °C.

The morphology of the 4-arm PLA based foams formulated with surfactants was investigated with SEM (**Figure 5.11**). Cross-sectional SEM images of foams prepared without surfactant at 23 °C were acquired as a reference and showed a regular distribution

of cells with an approximate diameter of 0.21 mm (**Figure 5.11a**). The incorporation of 5 wt% polysorbate 80 led to foams with a similar regular distribution of cells and smaller diameter of approximately 0.12 mm (**Figure 5.11b**). This decrease in cell size with a consistent cell distribution could be attributed to a well-dispersed population of polysorbate micelles acting as heterogeneous nucleation sites which promote bubble nucleation to a greater extent than the homogeneous nucleation which occurs during the foaming of neat PLA.[42] Foams prepared with 5 wt% poloxamer 188 showed a bimodal cell distribution composed of one population of larger cells with a diameter on the order of 10^{-1} mm among a population of notably smaller cells with a size on the order of 10^{-2} mm (**Figure 5.11c**). The bimodal bubble size distribution is indicative of competing nucleation mechanisms. This could be attributed to poor miscibility of poloxamer and CO_2,[57] leading to the precipitation of poloxamer particles that proceed to act as hetereogeneous nucleation sites which compete with bubble formation caused by homogeneous nucleation. Foams prepared with a combination of both surfactants showed a relatively regular distribution of cells with an approximate diameter of 0.23 mm. The preparation of foams with a regular cell distribution in the presence of poloxamer indicates that the polysorbate is able to serve as a compatibilizer for poloxamer and CO_2 and establishes a consistent mode of nucleation. SEM imaging of the foams prepared at higher foaming temperature (45 °C) showed a coarser cellular structure for neat PLA and all of the formulations with surfactants. This is expected as the higher temperature decreases CO_2 solubility which leads to a lower cell nucleation rate and ultimately fewer, larger cells. Furthermore, the increase in temperature enables an extended foam rise time which provides more opportunity for cell coalescence

events to occur. The formulation containing both poloxamer 188 and polysorbate 80 was found to have the most tolerant processing window, where the increased foaming temperature led to moderate increase in cell size (D ≈ 0.33 mm) while retaining a relatively regular cell distribution.

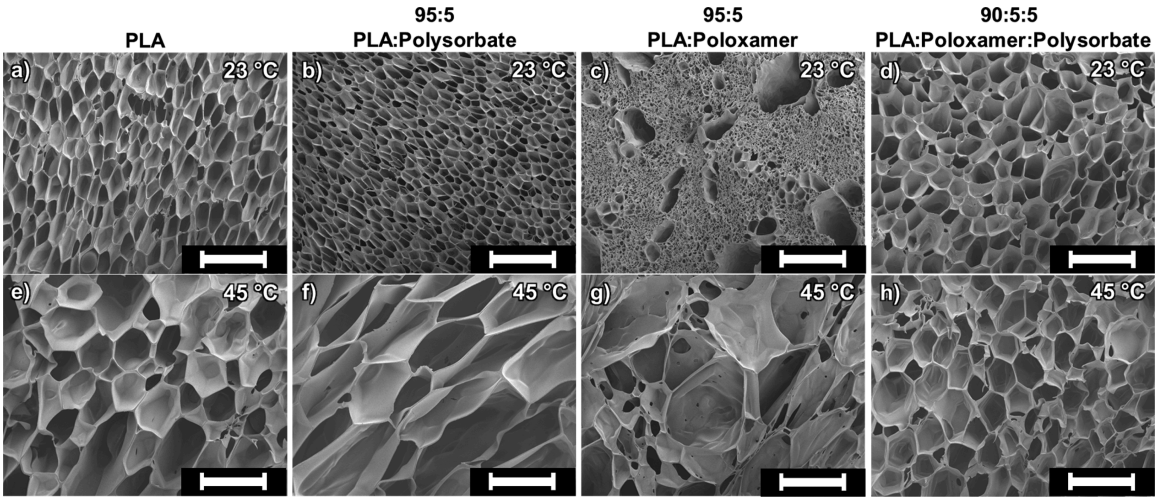

Figure 5.11. Scanning electron microscope images of PLA and PLA/surfactant blend foams prepared at (a−d) 23 °C and (e−h) 45 °C. All foams were prepared with 4-arm PLA (M_n = 50.5 kg/mol) and the surfactants were polysorbate 80 and poloxamer 188 incorporated at 5 wt% loadings. Scale bars are 1 mm.

Water uptake and delivery to cut flowers was tested through a time trial consisting of a flower stem (*Gerbera jamesonii*) cut at 45° and inserted 3 cm into a 100 cm^3 foam sample. The *Gerbera jamesonii* was selected due to its established sensitivity to water availability. Two control flowers (one in a dry container and a second in 100 mL tap water) were placed alongside a flower in commercial floral foam and another in PLA base formulation foam, both foams soaked to saturation in tap water before flower insertion. The water uptake for the commercial foam was >95% and the experimental PLA-based foam had a water uptake of 40%. The flowers were photographed every 2 h to monitor both general appearance and rigidity of their stems. The flower in air wilted within 6 h. The

flower in the commercial floral foam sample began to wilt after 36 h. The flower in the PLA base formulation foam began to wilt after 48 h, while the control in water did not wilt for more than 6 days. To test the utility of the PLA based foam having the ability to rewet, water was added to both the commercial floral foam and the PLA-based formulation foam after the flowers had wilted. Rigidity returned to the stem in the PLA foam as it reabsorbed water and delivered it to the flower. The flower in commercial foam, which does not rewet after the initial water absorption removes the surfactant coating, remained wilted.

Figure 5.12. Images of flower arrangement in PLA based floral foam prototype over the course of 132 h with water additions (ca. 10 mL) made every 24 h to maintain hydration.

With the base formulation outperforming commercial floral foam in its hydration of cut flower stems and matching the mechanical properties, we scaled up synthesis to make foam blocks large enough to hold a practical floral arrangement. Seven stems of a variety of flowers and decorative plants were inserted into a tap water soaked 500 cm^3 foam

at <1 cm spacing at approximately 30° angles. These results provide clear evidence that the 4-arm star PLA based formulations afford expanded materials that perform well as foams for the construction of decorative floral arrangements (**Figure 5.12**). Furthermore, we demonstrated that the PLA-based foams could be colored to mimic the appearance of commercial floral foams (**Figure 5.13**).

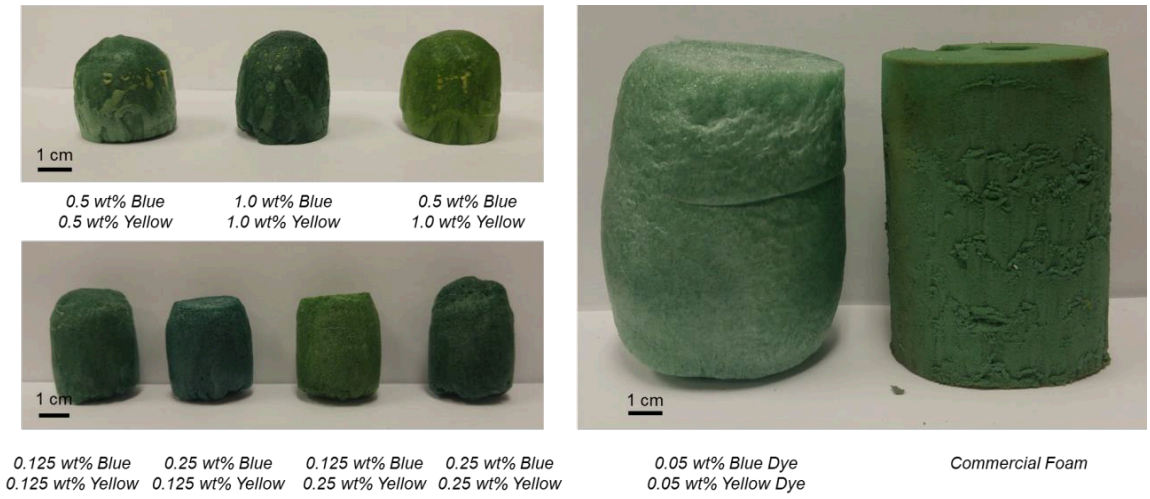

Figure 5.13. Photographs of foams with colorant additives composed of the 90:5:5 4-arm PLA:polysorbate 80:poloxamer 188 formulation and Keyplast™ dyes incorporated at the indicated loading as an additive wt% relative to the total mass of the PLA and surfactant blend. All samples were foamed at 50 °C with 6 MPa (gauge pressure CO_2). A commercial phenolic floral foam is shown for comparison.

5.5 Conclusions

PLA foams are a viable alternative for environmentally challenged foams currently produced from petrochemicals that are essentially nonrecyclable. We expect it to be safe as a consumer product, and as a biodegradable alternative, it can be used in biological applications like drug delivery and tissue scaffolds. The optimization of PLA foams for use in floral foam applications demonstrated the ability to control density over a range of values using both temperature variation and surfactant addition. The use of 3-arm and 4-arm star

polymers drastically improved the foaming characteristics of PLA and allowed for the consistent foaming of coherent, low-density, homogeneous foams, regardless of molar mass. The low-density foams had low compression strengths around 50 kPa, similar to that of commercial floral foam. Adding polysorbate surfactants further stabilized carbon dioxide bubble formation and facilitated greater foam growth at more mild conditions than previous works, at temperatures as low as 20 °C. Finally, the incorporation of poloxamer directly into the polymer formulation imparted significant hydrophilicity without notably modifying the mechanical properties of the foam. A base formulation for the production of floral foams made from compostable and renewable materials was optimized at mild conditions. It matched desired mechanical properties and outperformed the current commercial product in flower longevity trials.

5.6 References

[1] Ghaffari Mosanenzadeh, S.; Doutres, O.; Naguib, H. E.; Park, C. B.; Atalla, N. A. Numerical Scheme for Investigating the Effect of Bimodal Structure on Acoustic Behavior of Polylactide Foams. *Appl. Acoustics* **2015**, *88*, 75−83.

[2] Rouholamin, D.; Smith, P. J.; Ghassemieh, E. Control of Morphological Properties of Porous Biodegradable Scaffolds Processed by Supercritical CO_2 Foaming. *J. Mater. Sci.* **2013**, *48*, 3254−3263.

[3] Shoichet, M. S. Polymer Scaffolds for Biomaterials Applications. *Macromolecules* **2010**, *43*, 581−591.

[4] Mathieu, L. M.; Montjovent, M. O.; Bourban, P. E.; Pioletti, D. P.; Månson, J. A. E. Bioresorbable Composites Prepared by Supercritical Fluid Foaming. *J. Biomed. Mater. Res., Part A* **2005**, *75A*, 89−97.

[5] Smithers, V. L. Absorbent Material for Floral Arrangements. Patent No. US2753277, 1956.

[6] Groot, W.; van Krieken, J.; Sliekersl, O.; de Vos, S. Production and Purification of Lactic Acid and Lactide. In *Poly(Lactic Acid): Synthesis, Structures, Properties,*

Processing, and Application; Auras, R., Lim, L.-K., Selke, S. E. M., Tsuji, H., Eds.; John Wiley & Sons, Inc.: Hoboken, NJ, 2010.

[7] Nofar, M.; Park, C. B. Poly(Lactic Acid) Foaming. *Prog. Polym. Sci.* **2014**, *39*, 1721−1741.

[8] Huang, E.; Liao, X.; Zhao, C.; Park, C. B.; Yang, Q.; Li, G. Effect of Unexpected CO_2's Phase Transition on the High-Pressure Differential Scanning Calorimetry Performance of Various Polymers. *ACS Sustainable Chem. Eng.* **2016**, *4*, 1810−1818.

[9] Mahmood, S. H.; Keshtkar, M.; Park, C. B. Determination of Carbon Dioxide Solubility in Polylactide Acid with Accurate PVT Properties. *J. Chem. Thermodyn.* **2014**, *70*, 13−23.

[10] Li, G.; Li, H.; Turng, L. S.; Gong, S.; Zhang, C. Measurement of Gas Solubility and Diffusivity in Polylactide. *Fluid Phase Equilib.* **2006**, *246*, 158−166.

[11] Jacobs, L. J. M.; Kemmere, M. F.; Keurentjes, J. T. F. Sustainable Polymer Foaming Using High Pressure Carbon Dioxide: A Review on Fundamentals, Processes and Applications. *Green Chem.* **2008**, *10*, 731−738.

[12] Gruber, P. R. Poly(Lactide) Copolymer and Process for Manufacture Thereof. Patent No. US5359026, 1994.

[13] Najafi, N.; Heuzey, M.-C.; Carreau, P. J.; Therriault, D.; Park, C. B. Rheological and Foaming Behavior of Linear and Branched Polylactides. *Rheol. Acta* **2014**, *53*, 779−790.

[14] Pilla, S.; Kim, S. G.; Auer, G. K.; Gong, S.; Park, C. B. Microcellular Extrusion-Foaming of Polylactide with Chain-Extender. *Polym. Eng. Sci.* **2009**, *49*, 1653−1660.

[15] Pilla, S.; Kramschuster, A.; Yang, L. Q.; Lee, J.; Gong, S. Q.; Turng, L. S. Microcellular Injection-Molding of Polylactide with Chain-Extender. *Mater. Sci. Eng., C* **2009**, *29*, 1258−1265.

[16] Zhou, M.; Zhou, P.; Xiong, P.; Qian, X.; Zheng, H. H. Crystallization, Rheology and Foam Morphology of Branched PLA Prepared by Novel Type of Chain Extender. *Macromol. Res.* **2015**, *23*, 231−236.

[17] Li, S.; He, G.; Liao, X.; Park, C. B.; Yang, Q.; Li, G. Introduction of a Long-Chain Branching Structure by Ultraviolet-Induced Reactive Extrusion to Improve Cell Morphology and Processing Properties of Polylactide Foam. *RSC Adv.* **2017**, *7*, 6266−6277.

[18] Gruber, P. R.; Kolstad, J. J.; Witzke, D. R.; Hartmann, M. H.; Brosch, A. L. Viscosity-Modified Lactide Polymer Composition and Process for Manufacture Thereof. Patent No. US5594095, 1997.

[19] Legland, D.; Arganda-Carreras, I. & Andrey, P., MorphoLibJ: integrated library and plugins for mathematical morphology with ImageJ. *Bioinformatics* **2016,** *32*, 3532–3534.

[20] Brutman, J. P.; Delgado, P. A.; Hillmyer, M. A. Polylactide Vitrimers. *ACS Macro Letters* **2014**, *3*, 607-610.

[21] Spinu, M.; Ford, T. M. Degradable Foam Materials. Patent No. US5210108, 1993.

[22] Michaels, A. S.; Bixler, H. J. Solubility of Gases in Polyethylene. *J. Polym. Sci.* **1961**, *50*, 393−412.

[23] Food and Drug Administration (FDA). *Code of Federal Regulations*, Part 175, Title 21; FDA: Washington, DC, 2018.

[24] Kelly, C. A.; Howdle, S. M.; Shakesheff, K. M.; Jenkins, M. J.; Leeke, G. A. Viscosity Studies of Poly(DL-Lactic Acid) in Supercritical CO_2. *J. Polym. Sci., Part B: Polym. Phys.* **2012**, *50*, 1383−1393.

[25] Corneillie, S.; Smet, M. PLA Architectures: The Role of Branching. *Polym. Chem.* **2015**, *6*, 850−867.

[26] Nouri, S.; Dubois, C.; Lafleur, P. G. Effect of chemical and physical branching on rheological behavior of polylactide. *J. Rheol.* **2015**, *59*, 1045−1063.

[27] Dorgan, J. R.; Williams, J. S.; Lewis, D. N. Melt Rheology of Poly(Lactic Acid): Entanglement and Chain Architecture Effects. *J. Rheol.* **1999**, *43*, 1141−1155.

[28] De Gennes, P. G. Reptation of stars. *J. Phys. (Paris)* **1975**, *36*, 1199−1203.

[29] Kim, E. S.; Kim, B. C.; Kim, S. H. Structural effect of linear and star-shaped poly(L-lactic acid) on physical properties. *J. Polym. Sci., Part B: Polym. Phys.* **2004**, *42*, 939−946.

[30] Dorgan, J. R.; Janzen, J.; Clayton, M. P.; Hait, S. B.; Knauss, D. M. Melt rheology of variable L-content poly(lactic acid). *J. Rheol.* **2005**, *49*, 607−619.

[31] Chauvet, M.; Sauceau, M.; Baillon, F.; Fages, J. Mastering the Structure of PLA Foams Made with Extrusion Assisted by Supercritical CO_2. *J. Appl. Polym. Sci.* **2017**, *134*, 45067.

[32] Fujiwara, T.; Yamaoka, T.; Kimura, Y.; Wynne, K. J. Poly(Lactide) Swelling and Melting Behavior in Supercritical Carbon Dioxide and Post-Venting Porous Material. *Biomacromolecules* **2005**, *6*, 2370−2373.

[33] Liao, X.; Nawaby, A. V. Solvent Free Generation of Open and Skinless Foam in Poly(L-Lactic Acid)/Poly(D,L-Lactic Acid) Blends Using Carbon Dioxide. *Ind. Eng. Chem. Res.* **2012**, *51*, 6722−6730.

[34] Ren, Q.; Wang, J.; Zhai, W.; Su, S. Solid State Foaming of Poly(Lactic Acid) Blown with Compressed CO_2: Influences of Long Chain Branching and Induced Crystallization on Foam Expansion and Cell Morphology. *Ind. Eng. Chem. Res.* **2013**, *52*, 13411−13421.

[35] Zhang, X. D.; Macosko, C. W.; Davis, H. T.; Nikolov, A. D.; Wasan, D. T. Role of Silicone Surfactant in Flexible Polyurethane Foam. *J. Colloid Interface Sci.* **1999**, *215*, 270−279.

[36] Ashida, K. *Polyurethane and Related Foams: Chemistry and Technology*; CRC Press: Boca Raton, FL, 2006.

[37] Yeh, D. H.; Pennell, K. D.; Pavlostathis, S. G. Toxicity and Biodegradability Screening of Nonionic Surfactants Using Sediment-Derived Methanogenic Consortia. *Water Sci. Technol.* **1998**, *38*, 55−62.

[38] Yeh, D. H.; Pavlostathis, S. G. Anaerobic Biodegradability of Tween Surfactants Used as a Carbon Source for the Microbial Reductive Dechlorination of Hexachlorobenzene. *Water Sci. Technol.* **2005**, *52*, 343−349.

[39] Mao, H.; Hillmyer, M. A. Morphological Behavior of Polystyrene-block-Polylactide/Polystyrene-Block-Poly(Ethylene Oxide) Blends. *Macromol. Chem. Phys.* **2008**, *209*, 1647−1656.

[40] Sato, S.; Gondo, D.; Wada, T.; Kanehashi, S.; Nagai, K. Effects of Various Liquid Organic Solvents on Solvent-Induced Crystallization of Amorphous Poly(Lactic Acid) Film. *J. Appl. Polym. Sci.* **2013**, *129*, 1607−1617.

[41] Kaushiva, B. D. *Structure−Property Relationships of Flexible Polyurethane Foams.* Ph.D. Dissertation, Virginia Polytechnic Institute and State University, Blacksburg, VA, 1999.

[42] Spitael, P.; Macosko, C. W.; McClurg, R. B. Block Copolymer Micelles for Nucleation of Microcellular Thermoplastic Foams. *Macromolecules* **2004**, *37*, 6874−6882.

[43] Kiss, É.; Bertóti, I.; Vargha-Butler, E. I. XPS and Wettability Characterization of Modified Poly(Lactic Acid) and Poly(Lactic/Glycolic Acid) Films. *J. Colloid Interface Sci.* **2002**, *245*, 91−98.

[44] Kiss, É.; Takács, M. G.; Bertóti, I.; Vargha-Butler, E. I. Surface Properties of Poly(Lactic/Glycolic Acid)−Pluronic® Blend Films. *Polym. Adv. Technol.* **2003**, *14*, 839−846.

[45] Mahoney, C. M.; Yu, J.; Gardella, J. A. Depth Profiling of Poly(L-Lactic Acid)/Triblock Copolymer Blends with Time-of-Flight Secondary Ion Mass Spectrometry. *Anal. Chem.* **2005**, *77*, 3570−3578.

[46] Yu, J.; Mahoney, C. M.; Fahey, A. J.; Hicks, W. L.; Hard, R.; Bright, F. V.; Gardella, J. A. Phase Separation at the Surface of Poly(Ethylene Oxide)-Containing Biodegradable Poly(L-Lactic Acid) Blends. *Langmuir* **2009**, *25*, 11467−11471.

[47] Park, T. G.; Cohen, S.; Langer, R. Poly(L-Lactic Acid)/Pluronic Blends: Characterization of Phase Separation Behavior, Degradation, and Morphology and Use as Protein-Releasing Matrixes. *Macromolecules* **1992**, *25*, 116−122.

[48] Lee, J.-W.; Jeong, E. D.; Cho, E. J.; Gardella, J. A.; Hicks, W.; Hard, R.; Bright, F. V. Surface-Phase Separation of PEO-Containing Biodegradable PLLA Blends and Block Copolymers. *Appl. Surf. Sci.* **2008**, *255*, 2360−2364.

[49] Ahn, J. S.; Suh, J. M.; Lee, M.; Jeong, B. Slow Eroding Biodegradable Multiblock Poloxamer Copolymers. *Polym. Int.* **2005**, *54*, 842−847.

[50] Mosanenzadeh, S. G.; Naguib, H. E.; Park, C. B.; Atalla, N. Development of Polylactide Open-Cell Foams with Bimodal Structure for High-Acoustic Absorption. *J. Appl. Polym. Sci.* **2014**, *131*, 39518.

[51] Harris, L. D.; Kim, B. S.; Mooney, D. J. Open Pore Biodegradable Matrices Formed with Gas Foaming. *J. Biomed. Mater. Res.* **1998**, *42*, 396−402.

[52] Cuénoud, M.; Bourban, P.-E.; Plummer, C. J. G.; Månson, J.-A. E. Plasticization of Polylactide Foams for Tissue Engineering. *J. Cell. Plast.* **2012**, *48*, 409−432.

[53] Yu, P.; Mi, H. Y.; Huang, A.; Geng, L. H.; Chen, B. Y.; Kuang, T. R.; Mou, W. J.; Peng, X. F. Effect of Poly(Butylenes Succinate) on Poly(Lactic Acid) Foaming Behavior: Formation of Open Cell Structure. *Ind. Eng. Chem. Res.* **2015**, *54*, 6199−6207.

[54] Salerno, A.; Clerici, U.; Domingo, C. Solid-State Foaming of Biodegradable Polyesters by Means of Supercritical CO2/Ethyl Lactate Mixtures: Towards Designing Advanced Materials by Means of Sustainable Processes. *Eur. Polym. J.* **2014**, *51*, 1−11.

[55] Lee, P. C.; Naguib, H. E.; Park, C. B.; Wang, J. Increase of Open-Cell Content by Plasticizing Soft Regions with Secondary Blowing Agent. *Polym. Eng. Sci.* **2005**, *45*, 1445−1451.

[56] Nielsen, M.; Junge, H.; Kammer, A.; Beller, M. Towards a Green Process for Bulk-Scale Synthesis of Ethyl Acetate: Efficient Acceptorless Dehydrogenation of Ethanol. *Angew. Chem., Int. Ed.* **2012**, *51*, 5711−5713.

[57] Takishima, S.; O'Neil, M. L.; Johnston, K. P. Solubility of Block Copolymer Surfactants in Compressed CO2 Using a Lattice Fluid Hydrogen-Bonding Model. *Ind. Eng. Chem. Res.* **1997**, *36*, 2821−2833.

Chapter 6. Future Work

6.1 Block polymer charge mosaic thin films

Incremental progress has been made in the synthesis and characterization of solid-state block polyelectrolytes. Our work first focused on the development and characterization of thin films containing oppositely charged block polymer domains. After designing a postpolymerization modification strategy, we used reversible addition-fragmentation chain transfer polymerization (RAFT) for the synthesis of ABC triblock polymers in **Chapter 2**. While we successfully designed a system with a mild, 2-in-1 functionalization reaction using trimethylamine, we were unable to form self-assembled morphologies with long range order. Future work will need to continue using the strategy of neutral self-assembly followed by postpolymerization modification to reach systems with good long-range order and improved mechanical properties. Since the publication of our work, a new paper has been published achieving vertically oriented, positively charged cylinders with excellent long-range order dispersed in a negatively charged matrix.[1] While there is good order in the system, functionalization to high conversions led to practical problems with the films and there were some data that suggested potential morphological change during the reaction. Future research will need to focus on the development of polymers with clear microphase separation, a strong neutral support block, and long-range ordering that maintains morphology through functionalization.

Work will also be needed to improve the mechanical properties of the thin films to increase applicability in membrane separations. The polymers we synthesized in **Chapter 2** proved to be extremely brittle and incapable of withstanding any significant pressure without fracture. Using these materials as an active layer on a porous support requires

flexibility and integrity. One strategy may be to use a rubbery block as the neutral support and crosslink it after self-assembly, continuing the use of ABC triblock polymers by introducing flexibility to our demonstrated system. Unfortunately, the high osmotic pressure due to swelling of the polyelectrolyte may cause even a heavily crosslinked matrix to distort, damaging the morphology and introducing a new set of problems in characterization and application.

6.2 Polymerization-induced microphase separated monoliths

6.2.1 Synthesis of thin active layers for membrane separations

Because of the difficulties in thin film self-assembly and composite membrane fabrication, we approached the problem using polymerization-induced microphase separation (PIMS) in **Chapter 3**. PIMS will likely be a more successful approach to making scalable materials with desired properties. The aim in the future is to incorporate the charged PIMS materials we made into an active layer of a functional membrane. There are several possible strategies to incorporate these materials that should be the focus of future work.

The first proposed approach is to simply fabricate an extremely thin PIMS membrane. Some previous unpublished work in our group successfully synthesized remarkably thin PIMS samples by polymerizing the sample between thinly spaced pieces of glass, although there were myriad practical issues like delamination from the glass after synthesis and evaporation of monomer during the process. A second method has been proposed attempting a PIMS polymerization at an interface, allowing for the polymerization of a thin layer of macroinitiator solution, and therefore a thin, floating

PIMS layer that could simply be lifted out of a solution onto a porous support. A larger PIMS sample could also be mechanically reduced (sanded) down to a thickness of tens of microns and using certain tools, it may be possible to reduce the thickness even further. A sample that thin will likely be brittle on the macroscale but placing an ultrathin layer onto a solid porous support may give the mechanical integrity needed to withstand significant pressure.

A second proposed approach incorporates PIMS materials into the pores of an existing support. By soaking the homogeneous PIMS solution into a membrane and heating to form the PIMS, it may be possible to incorporate the PIMS directly into the support membrane, which gives significant support to the PIMS portion (it is supported on all sides every few hundred nanometers). Unfortunately, the chemical compatibility with the support can cause problems with the synthesis and the thickness and tortuosity of common membranes can lead to effective active layer thicknesses far larger than desired.

6.2.2 Synthesis of charge mosaic PIMS monoliths and controlling swelling

These approaches may allow the fabrication of a PIMS composite membrane, which is an important step towards their ultimate application. At the same time, the materials in **Chapter 3** only contain single charges. The goal of a charge mosaic membrane requires both positive and negative charges to be incorporated into the PIMS material. The creation of a charge mosaic PIMS is approached in **Appendix A**, which presents two early attempted strategies towards the incorporation of oppositely charged domains using mixed macroinitiators and block polymer macroinitiators to form tricontinuous materials. Finally,

a proposed design is presented for a block polymer PIMS monolith that uses a polyelectrolyte as the matrix domain.

The use of a PIMS material as an ion-exchange membrane raises a number of fundamental questions about the characteristics that make polyelectrolytes useful materials for the conduction of charged molecules. In **Appendix B**, we suggest a method for using block polymer macroinitiators to create a PIMS monolith with controlled swelling. By adding a degradable domain to the macroinitiator, a portion of the fabricated monolith can be etched away to allow for increased swelling. We hypothesize this model system will provide insight into the fundamental properties of polyelectrolytes that affect their ion conductivity including degree of swelling, morphology, and ion density.

6.3 Poly(vinylbenzyl chloride) and polystyrene

Chapter 4 explores the unexpected miscibility between polystyrene (PS) and poly(vinylbenzyl chloride (PVBC) observed in **Chapter 2**. While we attempted to measure the Flory-Huggins interaction parameter, we were unable to determine a precise value. Follow up work with neutron scattering of homogeneous blends will likely show a significant improvement in the incoherent scattering over the small-angle X-ray scattering we attempted and will likely allow a precise fitting to measure the parameter. Knowledge of the parameter will allow for future work on the solid-state physics of the PS-*b*-PVBC block polymers, which could be useful for a number of applications in solid state polyelectrolytes. The fact that PS and PVBC are miscible is in itself an interesting fundamental question of polymer physics (as PVBC and poly(4-chlorostyrene), an *almost*

identical monomer, have a much higher interaction parameter). The fundamental study of polymer miscibility would benefit from further exploration of this system.

6.4 Hydrophilic poly(lactide) foams

Hydrophilic floral foams are a niche application that polylactide (PLA) is well suited for as a compostable, biosourced polymer. Additionally, there are a number of other applications of hydrophilic foams that could build on our initial work in **Chapter 5**. For example, the biocompatibility and degradability of PLA foams have made them a common target material for use as tissue scaffolds and drug delivery systems. In these previous works, the hydrophobicity of PLA is a commonly cited problem. Our use of surfactants made the surface of the PLA hydrophilic without affecting its structural integrity even in aqueous environments, which could make these materials good candidates for biological applications. Our work also showed further evidence that a star polymer architecture increases the melt strength of PLA and makes it a more suitable material for certain processing conditions. While this has been suggested in the past, further work should be done on PLA architecture and its mechanical properties under expansion.

6.5 References

[1] Fultz, B. A.; Terlier, T.; Dunoyer de Segonzac, B.; Verduzco, R.; Kennemur, J. G. Nanostructured Films of Oppositely Charged Domains from Self-Assembled Block Copolymers. *Macromolecules* **2020**, *53*, 5638–5648.

Bibliography

Abreu, A. S.; Oliveira, M.; Rodrigues, P. V.; Moura, I.; Botelho, G.; Machado, A. V. Synthesis and characterization of polystyrene-block-poly(vinylbenzoic acid): a promising compound for manipulating photoresponsive properties at the nanoscale. *J. Mater. Sci.* **2015**, *50*, 2788–2796.

Ahmed, L. S.; Xia, J.; Dubin, P. L.; Kokufuta, E. Stoichiometry and the Mechanism of Complex Formation in Protein-Polyelectrolyte Coacervation. *J. Macromol. Sci., Part A: Pure Appl.Chem.* **1994**, *31*, 17−29.

Ahn, J. S.; Suh, J. M.; Lee, M.; Jeong, B. Slow Eroding Biodegradable Multiblock Poloxamer Copolymers. *Polym. Int.* **2005**, *54*, 842−847.

Albert, J. N. L.; Epps, T. H. Self-assembly of block copolymer thin films. *Mater. Today* **2010**, *13*, 24−33.

Alexandratos, S. D. Ion-Exchange Resins: A Retrospective from Industrial and Engineering Chemistry Research. *Ind. Eng. Chem. Res.* **2009**, *48*, 388−398.

AmberLite™ HPR9200 Cl Product Data Sheet, 1st ed.; Dupont, 2019; pp 1–4.

American Chemical Society National Historic Chemical Landmarks. Bakelite: the World's First Synthetic Plastic. *American Chemical Society*. http://www.acs.org/content/acs/en/education/whatischemistry/landmarks/bakelite.html (accessed June 9, 2020).

Anderson, K. S.; Hillmyer, M. A. Melt Chain Dimensions of Polylactide. *Macromolecules* **2004**, *37*, 1857–1862.

Antonov, M.; Mazzawi, M.; Dubin, P. L. Entering and Exiting the Protein−Polyelectrolyte Coacervate Phase via Nonmonotonic Salt Dependence of Critical Conditions. *Biomacromolecules* **2010**, *11*, 51−59.

Ashida, K. *Polyurethane and Related Foams: Chemistry and Technology*; CRC Press: Boca Raton, FL, 2006.

Auras, R. A.; Lim, L. T.; Selke, S. E. M.; Tsuji, H. *Poly(lactic acid): Synthesis, Structures, Properties, Processing, and Applications*; John Wiley & Sons, Inc.: Hoboken, NJ, 2010.

Baruth, A.; Rodwogin, M. D.; Shankar, A.; Erickson, M. J.; Hillmyer, M. A.; Leighton, C., Non-lift-off Block Copolymer Lithography of 25 nm Magnetic Nanodot Arrays. *ACS Appl. Mater. Interfaces* **2011**, *3*, 3472-3481.

Bates, F. S.; Fetters, L. J.; Wignall, G. D. Thermodynamics of Isotopic Polymer Mixtures: Poly(vinyl ethylene) and Poly(ethylethylene). *Macromolecules* **1988**, *21*, 1086–1094.

Bates, F. S.; Fredrickson, G. H. Block Copolymers–Designer Soft Materials. *Phys. Today* **1999**, *52*, 32−38.

Bates, F. S.; Wignall, G. D.; Koehler, W. C. Critical Behavior of Binary Liquid Mixtures of Deuterated and Protonated Polymers. *Phys. Rev. Lett.* **1985**, *55*, 2425–2428.

Bolto, B.; Hoang, M.; Tran, T. Review of Piezodialysis — Salt Removal with Charge Mosaic Membranes. *Desalination* **2010**, *254* (1-3), 1–5.

Boschan, R.; Merrow, R. T.; Van Dolah, R. W. The Chemistry of Nitrate Esters. *Chem. Rev.* **1955**, *55*, 485–510.

Boyd, G. E.; Larson, Q. V. The Binding of Quaternary Ammonium Ions by Polystyrenesulfonic Acid Type Cation Exchangers. *J. Am. Chem. Soc.* **1967**, *89*, 6038–6042.

Bronich, T. K.; Kabanov, A. V.; Kabanov, V. A.; Yu, K.; Eisenberg, A. Soluble Complexes from Poly(ethylene oxide)-*block*-polymethacrylate Anions and *N*-Alkylpyridinium Cations. *Macromolecules* **1997**, *30*, 3519−3525.

Brown, D. W. and Lowry R. E. Molecular weight standards from sulfonation of polystyrene. *J. Polymer Sci.* **1979**, *17*, 1039–1046.

Brunwin, D. M.; Fischer, E.; Henderson, J. F. Developments in Self-Reinforced Elastomers. *Journal of Polymer Science Part C* **1969**, *26*, 135–147.

Brutman, J. P.; Delgado, P. A.; Hillmyer, M. A. Polylactide Vitrimers. *ACS Macro Letters* **2014**, *3*, 607-610.

Campione, A.; Gurreri, L.; Ciofalo, M.; Micale, G.; Tamburini, A.; Cipollina, A. Electrodialysis for water desalination: A critical assessment of recent developments on process fundamentals, models and applications. *Desalination* **2018**, *434*, 121–160.

Cao, Y.-C.; Wang, X.; Mamlouk, M.; Scott, K. Preparation of alkaline anion exchange polymer membrane from methylated melamine grafted poly(vinylbenzyl chloride) and its fuel cell performance. *J. Mater. Chem.* **2011**, *21*, 12910−12916.

Carothers, W. H.; Williams, I.; Collins, A. M.; Kirby, J. E. Acetylene Polymers and Their Derivatives. Ii. a New Synthetic Rubber: Chloroprene and Its Polymers. *Journal of the American Chemical Society* **1931**, *53*, 4203–4225.

Chauvet, M.; Sauceau, M.; Baillon, F.; Fages, J. Mastering the Structure of PLA Foams Made with Extrusion Assisted by Supercritical CO_2. *J. Appl. Polym. Sci.* **2017**, *134*, 45067.

Chen, L.; Hallinan, D. T., Jr.; Elabd, Y. A.; Hillmyer, M. A. Highly Selective Polymer Electrolyte Membranes from Reactive Block Polymers. *Macromolecules* **2009**, *42*, 6075−6085.

Chen, X. C.; Jiang, X.; Balsara, N. P. Swelling of individual nanodomains in hydrated block copolymer electrolyte membranes. *J. Chem. Phys.* **2018**, *149*, 163325.

Chen, X. C.; Kortright, J. B.; Balsara, N. P. Water Uptake and Proton Conductivity in Porous Block Copolymer Electrolyte Membranes. *Macromolecules* **2015**, *48*, 5648–5655.

Choi, J.; Huh, J.; Carter, K. R.; Russell, T. P. Directed Self-Assembly of Block Copolymer Thin Films Using Minimal Topographic Patterns. *ACS Nano* **2016**, *10*, 7915−7925.

Chollakup, R.; Smitthipong, W.; Eisenbach, C. D.; Tirrell, M. Phase Behavior and Coacervation of Aqueous Poly(acrylic acid)-Poly(allylamine) Solutions. *Macromolecules* **2010**, *43*, 2518−2528.

Chopade, S. A.; Anderson, E. L.; Schmidt, P. W.; Lodge, T. P.; Hillmyer, M. A.; Bühlmann, P. Self-Supporting, Hydrophobic, Ionic Liquid-Based Reference Electrodes Prepared by Polymerization-Induced Microphase Separation. *ACS Sens.* **2017**, *2*, 1498–1504.

Corneillie, S.; Smet, M. PLA Architectures: The Role of Branching. *Polym. Chem.* **2015**, *6*, 850−867.

Couture, G.; Alaaeddine, A.; Boschet, F.; Ameduri, B. Polymeric materials as anion-exchange membranes for alkaline fuel cells. *Prog. Polym. Sci.* **2011**, *36*, 1521–1557.

Couture, G.; Améduri, B. Kinetics of RAFT homopolymerisation of vinylbenzyl chloride in the presence of xanthate or trithiocarbonate. *Eur. Polym. J.* **2012**, *48*, 1348−1356.

Cuénoud, M.; Bourban, P.-E.; Plummer, C. J. G.; Månson, J.-A. E. Plasticization of Polylactide Foams for Tissue Engineering. *J. Cell. Plast.* **2012**, *48*, 409−432.

De Gennes, P. G. Reptation of stars. *J. Phys. (Paris)* **1975**, *36*, 1199−1203.

De Gennes, P. G. *Scaling Concepts in Polymer Physics*; Cornell Univ. Press: Ithaca, New York, 1979.

Delaney, K. T.; Fredrickson, G. H. Theory of polyelectrolyte complexation−Complex coacervates are self-coacervates. *J. Chem. Phys.* **2017**, *146*, 224902.

Dieter, C. A.; Maupin, M. A.; Caldwell, R. R.; Harris, M. A.; Ivahnenko, T. I.; Lovelace, J. K.; Barber, N. L.; Linsey, K. S. *Estimated Use of Water in the United States in 2015*; U.S. Department of the Interior and U.S. Geological Survey: Reston, Virginia, 2018; pp 1–76.

Dobrynin, A. V.; Colby, R. H.; Rubinstein, M. Polyampholytes. *J. Polym. Sci., Part B: Polym. Phys.* **2004**, *42*, 3513−3538.

Dorgan, J. R.; Janzen, J.; Clayton, M. P.; Hait, S. B.; Knauss, D. M. Melt rheology of variable L-content poly(lactic acid). *J. Rheol.* **2005**, *49*, 607−619.

Dorgan, J. R.; Williams, J. S.; Lewis, D. N. Melt Rheology of Poly(Lactic Acid): Entanglement and Chain Architecture Effects. *J. Rheol.* **1999**, *43*, 1141−1155.

Einstein, A. Über Einen Die Erzeugung Und Verwandlung Des Lichtes Betreffenden Heuristischen Gesichttspunkt. *Annalen der Physik* **1905**, *322*, 132–148.

Elimelech, M.; Phillip, W. A. The Future of Seawater Desalination: Energy, Technology, and the Environment. *Science* **2011**, *333*, 712–717.

Ferris, A. F.; McLean, K. W.; Marks, I. G.; Emmons, W. D. Metathetical Reactions of Silver Salts in Solution. III. The Synthesis of Nitrate Esters. *J. Am. Chem. Soc.* **1953**, *75*, 4078.

Flory, P. J. Thermodynamics of High Polymer Solutions. *J. Chem. Phys.* **1941**, *9*, 660–660.

Flory, P. J. Thermodynamics of High Polymer Solutions. *J. Chem. Phys.* **1942**, *10*, 51–61.

Food and agriculture organization of the United Nations. Coping with Water Scarcity : an Action Framework for Agriculture and Food Security. **2012**, 1–100.

Food and Drug Administration (FDA). *Code of Federal Regulations*, Part 175, Title 21; FDA: Washington, DC, 2018.

Francisco, M. A.; Krylowski, J. Chemistry of Organic Nitrates: Thermal Chemistry of Linear and Branched Organic Nitrates. *Ind. Eng. Chem. Res.* **2005**, *44*, 5439–5446.

Freyer, J. L.; Brucks, S. D.; Campos, L. M. Fully charged: Maximizing the potential of cationic polyelectrolytes in applications ranging from membranes to gene delivery through rational design. *J. Polym. Sci., Part A: Polym. Chem.* **2017**, *55*, 3167−3174.

Fujimoto, T.; Ohkoshi, K.; Miyaki, Y.; Nagasawa, M. A New Charge-Mosaic Membrane from a Multiblock Copolymer. *Science* **1984**, *224*, 74−76.

Fujiwara, T.; Yamaoka, T.; Kimura, Y.; Wynne, K. J. Poly(Lactide) Swelling and Melting Behavior in Supercritical Carbon Dioxide and Post-Venting Porous Material. *Biomacromolecules* **2005**, *6*, 2370−2373.

Fultz, B. A.; Terlier, T.; Dunoyer de Segonzac, B.; Verduzco, R.; Kennemur, J. G. Nanostructured Films of Oppositely Charged Domains from Self-Assembled Block Copolymers. *Macromolecules* **2020**, *53*, 5638–5648.

Furia, T. E. *CRC Handbook of Food Additives*, Second Edition. CRC Press: Boca Raton, Florida, 1973; Vol. 1.

Gao, P.; Hunter, A.; Summe, M. J.; Phillip, W. A. A Method for the Efficient Fabrication of Multifunctional Mosaic Membranes by Inkjet Printing. *ACS Appl. Mater. Interfaces* **2016**, *8*, 19772−19779.

Geise, G. M.; Paul, D. R.; Freeman, B. D. Fundamental Water and Salt Transport Properties of Polymeric Materials. *Progress in Polymer Science* **2014**, *39*, 1–42.

Ghaffari Mosanenzadeh, S.; Doutres, O.; Naguib, H. E.; Park, C. B.; Atalla, N. A. Numerical Scheme for Investigating the Effect of Bimodal Structure on Acoustic Behavior of Polylactide Foams. *Appl. Acoustics* **2015**, *88*, 75−83.

Gleick, P. H. Water, Drought, Climate Change, and Conflict in Syria. *Weather, Climate, and Society* **2014**, *6*, 331–340.

Goldfeld, D. J.; Silver, E. S.; Radlauer, M. R.; Hillmyer, M. A. Synthesis and Self-Assembly of Block Polyelectrolyte Membranes through a Mild, 2-in-1 Postpolymerization Treatment. *ACS Appl. Poly. Mater.* **2020**, *2*, 817–825.

Goodyear, C. Improvement in the Mode of Preparing Caoutchouc with Sulphur for the Manufacture of Various Articles. February 24, 1839.

Graham, A. T.; Buchholz, F. L. *Modern Superabsorbent Polymer Technology*; Wiley-VCH: New York, 1998.

Greenlee, L. F.; Lawler, D. F.; Freeman, B. D.; Marrot, B.; Moulin, P. Reverse Osmosis Desalination: Water Sources, Technology, and Today•S Challenges. *Water Research* **2009**, *43*, 2317–2348.

Groot, W.; van Krieken, J.; Sliekersl, O.; de Vos, S. Production and Purification of Lactic Acid and Lactide. In *Poly(Lactic Acid): Synthesis, Structures, Properties, Processing, and Application*; Auras, R., Lim, L.-K., Selke, S. E. M., Tsuji, H., Eds.; John Wiley & Sons, Inc.: Hoboken, NJ, 2010.

Gruber, P. R. Poly(Lactide) Copolymer and Process for Manufacture Thereof. Patent No. US5359026, 1994.

Gruber, P. R.; Kolstad, J. J.; Witzke, D. R.; Hartmann, M. H.; Brosch, A. L. Viscosity-Modified Lactide Polymer Composition and Process for Manufacture Thereof. Patent No. US5594095, 1997.

Gucht, J. v. d.; Spruijt, E.; Lemmers, M.; Cohen Stuart, M. A. Polyelectrolyte complexes: bulk phases and colloidal systems. *J. Colloid Interface Sci*. **2011**, *361*, 407−422.

Guliyeva, A.; Vayer, M.; Warmont, F.; Faugère, A. M.; Andreazza, P.; Takano, A.; Matsushita, Y.; Sinturel, C. Thin Films with Perpendicular Tetragonally Packed Rectangular Rods Obtained from Blends of Linear ABC Block Terpolymers. *ACS Macro Lett.* **2018**, *7*, 789−794.

Haladjova, E.; Mountrichas, G.; Pispas, S.; Rangelov, S. Poly(vinylbenzyl trimethylammonium chloride) Homo and Block Copolymers Complexation with DNA. *J. Phys. Chem. B* **2016**, *120*, 2586−2595.

Harris, L. D.; Kim, B. S.; Mooney, D. J. Open Pore Biodegradable Matrices Formed with Gas Foaming. *J. Biomed. Mater. Res.* **1998**, *42*, 396−402.

Harry, K. J. Lithium dendrite growth through solid polymer electrolyte membranes. PhD Thesis, University of California, Berkeley: Berkeley, CA, 2016.

Haviland, D. B. Quantitative force microscopy from a dynamic point of view. *Curr. Opin. Colloid Interface Sci.* **2017**, *27*, 74−81.

He, Y.; He, W.; Wei, R.; Chen, Z.; Wang, X. Synthesizing Amphiphilic Block Copolymers Through Macromolecular Azo-Coupling Reaction. *Chem. Commun.* **2012**, *48*, 1036–1038.

Hickner, M. A.; Herring, A. M.; Coughlin, E. B. Anion exchange membranes: Current status and moving forward. *J. Polym. Sci., Part B: Polym. Phys.* **2013**, *51*, 1727−1735.

Hiemenz, P. C.; Lodge, T. P. *Polymer Chemistry, 2nd ed.*; CRC Press: Boca Raton, FL, 2007.

Higa, M.; Masuda, D.; Kobayashi, E.; Nishimura, M.; Sugio, Y.; Kusudou, T.; Fujiwara, N. Charge mosaic membranes prepared from laminated structures of PVA-based charged layers: 1. Preparation and transport properties of charged mosaic membranes. *J. Membr. Sci.* **2008**, *310*, 466−473.

Higgins, T. M.; Park, S. H.; King, P. J.; Zhang, C. J.; McEvoy, N.; Berner, N. C.; Daly, D.; Shmeliov, A.; Khan, U.; Duesberg, G.; Nicolosi, V.; Coleman, J. N. A Commercial Conducting Polymer as Both Binder and Conductive Additive for Silicon Nanoparticle-Based Lithium-Ion Battery Negative Electrodes. *ACS Nano* **2016**, *10*, 3702−3713.

Hirahara, K.; Takahashi, S.-I.; Iwata, M.; Fujimoto, T.; Miyaki, Y. Artificial Membranes From Multiblock Copolymers. 5. Transport Behaviors of Organic and Inorganic Solutes Through a Charge-Mosaic Membrane. *Industrial Engineering Chemistry Research* **1986**, No. 25, 305–313.

Huang, E.; Liao, X.; Zhao, C.; Park, C. B.; Yang, Q.; Li, G. Effect of Unexpected CO_2's Phase Transition on the High-Pressure Differential Scanning Calorimetry Performance of Various Polymers. *ACS Sustainable Chem. Eng.* **2016**, *4*, 1810−1818.

Hunt, J. N.; Feldman, K. E.; Lynd, N. A.; Deek, J.; Campos, L. M.; Spruell, J. M.; Hernandez, B. M.; Kramer, E. J.; Hawker, C. J. Tunable, high modulus hydrogels driven by ionic coacervation. *Adv. Mater.* **2011**, *23*, 2327−2331.

Hunt, T. V.; DeMott, J. M.; Ackerbauer, K. A.; Whittier, W. L.; Peksa, G. D. Single-dose sodium polystyrene sulfonate for hyperkalemia in chronic kidney disease or end-stage renal disease. *Clin. Kidney J.* **2019**, *12*, 408−413.

ImAFM Overview. Intermodulation Products AB, Sweden. https://intermodulation-products.com/support/tutorials (accessed June 7, 2019).

Isono, Y.; Ito, H.; Hirahara, K.; Fujimoto, T.; Miyaki, Y. Weak Acid-Strong Base Type Charge-Mosaic Membrane. I. Carboxylic Acid-Quaternary Amine System. *Journal of Membrane Science* **1989**, *43*, 205–216.

Isono, Y.; Tanisugi, H.; Endo, K.; Fujimoto, T.; Hasegawa, H.; Hashimoto, T.; Kawai, H. Morphological and Mechanical Properties of Multiblock Copolymers. *Macromolecules* **1983**, *16*, 5−10.

Jackson, G. L. Nanoconfined Water and Water-mediated Ion Transport in Model Lyotropic Liquid Crystals. PhD Thesis, University of Wisconsin-Madison: Madison, WI, 2018.

Jacobs, L. J. M.; Kemmere, M. F.; Keurentjes, J. T. F. Sustainable Polymer Foaming Using High Pressure Carbon Dioxide: A Review on Fundamentals, Processes and Applications. *Green Chem.* **2008**, *10*, 731−738.

Jenkins, A. D.; Kratochvíl, P.; Stepto, R. F. T.; Suter, U. W. Glossary of Basic Terms in Polymer Science (IUPAC Recommendations 1996). *Pure Applied Chemistry* **1996**, *68*, 2287–2311.

Jeon, C.; Han, J. J.; Seo, M. Control of Ion Transport in Sulfonated Mesoporous Polymer Membranes. *ACS Appl. Mater. Interfaces* **2018**, *10*, 40854–40862.

Jones, T. D.; Chaffin, K. A.; Bates, F. S.; Annis, B. K.; Hagaman, E. W.; Kim, M.-H.; Wignall, G. D.; Fan, W.; Waymouth, R. Effect of Tacticity on Coil Dimensions and Thermodynamic Properties of Polypropylene. *Macromolecules* **2002**, *35*, 5061–5068.

Kamber, N. E.; Jeong, W.; Waymouth, R. M. Organocatalytic Ring-Opening Polymerization. *Chem. Rev.* **2007**, *107*, 5813−5840.

Kaushiva, B. D. *Structure−Property Relationships of Flexible Polyurethane Foams.* Ph.D. Dissertation, Virginia Polytechnic Institute and State University, Blacksburg, VA, 1999.

Kelly, C. A.; Howdle, S. M.; Shakesheff, K. M.; Jenkins, M. J.; Leeke, G. A. Viscosity Studies of Poly(DL-Lactic Acid) in Supercritical CO_2. *J. Polym. Sci., Part B: Polym. Phys.* **2012**, *50*, 1383−1393.

Kelly, K. D.; Schlenoff, J. B. Spin-Coated Polyelectrolyte Coacervate Films. *ACS Appl. Mater. Interfaces* **2015**, *7*, 13980−13986.

Kennemur, J. G.; Hillmyer, M. A.; Bates, F. S. Synthesis, Thermodynamics, and Dynamics of Poly(4-tert-butylstyrene-b-methyl methacrylate). *Macromolecules* **2012**, *45*, 7228–7236.

Kershner, I. Aided by the Sea, Israel Overcomes an Old Foe: Drought. *New York Times*. May 30, 2015, p A1.

Kim, E. S.; Kim, B. C.; Kim, S. H. Structural effect of linear and star-shaped poly(L-lactic acid) on physical properties. *J. Polym. Sci., Part B: Polym. Phys.* **2004**, *42*, 939−946.

Kim, H.-C.; Park, S.-M.; Hinsberg, W. D. Block Copolymer Based Nanostructures: Materials, Processes, and Applications to Electronics. *Chem. Rev.* **2010**, *110*, 146–177.

Kim, S. Y.; Park, M. J.; Balsara, N. P.; Jackson, A. Confinement Effects on Watery Domains in Hydrated Block Copolymer Electrolyte Membranes. *Macromolecules* **2010**, *43*, 8128–8135.

Kimerling, A. S.; Rochefort, W. E.; Bhatia, S. R. Rheology of Block Polyelectrolyte Solutions and Gels: A Review. *Ind. Eng. Chem. Res*. **2006**, *45*, 6885−6889.

Kiss, É.; Bertóti, I.; Vargha-Butler, E. I. XPS and Wettability Characterization of Modified Poly(Lactic Acid) and Poly(Lactic/Glycolic Acid) Films. *J. Colloid Interface Sci.* **2002**, *245*, 91−98.

Kiss, É.; Takács, M. G.; Bertóti, I.; Vargha-Butler, E. I. Surface Properties of Poly(Lactic/Glycolic Acid)−Pluronic® Blend Films. *Polym. Adv. Technol.* **2003**, *14*, 839−846.

Kolomanska, J.; Johnston, P.; Gregori, A.; Dominguez, I. F.; Egelhaaf, H. -J.; Perrier, S.; Rivaton, A.; Dagron-Lartigau, C.; Topham, P. D. Design, synthesis and thermal

behaviour of a series of well-defined clickable and triggerable sulfonate polymers. *RSC Adv.* **2015**, *5*, 66554–66562.

Kraytsberg, A.; Ein-Eli, Y. Review of Advanced Materials for Proton Exchange Membrane Fuel Cells. *Energy Fuels* **2014**, *28*, 7303–7330.

Lacroix-Desmazes, P.; Delair, T.; Pichot, C.; Boutevin, B. Synthesis of Poly(chloromethylstyrene-b-styrene) Block Copolymers by Controlled Free-Radical Polymerization. *J. Polym. Sci., Part A: Polym. Chem.* **2000**, *38*, 3845−3854.

Larsen, M. B.; Van Horn, J. D.; Wu, F.; Hillmyer, M. A. Intrinsically Hierarchical Nanoporous Polymers via Polymerization-Induced Microphase Separation. *Macromolecules* **2017**, *50*, 4363–4371.

Laschewsky, A. Structures and Synthesis of Zwitterionic Polymers. *Polymers* **2014**, *6*, 1544−1601.

Lee, H.; Yanilmaz, M.; Toprakci, O.; Fu, K.; Zhang, X. A review of recent developments in membrane separators for rechargeable lithium-ion batteries. *Energy Environ. Sci.* **2014**, *7*, 3857–3886.

Lee, J.-W.; Jeong, E. D.; Cho, E. J.; Gardella, J. A.; Hicks, W.; Hard, R.; Bright, F. V. Surface-Phase Separation of PEO-Containing Biodegradable PLLA Blends and Block Copolymers. *Appl. Surf. Sci.* **2008**, *255*, 2360−2364.

Lee, P. C.; Naguib, H. E.; Park, C. B.; Wang, J. Increase of Open-Cell Content by Plasticizing Soft Regions with Secondary Blowing Agent. *Polym. Eng. Sci.* **2005**, *45*, 1445−1451.

Lee, S.; Bluemle, M. J.; Bates, F. S. Discovery of a Frank-Kasper Σ Phase in Sphere-Forming Block Copolymer Melts. *Science* **2010**, *330*, 349–353.

Legland, D.; Arganda-Carreras, I. & Andrey, P., MorphoLibJ: integrated library and plugins for mathematical morphology with ImageJ. *Bioinformatics* **2016,** *32*, 3532–3534.

Leitz, F. B.; Alexander, S. S.; de Winter, D. M.; Plummer, C. W. *Research on Piezodialysis: Second Report*. United States Department of the Interior: Washington, DC, 1970.

Leitz, F. B.; Alexander, S. S.; Douglas, A. S. *Research on Piezodialysis.* United States Department of the Interior: Washington, DC, 1969.

Leitz, F. B.; Sharr, J.; O'Meara, J. W.; Gillam, W. S.; Johnson, S. *Research on piezodialysis: third report.* United States Department of the Interior: Washington, DC, 1972.

Li, G.; Li, H.; Turng, L. S.; Gong, S.; Zhang, C. Measurement of Gas Solubility and Diffusivity in Polylactide. *Fluid Phase Equilib.* **2006**, *246*, 158−166.

Li, S.; He, G.; Liao, X.; Park, C. B.; Yang, Q.; Li, G. Introduction of a Long-Chain Branching Structure by Ultraviolet-Induced Reactive Extrusion to Improve Cell Morphology and Processing Properties of Polylactide Foam. *RSC Adv.* **2017**, *7*, 6266−6277.

Li, Y.; Jackson, A. C.; Beyer, F. L.; Knauss, D. M. Poly(2,6-dimethyl-1,4-phenylene oxide) Blended with Poly(vinylbenzyl chloride)-*b*-polystyrene for the Formation of Anion Exchange Membranes. *Macromolecules* **2014**, *47*, 6757−6767.

Liao, X.; Nawaby, A. V. Solvent Free Generation of Open and Skinless Foam in Poly(L-Lactic Acid)/Poly(D,L-Lactic Acid) Blends Using Carbon Dioxide. *Ind. Eng. Chem. Res.* **2012**, *51*, 6722−6730.

Lienkamp, K.; Schnell, I.; Groehn, F.; Wegner, G. Polymerization of Styrene Sulfonate Ethyl Ester by ATRP: Synthesis and Characterization of Macromonomers for Suzuki Polycondensation. *Macromol. Chem. Phys.* **2006**, *207*, 2066−2073.

Lloyd, W. G.; Durocher, T. E. Nucleophilic Displacements upon Poly(vinylbenzyl chloride). *J. Appl. Polym. Sci.* **1963**, *7*, 2025−2033.

Lopatin, G.; Newey, H. A. Ionic Block Copolymers as Piezodialysis Membranes. In *Reverse Osmosis Membrane Research*; Lonsdale, H. K., Podall, H. E., Eds.; Springer US: Boston, MA, 1972; pp 317–327.

Lowe, A. B.; McCormick, C. L. Synthesis and Solution Properties of Zwitterionic Polymers. *Chem. Rev.* **2002**, *102*, 4177–4190.

Luo, M.; Epps, T. H. Directed Block Copolymer Thin Film Self-Assembly: Emerging Trends in Nanopattern Fabrication. *Macromolecules* **2013**, *46*, 7567−7579.

M. Doucet, et al. *SasView*, Version 5.0.2. http://doi.org/10.5281/zenodo.3011184.

Mahmood, S. H.; Keshtkar, M.; Park, C. B. Determination of Carbon Dioxide Solubility in Polylactide Acid with Accurate PVT Properties. *J. Chem. Thermodyn.* **2014**, *70*, 13−23.

Mahoney, C. M.; Yu, J.; Gardella, J. A. Depth Profiling of Poly(L-Lactic Acid)/Triblock Copolymer Blends with Time-of-Flight Secondary Ion Mass Spectrometry. *Anal. Chem.* **2005**, *77*, 3570−3578.

Malhotra, S. L.; Lessard, P.; Blanchard, L. P. The Thermal Decomposition and Glass Transition Temperature of Poly(*p*-tert-butylstyrene). *J. Macromol. Sci., Chem.* **1981**, *A15*, 121−141.

Malhotra, S. L.; Lessard, P.; Minh, L.; Blanchard, L. P. Thermal Decomposition and Glass-Transition Temperature Study of Poly-*p*-methylstyrene. *J. Macromol. Sci., Chem.* **1980**, *14*, 517−540.

Mao, H.; Hillmyer, M. A. Morphological Behavior of Polystyrene-block-Polylactide/Polystyrene-Block-Poly(Ethylene Oxide) Blends. *Macromol. Chem. Phys.* **2008**, *209*, 1647−1656.

Mathieu, L. M.; Montjovent, M. O.; Bourban, P. E.; Pioletti, D. P.; Månson, J. A. E. Bioresorbable Composites Prepared by Supercritical Fluid Foaming. *J. Biomed. Mater. Res., Part A* **2005**, *75A*, 89−97.

Maul, J.; Frushour, B. G.; Kontoff, J. R.; Eichenauer, H.; Ott, K. -H.; Schade, C. "Polystyrene and Styrene Copolymers" *Ullmann's Encyclopedia of Industrial Chemistry* **2007**, Wiley-VCH, Weinheim.

Mauritz, K. A.; Moore, R. B. State of Understanding of Nafion. *Chem. Rev.* **2004**, *104*, 4535–4586.

Mays, J. W. and Hadjichristidis, N. Synthesis of high molecular weight near-monodisperse poly(4-methylstyrene) by anionic polymerization. *Polymer Bulletin* **1989**, *22*, 471–474.

Mendes, P. M.; Yeung, C. L.; Preece, J. A. Bio-nanopatterning of Surfaces. *Nanoscale Res. Lett.* **2007**, *2*, 373−384.

Merrifield, R. B. The Synthesis of a Tetrapeptide. *J. Am. Chem. Soc.* **1963**, *85*, 2149−2154.

Michaels, A. S.; Bixler, H. J. Solubility of Gases in Polyethylene. *J. Polym. Sci.* **1961**, *50*, 393−412.

Minneapolis Flour Milling Boom. *Minnesota Historical Society*. https://www.mnhs.org/millcity/learn/history/flour-milling (accessed June 9, 2020).

Miyaki, Y.; Iwata, M.; Fujita, Y.; Tanisugi, H.; Isono, Y.; Fujimoto, T. Artificial Membranes from Multiblock Copolymers. 2. Molecular Characterization and Morphological Behavior of Pentablock Copolymers of the ISIAI Type. *Macromolecules* **1984**, *17*, 1907−1912.

Moad, G.; Chong, Y. K.; Postma, A.; Rizzardo, E.; Thang, S. H. Advances in RAFT polymerization: the synthesis of polymers with defined end-groups. *Polymer* **2005**, *46*, 8458–8468.

Moad, G.; Rizzardo, E.; Thang, S. H. Radical addition−fragmentation chemistry in polymer synthesis. *Polymer* **2008**, *49*, 1079−1131.

Mondal, S.; Das, S.; Nandi, A. K. A Review on Recent Advances in Polymer and Peptide Hydrogels. *Soft Matter* **2020**, *16*, 1404–1454.

Mosanenzadeh, S. G.; Naguib, H. E.; Park, C. B.; Atalla, N. Development of Polylactide Open-Cell Foams with Bimodal Structure for High-Acoustic Absorption. *J. Appl. Polym. Sci.* **2014**, *131*, 39518.

Mühlebach, A.; Gaynor, S. G.; Matyjaszewski, K. Synthesis of Amphiphilic Block Copolymers by Atom Transfer Radical Polymerization (ATRP). *Macromolecules* **1998**, *31*, 6046–6052.

Muthukumar, M. 50th Anniversary Perspective: a Perspective on Polyelectrolyte Solutions. *Macromolecules* **2017**, *50*, 9528–9560.

Najafi, N.; Heuzey, M.-C.; Carreau, P. J.; Therriault, D.; Park, C. B. Rheological and Foaming Behavior of Linear and Branched Polylactides. *Rheol. Acta* **2014**, *53*, 779−790.

Neihof, R.; Sollner, K. A Quantitative Electrochemical Theory of the Electrolyte Permeability of Mosaic Membranes Composed of Selectively Anion-Permeable and Selectively Cation-Permeable Parts and Its Experimental Verification. I. an Outline of the Theory and Its Quantitative Test in Model Systems with Auxiliary Electrodes. *J. Phys. Chem.* **1950**, *54*, 157–176.

Neihof, R.; Sollner, K. A Quantitative Electrochemical Theory of the Electrolyte Permeability of Mosaic Membranes Composed of Selectively Anion-Permeable Parts, and Its Experimental Verification: II. a Quantitative Test of the Theory in Model Systems Which Do Not Involve the Use of Auxiliary Electrodes. *The Journal of General Physiology* **1955**, *38*, 613–622.

Nielsen, M.; Junge, H.; Kammer, A.; Beller, M. Towards a Green Process for Bulk-Scale Synthesis of Ethyl Acetate: Efficient Acceptorless Dehydrogenation of Ethanol. *Angew. Chem., Int. Ed.* **2012**, *51*, 5711−5713.

Nofar, M.; Park, C. B. Poly(Lactic Acid) Foaming. *Prog. Polym. Sci.* **2014**, *39*, 1721−1741.

Nouri, S.; Dubois, C.; Lafleur, P. G. Effect of chemical and physical branching on rheological behavior of polylactide. *J. Rheol.* **2015**, *59*, 1045−1063.

Nowak, A. P.; Breedveld, V.; Pakstis, L.; Ozbas, B.; Pine, D. J.; Pochan, D.; Deming, T. J. Rapidly recovering hydrogel scaffolds from self-assembling diblock copolypeptide amphiphiles. *Nature* **2002**, *417*, 424−428.

Odian, G. *Principles of Polymerization*; John Wiley & Sons, Inc.: Hoboken, New Jersey, 2004; pp 1–839.

Oh, J.; Seo, M. Photoinitiated Polymerization-Induced Microphase Separation for the Preparation of Nanoporous Polymer Films. *ACS Macro Lett.* **2015**, *4*, 1244–1248.

Overbeek, J. T. G.; Voorn, M. J. Phase Separation in Polyelectrolyte Solutions. Theory of Complex Coacervation. *J. Cell. Comp. Physiol.* **1957**, *49*, 7–26.

Park, M. J.; Balsara, N. P. Phase Behavior of Symmetric Sulfonated Block Copolymers. *Macromolecules* **2008**, *41*, 3678–3687.

Park, T. G.; Cohen, S.; Langer, R. Poly(L-Lactic Acid)/Pluronic Blends: Characterization of Phase Separation Behavior, Degradation, and Morphology and Use as Protein-Releasing Matrixes. *Macromolecules* **1992**, *25*, 116−122.

Parkes, A. Improvements in the Manufacture of Parkesine or Compound of Pyroxyline, and Also Solutions of Pyroxyline Known as Collodion. In *Patents for inventions*; 1857; pp 255–256.

Perry, S. L.; Leon, L.; Hoffmann, K. Q.; Kade, M. J.; Priftis, D.; Black, K. A.; Wong, D.; Klein, R. A.; Pierce, C. F.; Margossian, K. O.; Whitmer, J. K.; Qin, J.; de Pablo, J. J.; Tirrell, M. Chirality-Selected Phase Behaviour in Ionic Polypeptide Complexes. *Nature Communications* **2019**, *6*, 6052-6059.

Perry, S. L.; Li, Y.; Priftis, D.; Leon, L.; Tirrell, M. The Effect of Salt on the Complex Coacervation of Vinyl Polyelectrolytes. *Polymers* **2014**, *6*, 1756–1772.

Peterson, C.; Hillmyer, M. A. Fast Photochromic Dye Response in Rigid Block Polymer Thermosets. *ACS Appl. Polym. Mater*. **2019**, *1*, 2778–2786.

Philipp, B.; Dautzenberg, H.; Linow, K.-J.; Kötz, J.; Dawydoff, W. Polyelectrolyte Complexes - Recent Developments and Open Problems. *Prog. Polym. Sci.* **1989**, *14*, 91−172.

Pilla, S.; Kim, S. G.; Auer, G. K.; Gong, S.; Park, C. B. Microcellular Extrusion-Foaming of Polylactide with Chain-Extender. *Polym. Eng. Sci.* **2009**, *49*, 1653−1660.

Pilla, S.; Kramschuster, A.; Yang, L. Q.; Lee, J.; Gong, S. Q.; Turng, L. S. Microcellular Injection-Molding of Polylactide with Chain-Extender. *Mater. Sci. Eng., C* **2009**, *29*, 1258−1265.

Pinto, M. R.; Schanze, K. S. Conjugated Polyelectrolytes: Synthesis and Applications. *Synthesis* **2002**, *9*, 1293−1309.

Postma, A.; Davis, T. P.; Evans, R. A.; Li, G.; Moad, G.; O'Shea, M. S. Synthesis of Well-Defined Polystyrene with Primary Amine End Groups Through the Use of Phthalimido-Functional RAFT Agents. *Macromolecules* **2006**, *39*, 5293–5306.

Qin, J.; Priftis, D.; Farina, R.; Perry, S. L.; Leon, L.; Whitmer, J.; Hoffmann, K.; Tirrell, M.; de Pablo, J. J. Interfacial Tension of Polyelectrolyte Complex Coacervate Phases. *ACS Macro Lett.* **2014**, *3*, 565−568.

Rajesh, S.; Yan, Y.; Chang, H. -C.; Gao, H. Phillip, W. A. Mixed Mosaic Membranes Prepared by Layer-by-Layer Assembly for Ionic Separations. *ACS Nano* **2014**, *8*, 12338–12345.

Raviv, U.; Glasson, S.; Kampf, N.; Gohy, J.-F.; Jérôme, R.; Klein, J. Lubrication by charged polymers. *Nature* **2003**, *425*, 163−165.

Ren, Q.; Wang, J.; Zhai, W.; Su, S. Solid State Foaming of Poly(Lactic Acid) Blown with Compressed CO_2: Influences of Long Chain Branching and Induced Crystallization on Foam Expansion and Cell Morphology. *Ind. Eng. Chem. Res.* **2013**, *52*, 13411−13421.

Rouholamin, D.; Smith, P. J.; Ghassemieh, E. Control of Morphological Properties of Porous Biodegradable Scaffolds Processed by Supercritical CO_2 Foaming. *J. Mater. Sci.* **2013**, *48*, 3254−3263.

Rumyantsev, A. M.; Pan, A.; Ghosh Roy, S.; De, P.; Kramarenko, E. Y. Polyelectrolyte Gel Swelling and Conductivity vs Counterion Type, Cross-Linking Density, and Solvent Polarity. *Macromolecules* **2016**, *49*, 6630–6643.

Saba, S. A.; Lee, B.; Hillmyer, M. A. Tricontinuous Nanostructured Polymers via Polymerization-Induced Microphase Separation. *ACS Macro Lett.* **2017**, *6*, 1232–1236.

Sadoff, C. W.; Hall, J. W.; Grey, D.; Aerts, J. C. J. H.; Ait-Kadi, M.; Brown, C.; Cox, A.; Dadson, S.; Garrick, D.; Kelman, J.; McCornick, P.; Ringler, C.; Rosegrant, M.; Whittington, D.; Wiberg, D. Securing Water, Sustaining Growth: Report of the GWP/OECD Task Force on Water Security and Sustainable Growth. **2015**, 1–171.

Salerno, A.; Clerici, U.; Domingo, C. Solid-State Foaming of Biodegradable Polyesters by Means of Supercritical CO2/Ethyl Lactate Mixtures: Towards Designing Advanced Materials by Means of Sustainable Processes. *Eur. Polym. J.* **2014**, *51*, 1−11.

Sato, S.; Gondo, D.; Wada, T.; Kanehashi, S.; Nagai, K. Effects of Various Liquid Organic Solvents on Solvent-Induced Crystallization of Amorphous Poly(Lactic Acid) Film. *J. Appl. Polym. Sci.* **2013**, *129*, 1607−1617.

Schuh, K.; Prucker, O.; Rühe, J. Surface Attached Polymer Networks through Thermally Induced Cross-Linking of Sulfonyl Azide Group Containing Polymers. *Macromolecules* **2008**, *41*, 9284−9289.

Schulze, M. W.; Hillmyer, M. A. Tuning Mesoporosity in Cross-Linked Nanostructured Thermosets via Polymerization-Induced Microphase Separation. *Macromolecules* **2017**, *50*, 997–1007.

Scranton, A. B.; Rangarajan, B.; Klier, J. *Biomedical Applications of Polyelectrolytes;* Springer-Verlag: Berlin, Germany, 1995; Vol. *122*.

Scranton, A. B.; Rangarajan, B.; Klier, J. Biomedical Applications of Polyelectrolyles. *Adv. Polym. Sci.* **1995**, *122*, 1–53.

Security of Industrial Water Supply and Management; Atimtay, A. T., Sikdar, S. K., Eds.; 2011; pp 1–261.

Segalman, R. A. Patterning with block copolymer thin films. *Mater. Sci. Eng., R* **2005**, *48*, 191−226.

Seo, M.; Hillmyer, M. A. Reticulated Nanoporous Polymers by Controlled Polymerization-Induced Microphase Separation. *Science* **2012**, *336*, 1422–1425.

Seo, M.; Murphy, C. J.; Hillmyer, M. A. One-Step Synthesis of Cross-Linked Block Polymer Precursor to a Nanoporous Thermoset. *ACS Macro Lett*. **2013**, *2*, 617–620.

Serpico, J. M.; Ehrenberg, S. G.; Fontanella, J. J.; Jiao, X.; Perahia, D.; McGrady, K. A.; Sanders, E. H.; Kellogg, G. E.; Wnek, G. E. Transport and Structural Studies of Sulfonated Styrene−Ethylene Copolymer Membranes. *Macromolecules* **2002**, *35*, 5916–5921.

Shoichet, M. S. Polymer Scaffolds for Biomaterials Applications. *Macromolecules* **2010**, *43*, 581−591.

Sing, C. E.; Perry, S. L. Recent Progress in the Science of Complex Coacervation. *Soft Matter* **2020**, *16*, 2885–2914.

Smith, M. B. and March, J. *Advanced Organic Chemistry 6th ed.*; Wiley Interscience: Hoboken, NJ; 2007; pp 501–502.

Smithers, V. L. Absorbent Material for Floral Arrangements. Patent No. US2753277, 1956.

Sollner, K.; Gregor, H. P. Membrane Equilibria Which Involve Only the Ions of Strong in Organic Electrolytes. *Journal of the American Chemical Society* **1945**, *67*, 346–346.

Sphere. The Sphere Handbook: Humanitarian Charter and Minimum Standards in Humanitarian Response (Fourth Edition). **2018**, 1–458.

Spinu, M.; Ford, T. M. Degradable Foam Materials. Patent No. US5210108, 1993.

Spitael, P.; Macosko, C. W.; McClurg, R. B. Block Copolymer Micelles for Nucleation of Microcellular Thermoplastic Foams. *Macromolecules* **2004**, *37*, 6874−6882.

Spruijt, E.; Sprakel, J.; Lemmers, M.; Stuart, M. A. C.; van der Gucht, J. Relaxation Dynamics at Different Time Scales in Electrostatic Complexes: Time-Salt Superposition. *Phys. Rev. Lett.* **2010**, *105*, 1426–4.

Standardless absolute intensity calibration on SAXSLAB's SAXS instruments. Technical documentation for Xenocs, Inc.: Grenoble, France, Sept. 22, 2015. http://saxslab.com/wp-content/uploads/2015/08/standardless-AI-calibration_v1.3.pdf (accessed June 6, 2020).

Staudinger, H. Über Polymerisation. *Berichte der deutschen chemischen Gesellschaft A and B Series* **1920**, *53*, 1073–1085.

Strube, O. I. and Schmidt-Naake, G. Synthesis of Reactive Triblock Copolymers via Reversible Addition-Fragmentation Chain Transfer (RAFT) Polymerization. *Macromol. Symp*. **2009**, *275–276*, 13–23.

Subramani, A.; Jacangelo, J. G. Emerging Desalination Technologies for Water Treatment: a Critical Review. *Water Research* **2015**, *75*, 164–187.

Sundar, V. J.; Ramesh, R.; Rao, P. S.; Saravanan, P.; Sridharnath, B.; Muralidharan, C. Water Management in Leather Industry. *Journal of Scientific Industrial Research* **2001**, *60*, 443–450.

Takishima, S.; O'Neil, M. L.; Johnston, K. P. Solubility of Block Copolymer Surfactants in Compressed CO2 Using a Lattice Fluid Hydrogen-Bonding Model. *Ind. Eng. Chem. Res.* **1997**, *36*, 2821−2833.

Tang, C.; Lennon, E. M.; Fredrickson, G. H.; Kramer, E. J.; Hawker, C. J. Evolution of Block Copolymer Lithography to Highly Ordered Square Arrays. *Science* **2008**, *322*, 429−432.

Tang, C.; Sivanandan, K.; Stahl, B. C.; Fredrickson, G. H.; Kramer, E. J.; Hawker, C. J. Multiple Nanoscale Templates by Orthogonal Degradation of a Supramolecular Block Copolymer Lithographic System. *ACS Nano* **2010**, *4*, 285−291.

The United Nations World Water Development Report 2016: Water and Jobs; 2016. **2016**, 1–164.

The United Nations World Water Development Report 4. **2012**, *1-3*, 1–909.

Thermal Transitions of Homopolymers: Glass Transition & Melting Point. https://www.sigmaaldrich.com/technical-documents/articles/materials-science/polymer-science/thermal-transitions-ofhomopolymers.html (accessed June 7, 2019).

Thunhorst, K. L.; Noble, R. D.; Bowman, C. N. Preparation of Functionalized Polymers by Reactions of Poly(Vinylbenzyl Chloride). In *Polymer Modification*; Swift, G.;

Carraher, C. E.; Bowman, C. N., Eds.; Springer Science+Business Media, LLC: New York; 1997; pp 97–107.

Ting, W.-H.; Dai, S. A.; Shih, Y.-F.; Yang, I. K.; Su, W.-C.; Jeng, R.-J. Facile synthetic route toward poly(vinyl benzyl amine) and its versatile intermediates. *Polymer* **2008**, *49*, 1497−1505.

Wan, A. C. A.; Yim, E. K. F.; Liao, I.-C.; Le Visage, C.; Leong, K. W. Encapsulation of Biologics in Self-Assembled Fibers as Biostructural Units for Tissue Engineering. *J. Biomed. Mater. Res.* **2004**, *71A*, 586–595.

Wang, P.; Anderko, A.; Young, R. D. Modeling Electrical Conductivity in Concentrated and Mixed-Solvent Electrolyte Solutions. *Ind. Eng. Chem. Res.* **2004**, *43*, 8083–8092.

Wang, Q.; Schlenoff, J. B. The Polyelectrolyte Complex/Coacervate Continuum. *Macromolecules* **2014**, *47*, 3108−3116.

Wang, X.; Goswami, M.; Kumar, R.; Sumpter, B. G.; Mays, J. Morphologies of block copolymers composed of charged and neutral blocks. *Soft Matter* **2012**, *8*, 3036−3052.

Weinstein, J. N.; Caplan, S. R. Charge-Mosaic Membranes: Enhanced Permeability and Negative Osmosis with a Symmetrical Salt. *Science* **1968**, *161*, 70–72.

Wendt, P. The Control of Rubber in World War II. *Southern Economic Journal* **1947**, *13*, 203–227.

Werber, J. R.; Deshmukh, A.; Elimelech, M. The Critical Need for Increased Selectivity, Not Increased Water Permeability, for Desalination Membranes. *Environ. Sci. Technol. Lett.* **2016**, *3*, 112–120.

Yancheva, G.; Nowaczyk, N. R.; Mingram, J.; Dulski, P.; Schettler, G.; Negendank, J. F. W.; Liu, J.; Sigman, D. M.; Peterson, L. C.; Haug, G. H. Influence of the Intertropical Convergence Zone on the East Asian Monsoon. *Nature* **2007**, *445*, 74–77.

Yang, S. Y.; Ryu, I.; Kim, H. Y.; Kim, J. K.; Jang, S. K.; Russell, T. P. Nanoporous Membranes with Ultrahigh Selectivity and Flux for the Filtration of Viruses. *Adv. Mater.* **2006**, *18*, 709–712.

Yang, S.; Vishnyakov, A.; Neimark, A. V. Self-assembly in block polyelectrolytes. *J. Chem. Phys.* **2011**, *134*, 054104.

Yeh, D. H.; Pavlostathis, S. G. Anaerobic Biodegradability of Tween Surfactants Used as a Carbon Source for the Microbial Reductive Dechlorination of Hexachlorobenzene. *Water Sci. Technol.* **2005**, *52*, 343−349.

Yeh, D. H.; Pennell, K. D.; Pavlostathis, S. G. Toxicity and Biodegradability Screening of Nonionic Surfactants Using Sediment-Derived Methanogenic Consortia. *Water Sci. Technol.* **1998**, *38*, 55−62.

Yu, J.; Mahoney, C. M.; Fahey, A. J.; Hicks, W. L.; Hard, R.; Bright, F. V.; Gardella, J. A. Phase Separation at the Surface of Poly(Ethylene Oxide)-Containing Biodegradable Poly(L-Lactic Acid) Blends. *Langmuir* **2009**, *25*, 11467−11471.

Yu, P.; Mi, H. Y.; Huang, A.; Geng, L. H.; Chen, B. Y.; Kuang, T. R.; Mou, W. J.; Peng, X. F. Effect of Poly(Butylenes Succinate) on Poly(Lactic Acid) Foaming Behavior: Formation of Open Cell Structure. *Ind. Eng. Chem. Res.* **2015**, *54*, 6199−6207.

Zeldovich, K. B.; Khokhlov, A. R. Osmotically Active and Passive Counterions in Inhomogeneous Polymer Gels. *Macromolecules* **1999**, *32*, 3488–3494.

Zhang, W.; Zhao, Q.; Yuan, J. Porous Polyelectrolytes: The Interplay of Charge and Pores for New Functionalities. *Angew. Chem., Int. Ed*. **2018**, *57*, 6754−6773.

Zhang, X. D.; Macosko, C. W.; Davis, H. T.; Nikolov, A. D.; Wasan, D. T. Role of Silicone Surfactant in Flexible Polyurethane Foam. *J. Colloid Interface Sci.* **1999**, *215*, 270−279.

Zhang, Y.; Batys, P.; O'Neal, J. T.; Li, F.; Sammalkorpi, M.; Lutkenhaus, J. L. *ACS Cent. Sci*. **2018**, *4*, 638−644.

Zhao, Q.; An, Q. F.; Ji, Y.; Qian, J.; Gao, C. Polyelectrolyte complex membranes for pervaporation, nanofiltration and fuel cell applications. *J. Membr. Sci*. **2011**, *379*, 19−45.

Zhou, M.; Zhou, P.; Xiong, P.; Qian, X.; Zheng, H. H. Crystallization, Rheology and Foam Morphology of Branched PLA Prepared by Novel Type of Chain Extender. *Macromol. Res.* **2015**, *23*, 231−236.

Appendix A. Tricontinuous dual-charged PIMS for charge mosaic materials

* This work was completed in close collaboration with Dr. Eric Silver.

A.1. Introduction

Purification of saline water can be accomplished by electrodialysis and piezodialysis.[1] Both of these technologies rely on the selective transfer of ions through a membrane. An efficient way to pass ions while excluding neutral molecules is by constructing a polymer membrane that contains a supported polyelectrolyte, or charge-containing polymer. Since polyelectrolytes are typically soluble in water,[2] an attractive membrane material contains polyelectrolytes domains that percolate a water-insoluble and mechanically tough support structure.[3]

The charged domains are capable of transferring ions through the thickness of the separator when a suitable driving force (e.g., pressure or an electric field) is applied. Single fixed-charge-containing materials are useful for electrodialysis,[4] where electric fields are used to drive ions across the membrane, while a membrane containing both fixed positive and fixed negative charges could be used in a piezodialysis membrane, where water is desalinated by passing both anions and cations of a salt through the same membrane, leaving behind purified water on the high pressure side.[5–8]

A membrane used for piezodialysis relies on the concept of charge mosaic materials that contain both positive and negative charges, as described in **Chapter 1** and **Chapter 2**. The best materials for such applications have positive domains spatially separated from negative domains, where the distance between the domains is inversely proportional to the flux through the membrane. To make the highest efficiency water desalination membranes, the space between the positive and negative domains should be minimized. Previous block polymer work was able to make charge mosaic membranes on the length scale of microns,

and work detailed in **Chapter 2** made materials with domain spacing below 100 nm. Unfortunately, these materials were not mechanically robust enough to withstand the high pressures required for desalination and would require the fabrication of a composite membrane to be used successfully.

Building on the single-charged monolith work in **Chapter 3**, we target mechanically robust, high ion-density, dual-charged materials using polymerization-induced microphase separation (PIMS). PIMS monoliths have been made containing positive charges using poly(vinylbenzyl chloride) (PVBC) as a pre-cationic macroinitiator. The macroinitiator containing trithiocarbonate reversible addition-fragmentation chain transfer (RAFT) end-groups were dissolved into a mix of styrene (S) and divinylbenzene (DVB) with a radical initiator. After heating for 24 hours, the resulting solid monolith contained nanostructured percolating domains of PVBC throughout a solid, crosslinked S/DVB matrix. The PVBC domain was then functionalized using trimethylamine (TMA) and was shown to have interconnected domains that rejected a positively charged dye and successfully sequestered a negatively charged dye throughout its thickness. Functionalization was confirmed with attenuated total reflection infrared spectroscopy (ATR-IR) and the retention of microstructure confirmed using transmission small-angle X-ray scattering (SAXS). We believe this easy to synthesize material would work well as an anion exchange material.

A similar material with opposite charges was made using poly(*n*-octyl styrene sulfonic ester) (PoSSE) as a macroinitiator. Using the same synthetic process, functionalization with TMA gave a similarly robust material that absorbed positively

charged dye and rejected negatively charged dye. Characterization revealed no change in nanometer scale microstructure, making this material an excellent cation exchange material.

We now work towards a charge mosaic material by combining the pre-anionic and pre-cationic monomers into a single tricontinuous system. In one previous paper, a tricontinuous PIMS material was reported that contained both polyisoprene (PI) and polylactide (PLA) domains percolating through a DVB matrix.[9] The materials were made by simply dissolving both the PI and PLA macroinitiators in DVB with a radical initiator and heating. By selectively removing the PI, the PLA, or both domains, each domain was shown to be continuous, percolating through the entire nanostructured material. The porosities under each etching condition were shown to be additive, implying that the PI and PLA domains were completely separate from each other. TEM evidence supported the conclusion of a tricontinuous monolith.

Using similar methods, we attempt to create a tricontinuous PIMS consisting of a positively charged domain derived from PVBC macroinitiator, a negatively charged domain derived from PoSSE, and a neutral DVB matrix to hold the domains together as a continuous, but spatially separated charge mosaic.

A.2. Experimental

A.2.1. Materials

Unless otherwise noted, all chemicals were purchased from Sigma-Aldrich and used as received. Styrene (99%) was distilled after drying over calcium hydride. Azobisisobutyronitrile (AIBN) (98%) was recrystallized from methanol and dried under

reduced pressure. Divinylbenzene (80% technical grade), 4-chlorostyrene, and 4-vinylbenzyl chloride (90%) were run through a plug of basic alumina to remove inhibitors. Dichloromethane and tetrahydrofuran were purified via a GC-SPS-4-CM glass contour 800-L solvent purification system obtained from Pure Process Technologies (Nashua, NH). The chain transfer agent (4-Cyano-4-[(dodecylsulfanylthiocarbonyl)sulfanyl]pentanoic acid; CTA) was synthesized according to previous literature procedures.[10] *n*-octyl styrene sulfonic ester was synthesized following **Section 3.3.3**.

A.2.2. Instrumentation

NMR spectra were recorded on a Bruker Advance III HD 500 spectrometer. Chemical shifts are reported in δ units, expressed in ppm downfield from tetramethylsilane using residual protiosolvent as an internal standard ($CDCl_3$, ^1H: 7.26 ppm).

Size exclusion chromatography (SEC) was performed in THF (25 °C, 1 mL/min) on an Agilent Infinity 1260 HPLC system equipped with three Waters Styragel HR columns, a Wyatt DAWN HELEOS-II 18-angle laser light scattering detector, and a Wyatt Optilab T-rEX differential refractive index detector. Absolute weight-average molar mass was determined using light scattering detector with a d*n*/dc = 0.171 mL g^{-1} for PVBC, 0.1156 mL g^{-1} for PoSSE, and 0.185 mL g^{-1} for PS and P4ClS as determined using a batch d*n*/d*c* calculation (**Section 3.3.6**).

Thermal gravimetric analysis (TGA) was performed on a TA Instruments Q500 under house nitrogen at a heating rate of 10 °C min^{-1}. Differential scanning calorimetry (DSC) analyses were performed on a TA Instruments Discovery DSC using standard

aluminum T-zero pans with hermetic lids. Scans were conducted under house nitrogen at a heating or cooling rate of 10 °C min^{-1}.

Infrared spectroscopy measurements were performed on a Bruker Alpha Platinum ATR spectrometer with a built-in diamond attenuated total reflection set up and a DLaTGS detector.

Transmission small angle X-ray scattering (SAXS) measurements were performed on a SAXSLab GANESHA300XL instrument of the Characterization Facility at the University of Minnesota. Cu Kα X-rays (λ = 1.54 Å) generated by a Xenocs Geni3DX source were collimated through 2 sets of 4-bladed slits (JJ X-ray, A/S). 2D-SAXS patterns were acquired using a Dectris EIGER R 1M detector (7.72 cm x 7.99 cm rectangular area) with 1030 x 1065 pixels (75 μm x 75 μm pixel size) at a sample-to-detector distance of 46.8 cm. Samples were sealed in an ambient temperature holder with Kapton tape windows. All 2D-SAXS pattern were azimuthally-integrated to obtain one-dimensional scattered intensity I(q) versus q plots.

UV-vis spectroscopy was measured with a Shimadzu spectrometer. Spectra were obtained between 200 and 800 nm at 1 nm intervals. Dye concentration calibration curves were calculated using dilution of stock solutions.

Images of samples were taken using an Epson Perfection V600 Photo Flatbed Scanner or an iPhone 6S. The images were cropped and white balanced in Photoshop using the black text and white paper of the background to increase contrast (white balance applied evenly across each image).

A.2.3. Synthesis of polystyrene (PS)

An oven-dried Schlenk flask was fitted with a Teflon stopcock and flame dried three times, backfilling with 5 psig of argon (*g*) after each cycle. The flask was then placed under an atmosphere of argon (*g*) and charged with styrene monomer (5 mL, 4.53 g, 43.5 mmol, 3360 equiv.), CTA (0.0052 g, 0.013 mmol, 1 equiv.) and a 5 mL solution of AIBN (0.00065 g, 0.0038 mmol, 0.3 equiv.) in THF. The reaction was then degassed through three cycles of freeze-pump-thaw. After the last thawing, the flask was backfilled with 5 psig of argon (*g*) and sealed. The flask was placed in a preheated oil bath (100 °C) and stirred for 19 h. The reaction was stopped by submerging the flask in a N_2 (*l*) bath for 1 min and then warming to room temperature. The polymer was precipitated in methanol and then filtered through 0.2 μm pore PVDF membrane and the solid was dried under vacuum to yield PS as a white solid (1.138 g, 25% isolated yield, $M_{n,NMR}$ = 74 kg mol^{-1}, $M_{n,SEC}$ = 80 kg mol^{-1}, $M_{w,SEC}$ = 93 kg mol^{-1}, $Đ$ = 1.17) ^{1}H NMR (500 MHz, $CDCl_3$): δ 0.90 (4.46H, t, -CH_3), 1.45 (464H, multiplet, -CH_2- and -CH- backbone), 3.25 (2H, m, S-CH_2-), 6.59 (707H, m, Ar-H).

A.2.4. Synthesis of poly(4-chlorostyrene) (P4ClS)

An oven-dried Schlenk flask was fitted with a Teflon stopcock and flame dried three times, backfilling with 5 psig of argon (*g*) after each cycle. The flask was then placed under an atmosphere of argon (*g*) and charged with 4-chlorostyrene (2 mL, 2.31 g, 16.67 mmol, 3600 equiv.), CTA (0.0018 g, 0.0046 mmol, 1 equiv.) and AIBN (0.0002 g, 0.0013 mmol, 0.3 equiv.). The reaction was then degassed through three cycles of freeze-pump-thaw. After the last thawing, the flask was backfilled with 5 psig of argon (*g*) and

sealed. The flask was placed in a preheated oil bath (120 °C) and stirred for 3 h. The reaction was stopped by submerging the flask in a N_2 (*l*) bath for 1 min and then warming to room temperature. The polymer was precipitated in methanol and then filtered through a 0.2 μm pore PVDF membrane and the solid was dried under vacuum to yield P4ClS as a white solid (0.919 g, 40% isolated yield, $M_{n,NMR}$ = 92 kg mol^{-1}, $M_{n,SEC}$ = 97 kg mol^{-1}, $M_{w,SEC}$ = 137 kg mol^{-1}, $Đ$ = 1.41) ^{1}H NMR (500 MHz, $CDCl_3$): δ 0.88 (2H, t, -CH_3), 1.32 (2121H, m, -CH_2- and -CH-backbone), 3.74 (2H, m, -S-CH_2-), 6.40 (2654H, m, Ar-H).

A.2.5. Synthesis of poly(*n*-octyl styrene sulfonic ester) (PoSSE)

An oven-dried Schlenk flask was fitted with a Teflon stopcock and flame dried three times, backfilling with argon after each cycle. The flask was then placed under an atmosphere of argon and charged with *n*-octyl styrene sulfonate (oSSE) monomer (7.8 g, 26.3 mmol, 67 equiv.), 4-cyano-4-[(dodecylsulfanylthiocarbonyl)sulfanyl]pentanoic acid (CTA) (0.159 g, 0.393 mmol, 1 equiv.), and AIBN (0.0189 g, 0.115 mmol, 0.3 equiv.), and dissolved in dry THF (2.7 mL g^{-1} monomer). The reaction was freeze-pump-thawed three times and the reaction flask was backfilled with 5 psig of argon. The flask was placed in a preheated oil bath (60 °C) and stirred for five days. The reaction was stopped by submerging the reaction flask in a liquid N_2 bath for 1 min, and then warming to room temperature. Subsequently, the solution mixture was precipitated in methanol and filtered through a 0.2 μm pore PVDF membrane, and the isolated solid was dried under vacuum to yield PSSE as a white solid (4.19 g, 54% isolated yield, $M_{n,NMR}$ = 21 kg mol^{-1}, $M_{n,SEC}$ = 21 kg mol^{-1}, $M_{w,SEC}$ = 21 kg mol^{-1}, $Đ$ = 1.02) ^{1}H NMR (500 MHz, $CDCl_3$): δ (ppm) 0.91

(218H, s, -CH_3), 1.62 (1090H, m, -CH_2-), 3.25 (2H, br s, -S-CH_2-), 4.07 (142H, br s, O-CH_2-), 6.74 (126H, br s, Ar-*H*), 7.70 (140H, br s, Ar-*H*).

A.2.6. Synthesis of poly(*n*-octyl styrene sulfonic ester)-*b*-poly(4-chlorostyrene) (PoSSE–P4ClS)

An oven-dried Schlenk flask was fitted with a Teflon stopcock and flame dried three times, backfilling with 5 psig of argon (*g*) after each cycle. The flask was then placed under an atmosphere of argon (*g*) and charged with PSSE macroinitiator (0.0997 g, 0.0016 mmol, 1 equiv.), 4-chlorostyrene (1 mL, 1.155 g, 8.33 mmol, 5208 equiv.), and a 1 mL solution of AIBN (0.00009 g, 0.00048 mmol, 0.3 equiv.) in THF. The reaction was then degassed through three cycles of freeze-pump-thaw. After the last thawing, the flask was backfilled with 5 psig of argon (*g*) and sealed. The flask was placed in a preheated oil bath (100 °C) and stirred for 4 h. The reaction was stopped by submerging the flask in a N_2 (*l*) bath for 1 min and then warming to room temperature. The polymer was precipitated in methanol and then filtered through 0.2 μm pore PVDF membrane and the solid was dried under vacuum to yield PSSE-*b*-P4ClS as a white solid (0.324 g, 26% isolated yield, $M_{n,NMR}$ = 225 kg mol^{-1}, $M_{n,SEC}$ = 113 kg mol^{-1}, $M_{w,SEC}$ = 130 kg mol^{-1}, $Đ$ = 1.15) ^{1}H NMR (500 MHz, $CDCl_3$): δ 0.91 (3H, br s, -CH_3), 1.32 (25H, m, -CH_2- and -CH-backbone), 4.08 (2H, br s, -O-CH_2-), 6.40 (26H, m, Ar-H), 7.67 (2H, m, Ar-H).

A.2.7. Synthesis of poly(*n*-octyl styrene sulfonic ester)-*b*-poly(4-chlorostyrene)-*b*-poly(vinylbenzyl chloride) (PoSSE–P4ClS–PVBC)

An oven-dried Schlenk flask was fitted with a Teflon stopcock and flame dried three times, backfilling with 5 psig of argon (*g*) after each cycle. The flask was then placed

under an atmosphere of argon (*g*) and charged with PSSE-*b*-P4ClS macroinitiator (0.1004 g, 0.0014 mmol, 1 equiv.), vinylbenzyl chloride (0.25 mL, 0.27 g, 1.8 mmol, 1267 equiv.), and a 1 mL solution of AIBN (0.00008 g, 0.0004 mmol, 0.3 equiv.) in THF. The reaction was then degassed through three cycles of freeze-pump-thaw. After the last thawing, the flask was backfilled with 5 psig of argon (*g*) and sealed. The flask was placed in a preheated oil bath (100 °C) and stirred for 1 h. The reaction was stopped by submerging the flask in a N_2 (*l*) bath for 1 min and then warming to room temperature. The polymer was precipitated in methanol and then filtered through 0.2 μm pore PVDF membrane and the solid was dried under vacuum to yield PSSE-*b*-P4ClS-*b*-PVBC as a white solid (0.088 g, 24% isolated yield, $M_{n,NMR}$ = 78 kg mol^{-1}, $M_{n,SEC}$ = 27 kg mol^{-1}, $M_{w,SEC}$ = 31 kg mol^{-1}, $Đ$ = 1.10) ^{1}H NMR (500 MHz, $CDCl_3$): δ 0.91 (3H, br s, -CH_3), 1.32 (18H, m, -CH_2- and -CH- backbone). 4.07 (2H, br s, -O-CH_2- from SSE monomer), 4.54 (0.7H, br s, -CH_2-Cl from VBC monomer), 6.40 (15H, m, Ar-H), 7.70 (2H, m, Ar-H).

A.2.8. Synthesis of PIMS monoliths

Macroinitiator (either PVBC or PoSSE, 0.260 g or 0.390 g, for 20 wt% or 30 wt%) was combined in a scintillation vial with styrene (0.792 g or 0.693 g) and divinylbenzene (0.248 g or 0.237 g) mixed at a 4:1 S:DVB molar ratio. The solution was sonicated at room temperature for 20 min to dissolve the macroinitiator. After sonication, a scoop of AIBN (~1 mg) was added and stirred into the mixture. The PIMS solution was then divided into three silane treated vials. The headspace was purged with dry argon and the vials capped and then sealed with parafilm. The vials were then suspended in an oil bath at 70 °C for 24 hours. The solidified PIMS were removed from the oil bath and air-cooled to room

temperature. The vials were then shattered with a hammer to remove the solidified PIMS. The recovered PIMS were then placed under high vacuum overnight to remove residual monomer. PIMS monoliths were imaged and then sanded flat and polished using 600-5000 grit sandpaper to remove the skin layer and make a standard geometry.

A.2.9. Functionalization of PIMS

PIMS monoliths were functionalized by soaking in 3 mL of 45 wt% trimethylamine in water for 24 hours. After functionalization, the PIMS were rinsed in DI water and placed under high vacuum overnight to remove excess TMA. The dried monoliths were massed, imaged, and measured with ATR-IR to check functionalization.

A.2.10. Exposure of PIMS monoliths to dye solutions

PIMS monoliths were exposed to positively charged toluidine blue and negatively charged methyl red solutions to assess the polymer charges. 1 mg of toluidine blue or methyl red was dissolved into 100 mL of 0.1 M phosphate buffer in water mixed at a pH of 7.0. The solution was sonicated for 30 min to ensure dissolution of the dye. PIMS monoliths were placed into 15 mL polypropylene centrifuge tubes with 3 mL of dye stock solution and soaked for 24 h. After exposure, the PIMS were removed, rinsed in DI water, and dried with a delicate task wiper. The monoliths were weighed and imaged at each exposure step. UV-vis spectroscopy was used to assess the residual dye remaining in solution after exposure to the PIMS. The spectrometer was baselined with a cuvette of phosphate buffer and then used to measure the absorbance of each dye solution left after PIMS exposure and a control solution from a centrifuge tube without a sample.

The UV-vis absorption was calibrated using dilution of stock solutions that showed the following relationship between dye concentration and absorption for each dye:

Methyl Red: Absorbance = 35293 · (Concentration in M)

Toluidine Blue: Absorbance = 28622 · (Concentration in M) + 0.0337

Using the above calibration curve, the amount of dye remaining in solution was measured for each sample. Subtracting from the original amount of dye, the amount of absorbed dye was calculated for each PIMS sample.

A.3. Results and Discussion

A.3.1. Using multiple macroinitiators

To make a tricontinuous PIMS structure, the first strategy was following the procedure used previously by Saba *et al*. to produce a tricontinuous PIMS using PI and PLA.[9] In their work, they simply combined two macroinitiators into the starting PIMS solution, dissolving each into DVB and polymerizing the mixture. We attempted the same procedure using PVBC and PoSSE macroiniators, attempted both in pure DVB as had been done in the previous study, and also using 4:1 S/DVB, the monomer ratio used in **Chapter 3**.

After polymerizing for 24 hours, the hazy solution solidified into clear monoliths (**Figure A.1**) with a broad scattering peak in SAXS. The PIMS as made were exposed to positive and negative dye, and the unfunctionalized monoliths did not absorb any appreciable amount of dye and did not swell in water. The materials were then exposed to TMA for 24 hours.

(a)  (b)  (c) 

Figure A.1. PoSSE/PVBC blend PIMS (a) as made, (b) after exposure to TMA and toluidine blue solution, and (c) after exposure to methyl red.

After the TMA exposure, the materials began to lose their mechanical integrity. Small pieces started to flake off of the sample and cracks began to appear throughout the material. The longer the monoliths were exposed to aqueous solution, the more their mechanical integrity disintegrated. Soaking in dye trials revealed an unexpected phenomenon. The monoliths absorbed a significant amount of both positive and negative dyes, confirming that there was proper functionalization of both the PVBC domain and the PoSSE domain, yielding a charged material. However, the coloration suggested sequestration of the positive and negative dyes in different macroscale portions of the monolith (**Figure A.1b** and **c**). Further, the fractures in the monolith appeared along the line separating the two dye absorption regions, and the blue regions (several millimeters in size) that had absorbed the positively charged toluidine blue were peeling off of the similarly sized orange regions that had absorbed the negatively charged methyl red.

SAXS of the individual pieces that had separated after functionalization showed that both the orange and blue portions of the monolith gave scattering that was consistent with the characteristic disordered PIMS peak observed in other related systems (**Figure A.2**). We hypothesize that a strong difference in solubility between the PoSSE and PVBC

in S/DVB monomer resulted in macrophase separation of the microphase separated PIMS regions.

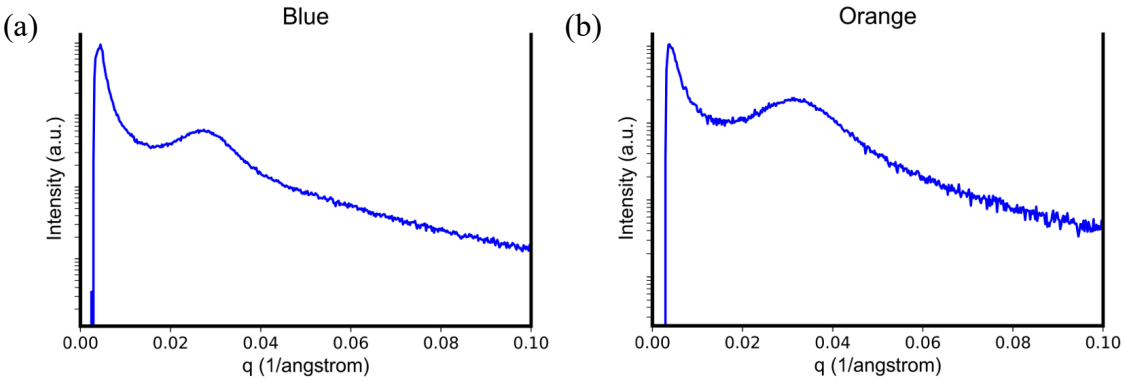

Figure A.2. Transmission SAXS data for (a) blue and (b) orange portions of the PoSSE/PVBC blend PIMS.

In **Chapter 4**, we had shown that PVBC has a remarkably small interaction parameter with polystyrene (PS), which likely means that it has a similarly small interaction with styrene monomer. In other words, it is extremely soluble. Similarly, in **Chapter 3**, we reported immense difficulty fabricating PoSSE PIMS at high macroinitiator molar masses or weight percents due to the sparing solubility of the polymer in S/DVB. We hypothesize that this causes the PVBC to swell into S/DVB rich domains with a different density from the S/DVB poor PoSSE domains before the PIMS process begins. As the material polymerizes in a stationary container, the density differences lead to macrophase separation, where the S/DVB rich PVBC phase drives out the PoSSE phase. These two different phases then each go through the PIMS process and form microstructured PIMS materials containing only one of the two macroinitiators. Because the macrophase separation progressed to macroscale domains much larger than the wavelength of light (on the millimeter scale), the difference in refractive index did not

cause appreciable light scattering, resulting in optical clarity. Once functionalized into polyelectrolytes, these separate phases delaminate into a positively charged PIMS and a negatively charged PIMS.

In an effort to circumvent the solubility issues, we synthesized two diblock polymers each containing a PS block at the end, (64k PoSSE)-*b*-(20k PS) and (24k PVBC)-*b*-(9k PS). We hypothesized that the added PS block would make the polymers more equally soluble and potentially better match the kinetics of the polymerization, as both macroinitiators would be growing the polymer matrix from an existing PS chain. At a total 30 wt% loading (15 wt% of each macroinitiator), the monomer solution was hazy, and the resulting monoliths behaved identically to samples made with a homopolymer PoSSE and PVBC macroinitiator blend. The addition of a PS block was therefore determined to be an unproductive strategy.

A.3.2. Block polymer macroinitiators

A.3.2.1 Coacervate PIMS

Due to solubility differences between PoSSE and PVBC in S/DVB monomers, the next strategy attempted to demonstrate successful PIMS synthesis using block polymers as macroinitiators. The use of block polymers in PIMS systems has not been previously reported but could solve the problem by covalently tying the opposing materials together. Even if one block was significantly more soluble than the other, it would necessarily be adjacent to the other block in the final material as it cannot physically macrophase separate.

The first example was made using a diblock polymer containing both a PoSSE and PVBC block. A diblock polymer with a 1:2.3 molar ratio of oSSE to VBC was made with

a molar mass (23 kg · mol^{-1} PoSSE)-*b*-(27 kg · mol^{-1} PVBC). The diblock polymer quickly dissolved in S/DVB at 30 wt% into an optically clear solution. The material was heated for 24 hours and solidified into an optically clear monolith that was sanded flat (**Figure A.3a**).

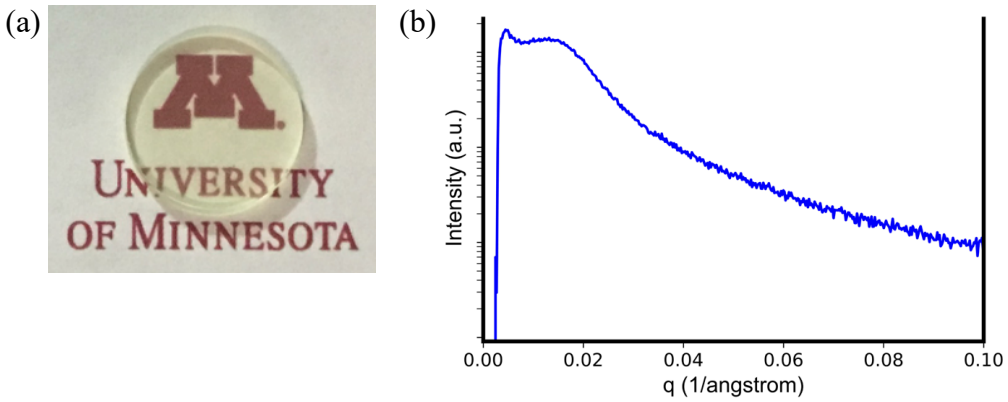

Figure A.3. (a) Image and (b) SAXS data for PoSSE-*b*-PVBC diblock PIMS.

The SAXS spectrum of the monolith showed the characteristic broad peak of a PIMS material (**Figure A.3b**) and it did not absorb any appreciable amount of dye or absorb water. The monolith was then functionalized by soaking in TMA for 24 hours. Unlike the monoliths in **Section A.3.1**, the material did not lose any mechanical integrity after functionalization, although it did swell with water. Dye trials showed the material absorbed only a small amount of methyl red dye (**Figure A.4**), which was consistent with expectations as the diblock macroinitiator had a higher number of VBC monomer units. It absorbed significantly less negatively charged methyl red than comparable monoliths containing only PVBC in **Chapter 3** and rejected all of the positively charged toluidine blue.

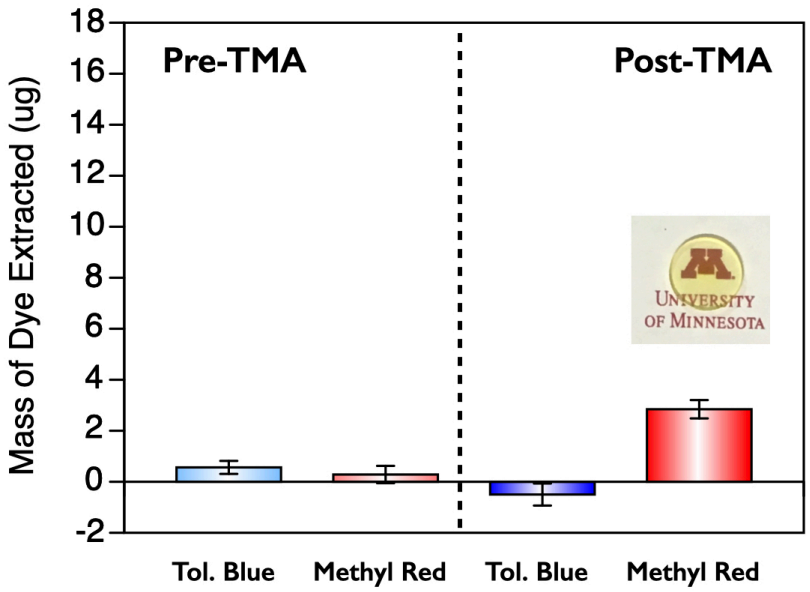

Figure A.4. Mass of dye extracted before and after TMA exposure of PoSSE-*b*-PVBC diblock PIMS.

We hypothesize that the successful PIMS contained a PVBC domain surrounding an inner layer of PoSSE domains. Since the diblock polymer only contained a CTA on one end, it is expected to form a core-shell structure within its percolating domain. Once functionalized, the PoSSE chain ends would be free to move in the swollen polyelectrolyte and could very well form a coacervate with the functionalized PVBC domain as the materials are entropically driven to charge cancel and release their counterions. The final material should, therefore, contain a continuous domain of neutral poly(styrene sulfonate)/poly(vinylbenzyl trimethylammonium) coacervate with a slight excess of fixed positive charges, thus allowing for some uptake of a negatively charged dye.

The formation of a successful PIMS structure using a diblock polymer indicates that the difficulties in solubility differences can likely be overcome using covalent links between the blocks. The formation of a coacervate confirms that the two blocks will

arrange into adjacent domains, which makes it likely that a tricontinuous material could be formed with this strategy.

A.3.2.2 Triblock macroinitiator

After successfully making a tricontinuous system that contains adjacent positive and negative domains, the next step is to separate these domains with a neutral domain, preventing their coalescence into a complex coacervate. The most straightforward method is to use a triblock macroinitiator that contains a neutral polymer between the two charged domains, which we expect to form a core with two surrounding shell layers. Such triblock materials were synthesized successfully in **Chapter 2**.

Unfortunately, this raises a complex problem detailed in **Chapter 2**, where we showed that PVBC was incapable of microphase separating from PS at achievable molar masses. In **Chapter 3**, we showed that it was still possible to see some microphase separation between PVBC and P(S/DVB) in a PIMS system when the crosslinked matrix reaches a sufficiently high molar mass. In the case of a triblock macroinitiator containing a PS midblock, however, we do not expect crosslinking to occur with the matrix formed during the PIMS process. In fact, in our idealized core-shell-shell model of the polyelectrolyte domain, we expect the PS domain from the triblock to be embedded within the polyelectrolyte, meaning it is neither a part of nor adjacent to the P(S/DVB) matrix. Situating the PS domain alongside the PVBC domain, we would therefore expect the two domains to mix freely, creating a PoSSE core with a PS/PVBC blended shell. A blended system will likely be difficult, if not impossible, to functionalize and is unlikely to sufficiently separate the positive and negative domains even if it does functionalize.

To get around this miscibility issue, we target a PoSSE-*b*-P4ClS-*b*-PVBC triblock macroinitiator, which we expect to microphase separate based on the thin films detailed in **Chapter 2**. While PoSSE is a different starting block from the poly(*n*-propyl styrene sulfonic ester) (PSSE) used in **Chapter 2**, the sulfonic esters all appear to show similar microphase separation behavior with polystyrene and its derivatives (with a relatively high χ and clear microphase separation). By ensuring that the P4ClS domain will then microphase separate from the PVBC domain, we expect four separate domains to be formed in a tetracontinuous structure.

Initial trials were completed using a (62k PoSSE)-*b*-(146k P4ClS)-*b*-(61k PVBC) triblock at a 30 wt% loading in a mix of 4:1 S:DVB. The solutions were difficult to dissolve into a homogeneous solution, and even once mixed were gel-like and hazy. The monoliths that formed were colored and hazy (**Figure A.5a**). The SAXS pattern showed no broad peak, indicating a lack of microstructure in the material (**Figure A.5b**). We attribute the lack of PIMS structure on the large molar mass of the triblock macroinitiator. PoSSE is not particularly soluble in the monomer mixture, and at a triblock molar mass of nearly 300 kg · mol^{-1}, it is not soluble enough at 30 wt% loading to mix evenly and likely has macrophase separation within the material.

(a) (b)

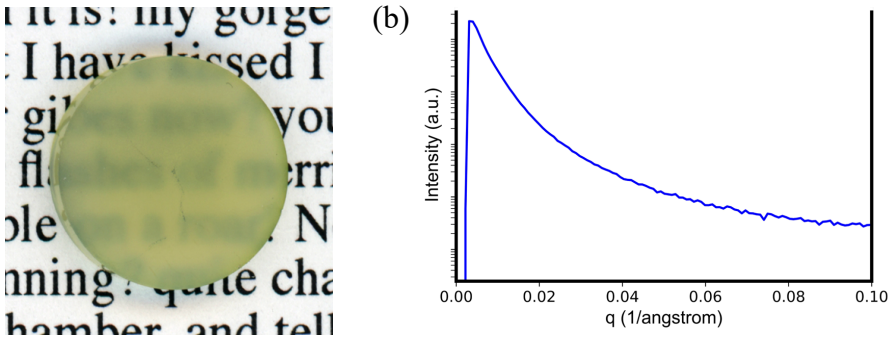

Figure A.5. (a) Image and (b) SAXS spectrum for (62k PoSSE)-(146k P4ClS)-(61k PVBC) PIMS.

We then attempted to make a monolith using a considerably smaller triblock, (29k PoSSE)-*b*-(27k P4ClS)-*b*-(17k PVBC) with a total molar mass of around 73 kg · mol^{-1}. At a 30 wt% loading, the polymer fully dissolved in the 4:1 S:DVB solution after 20 min of sonication. After adding the radical initiator and heating, the final PIMS monolith appeared cloudy, but transparent enough to see through. After attempting to remove it from the container, however, it was found to have no mechanical integrity, and broke apart into small pieces. The pieces of monolith did have a weak scattering bump by SAXS (**Figure A.6**), indicating the presence of some nanostructure.

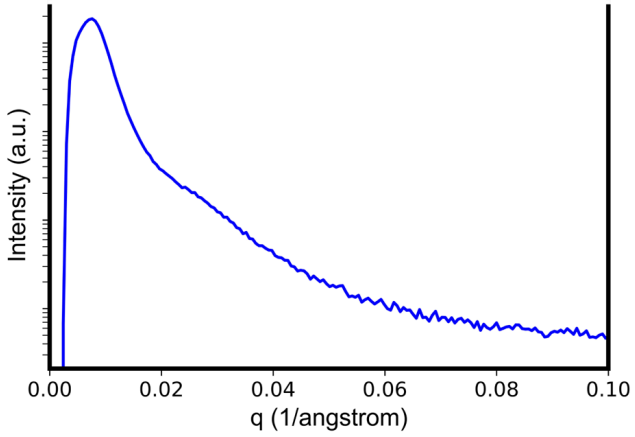

Figure A.6. SAXS scattering data for triblock (29k PoSSE)–(27k P4ClS)–(17k PVBC) PIMS.

Unfortunately, dye trials showed that while the monolith seemingly absorbed a small amount of blue and red dye on the surface, it did not permeate through the thickness of the material (**Figure A.7**). The lack of continuity is not entirely unexpected. At a 30 wt% loading, the actual loading of each of the individual polymers is quite small. Based on the mass distribution of the molar mass of the polymer, the monolith is only 12 wt% PoSSE

and 7 wt% PVBC. In **Chapter 3**, we found that loadings below 20 wt% of macroinitiator in a bicontinous PIMS system failed to consistently show continuity in the minority domains. It is therefore likely that the small amount of each individual polymer domain leads to discontinuous microstructure and the only accessible polyelectrolyte is located on the outer surface of the monolith.

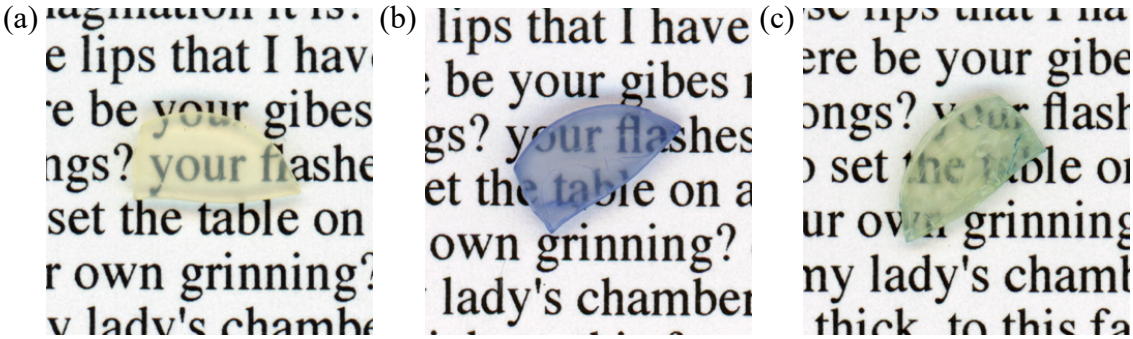

Figure A.7. PIMS monolith containing 30 wt% PoSSE–P4ClS–PVBC triblock polymer (a) after TMA exposure, (b) after exposure to toluidine blue solution, and (c) after exposure to methyl red solution.

Based on the theoretical structure of the tetracontinuous monolith, the loading would need to be increased markedly to reach a point where we would expect the domains to be continuous. A triblock macroinitiator would require at least a 60 wt% loading if it was an even 1:1:1 molar mass ratio between the blocks. Even then, it has not yet been proven whether the presence of multiple domains necessarily adjacent to each other (as in the case of a block polymer) will form a morphology with continuous domains at such loadings. A trial using the same triblock polymer at 60 wt% macroinitiator loading showed little promise; the monomer component fell far short of having enough liquid to even wet such a large amount of starting polymer, even after days of attempted dissolution. While the polymer was still relatively large (73 kg · mol^{-1}), it is synthetically difficult to reach a

triblock polymer much smaller than 10 kg · mol^{-1} per block, which in the ideal case is only half the molar mass. Even then, PIMS studies in **Chapter 3** had significant difficulties achieving loadings >50 wt%, even with small (<20 kg · mol^{-1}) homopolymers due to practical solubilities and gelation. It therefore seems unlikely that we will achieve a desired tetracontinuous PIMS microstructure with a triblock polymer macroinitiator approach.

A.3.3. PVBC reverse PIMS

One of the strategies to reduce the needed loading of macroinitiator is to make use of the matrix domain as a charged polyelectrolyte domain. By using a PoSSE-*b*-P4ClS diblock polymer as the initiator in a VBC/DVB monomer solution, we would expect the final PIMS to contain a percolating core-shell structure of PoSSE surrounded by P4ClS, interwoven through a crosslinked matrix of PVBC. To reach a balanced ratio of charges, the monolith would require a 66 wt% loading of a 1:1 PoSSE:P4ClS diblock polymer (although that could be reduced below 60 wt% with a smaller P4ClS block). While that is still a high loading, a diblock polymer can be practically produced at smaller molar masses than a triblock polymer. Assuming charge balance is not a necessity, it would also be expected to contain tricontinuous domains at loadings as low as 40 wt%, which has been readily achievable in homopolymer systems.

Producing this system requires several complementary properties. The first is that a PoSSE–P4ClS macroinitiator be soluble in a mix of VBC/DVB at high enough loadings to make a PIMS monolith with interconnected domains. Secondly, the kinetics of the polymerization must fit within the PIMS regime. The rate of polymerization plays an important role in trapping the disordered bicontinuous PIMS state. Previous systems have

shown difficulty producing PIMS with other monomers, and although there have been examples with acrylates and several styrene derivatives,[11,12] some monomers have failed to successfully produce PIMS. For example, as a part of work in **Chapter 3** as well as earlier work in this chapter, we were never able to successfully produce a microstructured PIMS monolith using 4ClS/DVB as the matrix monomers.

The first trial in using PVBC as a matrix monomer is to attempt the fabrication of a bicontinuous PIMS using a neutral polymer as the macroinitiator. PIMS monoliths were made with 30 wt% loadings of both 56 kg · mol^{-1} PS and 97 kg · mol^{-1} P4ClS in a 4:1 molar ratio of VBC:DVB. Both macroinitiators rapidly dissolved into clear solutions, which generated solid, transparent PIMS after heating with radical initiator. Both samples showed broad peaks in transmission SAXS indicative of PIMS microstructure (**Figure A.8**).

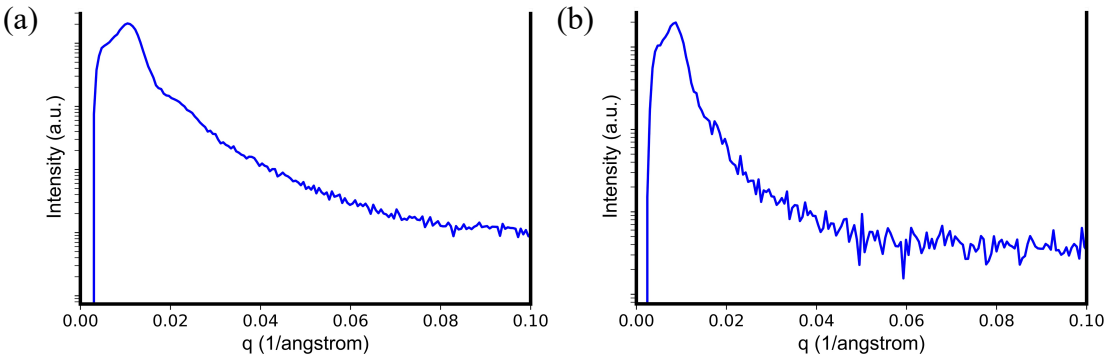

Figure A.8. Transmission SAXS data for (a) PS and (c) P4ClS reverse PIMS.

Both samples were subsequently soaked in TMA solution and showed significantly cracking throughout the samples (**Figure A.9**). We hypothesize that the cracking is caused by the significant deformation of the matrix domain as it swells. The structural change causes the neutral, co-continuous macroinitiator phase to crack, but the crosslinked PVBC

phase around it holds the monolith sample together. Despite the visible fractures, both samples remained coherent as single pieces and were shown to sequester a significant amount of negatively charged methyl red dye after soaking overnight.

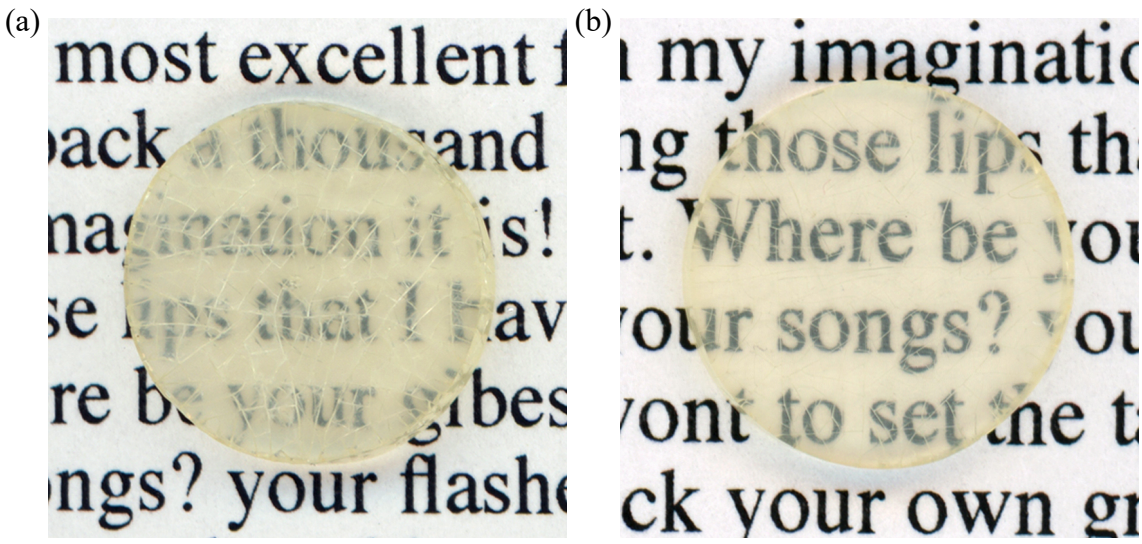

Figure A.9. Images of PVBC reverse PIMS with (a) PS and (b) P4ClS macroinitiators after soaking in TMA.

A.4. Conclusions

The fabrication of a dual-charged material with separate positive and negative domains crossing through the thickness of the sample is desirable for water desalination technology through piezodialysis. Building on work in **Chapter 3** that successfully made bicontinuous PIMS monoliths with either negative or positive charge, we attempted to combine the materials into a single sample. Using procedures based on the only previous example of tricontinuous PIMS, we were unable to successfully fabricate a dual-charged system due to solubility differences in the macroinitiators. We then moved to a block polymer macroinitiator approach by combining the different desired domains into a block polymer, covalently linking the materials before the PIMS formation. Unfortunately, the

high loading of macroinitiator required to create four continuous domains is unachievable within the solubility constraints of our materials. Finally, a promising approach is presented that reverses the role of the matrix by using VBC as the crosslinked monomer in the PIMS system. Initial studies with neutral homopolymers show successful PIMS fabrication and suggest a diblock PoSSE–P4ClS polymer may be able to achieve the desired charge mosaic result.

A.5. References

[1] Bolto, B.; Hoang, M.; Tran, T. Review of piezodialysis — salt removal with charge mosaic membranes. *Desalination* **2010**, *254*, 1–5.

[2] Scranton, A. B.; Rangarajan, B.; Klier, J. Biomedical Applications of Polyelectrolyles. *Adv. Polym. Sci.* **1995**, *122*, 1–53.

[3] Fujimoto, T.; Ohkoshi, K.; Miyaki, Y.; Nagasawa, M. A New Charge-Mosaic Membrane from a Multiblock Copolymer. *Science* **1984**, *224*, 74–76.

[4] Campione, A.; Gurreri, L.; Ciofalo, M.; Micale, G.; Tamburini, A.; Cipollina, A. Electrodialysis for water desalination: A critical assessment of recent developments on process fundamentals, models and applications. *Desalination* **2018**, *434*, 121–160.

[5] Leitz, F. B.; Alexander, S. S.; Douglas, A. S. *Research on Piezodialysis.* United States Department of the Interior: Washington, DC, 1969.

[6] Leitz, F. B.; Alexander, S. S.; de Winter, D. M.; Plummer, C. W. *Research on Piezodialysis: Second Report*. United States Department of the Interior: Washington, DC, 1970.

[7] Leitz, F. B.; Sharr, J.; O'Meara, J. W.; Gillam, W. S.; Johnson, S. *Research on piezodialysis: third report.* United States Department of the Interior: Washington, DC, 1972.

[8] Rajesh, S.; Yan, Y.; Chang, H. -C.; Gao, H. Phillip, W. A. Mixed Mosaic Membranes Prepared by Layer-by-Layer Assembly for Ionic Separations. *ACS Nano* **2014**, *8*, 12338–12345.

[9] Saba, S. A.; Lee, B.; Hillmyer, M. A. Tricontinuous Nanostructured Polymers via Polymerization-Induced Microphase Separation. *ACS Macro Lett.* **2017**, *6*, 1232–1236.

[10] Moad, G.; Chong, Y. K.; Postma, A.; Rizzardo, E.; Thang, S. H. Advances in RAFT polymerization: the synthesis of polymers with defined end-groups. *Polymer* **2005**, *46*, 8458–8468.

[11] Peterson, C.; Hillmyer, M. A. Fast Photochromic Dye Response in Rigid Block Polymer Thermosets. *ACS Appl. Polym. Mater*. **2019**, *1*, 2778–2786.

[12] Larsen, M. B.; Van Horn, J. D.; Wu, F.; Hillmyer, M. A. Intrinsically Hierarchical Nanoporous Polymers via Polymerization-Induced Microphase Separation. *Macromolecules* **2017**, *50*, 4363–4371.

Appendix B. Controlled swelling of polyelectrolyte PIMS monoliths using degradable poly(lactide) spacers

* The theoretical basis for this work was assembled in close collaboration with Dr. Eric Silver.

B.1. Introduction

In **Chapter 3**, we described a method for making either positively or negatively charged materials using polymerization-induced microphase separation (PIMS). The straightforward synthesis used a pre-ionic macroinitiator dissolved in a blend of styrene (S) and divinylbenzene (DVB) that was radically chain extended. During the polymerization, the enthalpic drive for the materials to microphase segregate as the macroinitiator chain extends leads to a bicontinuous nanostructure consisting of interconnected domains.

Crosslinking the glassy matrix freezes it in place, which means the macroinitiator domain occupies a fixed volume. Once this is converted to a polyelectrolyte, the domain is driven to swell in the presence of water. However, the osmotic pressure cannot lead to domain volume increases without fracturing the matrix material. As a result, a polyelectrolyte-containing PIMS can consist of high ion densities and relatively low hydration levels.

Such confined polyelectrolytes are intriguing because systems with restricted swelling are of high interest for ion transfer as the ion density in a polyelectrolyte plays a substantial role in the transport abilities of the domain.[1] Theory predicts a maximum in conductivity as a function of swelling; decreasing swelling continually increases conductivity as the ion density increases until reaching such low hydration that there is not enough water to facilitate ion transport, in which case the conductivity rapidly decreases.[2] Systematically controlling the swelling of a polyelectrolyte system is challenging due to the extremely high osmotic pressures. Strategies include controlling the hydrophobicity of

the monomers,[3] decreasing the functionality of the monomers,[4] or synthesizing highly crosslinked systems.[5] These strategies suffer from a range of uncontrollable factors that likely influence the ion transport properties regardless of swelling. For example, by controlling the hydrophobicity, the overall swelling decreases, but studies have shown that the materials simply form high charge density swollen subdomains alongside hydrophobic subdomains.[6] Adjusting crosslink density changes mechanical properties and leads to spatial inhomogeneities that can impact the ion transport properties.[7]

Thus, there is a need for a simple and easily tuned system to evaluate the effect of swelling of polyelectrolytes on ion conductivity. In our proposed PIMS system, we control several parameters that influence the type of counterion and the size of the ionic domain. Postpolymerization functionalization polymer ensures each monomeric unit contains a charge, and thus we expect that the polyelectrolyte domain should be evenly hydrated. A glassy, crosslinked matrix maintains mechanical integrity and ensures that the polyelectrolyte cannot physically expand beyond its occupied volume, provided the matrix material retains its integrity, even after charging and the covalent link between the polyelectrolyte and the crosslinked domain restricts the polyelectrolyte from dissolving in the media.

B.2. Experimental

B.2.1. Materials

Unless otherwise noted, all chemicals were purchased from Sigma-Aldrich and used as received. Styrene (99%) was distilled after drying over calcium hydride. Azobisisobutyronitrile (AIBN) (98%) was recrystallized from methanol and dried under

reduced pressure. Divinylbenzene (80% technical grade) was run through a plug of basic alumina to remove inhibitors. Dichloromethane and tetrahydrofuran were purified via a GC-SPS-4-CM glass contour 800-L solvent purification system obtained from Pure Process Technologies (Nashua, NH). The chain transfer agent (4-Cyano-4-[(dodecylsulfanylthiocarbonyl)sulfanyl]pentanoic acid; CTA) was synthesized according to previous literature procedures.[8] (±)-Lactide was donated by Altasorb and recrystallized three times from toluene prior to use. Poly(*n*-octyl styrene sulfonic ester) was synthesized following **Section 3.3.3** and **Section 3.3.4**.

B.2.2. Instrumentation

NMR spectra were recorded on a Bruker Advance III HD 500 spectrometer. Chemical shifts are reported in δ units, expressed in ppm downfield from tetramethylsilane using residual protiosolvent as an internal standard ($CDCl_3$, ^1H: 7.26 ppm). Size exclusion chromatography (SEC) was performed in THF (25 °C, 1 mL/min) on an Agilent Infinity 1260 HPLC system equipped with three Waters Styragel HR columns, a Wyatt DAWN HELEOS-II 18-angle laser light scattering detector, and a Wyatt Optilab T-rEX differential refractive index detector. Absolute weight-average molar mass was determined using light scattering detector with a dn/dc = 0.1156 mL g^{-1} for PoSSE as determined using a batch d*n*/d*c* calculation (**Section 3.3.6**). Thermal gravimetric analysis (TGA) was performed on a TA Instruments Q500 under house nitrogen at a heating rate of 10 °C min^{-1}. Differential scanning calorimetry (DSC) analyses were performed on a TA Instruments Discovery DSC using standard aluminum T-zero pans with hermetic lids. Scans were conducted under house nitrogen at a heating or cooling rate of 10 °C min^{-1}. Infrared spectroscopy

measurements were performed on a Bruker Alpha Platinum ATR spectrometer with a built-in diamond attenuated total reflection set up and a DLaTGS detector. Transmission small angle X-ray scattering (SAXS) measurements were performed on a SAXSLab GANESHA300XL instrument of the Characterization Facility at the University of Minnesota. Cu Kα X-rays (λ = 1.54 Å) generated by a Xenocs Geni3DX source were collimated through 2 sets of 4-bladed slits (JJ X-ray, A/S). 2D-SAXS patterns were acquired using a Dectris EIGER R 1M detector (7.72 cm x 7.99 cm rectangular area) with 1030 x 1065 pixels (75 μm x 75 μm pixel size) at a sample-to-detector distance of 46.8 cm. Samples were sealed in an ambient temperature holder with Kapton tape windows. All 2D-SAXS pattern were azimuthally-integrated to obtain one-dimensional scattered intensity I(q) versus q plots.

B.2.3. Synthesis of alcohol terminated CTA derivative

Alcohol-terminated CTA was made by coupling a single ethylene glycol unit to the end of the carboxylic acid-terminated CTA (4-Cyano-4-[(dodecylsulfanylthiocarbonyl)sulfanyl]pentanoic acid). CTA (0.5 g, 1.2 mmol, 1 equiv.) was mixed with 1-ethyl-3-(3-dimethylaminopropyl)carbodiimide (EDC) (0.261 g, 1.7 mmol, 1.4 equiv.) in 200 mL of dry DCM in a 250 mL oven-dried round bottom flask at 0 °C. Add 4-dimethylaminopyridine (0.015 g, 0.12 mmol, 0.1 equiv.) and stir vigorously for 1 h at 0 °C. Transfer to oven-dried addition funnel. Add DCM solution dropwise to a vigorously stirring flask of ethylene glycol (100 mL, excess) at 0 °C. Let warm to room temperature and stir overnight. Wash reaction mixture in a 500 mL separatory funnel with 3x200 mL deionized water and 1x200 mL brine solution. Dry with magnesium sulfate and

remove DCM by rotary evaporation. Dry overnight under high vacuum to recover a yellow oil (85.2 mg, 15% crude yield).

The product was purified using flash chromatography in 9:1 hexanes:ethyl acetate and isolated as the third spot at $R_f \sim 0.1$. After solvent removal through rotary evaporation and drying under reduced pressure, the product was isolated as a pale yellow oil (13.8 mg, 2.5% isolated yield). ^{1}H NMR (500 MHz, $CDCl_3$): δ 0.88 (3H, t, -C*H*$_3$, *J* = 6.73 Hz), 1.26 (16H, br s, -(C*H*$_2$)$_8$-), 1.39 (2H, br m, S-CH$_2$-CH$_2$-C*H*$_2$-), 1.69 (2H, m, S-CH$_2$-C*H*$_2$-), 1.89 (3H, s, -C-C*H*$_3$), 2.39 (1H, m, -O$_2$C-CH$_2$-C(*H*)H-C), 2.55 (1H, m, -O$_2$C-CH$_2$-C(*H*)H-C), 2.68 (2H, t, -O$_2$C-C*H*$_2$-, *J* = 7.94 Hz), 3.33 (2H, t, C*H*$_2$-S, *J* = 7.45 Hz), 3.85 (2H, br s, HO-C*H*$_2$-CH$_2$-), 4.26 (2H, br s, HO-CH$_2$-C*H*$_2$-).

B.2.4. Synthesis of poly(*n*-octyl styrene sulfonic ester) (PoSSE) from pentanol CTA

An oven-dried Schlenk flask was fitted with a Teflon stopcock and flame dried three times, backfilling with argon (*g*) after each cycle. The flask was then placed under an atmosphere of argon (*g*) and charged with *n*-octyl styrene sulfonate (oSSE) monomer (5.2045 g, 17.56 mmol, 156 equiv.), 4-cyano-4-[(dodecylsulfanylthiocarbonyl)sulfanyl]-pentanol (CTA) (0.0438 g, 0.1124 mmol, 1 equiv.), and AIBN (0.0136 g, 0.0337 mmol, 0.3 equiv.), and dissolved in dry THF (13.5 mL). The reaction was then put through three cycles of freeze-pump-thaw, after which the reaction flask was backfilled with 5 psig of argon (*g*) and sealed. The flask was placed in a preheated oil bath (60 °C) and stirred for five days. The reaction was stopped by submerging the reaction flask in a N_2 (*l*) bath for 1 min, and then warming to room temperature. Subsequently, the solution mixture was

precipitated in methanol and filtered through a 0.2 μm pore PVDF membrane, and the isolated solid was dried under vacuum to yield PoSSE as a pale yellow solid.

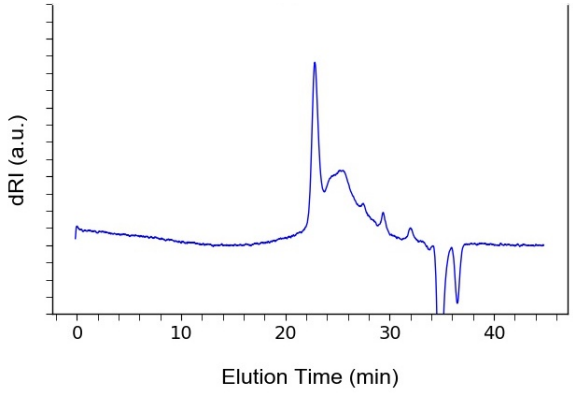

Figure B.1. SEC chromatogram of PoSSE synthesized with pentanol CTA showing multimodal and disperse molar mass distribution.

B.2.5. Synthesis of poly(lactide) (PLA) from pentanol CTA

An oven-dried Schlenk flask was fitted with a Teflon stopcock and moved into a dry N_2 glovebox. The flask was then loaded with (±)-lactide monomer (2.0 g, 13.88 mmol, 69 equiv.), 4-cyano-4-[(dodecylsulfanylthiocarbonyl)sulfanyl]-pentanol (CTA) (0.0779 g, 0.02 mmol, 1 equiv.), and 1,8-Diazabicyclo(5.4.0)undec-7-ene (DBU) (0.0305 g, 0.02 mmol, 1 equiv.), and dissolved in dry DCM (14 mL, 1 M lactide concentration). The reaction was then sealed and removed from the glovebox. The flask was stirred for 1 h at room temperature. The reaction was stopped by adding a scoop of benzoic acid (~10 mg) and stirring. Subsequently, the solution mixture was precipitated in methanol and decanting the supernatant three times. The isolated solid was dried under vacuum to yield PLA-CTA as a clear solid. $M_{n,SEC}$ = 11.7 kg · mol^{-1}, $Đ$ = 1.45.

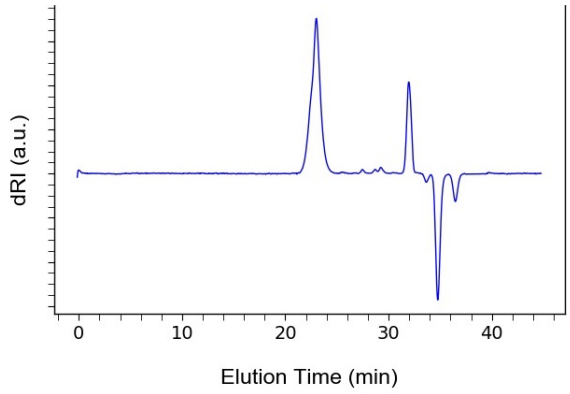

Figure B.2. SEC chromatogram of PLA synthesized with pentanol CTA.

B.2.6. Synthesis of poly(*n*-octyl styrene sulfonic ester) (PoSSE) from PLA-CTA

An oven-dried Schlenk flask was fitted with a Teflon stopcock and flame dried three times, backfilling with argon (*g*) after each cycle. The flask was then placed under an atmosphere of argon (*g*) and charged with *n*-octyl styrene sulfonate (oSSE) monomer (1.522 g, 5.13 mmol, 86 equiv.), PLA-CTA (0.70 g, 0.0597 mmol, 1 equiv.), and AIBN (0.0071 g, 0.017 mmol, 0.3 equiv.), and dissolved in dry THF (4.11 mL). The reaction was then put through three cycles of freeze-pump-thaw, after which the reaction flask was backfilled with 5 psig of argon (*g*) and sealed. The flask was placed in a preheated oil bath (60 °C) and stirred for five days. The reaction was stopped by submerging the reaction flask in a N_2 (*l*) bath for 1 min, and then warming to room temperature. Subsequently, the solution mixture was precipitated in methanol, centrifuged, and decanted before drying under reduced pressure. PLA-PoSSE-CTA was isolated as a pale yellow solid.

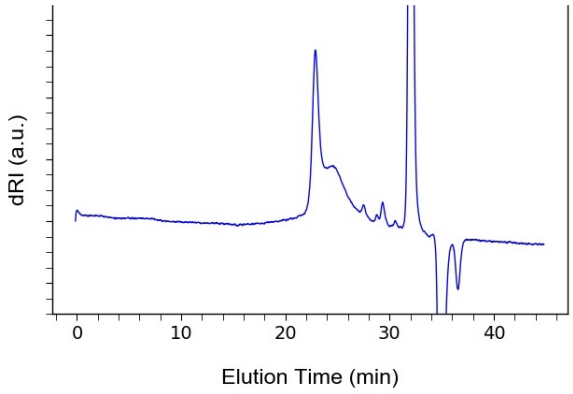

Figure B.3. SEC chromatogram of PLA-PoSSE-CTA showing multimodal and disperse molar mass distribution.

B.3. Results and Discussion

The charged monoliths demonstrated in **Chapter 3** only swell 4-6% with water after functionalization (estimated to be roughly two water molecules per charged monomer). To tune the hydration level, our goal is to open up volume for the polyelectrolyte domain by synthesizing monoliths with a PLA domain adjacent to a protected polyelectrolyte domain. Using a soluble block polymer comprised of PLA-b-PoSSE macroCTA instead of a homopolymer macroinitiator will yield a tricontinuous PIMS monolith containing three domains–a neutral matrix domain consisting of PS/PDVB and a phase segregated domain for the immiscible and covalently-linked PLA and PSSE (**Figure B.4**).

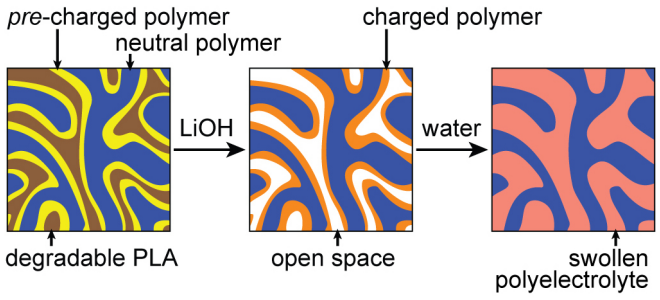

Figure B.4. Diagram of PIMS synthesized with a *pre*-charged domain and a degradable PLA domain which will etch out when functionalized, leaving open space for the polyelectrolyte to swell with water.

Treatment with a lithium hydroxide solution should etch the PLA and hydrolyze the sulfonic ester to the poly(lithium styrene sulfonate). PLA removal opens volume in the domain for the polyelectrolyte to swell, increasing the water content and decreasing the overall charge density in the material. In essence, we propose tuning the amount of polyelectrolyte swelling, as the larger the starting PLA chain, the more space will be available for the chains to swell after etching of the pores.

The first step is to synthesize a PLA-PoSSE-CTA block polymer to use as a macroinitiator. To compare the swelling between different monolith samples, it is advantageous to keep the number of charges constant. A good comparison will keep the same molar mass PoSSE block and vary the length of the PLA block attached to the end, allowing for different amounts of swelling space for the same amount of polyelectrolyte. The PLA synthesis, therefore, should be the second step in the synthesis. To grow the PLA, however, the PoSSE macroinitiator needs to be alcohol terminated with high end-group fidelity. We therefore target a RAFT CTA containing an alcohol-terminated Z group that can be used to grow PoSSE.

The simplest solution is to use the commercially available analog of the CTA used to grow PoSSE in **Chapter 3**. 4-cyano-4-[(dodecylsulfanylthiocarbonyl)sulfanyl]-pentanol can be purchased and used as is. Unfortunately, multiple attempts at the five-day polymerization (following the procedure in **Section 3.3.4**) were unsuccessful at synthesizing a low dispersity polymer with controlled molar mass (**Figure B.1**). In fact, every trial resulted in multi-modal SEC traces indicative of problems with chain initiation.

We hypothesize that the slight electronic differences between a carboxylic acid-terminated and a hydroxy-terminated CTA were enough to disrupt initiation of the PoSSE chains, making the already slow RAFT polymerization impractical.

To try to solve the initiation problem, we then tried to synthesize PLA from the hydroxyl end-group *before* oSSE polymerization. PLA is most commonly made through the catalyzed ring-opening polymerization of lactide. The most common industrial catalyst is tin(II) octanoate, but a variety of other metal and organo-catalysts have been developed,[10] most notably 1,8-Diazabicyclo(5.4.0)undec-7-ene (DBU),[11] which readily polymerizes lactide off of an alcohol initiator at room temperature.

Polymerizing lactide using tin catalysts is usually done in the melt at elevated temperatures, which is unsuitable for some trithiocarbonate RAFT CTAs that can thermally dissociate and undergo side reactions during polymerization. While PLA has been successfully polymerized with a tin catalyst in a previous synthesis (in a simultaneous RAFT/ROTEP polymerization) using 2-(benzylsulfanylthiocarbonylsulfanyl) ethanol,[12] trials using the cyano containing CTAs in our study (containing either a pentanoic acid or pentanol end group) showed severe degradation of the material and no resulting polymer. For that reason, our goal is to use a DBU catalyzed polymerization to grow PLA from the pentanol initiator.

First, PLA was polymerized from the pentanol CTA using DBU in DCM. The polymerization resulted in a somewhat disperse ($Đ$ = 1.45) polymer that was close to the target molar mass (**Figure B.2**). The PLA-CTA was then used as a macroinitiator to polymerize oSSE through the same five-day RAFT polymerization. The resulting diblock

polymer, however, had poor control of molar mass and a multimodal SEC trace (**Figure B.3**), similar to the result of the first oSSE polymerizations using the pentanol CTA. The PLA extension did not increase the efficiency of the initiation and did not solve the oSSE polymerization problems.

Another potential solution to the electronic differences is to instead use a *more* similar CTA that is modified to contain a hydroxy-terminated Z group. Starting with 4-cyano-4-[(dodecylsulfanylthiocarbonyl)sulfanyl]-pentanoic acid, we want to couple an ethylene glycol chain to the carboxylic acid, similar to a procedure shown by Oh and Seo.[9] Instead of using oxalyl chloride, we instead coupled the alcohol end-group of the ethylene glycol to the carboxylic acid end-group of the pentanoic acid CTA using 1-ethyl-3-(3-dimethylaminopropyl)carbodiimide (EDC) (**Section B.2.3**). The successful synthesis allowed us to easily make a small amount of CTA to use for the synthesis of PoSSE, which we believe will be electronically closer to the carboxylic acid-terminated CTA used in **Chapter 3** to make low dispersity, well-controlled polymers.

After growth of the PLA at several molar masses, yielding a library of macroinitiators with the same number of PoSSE monomers but differing PLA lengths, a variety of PIMS can be made, where the weight percent is shifted from 20% for the PoSSE macroCTA alone to higher amounts to compensate for lower PoSSE fractions in the block polymer. Then, a 1:1 PLA:PoSSE polymer would make a PIMS with 40 wt% macroinitiator such that the sample contains the same number of total sulfonic esters.

The PIMS can then be functionalized with lithium hydroxide. While it may seem advantageous to use a previously designed system and functionalize with trimethylamine

(as was done in **Chapter 3**), early trials show that even after several days in TMA solution, bulk PLA does not lose any significant mass. In addition, the use of lithium hydroxide as the base leaves lithium as the sulfonic acid counterion in the functionalized polyelectrolyte, a more application-related and well-studied ion for conductivity testing.

With several PIMS samples containing the same number of charges, we should be able to confirm the expected difference in swelling by measuring the dry and wet mass of the samples. Using ATR-IR, we will be able to confirm complete degradation of the PLA and complete functionalization of the sulfonic ester. Transmission SAXS will demonstrate the nanostructured domains of the material and dye trials can be used (as in **Chapter 3** and **Appendix A**) to demonstrate interconnectivity of the domains. We then hope to do electrochemical impedance spectroscopy to measure the ion conductivity of the material to gain insight into the effect of swelling on ion transfer properties of the materials.

B.4. Conclusions

The behavior of polyelectrolytes at different amounts of swelling is of high interest for applications in batteries, fuel cells, and purification technologies. While many studies have attempted to control the swelling to investigate its effects, there have always been caveats that complicated the results. Using charged PIMS, it is likely we will be able to establish a well-controlled system that can vary the swelling of a material by physical confinement, eliminating the problems associated with crosslinking polyelectrolytes, changing charge density, and modifying functionalization. By measuring the ion conductivity and transfer properties of the different materials, we may be able to gain new fundamental insights into the behavior of charged materials. So far, we have designed a

plan for the synthesis and successfully produced a hydroxyl-terminated CTA that can be used to build a diblock polymer macroinitiator. After synthesizing the diblock polymers, they can easily be made into PIMS with controlled swelling ratios, allowing for exploration of various fundamental properties.

B.5. References

[1] Chen, X. C.; Kortright, J. B.; Balsara, N. P. Water Uptake and Proton Conductivity in Porous Block Copolymer Electrolyte Membranes. *Macromolecules* **2015**, *48*, 5648–5655.

[2] Wang, P.; Anderko, A.; Young, R. D. Modeling Electrical Conductivity in Concentrated and Mixed-Solvent Electrolyte Solutions. *Ind. Eng. Chem. Res.* **2004**, *43*, 8083–8092.

[3] Chen, X. C.; Jiang, X.; Balsara, N. P. Swelling of individual nanodomains in hydrated block copolymer electrolyte membranes. *J. Chem. Phys.* **2018**, *149*, 163325.

[4] Park, M. J.; Balsara, N. P. Phase Behavior of Symmetric Sulfonated Block Copolymers. *Macromolecules* **2008**, *41*, 3678–3687.

[5] Rumyantsev, A. M.; Pan, A.; Ghosh Roy, S.; De, P.; Kramarenko, E. Y. Polyelectrolyte Gel Swelling and Conductivity vs Counterion Type, Cross-Linking Density, and Solvent Polarity. *Macromolecules* **2016**, *49*, 6630–6643.

[6] Kim, S. Y.; Park, M. J.; Balsara, N. P.; Jackson, A. Confinement Effects on Watery Domains in Hydrated Block Copolymer Electrolyte Membranes. *Macromolecules* **2010**, *43*, 8128–8135.

[7] Zeldovich, K. B.; Khokhlov, A. R. Osmotically Active and Passive Counterions in Inhomogeneous Polymer Gels. *Macromolecules* **1999**, *32*, 3488–3494.

[8] Moad, G.; Chong, Y. K.; Postma, A.; Rizzardo, E.; Thang, S. H. Advances in RAFT Polymerization: the Synthesis of Polymers with Defined End-Groups. *Polymer* **2005**, *46*, 8458–8468.

[9] Oh, J.; Seo, M. Photoinitiated Polymerization-Induced Microphase Separation for the Preparation of Nanoporous Polymer Films. *ACS Macro Lett.* **2015**, *4*, 1244–1248.

[10] Auras, R. A.; Lim, L. T.; Selke, S. E. M.; Tsuji, H. *Poly(lactic acid): Synthesis, Structures, Properties, Processing, and Applications*; John Wiley & Sons, Inc.: Hoboken, NJ, 2010.

[11] Kamber, N. E.; Jeong, W.; Waymouth, R. M. Organocatalytic Ring-Opening Polymerization. *Chem. Rev.* **2007**, *107*, 5813−5840.

[12] Seo, M.; Murphy, C. J.; Hillmyer, M. A. One-Step Synthesis of Cross-Linked Block Polymer Precursor to a Nanoporous Thermoset. *ACS Macro Lett*. **2013**, *2*, 617–620.